frontiers | Research Topics

Advanced biomaterials for osteochondral regeneration

Edited by
Le Yu, Qian Feng, Chen Yang and Mei Wei

Published in
Frontiers in Bioengineering and Biotechnology
Frontiers in Materials

ISSN 1664-8714
ISBN 978-2-83251-198-5
DOI 10.3389/978-2-83251-198-5

About Frontiers

Frontiers is more than just an open access publisher of scholarly articles: it is a pioneering approach to the world of academia, radically improving the way scholarly research is managed. The grand vision of Frontiers is a world where all people have an equal opportunity to seek, share and generate knowledge. Frontiers provides immediate and permanent online open access to all its publications, but this alone is not enough to realize our grand goals.

Frontiers journal series

The Frontiers journal series is a multi-tier and interdisciplinary set of open-access, online journals, promising a paradigm shift from the current review, selection and dissemination processes in academic publishing. All Frontiers journals are driven by researchers for researchers; therefore, they constitute a service to the scholarly community. At the same time, the *Frontiers journal series* operates on a revolutionary invention, the tiered publishing system, initially addressing specific communities of scholars, and gradually climbing up to broader public understanding, thus serving the interests of the lay society, too.

Dedication to quality

Each Frontiers article is a landmark of the highest quality, thanks to genuinely collaborative interactions between authors and review editors, who include some of the world's best academicians. Research must be certified by peers before entering a stream of knowledge that may eventually reach the public - and shape society; therefore, Frontiers only applies the most rigorous and unbiased reviews. Frontiers revolutionizes research publishing by freely delivering the most outstanding research, evaluated with no bias from both the academic and social point of view. By applying the most advanced information technologies, Frontiers is catapulting scholarly publishing into a new generation.

What are Frontiers Research Topics?

Frontiers Research Topics are very popular trademarks of the *Frontiers journals series*: they are collections of at least ten articles, all centered on a particular subject. With their unique mix of varied contributions from Original Research to Review Articles, Frontiers Research Topics unify the most influential researchers, the latest key findings and historical advances in a hot research area.

Find out more on how to host your own Frontiers Research Topic or contribute to one as an author by contacting the Frontiers editorial office: frontiersin.org/about/contact

Advanced biomaterials for osteochondral regeneration

Topic editors

Le Yu — Ohio University, United States

Qian Feng — Chongqing University, China

Chen Yang — University of Chinese Academy of Sciences, China

Mei Wei — Ohio University, United States

Citation

Yu, L., Feng, Q., Yang, C., Wei, M., eds. (2023). *Advanced biomaterials for osteochondral regeneration*. Lausanne: Frontiers Media SA.

doi: 10.3389/978-2-83251-198-5

Table of contents

frontiers | Frontiers in Materials

ORIGINAL RESEARCH
published: 02 June 2022
doi: 10.3389/fmats.2022.896516

3D-Printing Assisted SF-SA Based MgP Hybrid Hydrogel Scaffold for Bone Tissue Engineering

*Qiuyi Mao, Bowen Zhu, Hai Zhuang and Shoushan Bu**

Department of Stomatology, First Affiliated Hospital of Nanjing Medical University, Nanjing, China

A new prototype of hybrid silk fibroin and sodium alginate (SF-SA) based osteogenic hydrogel scaffold with a concentration of 2.5% magnesium phosphate (MgP) based gel was prepared with the assistance of an extrusion-based three-dimensional (3D) printing machine in this study. To determine the optimum ratio of MgP-based gel in the hydrogel, a series of physical and biochemical experiments were performed to determine the proper concentration of MgP in two-dimensional hydrogel films, as well as the cell compatibility with these materials in sequence. The SF-SA hydrogel with 2.5wt% magnesium phosphate (SF-SA/MgP) stood out and then was used to fabricate 3D hydrogel scaffolds according to the consequences of the experiments, with SF-SA hydrogel as a control. Then the morphology and osteogenic activity of the scaffolds were further characterized by field emission scanning electron microscope (SEM), calcium mineralization staining, and reverse transcription-polymerase chain reaction (rt-PCR). The SF-SA/MgP hydrogel scaffold promoted the adhesion of rat mesenchymal stem cells with higher degrees of efficiency under dynamic culture conditions. After co-culturing in an osteogenic differentiation medium, cells seeded on SF-SA/MgP hydrogel scaffold were shown to have better performance on osteogenesis in the early stage than the control group. This work illustrates that the 3D structures of hybrid SF-SA/MgP hydrogel are promising headstones for osteogenic tissue engineering.

Keywords: 3D-printing, hydrogel scaffold, silk fibroin, magnesium phosphate, bone tissue engineering

OPEN ACCESS

Edited by:
Chen Yang,
Wenzhou Institute, University of Chinese Academy of Sciences, China

Reviewed by:
Yingji Mao,
Bengbu Medical College, China
Akalabya Bissoyi,
University of Warwick, United Kingdom

****Correspondence:***
Shoushan Bu
bushsh@vip.sina.com

Specialty section:
This article was submitted to Biomaterials, a section of the journal Frontiers in Materials

Received: *21 March 2022*
Accepted: *22 April 2022*
Published: *02 June 2022*

Citation:
Mao Q, Zhu B, Zhuang H and Bu S (2022) 3D-Printing Assisted SF-SA Based MgP Hybrid Hydrogel Scaffold for Bone Tissue Engineering. Front. Mater. 9:896516. doi: 10.3389/fmats.2022.896516

1 INTRODUCTION

The application of additive manufacture (3D printing technology) has revolutionized bone tissue engineering due to its remarkable ability in simulating tissues by producing precise layer-by-layer deposition of bioactive and biocompatible materials (Murphy and Atala, 2014; Markstedt et al., 2015; Daly et al., 2016a; Groll et al., 2016). This advanced technology has helped to establish models of tumor, drug-releasing, and organ grafts since it was first introduced in 1998 (Kim et al., 1998). Key to the successful application of 3D-printing technology in bone tissue engineering is an appropriate selection of ink based on the working mode of the 3D printing machine such as drops inkjet (Saunders and Derby, 2014), micro-valve dispensing (Gudapati et al., 2016), laser-assisted techniques (Sorkio et al., 2018), and continuous micro-extrusion (Ozbolat and Hospodiuk, 2016). As the most frequently used mode used in bone tissue engineering, extrusion-based printing products show excellent performance on versatility, multiple modes of solidification, and towel adaptation in printing complex structures (Ozbolat and Hospodiuk, 2016; Placone and Engler, 2018). An applicable bioactive ink should be well extrudable to prevent blockage and able to produce 3D

structures with high shape fidelity and mechanical stability. An appropriate bioactive ink should also behave like the extracellular matrix: it can protect cells, provide a stable environment, and subsequently promote the functional expression of cells (Parak et al., 2019). Although many investigations have been conducted by other researchers, an applicable single-component hydrogel with multiple features to greatly fit extrusion-based 3D printing machines has not been achieved (Zhang et al., 2014; Pei et al., 2016; Du et al., 2019).

During the process of optimizing cellular function and tissue integration, the bioactivity of bioink is a critical factor as it is crucial to the creation of a microenvironment similar to extracellular matrix (ECM) in bone. The bioactivity of current hydrogel-based bioinks needs to be improved in cell biocompatibility and bioactivity (adhesion and proliferation), hydrophilicity, osteoconductivity, and osteoinductivity (Ma et al., 2018). One promising approach is to blend inorganic bioactive components with organic matrices, which has been widely used in tissue engineering in recent years (Laurenti et al., 2016).

Silk fibroin (SF), natural polymeric fibrin consisting of 18 amino acids (Palcone et al., 2018; Parak et al., 2019) derived from *Bombyx mori* cocoons, has excellent mechanical properties, biocompatibility, and biodegradability (Du et al., 2019). The applications of SF in biomedicine and 3D printing have been extensively reported in recent years (Wang et al., 2008; Cao and Wang, 2009; Jiang et al., 2009; Shi et al., 2017; Zhong et al., 2019). The featured gelation process of the SF solution would take place under specified conditions on account of the conformational transitions during which the SF molecule chain transfers from random coil to β-sheet (Wang et al., 2008). Among those conditions, Polyethylene glycol (PEG) gelated SF hydrogel was successfully applied as an injectable tissue repair material in a recent study (Wang et al., 2015). However, pure SF gelation was shown to lack osteogenic activity *in vivo* (Zhang et al., 2011), and the natural fibroin is difficult to degrade because of its special crystallization and orientation, as well as compact structure (Cao and Wang, 2009).

Sodium alginate, which was extracted from native brown seaweed (Phaeophyceae) and composed of two uronic acids, β (1–4) linked D-mannuronic acid (M) and α (1–4) linked L-guluronic acid (G) (Lee and Mooney, 2012; Venkatesan et al., 2015), was shown to be another prominent biopolymer for the fabrication of hydrogels (de Moraes et al., 2014; Gong et al., 2016). SA has been widely used as a kind of biomaterial for biomedical applications not only because SA regulates the biodegradation of SF (Zheng et al., 2018; Wang et al., 2020) but also because it helps stabilize organization on the surface to maintain inner stability when exposed to calcium chloride (Smrdel et al., 2006).

In this study, we novelty prepared multiple crosslinking hydrogels with inorganic material magnesium phosphate-based gels. Magnesium phosphate is considered a potential solution to promoting the osteogenic activity function of the hydrogel. Indeed, in recent years, magnesium phosphate (Klammert et al., 2011; Mestres and Ginebra, 2011; Babaie et al., 2016; Babaie et al., 2017) has captured more attention as an alternative for bone replacement. As highlighted by Ostrowski et al. (2016) and Nabiyouni et al. (2018), many MgP phases, such as struvite ($MgNH_4PO_46H_2O$) or newberyite ($MgHPO_43H_2O$) have advantages of better solubility and smaller tendency while transforming into lower soluble phases *in vivo* (Tamimi et al., 2011), since Mg^{2+} ions suppress Hydroxyapatite formation by stabilizing gel-like amorphous calcium phosphate phases to inhibit crystal growth (Yang et al., 2011). This inhibition leads to faster resorption and is likely to pronounce bone regeneration capacity, which has already been demonstrated in a couple of studies carried out in small animal models (Kanter et al., 2018). However, a notable weakness of magnesium phosphate as a blended material applied in extrusion-based 3D printing machines is the clogging of particles that may lead to blockage during extrusion. Previous research has proposed a potential solution to overcoming this—the novel thixotropic magnesium phosphate-based gel (TMP-BG) for 3D bioprinting (Laurenti et al., 2016; Chen et al., 2020). TMP-BG was shown to have excellent printability (Chen et al., 2018).

To optimize the performance of the composites, a new type of 3D-print assisted hybrid SF-SA/MgP hydrogel scaffold was prepared in this study. To adequately utilize the advantages of the composites in hydrogel and minimize their shortages simultaneously, formulations were adjusted and MgP concentration was made in different ratios. Next, the mechanical properties, rheological, bioactivity, *in vitro* behaviors, and printability were characterized and optimized. Then living cells were co-cultured with the hybrid hydrogel scaffolds. Their viability and osteogenic differentiation ability in printed constructs were evaluated. The hybrid mechanisms of the hydrogel scaffolds were also explored in this step.

The objective was to find an alternative scaffold with the assistance of 3D printing technology that promotes osteodifferentation in the early stage and matches degradation with new bone deposition. To achieve the goal, a new prototype of hybrid hydrogel consisting of sodium alginate and MgP-based gel in PEG-gelated silk fibroin hydrogel was created to strengthen the mechanical properties of hydrogel and balance the degradation rate with the newly formed tissues. Previous studies have demonstrated that pore size and the 3D spatial structure of the scaffolds are key factors for cell proliferation, differentiation, and extracellular matrix (ECM) production during bone regeneration (Gudapati et al., 2016; Ma et al., 2018). It has been shown that in bone repair, cells prefer scaffolds with pore sizes between 100 and 300 μm for better proliferation, differentiation, and ECM production ability (Ma et al., 2018). Hence, a 3D-printing hydrogel scaffold with macropores around 200 μm was highly preferred in our study.

2 MATERIALS AND METHODS

2.1 Materials

Silk fibroin was used as the fundamental component of the scaffolds. Thixotropic magnesium phosphate-based gel was made of magnesium hydroxide, sodium hydroxide, and phosphoric acid (Huge, Shanghai). The hydrogels were cross-

TABLE 1 | Formulations of SF-SA/MgP hybrid bioinks.

Formulations	Silk Fibroin (%w/v)	Mg (%w/v)	SA (%w/v)	pH
Mg0	5.0	0	0.5	7.75
Mg1	5.0	1.0	0.5	7.58
Mg2.5	5.0	2.5	0.5	7.63
Mg3	5.0	3	0.5	7.70

linked using PEG-400 (Aladdin, Shanghai), sodium alginate (Macklin, Shanghai), and calcium chloride (Huge, Shanghai).

2.2 Experimental Methods

2.2.1 Preparation of the Silk Fibroin and Sodium Alginate and SF-SA/MgP Hydrogel 2D Films

Silk fibroin/sodium alginate solution was made with a mass of 1 g lyophilized silk fibroin protein particles (Simatech, China) in a volume of 10 ml 0.5% sodium alginate solution. The bioactive nano inorganic MgP hydrogel material was made based on a previous report (Chen et al., 2020). Specifically, the molar ratios of $NaOH/H_3PO_4/Mg(OH)_2$ were 2.87/2/1. The solution and MgP-based gel were mixed in different ratios (**Table 1**), and the acquired liquid was termed M0, M1, M2.5, and M3, in which the concentrations of magnesium phosphate were 0%, 1%, 2.5%, and 3%, respectively. Then the different ratios of mixed solution were quickly and intensely stirred to form a homogeneous slurry. The formulations of SF-SA and SF-SA/MgP gels were optimized experimentally based on the gelation properties. We found that the hydrogel would collapse when the concentration of MgP was over 5%. Afterward, an equivalent volume of 80% PEG-400 was added to facilitate the gelation of silk fibroin. The solvent was added to separate wells of a 24-well-plate at a volume sufficient to coat the base of the well before its gelation at 37°C. The 0.2M $CaCl_2$ solution was added to each well to make SA crosslink with Ca^{2+} to obtain a firmer surface before the next step. Then all the wells were washed three times with ddH_2O and PBS in turn to exclude PEG and Cl^- ions and were sterilized by 30 min exposure to UV light in a biological safety cabinet. Plates were either seeded with cells immediately or stored at 4°C until use. Moreover, SF-SA hydrogel was prepared as a control.

2.2.2 Spectroscopic Characterization

Fourier transform infrared (FT-IR) spectroscopy was carried out to have a better understanding of the properties of individual materials. The spectra of Lyophilized SF-SA/MgP hydrogels and SF-SA hydrogel, collected from wavelength 4,000 to 400 cm^{-1} with a resolution of 4 cm^{-1} were analyzed by using an FT-IR spectrometer (IN10, Thermo Scientific).

2.2.3 Rheological Characterization

Rheological measurements were carried out on a Rotational Rheometer (Thermo HAAKE MARS60) at room temperature. The samples were all reached into a state of equilibrium for 60 s before measurement. A parallel plate (35 mm) was used for the four formulated inks, and the shear viscosity was measured at shear rates from 0.01 to 1,000 s^{-1}. A pressure of 10 Pa was chosen for the oscillation frequency measurements conducted at a frequency range of 10^{-1}–10 Hz. The 100s^{-1} shear rate was estimated to be the maximum shear rate experienced by the SF-SA-based hydrogels during the 3D printing process.

2.2.4 *In vitro* Cellular Activities

2.2.4.1 Rat Bone Mesenchymal Stem Cell Isolation and Culture

Rat BMSCs were extracted from the bone marrow of 4-week-old Sprague–Dawley rats (Nanjing Medical University Experimental Animal Center, China). All experiments related to the use of animals were approved by the Institutional Animal Care and Use Committee, following the procedure for Animal Experimental Ethical Inspection of Jiangsu Province Hospital, which is affiliated with Nanjing Medical University. In accordance with previous research (Jiang et al., 2009), the rats were euthanized by the injection of overdosed 10% chloral hydrate. Then the femurs were cut off and separated into pieces at the epiphysis, and the bone marrow was quickly rinsed using PBS supplemented with 2% streptomycin and penicillin. The harvested cells were incubated in Mesenchymal Stem Cell Medium (MSCM) supplemented with 15% FBS, 100 U/mL streptomycin, and 100 U/mL penicillin at 37°C in an atmosphere containing 5% CO_2. The growth medium was refreshed every 3 days.

2.2.4.2 Assessment of Cell Proliferation and Viability

A CCK-8 assay (n = 3) (Cell Proliferation Kit; Dojindo Laboratories, Japan) was conducted to evaluate cell proliferation on hybrid hydrogels and cytotoxicity. For the CCK-8 assay, the cell-seeded hydrogels were incubated in a 24-well plate (5×10^4 cell/well) in Dulbecco's modified eagle's medium (DMEM) supplemented with 10% FBS, 100 U/mL streptomycin and 100 U/mL penicillin while pure BMSCs was set as control. At different time points of co-culture (1, 3, 5, and 7 days) after cell-seeding on the hydrogels, the wells were switched with fresh medium (300 μL) and then the cck-8 solution (30 μL) was added to incubate for 2.5 h. The optical density at 450 nm absorbance was measured by using a microplate reader after a 100 μL volume of supernatant was added to a new 96-well plate.

2.2.4.3 Cell Adhesion and Morphology

The analysis of cell adhesion and morphology on scaffolds was performed by nuclei staining with F-actin with phalloidin (Actin-Tracker Red-594, Beyotime Biotechnology, China) and fixed in Antifade Mounting Medium with DAPI (P0131, Beyotime Biotechnology, China). Specifically, BMSCs (passage 3) seeded on hydrogel films in a 24-well plate (2×10^4 cells/well) were fixed with 4% paraformaldehyde (Biosharp Life Sciences, China) for at least 30 min and washed with PBS on day 3 and day 7. Cytoskeletal actin filaments were stained with FITC-phalloidin at 1/80 dilution (200 T/ml) in PBS and incubated for 1 h at 37°C, followed by three times PBS washing. The nuclei staining was carried out by incubation for 3 min at room temperature with DAPI. The whole staining procedure should be protected from light. Finally, the samples (n = 3) were observed by fluorescence microscopy.

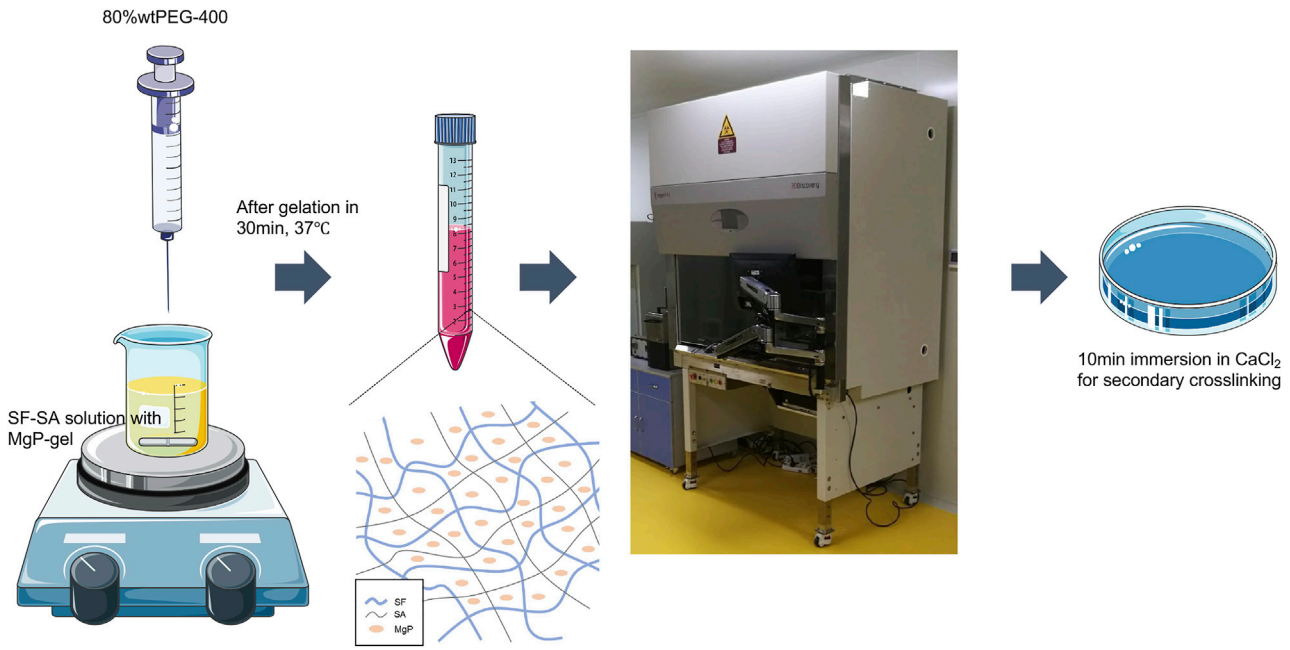

FIGURE 1 | The flow chart is an illustration of how the SF-SA and SF-SA/MgP hydrogel scaffolds were fabricated. The whole process was in a sterilized environment.

2.2.4.4 Alkaline Phosphatase Activity

To measure alkaline phosphatase activity, BMSCs were plated in 24-well culture plates (2×10^4 cells/mL) with osteogenic differentiation medium (ODM). To be detailed, the ODM was a mixture of 100 μM dexamethasone (Sigma-Aldrich), 10 mM β-glycerophosphate (Sigma-Aldrich), and 50 μM ascorbate-2-phosphate (Sigma-Aldrich) with the DMEM medium. To avoid the interference from silk fibroin protein in the extraction of cell proteins, the ODM used in this section was further prepared according to the International Organization for Standardization (ISO)-10993-5. Specifically, hydrogel films were immersed in ODM for 24 h before the extracts of the hydrogel were filtrated for cell culturing. After the cells were cultured in ODM for 7 days, the cells were washed with PBS 3 times before being lysed in 200 μL 0.1% Triton X-100 on ice for 10 min. Afterward, the ALP activity was evaluated colorimetrically with the Alkaline Phosphatase Assay Kit (P0321, Beyotime Biotechnology, China). The optical density (λ = 405 nm) was analyzed by using a microplate reader (SpectraMaxM2e, MD). Staining of ALP enzyme was also performed by a BCIP/NBT alkaline phosphatase color development kit (Beyotime, China) for visualization.

2.2.5 Fabrication of 3D Silk Fibroin and Sodium Alginate and SF-SA/MgP Hydrogel Scaffolds

The selected ratio of SF-SA/MgP was based on the cell proliferation and early osteodifferentiation performance of three hybrid SF-SA/MgP hydrogel films. To fabricate the 3D scaffold with the MgP-based hydrogel bioink, the final chosen concentration of M2.5 (SF-SA/MgP with the concentration of MgP 2.5%wt), and M0 hydrogel (SF-SA) was set as the control group. The fabrication was performed using a 3D printing system (3D Discovery, regenHU, Switzerland), and the whole fabrication process is shown in **Figure 1**. The diameter of the applied single nozzle was 510 μm and the moving speed was set as 6 mm/s, the pneumatic pressure was configured at 100 kPa. When the process of printing was finished, the structures were further cross-linked by immersion in 0.2 M $CaCl_2$ to maintain outside shape and enhance structural stability. At last, the structure was washed with PBS 3 times to exclude PEG and Cl^- ions.

2.2.6 Scanning Electron Microscopy

The morphology of all hydrogel scaffolds was investigated using scanning electron microscopy (MAIA3 TESCAN). All the hydrogel scaffolds were pre-lyophilized and coated with palladium prior to SEM observation.

2.2.7 Analysis of Osteodifferentiation on 3D Hydrogel Structures

Alizarin Red S staining of the scaffolds was carried out to analyze calcium mineralization. The scaffolds were washed twice with PBS and then fixed in 4% paraformaldehyde. After fixing for 30 min, all samples were washed again with PBS 3 times. Then 0.2% Alizarin Red S (Shanghaiyuanye Bio-Technology Co., Ltd., China) was added to react with calcium nodules for 5 min. The stained samples were then rinsed with PBS until the remaining red dye was completely removed. The optical images of the samples were captured by a stereomicroscope. To qualify the calcium mineral density, the obtained optical density (λ = 562 nm) was measured by a microplate reader after the stained samples were lysed with 10% cetylpyridinium chloride (CPC) dissolved in ddH_2O for 1 h.

TABLE 2 | Primer sequences used for this study.

Gene	Primer Pairs	Primer Sequence (5′-3′)
ALP	Forward	aacatcagggacattgacgtg
	Reverse	gtatctcggtttgaagctcttcc
OPN	Forward	atgatggccgaggtgatagt
	Reverse	accattcaactcctcgcttt
OCN	Forward	agcaaaggtgcagcctttgt
	Reverse	gcgcctgggtctcttcact
GAPDH	Forward	gcaccgtcaaggctgagaac
	Reverse	tggtgaagacgccagtgga

A quantitative real-time polymerase chain reaction (RT-PCR) for the BMSCs co-culture with hydrogel scaffolds was conducted on day 7 and day 14, to measure the relative gene expression levels of alkaline phosphatase (ALP), osteocalcin (OCN), and osteopontin (OPN) (Primer sequence showed in **Table 2**). The normalized housekeeping gene was Glyceraldehyde-3-phosphatedehydrogenase (GAPDH). RNA isolation was performed with Takara minibest universal RNA extraction kit and then cDNA was synthesized by PrimeScript RT Master Mix (Perfect Real Time) (Takara, Japan). The RT-PCR was performed by QuantStudio™ 6 and 7 Flex Real-Time PCR Systems (Applied Biosystems, United States) and the TB Green Premix Ex Taq II (Takara, Japan) following the manufacturer's protocols. All reactions were run in quintuplicate for each sample and each gene.

2.3 Statistical Analysis

All obtained data was used processed and analyzed with OriginPro 8 (OriginLab) and Prism 9 (GraphPad) for statistical analyses. ANOVA analysis of variance test was applied in this study based on the number of variables, and comparison between groups was with Turkey test. In all the analyses, $p < 0.05$ was considered statistically significant ($^{*}p < 0.05$, $^{**}p < 0.01$, $^{****}p < 0.0001$).

3 RESULTS

3.1 Scaffold Characterization

Fourier transform infrared (FT-IR) spectroscopy was applied to observe the material properties by analyzing specific absorption peaks to determine the structure of organic compounds in lyophilized SF-SA and SF-SA/MgP particles. As the **Figure 2A** illustrated, all the samples showed specific peaks at 1,634 cm^{-1} (alkyl C-H stretching vibrations), 1,528 cm^{-1}, corresponding to bending vibration of amide nitrogen and hydrogen, and the carbonyl group of carboxy anion after carboxylic acid salt was also peaked near this region, proving the presence of β-sheet in silk fibroin (Kweon et al., 2001). Peaks at 1,460 and 1,353 cm^{-1} corresponded to alkyl C-H bending vibration, 1,249 cm^{-1} to carbon-nitrogen stretching vibration, and 1,103 cm^{-1} to C-O-C stretching vibration. In addition, a broad peak at 3,416 cm^{-1} corresponded to amino and O-H stretching vibration (the area with hydrogen bond was broad), and peaks at 948 cm^{-1} and 840 cm^{-1} were fingerprint areas of organic materials, revealing the presence of $(HPO_4)^{2-}$ (Chen et al., 2018). Overall, with an increased concentration of MgP, the infrared spectra deviation in M1 and M2.5 was not as significant as that in M3, illustrating that the transformation of β-sheet was not obliviously affected by the mixture in M1 and M2.5. In all MgP-added groups, the absorption peak of phosphate between 1,200 and 1,000 cm^{-1} (Vivekanandan et al., 1997; Zhang and Darvell, 2010; Yu et al., 2013) was very weak, presumably overlapped by the ether bond of organic materials.

3.2 Rheological

To determine the effect of MgP made on the rheological property of the hydrogel bioink, M0, M1, M2.5, and M3 were prepared only with PEG gelation. As the results showed in **Figure 2B**, the increasing content of MgP promoted the shear-thinning under a high-speed shear. Notably, the addition of magnesium phosphate increased the static viscosity of the material at the beginning. When the material was subjected to shearing, the shear viscosity of the material with MgP decreased more. Next, as the shear rate increased, this shear thinning effect is further enhanced. The relationship between the storage modulus (G′) and loss modulus (G″) of the four samples is shown in **Figure 2C**. In the frequency ranging from 0.1 to 10 Hz, all samples were basically in line with G′> G″, proving that the material in this frequency range was a viscoelastic solid material. From low frequency to high frequency, the storage modulus change curve of the four materials was stable and slightly increased when the frequency is under 10 Hz. In the dynamic modulus of the four samples, the hydrogels with MgP were higher, and the loss modulus was M2.5 > M1 > M3 > M0 as shown.

3.3 Cell Proliferation and Viability

Figure 3A showed the evolution of the BMSCs proliferation performed by a CCK-8 assay (displayed as mean OD value) over 7 days. The average cell viability in the former three experimental groups was not significantly different from the control group in the first 3 days, suggesting that the chemical compositions of the hydrogels were cytocompatible with BMSCs at an early stage. At the interval time of day 5, the proliferation of BMSC on hydrogel films was slightly lower than in the control group but there was no significant difference among the four experimental groups. On day 7, The proliferation result of M2.5 was superior than other hydrogel groups but was still lower than control. Notably, for groups M0, M1, and M2.5, the lower cell viability in hydrogel films can be explained by the fragile construction of films and the degradation of hydrogels. For M3, however, an overdosed MgP content may be unbeneficial for cell proliferation because of an excessive release of Mg^{2+} or rapid degradation of hydrogel films. Additionally, the successive refreshment of the culture medium through aspiration and the washing procedure may also result in a decrease in the cell number.

In fluorescence microscopy images, the BMSCs adhesion on hydrogel films was the cells seeded on days 3 and 7. The F-actin filaments of the cell cytoskeleton and cell nuclei were stained with phalloidin (red) and DAPI (blue), respectively. **Figures 3B–E**

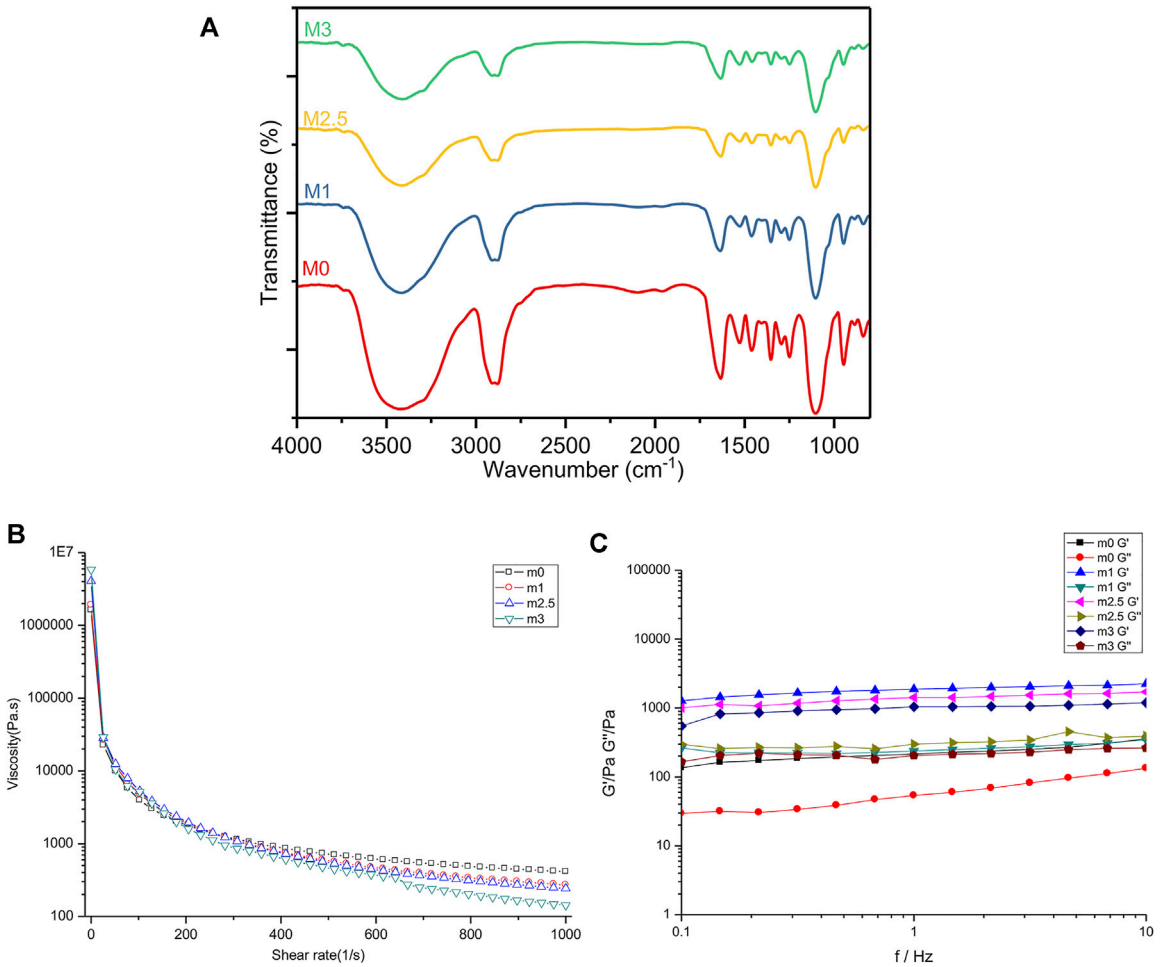

FIGURE 2 | Mechanical characteristics of m0, m1, m2.5, and m3 hydrogels. **(A)** FT-IR spectra of four films after lyophilization. **(B,C)** rheological analyses of four hydrogels before crosslinking with $CaCl_2$. **(B)** flow curves of hybrid bioinks with a shear rate from 0.1% to 100%. **(C)** G′ and G″ of four hydrogels under the mode of frequency sweep ranging from 0.1 to 10 Hz.

confirmed that the cells on the M2.5 and M3 scaffold tended to form cell aggregates and a non-uniform distribution on the films (**Figures 3D,E**), whereas BMSCs seeded on M0 and M1 (**Figures 3B,C**) showed a more homogeneous distribution on day 3. When it comes to day 7, BMCs on four scaffolds (**Figures 3B–E**) all displayed uniform distribution with a high cell density, proving that the surfaces of four kinds of hydrogel films all presented to be positive for cell adhesion and viability.

3.4 Alp Activity

The ALP expression is a key characteristic of osteogenic differentiation in the early stage of cell differentiation, reflecting the ability of osteoblasts to synthesize collagen I and to form a bone matrix (Basdra and Komposch, 1997). On day 7, the cells in a 24-well-plate induced by the extracts of four hydrogels were stained with a BCIP/NBT alkaline phosphatase color development kit. As **Figures 4A–H** showed, the M2.5 and M3 groups had deeper colors than M0 and M1 groups. **Figure 3I** showed the ALP activity on the same plate. The difference in ALP activity between the low content of MgP and high MgP content groups was significant ($p < 0.05$). The ALP activity of the M2.5 was the highest reaching 12.49 U/gprot and M3 reaches to12.20 U/gprot. Both the high content MgP groups were showing significantly higher alp activities than M0 and M1 groups, where the value was only 4.49 U/gprot and 8.54 U/gprot, respectively.

3.5 Scanning Electron Microscope

The stereomicroscope and SEM images of the fabricated SF-SA and SF-SA/MgP scaffolds were shown in **Figure 5A,B**. In stereomicroscope, the surface of SF-SA was smoother and more uniform. On the contrary, in SEM images, the micro-pores of SF-SA/MgP were more homogeneous and evenly distributed, as the average micro-pores diameter was around 57.885 ± 5.341 μm while the pore size in SF-SA ranged from 31.25 to 88.18 μm. The energy spectrum (**Figure 5E–I** of SF-SA/MgP also showed that the elements of Ca, Na, P, and Mg were evenly distributed on the surface of

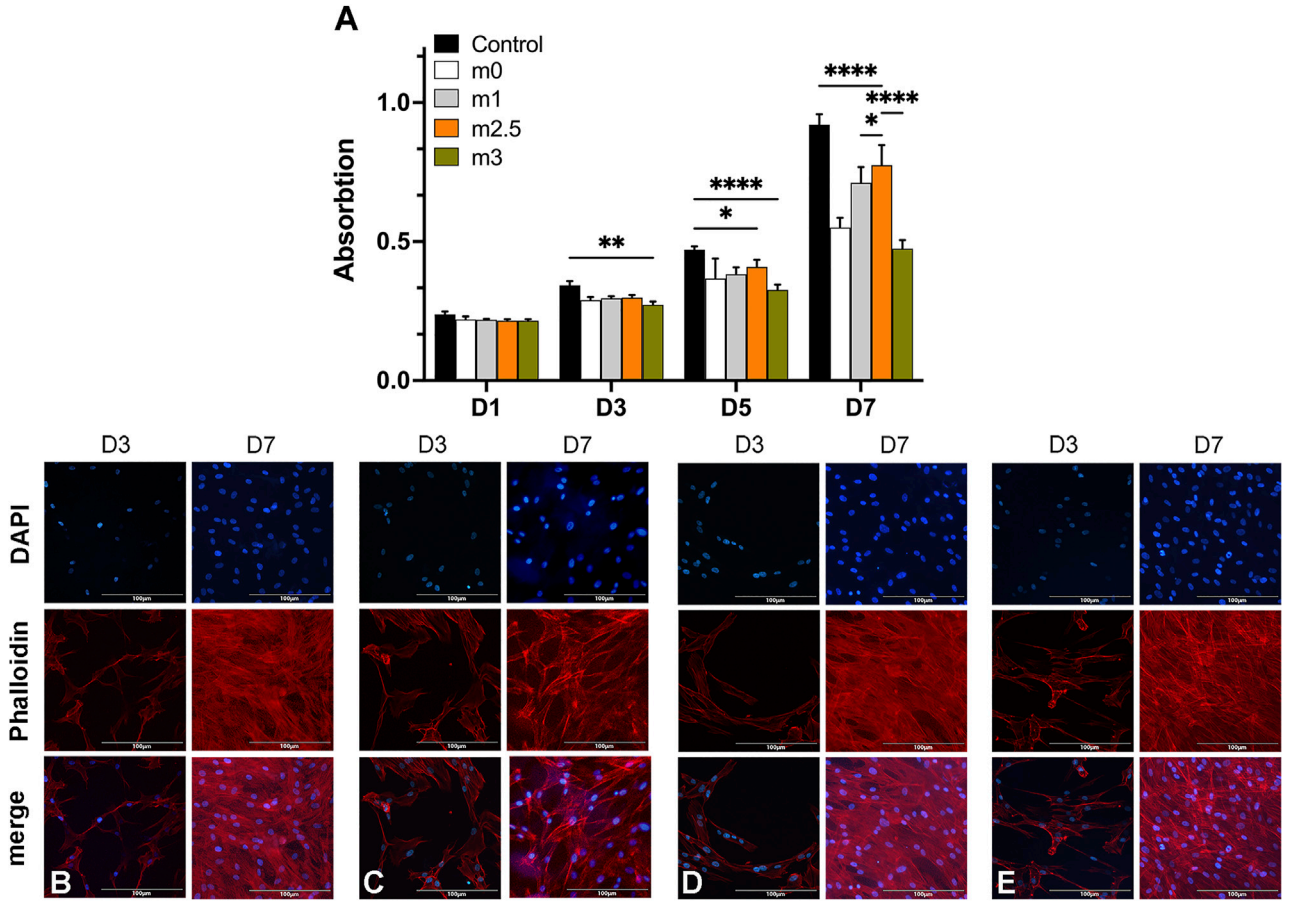

FIGURE 3 | (A) CCK8 assay of BMSCs on 2D hydrogel films at different time intervals (Day 1, 3, 5, and 7). **(B–E)** cells on films stained with DAPI (blue) and phalloidin (red) on day 3 and day 7.

scaffolds, proving that nano MgP particles were homogeneously distributed in the hydrogel scaffold. Moreover, a step-by-step crosslinking process in fabrication maintained its good injectability first during 3D printing, and further prevented the solid-liquid separation after immersion in $CaCl_2$.

3.6 Osteodifferentiation on 3D Hydrogel Structures

Figure 6A demonstrated the results of calcium deposition/mineralization by staining with alizarin red on day 14. As shown in the figure, the color of alizarin red was deeper as a result of the mixture of MgP. The quantification results were illustrated in **Figure 6B** where the OD values of SF-SA/MgP hydrogel were significantly higher, in correspondence with the staining results and previous alp activity analysis. For rt-PCR, **Figures 6C–E** showed the expression level of the osteogenic genes ALP, OCN, and OPN on day 7 and day 14. The gene expression of cells seeded on SF-SA/MgP scaffolds all presented higher levels than on SF-SA scaffolds, indicating that the osteogenic differentiation process of BMSCs on scaffolds was affected by the MgP component.

4 DISCUSSION

In our previous study, we designed an injectable silk-MgP hydrogel for the repair of the defect in bone tissues. However, in follow-up experiments we found that this kind of injectable hydrogel was seriously stuck with the loading plate of the 3D-print machine, making it impossible for a pre-designed scaffold to be fabricated and defect repaired. To overcome this issue, we made improvements by adding a low concentration of sodium alginate, with which we were able to fabricate a hydrogel bioink that can be applied for an extrusion 3D-print system.

In this newly hydrogel bioink, SF was the main component for the fabrication of the scaffold as SF is a natural polymer with excellent biocompatibility that can mimic the function of extracellular materials. There have been many reports on the successful application of SF-made 3D-printed scaffolds (Zhong et al., 2019; Kim et al., 2021a; Kim et al., 2021b).

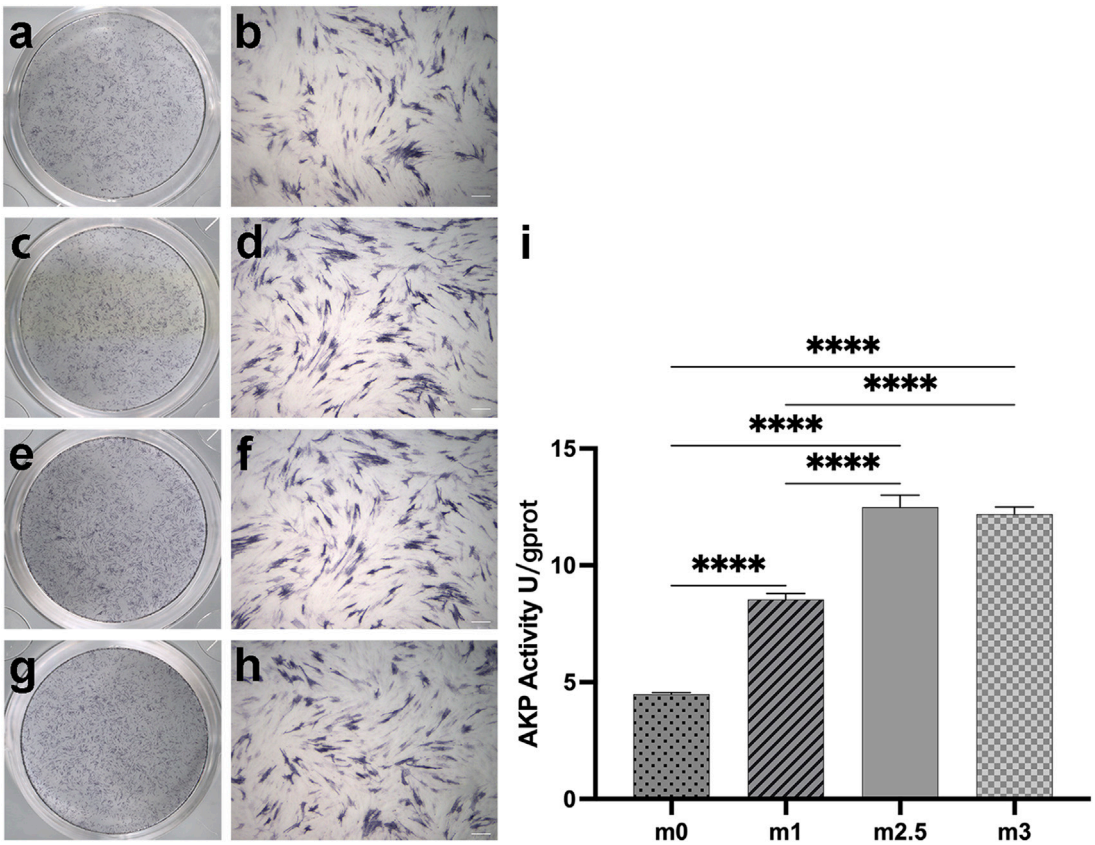

FIGURE 4 | (A–H): alp staining pictures after 7 days of cell culture, M0 **(A,B)**, M1 **(C,D)**, M2.5 **(E,F)**, and M3 **(G,H)** under scanning and 10× microscope. **(I)** the different alp activities in quantitative. Scale bar for 200 μm.

Theoretically, the silk protein can be catalytically hydrolyzed into amino acids under the action of proteolytic enzymes, then those amino acids would be metabolized by the body (Zheng et al., 2018). A recent study also revealed that the addition of sodium alginate can regulate the degradation rate of SF (Wang et al., 2020). The intermolecular covalent bonds and hydrogen bonds of SA macromolecule help SA form an interactive polymer network structure with SF which can affect the amount of silk II in SF hydrogel (Wang et al., 2020). In the following stage, the printed scaffold would be soaked into 0.2 M $CaCl_2$ to further reinforce the scaffold and better maintain its stability (Hua et al., 2010; Hong et al., 2016). The selection of 0.5%wt of SA is based on the fact that the transition of silk fibroin molecular in the follow-up experiments would not be affected while the viscosity of the SF solution was improved in this concentration, which is beneficial for the dispersion of MgP nanoparticles.

A thixotropic magnesium phosphate was also applied in this study in the form of nanoparticles instead of the traditional inorganic MgP particles. Laurenti, et al. were the first research group to study the fabrication and application of magnesium phosphate-based gel in bone repair (Laurenti et al., 2016). The MgP nanoparticles can evenly spread in the solution as a result of the ionization; the positive and negative charges simultaneously present lead to electrostatic and van der Waals interactions (Roth and Lenhoff, 1995). The particles dispersed in the solution, forming a 3D network known as the "house of cards" structure. (Barnes, 1997; Mewis and Wagner, 2009). By applying mechanical forces, thixotropic materials can be liquefied to flow; when the mechanical stress stops, the particles were driven into contact by Brownian motion to reform the 3D network again and the liquid-like dispersion is converted to solid-like gel. (Mewis and Wagner, 2009; Bergaya and Lagaly, 2013).

Generally, the hybrid hydrogel was confirmed to be a satisfying bioink for 3D scaffold production. The FT-IR spectrum of four hydrogel films shared similar structures with no obvious deviation, illustrating that the amount of MgP nanoparticles would not affect the transformation to the β-sheet in the SF solution. The absorption bands at a frequency ranging from 1,620 to 1,640 cm^{-1} and 1,695 to 1700 cm^{-1} corresponded to the functional groups in silk II form (Hu et al., 2006). As **Figure 2A** showed, the peaks at 1,634 cm^{-1} represented the existence of β-sheet structure (Kweon et al., 2001), but the value of transmittances decreased as the amount of the MgP increased.

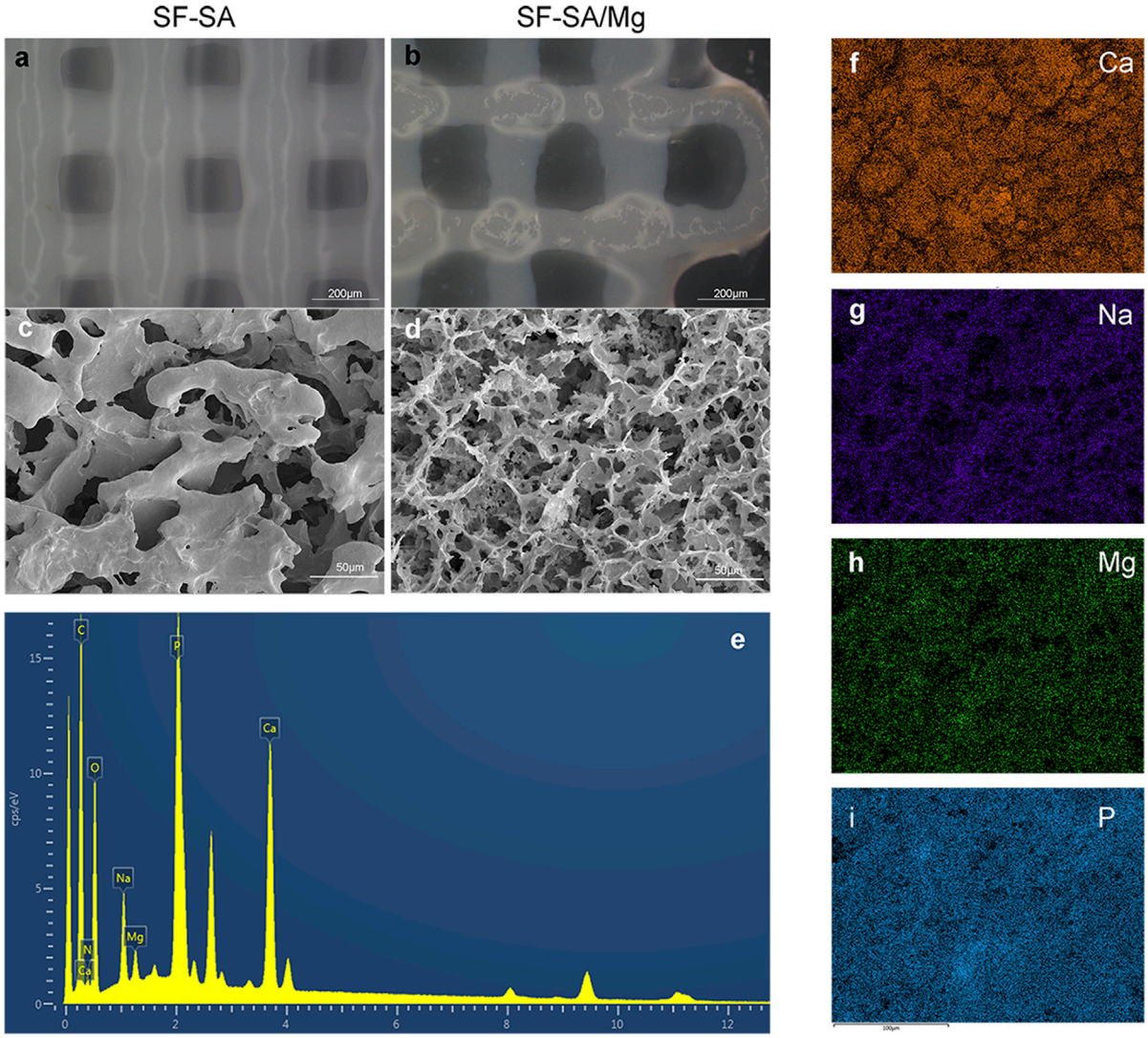

FIGURE 5 | Images of 3D-printed SF-SA **(A)** and SF-SA/MgP **(B)** scaffolds under stereoscopy, SEM images of the surface morphology of SF-SA **(C)** hydrogel and SF-SA/MgP **(D)** scaffolds. **(E–I)**: the surface of EDS of SF-SA/MgP scaffold.

For rheological analysis, an ideal substance for extrusion-based 3D printing should be shear-thinning, thixotropic, easily extruded, and with fine formability (Chung et al., 2013; Schuurman et al., 2013; Ozbolat and Hospodiuk, 2016). The four hydrogels in our study all showed well shear-thinning properties. The G' value was higher than that of G'' in frequency sweep mode in all samples, showing that the G' and G'' were independent of the change in frequency. This result indicated the gel-like behavior and a stable decentralized system of the bio-ink (Malkin et al., 2004).

To study the biocompatibility and bioactivity of the components in the hydrogel, MSCs were first seeded on 2D hydrogel films for cell viability and then incubated with extractions of biomaterials for ALP activity because the hydrogel films would collapse after 5 days due to the swelling of hydrogel. As shown in **Figure 3**, the CCK-8 analysis was in contradiction with the fluorescent staining. The decreased OD value in M3 on day 7 can be explained by the crack of hydrogel and washing with PBS. The extractions of hydrogels contained the releasing of Mg^{2+} with different concentrations; the results of CCK-8 and ALP activity exquisitely reflected the proper concentration of MgP which optimally promoted the osteogenic activity. The results of proliferation analysis and ALP activity were in accordance with a previous study (Wang et al., 2017), which revealed that low Mg^{2+} concentration (i.e., 0.1×10^{-3} M) had an inhibitory effect on the differentiation of

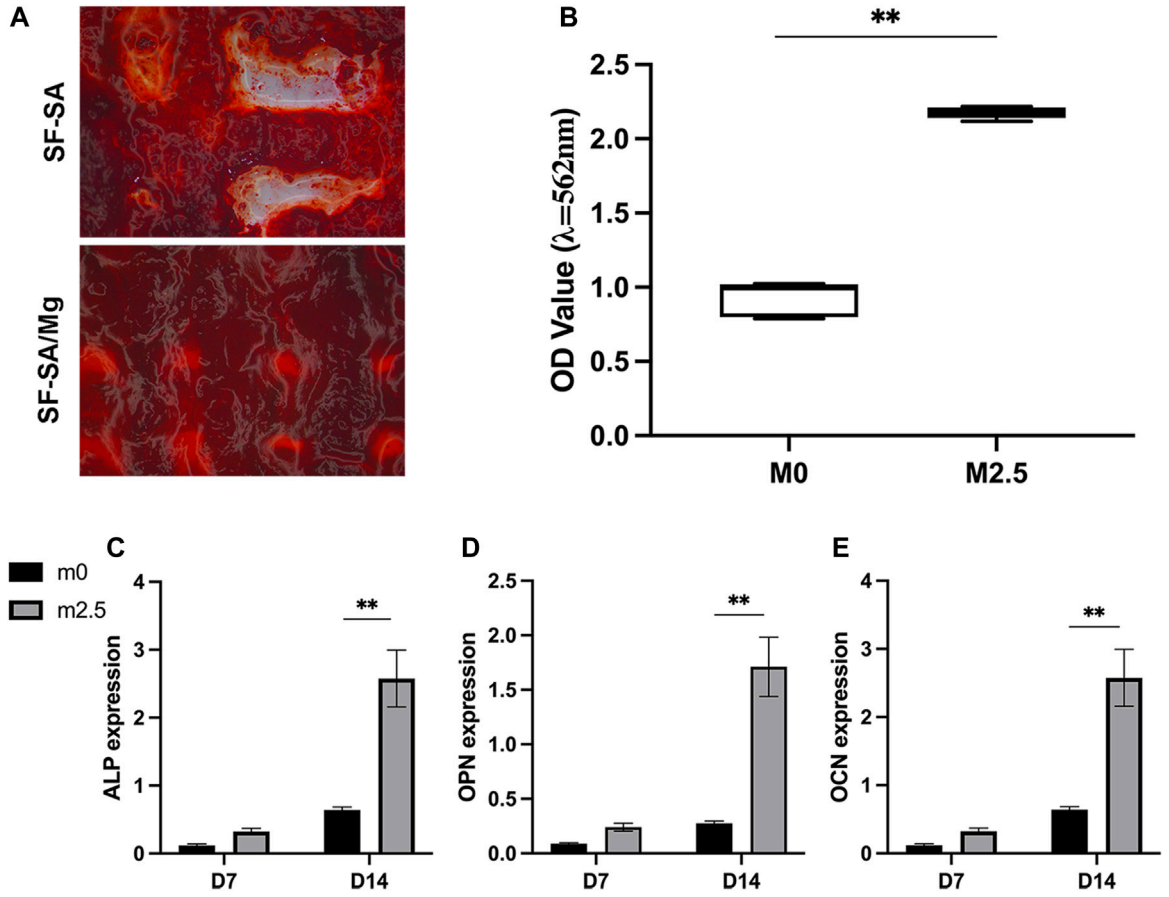

FIGURE 6 | 3D structures of SF-SA and SF-SA/MgP hydrogel scaffolds co-cultured with BMSCs on day 14. Alizarin staining **(A)**, and qualification by 10% CPC **(B)**. ALP, OCN, and OPN expression of each sample on days 7 and 14 **(C–E)**.

osteoblasts while an overdosed Mg^{2+} concentration (i.e., 18×10^{-3} M) was harmful to osseous metabolism (Basdra and Komposch, 1997; Wang et al., 2017).

In the process of the 3D scaffold fabrication, the air pressure was set at 100kPa, far less than the 0.45 MPa as described by Andrew C Daly, et al (Daly et al., 2016b). **Figures 5A,B** showed the shape fidelity and accuracy of the scaffold, reflected by the bar width and smoothness after the 4-layer printing. The SF-SA scaffold had a smoother surface but wider line than the SF-SA/MgP scaffold since SF-SA/MgP bio-ink had better recovery. The diameter of the syringe was finally set at 510 μm because the MgP nanoparticles would clog and block the finer syringe. This may be explained by the uneven gelation of the hydrogel. To overcome this problem, several improvements were proposed, such as the extension of stirring, ultrasonic, and syringe replacement with a conical nozzle. However, no feasible and sustainable solution had been found. Micro morphology of the scaffolds under SEM (**Figure 5C,D**) showed that the micropores of SF-SA/MgP were better for the medium penetration and absorption, as well as cell migration and adhesion. The results also explained why the performance of cell proliferation on M2.5 suppressed the performance on M0 because the M0 film had a smoother surface and more unevenly distributed micropores, making it difficult for cell attachment especially when the cell confluency reached over 80%.

5 CONCLUSION

The combination of MgP-based gel with silk fibroin and a low concentration of sodium alginate has been shown in previous research to be a highly effective hybrid hydrogel for 3D printing. We constructed an SF-SA/MgP hydrogel scaffold for bone tissue engineering with a content of 2.5% MgP. This hydrogel scaffold had good porosity with macro-pores around 200 μm between bars and outstanding biochemical properties that are beneficial to the growth of BMSCs. The mean diameter of micro-pores was 57.885 ± 5.341 μm. Moreover, as a bioactive hydrogel, it positively stimulated the osteogenic activity of cells due to the release of Mg^{2+}. Although the softness of SF-SA/MgP hydrogel can provide a microenvironment similar to ECM to use as cell-loaded bioink, it cannot be applied in force-loading structures like mandibular. The absence of experiments *in vivo* cannot explain the relationship between osteogenesis and degradation in detail.

Overall, this 3D-printing SF-SA/MgP hydrogel provides a potential solution to the bone defect issue and has the potential to be put into practice in future bone tissue engineering.

DATA AVAILABILITY STATEMENT

The datasets presented in this study can be found in online repositories. The names of the repository/repositories and accession number(s) can be found below: https://www.ncbi.nlm.nih.gov/genbank/, MK061162 https://www.ncbi.nlm.nih.gov/genbank/, HQ234608.1 https://www.ncbi.nlm.nih.gov/genbank/, AY663810.1 https://www.ncbi.nlm.nih.gov/genbank/, KY418007.1.

ETHICS STATEMENT

The animal study was reviewed and approved by the Animal Ethical and Welfare Committee of Nanjing Medical University.

AUTHOR CONTRIBUTIONS

QM and SB contributed to the conception and design of the study. QM conducted the experiments mentioned in the manuscript. QM performed the statistical analysis and wrote the first draft of the manuscript. BZ and HZ wrote sections of the manuscript. SB is in charge of proofreading and revising the manuscript. All authors contributed to manuscript revision, read, and approved the submitted version.

FUNDING

The study is kindly funded by the National Natural Science Foundation of China (81670967) and the Jiangsu Provincial Department of Health (H201504).

REFERENCES

Babaie, E., Lin, B., and Bhaduri, S. B. (2017). A New Method to Produce Macroporous Mg-Phosphate Bone Growth Substitutes. *Mater. Sci. Eng. C* 75, 602–609. doi:10.1016/j.msec.2017.02.111

Babaie, E., Lin, B., Goel, V. K., and Bhaduri, S. B. (2016). Evaluation of Amorphous Magnesium Phosphate (AMP) Based Non-Exothermic Orthopedic Cements. *Biomed. Mat.* 11 (5), 055010. doi:10.1088/1748-6041/11/5/055010

Barnes, H. A. (1997). Thixotropy—A Review. *J. Newt. Fluid Mech.* 70 (1), 1–33. doi:10.1016/s0377-0257(97)00004-9

Basdra, E. K., and Komposch, G. (1997). Osteoblast-Like Properties of Human Periodontal Ligament Cells: An *In Vitro* Analysis. *Eur. J. Orthod.* 19 (6), 615–621. doi:10.1093/ejo/19.6.615

Bergaya, F., and Lagaly, G. (2013). *Handbook of Clay Science*. Oxford: Newnes.

Cao, Y., and Wang, B. (2009). Biodegradation of Silk Biomaterials. *Int. J. Mol. Sci.* 10 (4), 1514–1524. doi:10.3390/ijms10041514

Chen, Y., Wang, Y., Yang, Q., Liao, Y., Zhu, B., Zhao, G., et al. (2018). A Novel Thixotropic Magnesium Phosphate-Based Bioink with Excellent Printability for Application in 3D Printing. *J. Mat. Chem. B* 6 (27), 4502–4513. doi:10.1039/c8tb01196f

Chen, Y., Xiong, X., Liu, X., Cui, R., Wang, C., Zhao, G., et al. (2020). 3D Bioprinting of Shear-Thinning Hybrid Bioinks with Excellent Bioactivity Derived from Gellan/Alginate and Thixotropic Magnesium Phosphate-Based Gels. *J. Mat. Chem. B* 8 (25), 5500–5514. doi:10.1039/d0tb00060d

Chung, J. H. Y., Naficy, S., Yue, Z., Kapsa, R., Quigley, A., Moulton, S. E., et al. (2013). Bio-ink Properties and Printability for Extrusion Printing Living Cells. *Biomater. Sci.* 1 (7), 763–773. doi:10.1039/c3bm00012e

Daly, A. C., Critchley, S. E., Rencsok, E. M., and Kelly, D. J. (2016). A Comparison of Different Bioinks for 3D Bioprinting of Fibrocartilage and Hyaline Cartilage. *Biofabrication* 8 (4), 045002. doi:10.1088/1758-5090/8/4/045002

Daly, A. C., Cunniffe, G. M., Sathy, B. N., Jeon, O., Alsberg, E., and Kelly, D. J. (2016). 3D Bioprinting of Developmentally Inspired Templates for Whole Bone Organ Engineering. *Adv. Healthc. Mat.* 5 (18), 2353–2362. doi:10.1002/adhm.201600182

de Moraes, M. A., Silva, M. F., Weska, R. F., and Beppu, M. M. (2014). Silk Fibroin and Sodium Alginate Blend: Miscibility and Physical Characteristics. *Mater. Sci. Eng. C* 40, 85–91. doi:10.1016/j.msec.2014.03.047

Du, X., Wei, D., Huang, L., Zhu, M., Zhang, Y., and Zhu, Y. (2019). 3D Printing of Mesoporous Bioactive Glass/Silk Fibroin Composite Scaffolds for Bone Tissue Engineering. *Mater. Sci. Eng. C* 103, 109731. doi:10.1016/j.msec.2019.05.016

Gong, X., Branford-White, C., Tao, L., Li, S., Quan, J., Nie, H., et al. (2016). Preparation and Characterization of a Novel Sodium Alginate Incorporated Self-Assembled Fmoc-FF Composite Hydrogel. *Mater. Sci. Eng. C* 58, 478–486. doi:10.1016/j.msec.2015.08.059

Groll, J., Boland, T., Blunk, T., Burdick, J. A., Cho, D.-W., Dalton, P. D., et al. (2016). Biofabrication: Reappraising the Definition of an Evolving Field. *Biofabrication* 8 (1), 013001. doi:10.1088/1758-5090/8/1/013001

Gudapati, H., Dey, M., and Ozbolat, I. (2016). A Comprehensive Review on Droplet-Based Bioprinting: Past, Present and Future. *Biomaterials* 102, 20–42. doi:10.1016/j.biomaterials.2016.06.012

Hong, S. H., Shin, M., Lee, J., Ryu, J. H., Lee, S., Yang, J. W., et al. (2016). STAPLE: Stable Alginate Gel Prepared by Linkage Exchange from Ionic to Covalent Bonds. *Adv. Healthc. Mat.* 5 (1), 75–79. doi:10.1002/adhm.201400833

Hu, X., Kaplan, D., and Cebe, P. (2006). Determining Beta-Sheet Crystallinity in Fibrous Proteins by Thermal Analysis and Infrared Spectroscopy. *Macromolecules* 39 (18), 6161–6170. doi:10.1021/ma0610109

Hua, S., Ma, H., Li, X., Yang, H., and Wang, A. (2010). pH-Sensitive Sodium Alginate/Poly(Vinyl Alcohol) Hydrogel Beads Prepared by Combined Ca2+ Crosslinking and Freeze-Thawing Cycles for Controlled Release of Diclofenac Sodium. *Int. J. Biol. Macromol.* 46 (5), 517–523. doi:10.1016/j.ijbiomac.2010.03.004

Jiang, X., Zhao, J., Wang, S., Sun, X., Zhang, X., Chen, J., et al. (2009). Mandibular Repair in Rats with Premineralized Silk Scaffolds and BMP-2-Modified bMSCs. *Biomaterials* 30 (27), 4522–4532. doi:10.1016/j.biomaterials.2009.05.021

Kanter, B., Vikman, A., Brückner, T., Schamel, M., Gbureck, U., and Ignatius, A. (2018). Bone Regeneration Capacity of Magnesium Phosphate Cements in a Large Animal Model. *Acta Biomater.* 69, 352–361. doi:10.1016/j.actbio.2018.01.035

Kim, E., Seok, J. M., Bae, S. B., Park, S. A., and Park, W. H. (2021). Silk Fibroin Enhances Cytocompatibilty and Dimensional Stability of Alginate Hydrogels for Light-Based Three-Dimensional Bioprinting. *Biomacromolecules* 22 (5), 1921–1931. doi:10.1021/acs.biomac.1c00034

Kim, S. H., Hong, H., Ajiteru, O., Sultan, M. T., Lee, Y. J., Lee, J. S., et al. (2021). 3D Bioprinted Silk Fibroin Hydrogels for Tissue Engineering. *Nat. Protoc.* 16 (12), 5484–5532. doi:10.1038/s41596-021-00622-1

Kim, S. S., Utsunomiya, H., Koski, J. A., Wu, B. M., Cima, M. J., Sohn, J., et al. (1998). Survival and Function of Hepatocytes on a Novel Three-Dimensional Synthetic Biodegradable Polymer Scaffold with an Intrinsic Network of Channels. *Ann. Surg.* 228 (1), 8–13. doi:10.1097/00000658-199807000-00002

Klammert, U., Ignatius, A., Wolfram, U., Reuther, T., and Gbureck, U. (2011). *In Vivo* degradation of Low Temperature Calcium and Magnesium Phosphate Ceramics in a Heterotopic Model. *Acta Biomater.* 7 (9), 3469–3475. doi:10.1016/j.actbio.2011.05.022

Kweon, H., Ha, H. C., Um, I. C., and Park, Y. H. (2001). Physical Properties of Silk Fibroin/Chitosan Blend Films. *J. Appl. Polym. Sci.* 80 (7), 928–934. doi:10.1002/app.1172

Laurenti, M., Al Subaie, A., Abdallah, M.-N., Cortes, A. R. G., Ackerman, J. L., Vali, H., et al. (2016). Two-Dimensional Magnesium Phosphate Nanosheets Form

Highly Thixotropic Gels that Up-Regulate Bone Formation. *Nano Lett.* 16 (8), 4779–4787. doi:10.1021/acs.nanolett.6b00636

Lee, K. Y., and Mooney, D. J. (2012). Alginate: Properties and Biomedical Applications. *Prog. Polym. Sci.* 37 (1), 106–126. doi:10.1016/j.progpolymsci.2011.06.003

Ma, H., Feng, C., Chang, J., and Wu, C. (2018). 3D-Printed Bioceramic Scaffolds: From Bone Tissue Engineering to Tumor Therapy. *Acta Biomater.* 79, 37–59. doi:10.1016/j.actbio.2018.08.026

Malkin, A. Y., Masalova, I., Slatter, P., and Wilson, K. (2004). Effect of Droplet Size on the Rheological Properties of Highly-Concentrated w/o Emulsions. *Rheol. Acta* 43 (6), 584–591. doi:10.1007/s00397-003-0347-2

Markstedt, K., Mantas, A., Tournier, I., Martínez Ávila, H., Hägg, D., and Gatenholm, P. (2015). 3D Bioprinting Human Chondrocytes with Nanocellulose-Alginate Bioink for Cartilage Tissue Engineering Applications. *Biomacromolecules* 16 (5), 1489–1496. doi:10.1021/acs.biomac.5b00188

Mestres, G., and Ginebra, M.-P. (2011). Novel Magnesium Phosphate Cements with High Early Strength and Antibacterial Properties. *Acta Biomater.* 7 (4), 1853–1861. doi:10.1016/j.actbio.2010.12.008

Mewis, J., and Wagner, N. J. (2009). Thixotropy. *Adv. Colloid Interface Sci.* 147-148, 214–227. doi:10.1016/j.cis.2008.09.005

Murphy, S. V., and Atala, A. (2014). 3D Bioprinting of Tissues and Organs. *Nat. Biotechnol.* 32 (8), 773–785. doi:10.1038/nbt.2958

Nabiyouni, M., Brückner, T., Zhou, H., Gbureck, U., and Bhaduri, S. B. (2018). Magnesium-Based Bioceramics in Orthopedic Applications. *Acta Biomater.* 66, 23–43. doi:10.1016/j.actbio.2017.11.033

Ostrowski, N., Roy, A., and Kumta, P. N. (2016). Magnesium Phosphate Cement Systems for Hard Tissue Applications: A Review. *ACS Biomater. Sci. Eng.* 2 (7), 1067–1083. doi:10.1021/acsbiomaterials.6b00056

Ozbolat, I. T., and Hospodiuk, M. (2016). Current Advances and Future Perspectives in Extrusion-Based Bioprinting. *Biomaterials* 76, 321–343. doi:10.1016/j.biomaterials.2015.10.076

Parak, A., Pradeep, P., du Toit, L. C., Kumar, P., Choonara, Y. E., and Pillay, V. (2019). Functionalizing Bioinks for 3D Bioprinting Applications. *Drug Discov. Today* 24 (1), 198–205. doi:10.1016/j.drudis.2018.09.012

Pei, P., Qi, X., Du, X., Zhu, M., Zhao, S., and Zhu, Y. (2016). Three-Dimensional Printing of Tricalcium Silicate/Mesoporous Bioactive Glass Cement Scaffolds for Bone Regeneration. *J. Mat. Chem. B* 4 (46), 7452–7463. doi:10.1039/c6tb02055k

Placone, J. K., and Engler, A. J. (2018). Recent Advances in Extrusion-Based 3D Printing for Biomedical Applications. *Adv. Healthc. Mater* 7 (8), e1701161. doi:10.1002/adhm.201701161

Roth, C. M., and Lenhoff, A. M. (1995). Electrostatic and van der Waals Contributions to Protein Adsorption: Comparison of Theory and Experiment. *Langmuir* 11 (9), 3500–3509. doi:10.1021/la00009a036

Saunders, R. E., and Derby, B. (2014). Inkjet Printing Biomaterials for Tissue Engineering: Bioprinting. *Int. Mater. Rev.* 59 (8), 430–448. doi:10.1179/1743280414y.0000000040

Schuurman, W., Levett, P. A., Pot, M. W., van Weeren, P. R., Dhert, W. J. A., Hutmacher, D. W., et al. (2013). Gelatin-methacrylamide Hydrogels as Potential Biomaterials for Fabrication of Tissue-Engineered Cartilage Constructs. *Macromol. Biosci.* 13 (5), 551–561. doi:10.1002/mabi.201200471

Shi, W., Sun, M., Hu, X., Ren, B., Cheng, J., Li, C., et al. (2017). Structurally and Functionally Optimized Silk-Fibroin-Gelatin Scaffold Using 3D Printing to Repair Cartilage Injury *In Vitro* and *In Vivo*. *Adv. Mater* 29 (29), 1701089. doi:10.1002/adma.201701089

Smrdel, P., Bogataj, M., Podlogar, F., Planinšek, O., Zajc, N., Mazaj, M., et al. (2006). Characterization of Calcium Alginate Beads Containing Structurally Similar Drugs. *Drug Dev. Industrial Pharm.* 32 (5), 623–633. doi:10.1080/03639040600599863

Sorkio, A., Koch, L., Koivusalo, L., Deiwick, A., Miettinen, S., Chichkov, B., et al. (2018). Human Stem Cell Based Corneal Tissue Mimicking Structures Using Laser-Assisted 3D Bioprinting and Functional Bioinks. *Biomaterials* 171, 57–71. doi:10.1016/j.biomaterials.2018.04.034

Tamimi, F., Nihouannen, D. L., Bassett, D. C., Ibasco, S., Gbureck, U., Knowles, J., et al. (2011). Biocompatibility of Magnesium Phosphate Minerals and Their Stability under Physiological Conditions. *Acta Biomater.* 7 (6), 2678–2685. doi:10.1016/j.actbio.2011.02.007

Venkatesan, J., Bhatnagar, I., Manivasagan, P., Kang, K.-H., and Kim, S.-K. (2015). Alginate Composites for Bone Tissue Engineering: A Review. *Int. J. Biol. Macromol.* 72, 269–281. doi:10.1016/j.ijbiomac.2014.07.008

Vivekanandan, K., Selvasekarapandian, S., Kolandaivel, P., Sebastian, M. T., and Suma, S. (1997). Raman and FT-IR Spectroscopic Characterisation of Flux Grown KTiOPO4 and KRbTiOPO4 Non-Linear Optical Crystals. *Mater. Chem. Phys.* 49 (3), 204–210. doi:10.1016/s0254-0584(97)80165-4

Wang, J., Ma, X.-Y., Feng, Y.-F., Ma, Z.-S., Ma, T.-C., Zhang, Y., et al. (2017). Magnesium Ions Promote the Biological Behaviour of Rat Calvarial Osteoblasts by Activating the PI3K/Akt Signalling Pathway. *Biol. Trace Elem. Res.* 179 (2), 284–293. doi:10.1007/s12011-017-0948-8

Wang, X., Kluge, J. A., Leisk, G. G., and Kaplan, D. L. (2008). Sonication-Induced Gelation of Silk Fibroin for Cell Encapsulation. *Biomaterials* 29 (8), 1054–1064. doi:10.1016/j.biomaterials.2007.11.003

Wang, X., Partlow, B., Liu, J., Zheng, Z., Su, B., Wang, Y., et al. (2015). Injectable Silk-Polyethylene Glycol Hydrogels. *Acta Biomater.* 12, 51–61. doi:10.1016/j.actbio.2014.10.027

Wang, Y., Fan, S., Li, Y., Niu, C., Li, X., Guo, Y., et al. (2020). Silk Fibroin/Sodium Alginate Composite Porous Materials with Controllable Degradation. *Int. J. Biol. Macromol.* 150, 1314–1322. doi:10.1016/j.ijbiomac.2019.10.141

Yang, X., Xie, B., Wang, L., Qin, Y., Henneman, Z. J., and Nancollas, G. H. (2011). Influence of Magnesium Ions and Amino Acids on the Nucleation and Growth of Hydroxyapatite. *CrystEngComm* 13 (4), 1153–1158. doi:10.1039/c0ce00470g

Yu, H., Deng, D., Li, Y., Xu, S., Li, Y., Yu, C., et al. (2013). Electronic Structure and Luminescent Properties of Ca5(PO4)2(SiO4):Eu2+ Green-Emitting Phosphor for white Light Emitting Diodes. *Opt. Commun.* 289, 103–108. doi:10.1016/j.optcom.2012.09.069

Zhang, H., and Darvell, B. W. (2010). Synthesis and Characterization of Hydroxyapatite Whiskers by Hydrothermal Homogeneous Precipitation Using Acetamide. *Acta Biomater.* 6 (8), 3216–3222. doi:10.1016/j.actbio.2010.02.011

Zhang, J., Zhao, S., Zhu, Y., Huang, Y., Zhu, M., Tao, C., et al. (2014). Three-Dimensional Printing of Strontium-Containing Mesoporous Bioactive Glass Scaffolds for Bone Regeneration. *Acta Biomater.* 10 (5), 2269–2281. doi:10.1016/j.actbio.2014.01.001

Zhang, W., Wang, X., Wang, S., Zhao, J., Xu, L., Zhu, C., et al. (2011). The Use of Injectable Sonication-Induced Silk Hydrogel for VEGF165 and BMP-2 Delivery for Elevation of the Maxillary Sinus Floor. *Biomaterials* 32 (35), 9415–9424. doi:10.1016/j.biomaterials.2011.08.047

Zheng, A., Cao, L., Liu, Y., Wu, J., Zeng, D., Hu, L., et al. (2018). Biocompatible Silk/Calcium Silicate/Sodium Alginate Composite Scaffolds for Bone Tissue Engineering. *Carbohydr. Polym.* 199, 244–255. doi:10.1016/j.carbpol.2018.06.093

Zhong, N., Dong, T., Chen, Z., Guo, Y., Shao, Z., and Zhao, X. (2019). A Novel 3D-Printed Silk Fibroin-Based Scaffold Facilitates Tracheal Epithelium Proliferation *In Vitro*. *J. Biomater. Appl.* 34 (1), 3–11. doi:10.1177/0885328219845092

Conflict of Interest: The authors declare that the research was conducted in the absence of any commercial or financial relationships that could be construed as a potential conflict of interest.

Publisher's Note: All claims expressed in this article are solely those of the authors and do not necessarily represent those of their affiliated organizations, or those of the publisher, the editors, and the reviewers. Any product that may be evaluated in this article, or claim that may be made by its manufacturer, is not guaranteed or endorsed by the publisher.

frontiers | Frontiers in Bioengineering and Biotechnology

ORIGINAL RESEARCH
published: 08 June 2022
doi: 10.3389/fbioe.2022.915181

VEGF-Loaded Heparinised Gelatine-Hydroxyapatite-Tricalcium Phosphate Scaffold Accelerates Bone Regeneration *via* Enhancing Osteogenesis-Angiogenesis Coupling

Xu Chen[1,2†], Chun-Yan Gao[1†], Xiao-Yang Chu[3], Chun-Yan Zheng[1], Ying-Yi Luan[4], Xin He[1], Kai Yang[4] and Dong-Liang Zhang[1]**

[1]Department of Orthodontics, Beijing Stomatological Hospital, Capital Medical University School of Stomatology, Capital Medical University, Beijing, China, [2]Department of Stomatology, Eighth Medical Center of Chinese PLA General Hospital, Beijing, China, [3]Department of Stomatology, Fifth Medical Center of Chinese PLA General Hospital, Beijing, China, [4]Prenatal Diagnosis Center, Beijing Obstetrics and Gynecology Hospital, Capital Medical University, Beijing, China

Background: Bone tissue defect, one of the common orthopaedicdiseases, is traumatizing and affects patient's lifestyle. Although autologous and xenograft bone transplantations are performed in bone tissue engineering, clinical development of bone transplantation is limited because ofvarious factors, such as varying degrees of immune rejection, lack of bone sources, and secondary damage to bone harvesting.

Methods: We synthesised a heparinised gelatine-hydroxyapatite-tricalcium phosphate (HG-HA-TCP) scaffold loaded with sustained-release vascular endothelial growth factor (VEGF) analysed their structure, mechanical properties, and biocompatibility. Additionally, the effects of HG-HA-TCP (VEGF) scaffolds on osteogenic differentiation and vascularisation of stem cells from human exfoliated deciduous teeth (SHED) *in vitro* and bone regeneration *in vivo* were investigated.

Results: HG-HA-TCP scaffold possessed good pore structure, mechanical properties, and biocompatibility. HG-HA-TCP scaffold loaded with VEGF could effectively promote SHED proliferation, migration, and adhesion. Moreover, HG-HA-TCP (VEGF) scaffold increased the expression of osteogenesis- and angiogenesis-related genes and promoted osteogenic differentiation and vascularisation in cells. *In vivo* results demonstrated that VEGF-loaded HG-HA-TCP scaffold improved new bone regeneration and enhanced bone mineral density, revealed byhistological, micro-CT and histochemical straining analyses. Osteogenic and angiogenic abilities of the three biological scaffolds wereranked as follows: HG-HA-TCP (VEGF) > G-HA-TCP (VEGF) > G-HA-TCP.

Abbreviations: ALP, alkaline phosphatase; BMD, bone mineral density; BSP, bone salivary protein; BV/TV, bone volume/total volume; CCK-8, cell counting kit-8; H&E, haematoxylin eosin; GAPDH, glyceraldehyde-3-phosphate dehydrogenase; HG-HA-TCP, heparinised gelatin-hydroxyapatite-tricalcium phosphate; OCN, osteogenesis-related gene osteocalcin; OSX, osterix; qRT-PCR, quantitative real time polymerase chain reaction; RUNX2, runt-related transcription factor 2; SHED, stem cells fromhuman exfoliated deciduous teeth; VEGF, vascular endothelial growth factor.

OPEN ACCESS

Edited by:
Chen Yang,
University of Chinese Academy of Sciences, China

Reviewed by:
Long Bai,
East China University of Science and Technology, China
Yingji Mao,
Bengbu Medical College, China

***Correspondence:**
Dong-Liang Zhang
zhangdongliang@mail.ccmu.edu.cn
Kai Yang
yk19830919@ccmu.edu.cn

†These authors have contributed equally to this work

Specialty section:
This article was submitted to Biomaterials, a section of the journal Frontiers in Bioengineering and Biotechnology

Received: 07 April 2022
Accepted: 06 May 2022
Published: 08 June 2022

Citation:
Chen X, Gao C-Y, Chu X-Y, Zheng C-Y, Luan Y-Y, He X, Yang K and Zhang D-L (2022) VEGF-Loaded Heparinised Gelatine-Hydroxyapatite-Tricalcium Phosphate Scaffold Accelerates Bone Regeneration via Enhancing Osteogenesis-Angiogenesis Coupling. Front. Bioeng. Biotechnol. 10:915181. doi: 10.3389/fbioe.2022.915181

Conclusion: HG-HA-TCP (VEGF) scaffold with good biocompatibility could create an encouraging osteogenic microenvironment that could accelerate vessel formation and osteogenesis, providing an effective scaffold for bone tissue engineering and developing new clinical treatment strategies for bone tissue defects.

Keywords: heparin, VEGF, gelatine, hydroxyapatite, tricalcium phosphate, bone regeneration

HIGHLIGHTS

- HG-HA-TCP scaffold had good pore structure, mechanical properties, and biocompatibility.
- VEGF-loaded HG-HA-TCP scaffold could effectively promote SHED proliferation, migration, and adhesion.
- VEGF-loaded HG-HA-TCP scaffold could effectively promote osteogenic differentiation and vascularisation.
- VEGF-loaded HG-HA-TCP scaffold improved new bone regeneration and enhanced bone mineral density.

INTRODUCTION

Bone tissue defect, a common orthopaedic disease, is primarilycaused by trauma, developmental deformity, revision surgery, osteomyelitis. It causesgreat pain (Zhu et al., 2022). The most common solution for bone defect restoration is to gain bone mass through transplantation of bone tissue engineering scaffolds, which are commonly considered autologous bones and xenografts (Zizzari et al., 2016). However, an autologous bone graft is limited in source, prone to infection in the donor site, and involvescomplicated surgical procedures, causing considerable limitations to its development. At this stage, the application of autologous bone grafts cannot provide satisfactory results for bone defect repair (Fillingham and Jacobs, 2016).

On the other hand, an allogeneic bone graft has structural properties similar to autologous bone and is easy to obtain and process, yet it risks immune rejection and infection (Wu et al., 2021). Therefore, researchand development of alternative pathways for bone defect repair have been a hotspot for research. Bone tissue engineering emerged, and synthetic biomaterials have also been widely studied and applied to solve the problem of bone defect repair (Wang et al., 2019).

Bone tissue engineering is a discipline that couples cell biology with material science to construct tissues or organs *in vitro* and *in vivo*, with three elements of seed cells, biomaterials, and biological factors (Marolt et al., 2010; Roddy et al., 2018). An optimal bone biomaterial should possess satisfactory mechanical properties, excellent biocompatibility and degrade at a moderate rate to match bone regeneration, which is crucial to bone defect repair (Mistry and Mikos, 2005). All artificial bone materials have evolved and refined, including glass ceramics, metals, and organic polymers (Dorozhkin, 2010). Since it is difficult for a single scaffold material to meet the material requirement of bone tissue engineering, two or more scaffold materials are often used after compounding (Gu et al., 2022). Tricalcium phosphate (TCP) and hydroxyapatite (HA) are important components of human bones and are extensively studied in artificial bone materials (Konovalenko et al., 2021). Gelatine (G) is a soluble collagen substitute with the advantages of low antigenicity, easy use, and low price; it is widely used in bone tissue engineering (Salehi et al., 2018). A previous study indicated that HA crystals could increase the strength of collagen, which could also enhance the toughness of HA crystals (Wolters et al., 2017). In our previous study, a G-HA-TCP composite scaffold was constructed, and it was confirmed by *in vitro* experiments that it could induce fine osteogenesis of human dental pulp stem cells (SHED) (Gu et al., 2018).

Bone tissue is highly vascularised; itsrenewal involvesinteraction between osteogenesis and angiogenesis, further leading to bone formation and tissue repair (Clark et al., 2015). Bone regeneration depends on successful angiogenesis, which is highly related toselecting tissue-engineered grafts (Novosel et al., 2011; Diomede et al., 2020). An optimal scaffold should ensure the development of a vascular network, providing a positive and appropriate microenvironment fortissue engineering and renewal (Martino et al., 2015). A wide range of growth factors can promote the vascularisation of seed cells and bone tissue material complexes. Among them, vascular endothelial growth factor (VEGF), also an angiogenesis factor, has the most potent ability to rebuild blood vessels and is often used in combination with scaffolds to improve osteogenic efficiency (Zha et al., 2021). *In vivo*, VEGF can be reserved in the natural extracellular matrix by its interactionwith sulphated glycosaminoglycans (such as heparin or heparan sulphate), and many studies mimicked the *in vivo* situation by complexing the scaffold with heparin to maintain the biological activity of VEGF while controlling itsrelease (Claassen et al., 2017).

However, whether VEGF-loaded heparinised G-HA-TCP (HG-HA-TCP) scaffold could regulate osteogenesis-angiogenesis coupling and bone regeneration has not been studied before. Previous research of our group found that G-HA-TCP could induce the osteogenic differentiation of SHED *in vitro*, which laid the foundation for present research. In the current study, we fabricated an HG-HA-TCP scaffold, and the physical properties, biocompatibility, and osteogenic properties after loading with VEGF were further observed and studied.

MATERIALS AND METHODS

The schematic diagram of whole process of the experiments was demonstrated in **Figure 1**.

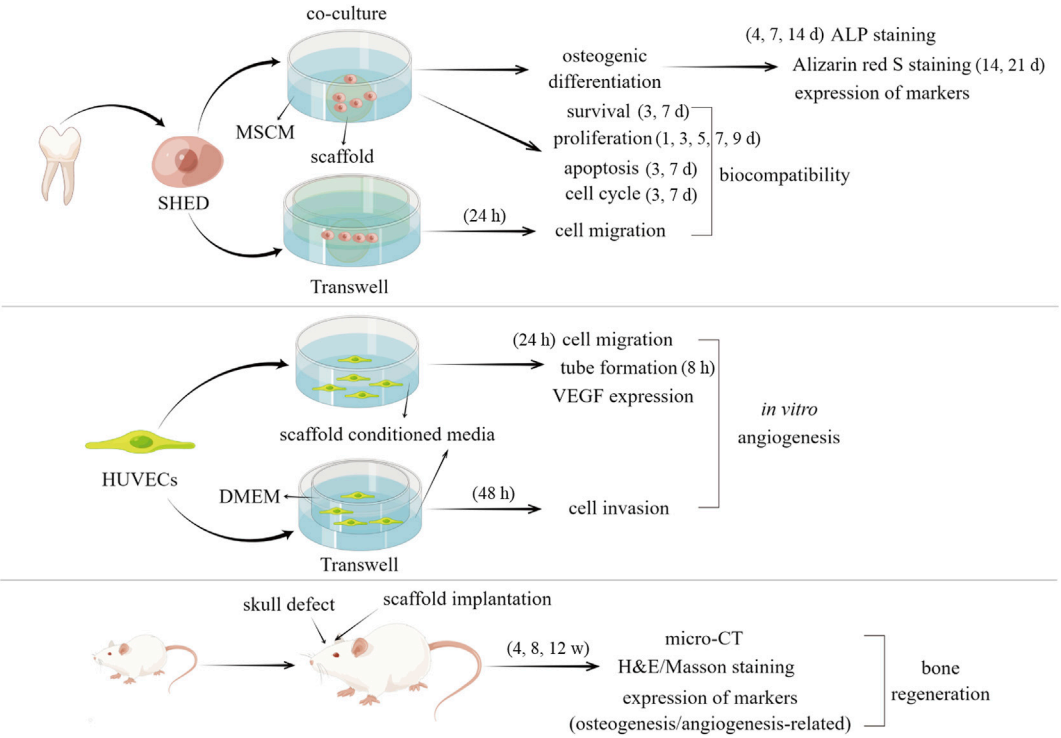

FIGURE 1 | Diagram of the whole process of this study.

Synthesis of G-HA-TCP Scaffold

The mechanical strength of HA is similar to that of normal bone tissue, but it has the disadvantages of poor mechanical properties, high brittleness, easy fracture, and refractory degradation. TCPbioceramics are similar to natural inorganic bone components with good osteoconductivity, osteoinductivity and biocompatibility, which are non-toxic and can be degraded and absorbed. However, it has the disadvantages of fast degradation, poor plasticity and unstable mechanical properties. Therefore, HA and TCP are often used in combination to complement each other for better performance of the stent. G has the characteristics of low strength, high brittleness, easy water absorption and swelling, and extremely low strength and elastic modulus after swelling. The properties of gelatin porous scaffolds are usually improved by physical modification and chemical cross-linking. G-HA-TCP was synthesised as per a previous study (Gu et al., 2018). In brief, G, HA, and TCP (at a proportion of 10:1:1) were added to ultrapure water and sonicated for 20 min, followed by a hot-water bath for 1 h. Sodium chloride was added as a pore-forming agent in the mixtureand simultaneously mixed with glutaraldehyde as a cross-linking agent. After incubating for 30 min, the formed scaffold was sodden and cleaned with ultrapure water for 12 h and aged 24 h under room temperature to obtain a gel-like 3D porous G-HA-TCP scaffold.

Conjugation of Heparin Onto G-HA-TCP Scaffold

G-HA-TCP scaffold was submerged in MES buffer for 2 h to prepare scaffold solution. Besides, N-Hydroxysuccinimide (NHS) and 1-(3-Dimethylaminopropyl)-3-ethylcarbodiimide hydrochloride (EDC) were added tothe heparin solution and incubated for 15 min to stimulate heparin (with a molar proportion of EDC:NHS as 1:1). Subsequently, scaffold solution was mixed into heparin solution with gentle stirring for 24 h atroom temperature. Finally, distilled water was used to rinse the scaffold to remove sideproducts. After freeze-drying, HG-HA-TCP material was obtained.

Microstructural Characterisation of Scaffolds

Freeze-dried G-HA-TCP and HG-HA-TCP scaffolds were fixed on the conductive tape on the sample holder, which was furtherplaced in the gold steaming chamber and gold was sprayed when it reached a vacuum state. Carl Zeiss scanning electron microscope (SEM) was used to observe surface morphology, pore distribution, and pore size of scaffolds under an energy dispersive spectrum voltage of 3 kV.

Preparation of Scaffolds Loaded With VEGF

VEGF-loaded scaffolds were prepared by the adsorption method. Briefly, 2 μg of recombinant human VEGF165

(127464-60-2, Peprotech, Rocky Hill, NJ, United States) was dissolved in 2 ml of ultrapure water consisting of 0.1% bovine serum albumin (BSA). Further, ethylene-oxide-sterilised HG-HA-TCP and G-HA-TCP scaffolds were placedin VEGF solution and keptat 4°C for 18 h. After washing, VEGF loaded scaffolds were dried under vacuum conditions and stored under room temperature.

Isolation and Identification of SHED

Twenty children with retained deciduous teeth treated in the Department of Paediatric Stomatology of our hospital were selected. With the notification and consent of their guardians, extracted deciduous teeth were obtained. The current study obtained approval fromthe Ethics Committee of Capital Medical University, Beijing, China (No. CMUSH-IRB-KJ-PJ-2020-02). The surface of the tooth was sanitised with 75% ethanol; the pulp was detached under hygienic conditions, cut into asizeof 1–1.5 mm^3, and digestedwith 0.4% neutral protease and 0.3% type I collagenase for 30 min at 37°C. MSCM medium (HyClone, United States) containing 20% foetal bovine serum (FBS; Gibco, United States) was addedto cease theenzymatic activity. After the digestion was terminated, cells were transferred to a 60-mm Petri dish with an MSCM medium supplemented with 100 U/mL streptomycin (Gibco), 100 U/mL penicillin (Gibco), and 15% FBS in 10% CO_2 at 37°C for conventional culture, and the medium was changed every 2–3 days.

Flow cytometry was performed to detect surface antigens to analyse the expression of specific mesenchymal protein markers. The third-generation SHED was harvested, 1×10^6 cells were resuspended in50 µl cold PBS. Further, cells were tagged with phycoerythrin (PE)-conjugated antibodies against CD105 (4300023, eBioscience, San Diego, CA, United States) and CD34 (119307, Biolegend, San Diego, CA, United States) and fluorescein isothiocyanate (FITC)-conjugated antibodies targeting CD44 (103,005, Biolegend), CD90 (328107, Biolegend), CD45 (304005, Biolegend), CD14 (301803, Biolegend), and CD11b (4271325, eBioscience). After 30 min of incubation, cells were rinsed with cold PBS solution and placed in BD Accuri™ C6 Plus flow cytometer (BD Biosciences, Bedford, MA, United States) for detection. Data were analysed using Cell Quest software (BD Biosciences). For the detection of cell differentiation, cells were treated with osteogenic (HUXXC-90021) and adipogenic (HUXXC-90031) induction medium (Cyagen, Guangzhou, China) for 2–3 weeks. Further, cells were assessed with Alizarin red S and Oil red O staining.

Co-Culture of Cells and Scaffolds

Third-generation SHED wasdigested with 0.25% trypsin, and MSCM medium was added to make a cell suspension. Ethylene-oxide-sterilised scaffold material was placed in the third-generation cell suspension containing 1×10^5 cells, then shookfor 1 h at 37°C. Further, thescaffold materials were taken out and placed in a petri dish, onto which the remaining cell suspension was dripped. After 4 h, it was cultured in an MSCM medium.

Cell Proliferation Assay

Cell proliferation assay was conducted with CCK-8 kits (CK04, DoJinDo, Japan). Briefly, cell suspension (100 µl/well) was seeded in a 96-well plate, and the cells were co-cultured with the scaffold after pre-incubationof 24 h (37°C, 5% CO_2). On days 1, 3, 5, 7, and 9 of co-culture of cells and scaffolds, 10 µl of CCK-8 solution was added to the cells. After incubation for 4 h, the absorbance of each well was measured at 450 nm usinga microplate reader.

Live/Dead Cell Staining

Cells on scaffolds on days 3 and 7 of culture were stained with LIVE DEAD Viability Cytotoxicity Kit (1976809, Invitrogen, Carlsbad, CA, United States) for cell survival imaging assay. Briefly, 0.5 µl Calcein AM (stains live cells, glows green) and 2 µl Eth DB (stains dead cells, glows red) were added to 1 ml PBS solution to prepare a working staining solution. Cells were cultured for 15–20 min at room temperature in the dark and observed usinga fluorescence microscope as soon as possible after the incubation. The proportion of living and dead cells wascounted, and the cells were photographed.

Migration and Invasion Assays

Invasive (HUVECs, from ATCC) and migratory (SHED) abilities of cells were evaluated usingMatrigel-coated inserts (BD Biosciences) and Transwell assay inserts (8 µm PET, 24-well Millicell), respectively. Overall, 200 µl MSCM or DMEM containing 2×10^5 cells and 800 µl medium comprising 10% FBS and various scaffolds were added to the upper and lower compartments. The cells were cultured at 37°C with 5% CO_2 for 48 h (invasion) or 24 h (migration). The invaded or migrated cells of the lower chambers were rinsed 3 times with PBS and fixed with paraformaldehyde for 10 min. After rinsing and air-drying, the cells were stained with 0.1% crystal violet for 10 min and observed usinga microscope.

Cell Cycle Detection

A cell cycle detection kit was purchased from Bioss (BA00204, Beijing, China). After co-cultivation with scaffolds for 3 or 7 days, supernatant liquid of cells was collected, cells were trypsinised, and MSCM was added. After washing cells twice with PBS, 70% ethanol was added to the cells. Cells were fixed at 4°C for 24 h and centrifuged (2000 rpm, 5 min), then removedthe supernatant. PBS was added to the cells, and the suspension was centrifuged (2000 rpm, 5 min) again, followed by the removal of the supernatant. The cells wereresuspended in 100 µl RNase A and placed in a water bath at 37°C for 30 min. Further, 400 µl PI was added to the cells, incubated at 4°C for 30 min in the dark. The cell cycle was examined using flow cytometry.

Apoptosis Analysis

The apoptosis kit was purchased from Nanjing KGI Biotechnology (KGA108-1, Nanjing, China). After co-cultivation of cells and scaffolds for 3 or 7 days, cells were harvested by trypsinisation without EDTA, rinsed twice with PBS, and resuspended in 500 µl of binding buffer. Further, the cells were incubated with 10 µl Annexin V-FITC in the dark for 10 min atroom temperature. Additionally, 5 µl of PI was added to

the cells, and they were incubatedfor another 5 min under the same experimental conditions. Cell apoptosis was examined usingflow cytometry.

Analysis of Alkaline Phosphatase Activity

SHED wasseeded into three groups of scaffold materials in an osteogenic medium (HUXXC-90021, Cyagen) at a seeding density of 1×10^4 cells/well. After 4, 7, and 14 days of culture, the culture mediumwas removed, and ALP activity was measured per the manufacturer's instructions withthe alkaline phosphatase detection kit.

Alizarin Red S Staining

Alizarin red S staining solution (ALIR-10001, Cyagen) was used in the present procedure. Overall, 1×10^4 cells/well were seeded into 6-well plates and incubated with osteogenic medium at37°C with 5% CO_2 for 24 h. The initial medium was replaced every 2 days after incubation. After 14 and 21 days of incubation, cells were rinsed twice with PBS andfixed with 4% paraformaldehyde for 30 min. After PBS rinsing 2–3 times, cells were stained with 2 ml Alizarin red S staining solution for 10 min and decolourised. Further, 2 ml PBS was added to each well. After 15 min of incubation, absorbance was measured at 490 nm using a microplate reader.

Quantitative Real-Time Polymerase Chain Reaction

Third-generation SHED wasseeded in 6-well plates at a density of 1×10^4 cells/well and co-cultured with osteogenic medium and scaffolds for 14 and 21 days to obtain cell pellets. Total RNA was extracted with TRIzol reagent (Invitrogen, Carlsbad, CA, United States), and cDNA was synthesised using PrimeScript RT Master Mix Perfect Real-Time Kit (Takara, Nanjing, China). SYBR Select MasterMix (Takara) was used for qRT-PCR assay to detect the expression of osteogenic differentiation markers, including ALP, bone salivary protein (BSP), runt-related transcription factor 2 (RUNX2), osterix (OSX), osteocalcin (OCN), and VEGF (in SHED and HUVECs). Glyceraldehyde-3-phosphate dehydrogenase (GAPDH) was usedas an internal reference gene. All primers used in the current study was purchased from Genechem (Shanghai, China).

Western Blotting

Osteogenic medium, scaffolds, and seeded cells were collected and co-cultured for 21 days to obtain cells. RIPA lysis buffer (Beyotime Biotechnology, Shanghai, China) was added to extract total cell proteins. Protein concentration was detected usingthe BAC method (Beyotime Biotechnology), and a 4 μg/μl protein solution was prepared. The proteinswereseparated by 12% SDS-PAGE electrophoresis and transferred to a PVDF membrane (Millipore, Billerica, MA, United States). After blockingwith 5% skimmed milk for 1 h, membranes were cultured with primary antibodies as follows: ALP (1:1000, ab229126, Abcam, Cambridge, United Kingdom), BSP (1:1000, #5468, Cell Signaling Technology), OCN (1:1000, ab133612, Abcam), OSX (1:1000, ab209484, Abcam), RUNX2 (1:1000, ab236639, Abcam), OCT4 (1:1000, ab181557, Abcam), SOX2 (1:1000, ab92494, Abcam), Nanog (1:1000, ab109250, Abcam), VEGF (1:1000, bs-0279R, Bioss), and GAPDH (1:2500, ab9485, Abcam). The next day, secondary antibodies (A0208, Beyotime Biotechnology) were added to the membrane, and the protein bands were detected usingECL (NCI5079, Thermo Fisher Scientific, Shanghai, China).

Wound Healing Assay

Different scaffold solutions were prepared before the wound healing assay by adding DMEM + 1% BSA with different scaffolds for 24 h at a scaffold surface area to a media volume proportion of 1.25 cm^2/ml. To prepare scaffold/monocyte conditioned media, monocytes were incubated in scaffold solutions for 24 h. HUVEC cells were inoculated in 24-well cell culture plates. DMEM medium was discarded when cell confluence reached 90%, and serum-free medium was added for 24 h. When cell confluence reached 100%, cells were scratched using apipette tip, and a corresponding conditioned medium from various scaffolds was added. Cell scratches were photographed using an inverted microscope. The scratch area S at 0 (S0) and 24 h (S24) wereanalysed using ImageJ software. The cell migration rate was calculated as follows:

$$\text{Cell migration rate} = (S0 - S24)/S24 \times 100\%$$

Matrigel Tubule Formation Experiment

The effects of scaffolds on the formation of the vascular tube by HUVEC cells were evaluated usingan *in vitro* angiogenesis assay kit (Corning). Cells (1.5×10^4 cells/well) were seeded in a Matrigel-coated 96-well plate and incubated for 8 h in various conditioned media. An inverted microscope was used for observing the formation of tubular structures in endothelial cells, and three areas of view in each well were selected randomly for photographing.

In vivo Implantation

Thirty-six male SD rats (Beijing Charles River Laboratories) weighing 250–300 g was placed in a clean and sterile environment with an ambient temperature of 22 ± 1°C and a day-night cycle of 12 h. They were divided randomly into control, G-HA-TCP scaffold, G-HA-TCP (VEGF), and HG-HA-TCP (VEGF) groups. Rats were anaesthetized by intraperitoneal injection of sodium pentobarbital (30 mg/kg). The periosteum was detached from the bone surface, drilled to create a circular skull defect with a diameter of 5 mm and implanted with various scaffolds. After implantation, skull tissue was collected for follow-up evaluation after 4, 8, and 12 weeks of implantation. For animal experiments, approval was obtained from the Ethics Committee of Capital Medical University (Beijing, China; MDKN-2021–046).

Micro-CT Analysis

SD rats in each group (n = 6) were anaesthetized using3% pentobarbital sodium. Further, a micro-CT system was used to calculate the bone mineral density (BMD) and bone volume/total volume (BV/TV) fraction of regenerated bone in the calvarial

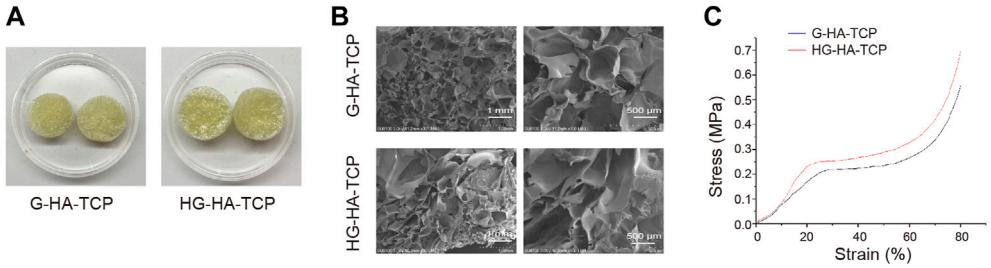

FIGURE 2 | Characteristics of scaffolds. **(A)** Surface morphology of scaffolds. **(B)** Internal structure of scaffolds as observed usingSEM. **(C)** Stress-strain curve of scaffolds.

defect. The micro-CT device was set with a tomographic rotation of 180° at 85 kV and 135 mA.

Histology Evaluation

Rats were sacrificed at 4, 8, and 12 weeks after implantation, and the scaffold and surrounding tissues were collected. The sample was soaked in 10% formalin for 48 h, and ethylenediaminetetraacetic acid (EDTA) solution (pH = 8.0, 0.5 M) was added for decalcification for 30 days. The decalcified samples were embedded in paraffin and sliced into thick sections of 4 μm for histological observation. To assess the regeneration of skull defect, slices were stained with Masson's trichrome and haematoxylin and eosin (H&E). In the current study, the 3Dhistech Pannoramic Scan slide scanning system was used to scan the bone tissue sections after H&E and Masson staining. Case Viewer software was used for observation and analysis.

Immunohistochemical Analysis

For immunohistochemistry, tissue sections were blocked with 5% BSA for 30 min and cultured with primaryanti-BMP2 (1:200, PA5-85956, Thermo Fisher), anti-CD31 (1:50, PA5-16301, Thermo Fisher), anti-RUNX2 (1:200, PA5-82787, Thermo Fisher), and anti-vWF (1:100, PA5-16634, Thermo Fisher). The optical density of immunohistochemical staining results was quantitatively evaluated usingImage J software.

Data Analysis

Measurement data were expressed as mean ± standard deviation (SD). Comparison between experimental groups wasconducted usinga one-way analysis of variance, followed by Tukey's multiple comparisons tests using SPSS 19.0 (SPSS Inc., Chicago, IL, United States) or GraphPad Prism seven software (GraphPad Software, La Jolla, CA, United States). $p < 0.05$ was consideredsignificant.

RESULTS

Characteristics of Scaffolds

First, we observed the characteristics of HG-HA-TCP and G-HA-TCPscaffolds. Both scaffolds were faint yellow incolour with loose and porous surfaces, and HG-HA-TCP hada brighter gloss than G-HA-TCP (**Figure 2A**). Scanning electron microscopy revealed that the pore size of the G-HA-TCP scaffold ranged from 70–200 μm with large porosity. HG-HA-TCP scaffold had alternating pore sizes, and the pore size range was 50–200 μm. Besides, clear pore structure could be seen in scaffolds, with large porosity, rich pores, and uniform distribution (**Figure 2B**). Results of the stress-strain curve of the scaffolds revealed that it was smooth when the deformation was 0%–20%. When the stress reached 0.2 MPa, the G-HA-TCP scaffold was yielded, and when the stress reached 0.25 MPa, the HG-HA-TCP scaffold was yielded. However, no notable difference was observed in the elastic moduli of the two scaffolds (**Figure 2C**). The results revealed that prepared HG-HA-TCP scaffolds were partially modified based on G-HA-TCP scaffolds, and the mechanical properties did not change markedly. With suitable pore size and wide pore size distribution, scaffold materials could meet the requirements of angiogenesis and cell ingrowth and wereoperational during bone tissue engineering.

Isolation and Identification of SHED

The isolated cells had a typical fibroblast-like morphology (**Figure 3A**). Flow cytometricanalysis revealed that the cells expressed the mesenchymal stem cell markers CD44, CD90, and CD105, whereas the hematopoietic cell markers CD11b, CD34, CD45, and CD14 were negatively expressed (**Figure 3B**). Additionally, we detected multipotency of SHED. After induction in osteogenic and adipogenic media, the corresponding staining was performed to detect their differentiation ability; isolated cells had osteogenic and adipogenic differentiation abilities (**Figure 3C**). Collectively, SHED was isolated successfully.

Scaffold Materials Have Good Biocompatibility

After co-culturing cells and scaffolds, we first detected cell proliferation usingthe CCK-8 assay. All three scaffolds could promote cell proliferation compared with the scaffold-free control group. G-HA-TCP (VEGF) promoted cell proliferation markedly better than G-HA-TCP but weaker than HG-HA-TCP (VEGF) (**Figure 4A**). LIVE/DEAD assays revealed that all three scaffold materials increased cell survival rate compared withthe scaffold-free control group. Moreover, cells in HG-HA-TCP

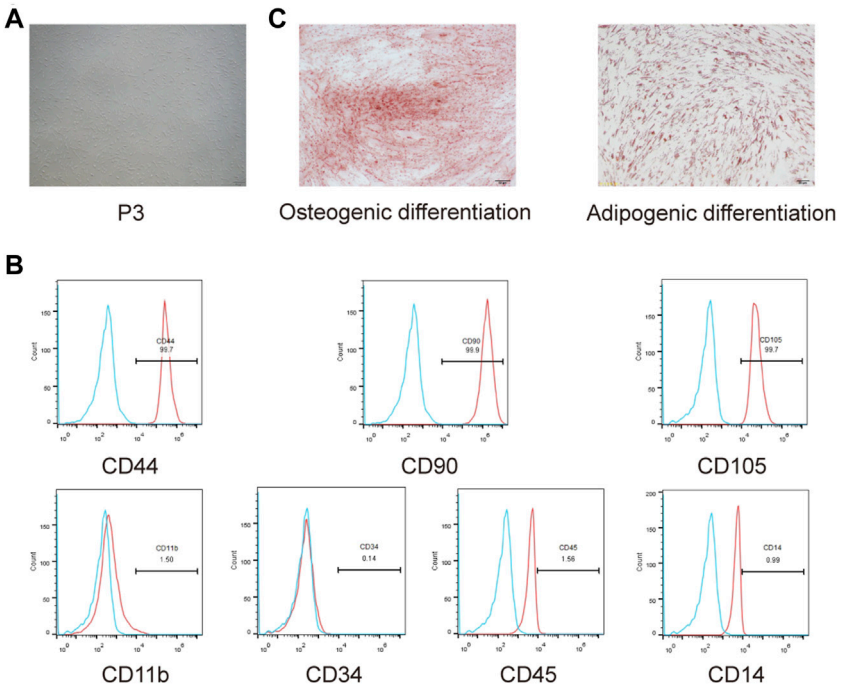

FIGURE 3 | Isolation and identification of SHED. **(A)** Morphology observation of isolated cells from exfoliated deciduous teeth. **(B)** CD44, CD90, CD105, CD11b, CD34, CD45, and CD14 expressions were measured usingflow cytometry. **(C)** Osteogenic andadipogenic differentiation abilities of isolated cells were assessed.

(VEGF) group displayed better viability thanother groups (**Figure 4B**). Additionally, the migrated cells were increased in scaffold groups compared to the scaffold-free control group, and the number of migrated cells in the G-HA-TCP (VEGF) group was more than that in the G-HA-TCP scaffold groupbut less than that in HG-HA-TCP (VEGF) group (**Figure 4C**). Additionally, the number of cells in the G1 phase of HG-HA-TCP (VEGF) and G-HA-TCP (VEGF) groups was lower than that in the G-HA-TCP scaffold group (**Figure 4D**). The rate of cell apoptosis in the G-HA-TCP (VEGF) group was lower than that in G-HA- TCP scaffold group but higher than that in HG-HA-TCP (VEGF) group (**Figure 4E**). The above results revealed that HG-HA-TCP (VEGF) scaffold could promote cell proliferation, adhesion, and migration and had good biocompatibility, which could be applied in bone tissue engineering.

HG-HA-TCP (VEGF) Promotes Osteogenic Differentiation of SHED

To further analyse the promoting effect of HG-HA-TCP (VEGF) on osteogenic differentiation of SHED, we first detected ALP activity inthe cells by ALP staining. All three scaffolds improved the osteogenic differentiation of ALP activity compared with the scaffold-free control group. ALP activity in G-HA-TCP (VEGF) group was higher than that in the G-HA-TCP group but lower than that in HG-HA-TCP (VEGF) group (**Figure 5A**). Results of cell mineralisation detected usingAlizarin red S staining revealed that the content of Alizarin red S in scaffold material groups was increased compared with that in the scaffold-free control group. However, the staining colour of the HG-HA-TCP (VEGF) group was more profoundthan that of the G-HA-TCP (VEGF) group at each time point, and the staining colour of the G-HA-TCP (VEGF) group was deeper than that of G-HA-TCP group (**Figure 5B**). qRT-PCR revealed that the expressions of BSP, ALP, RUNX2, OSX, OCN, and VEGF were upregulated in the cells of the HG-HA-TCP (VEGF) group, which werebetter than thoseinthe G-HA-TCP (VEGF) and G-HA-TCP groups (**Figure 5C**). Variations of ALP, BSP, OCN, OSX, RUNX2, OCT4, SOX2, Nanog, and VEGF in scaffold material groups increased dramatically. Moreover, HG-HA-TCP (VEGF) group accounted for the highest expressions in terms of the above factors, followed by G-HA-TCP (VEGF) and G-HA-TCP groups (**Figure 5D**). The HG-HA-TCP (VEGF) scaffold could promote osteogenic differentiation of SHED, and its effect surpassed that of G-HA-TCP (VEGF) and G-HA-TCP scaffolds.

HG-HA-TCP (VEGF) Promotes Endothelial Cell Angiogenesis

To analyse the promoting effect of HG-HA-TCP (VEGF) on endothelial cell angiogenesis, we first performeda wound-healing assay to detect cell migration. All three scaffold materials could promote cell migration compared with the scaffold-free control group. The efficacy of the HG-HA-TCP (VEGF) scaffold to promote cell migration was better than that of the G-HA-TCP

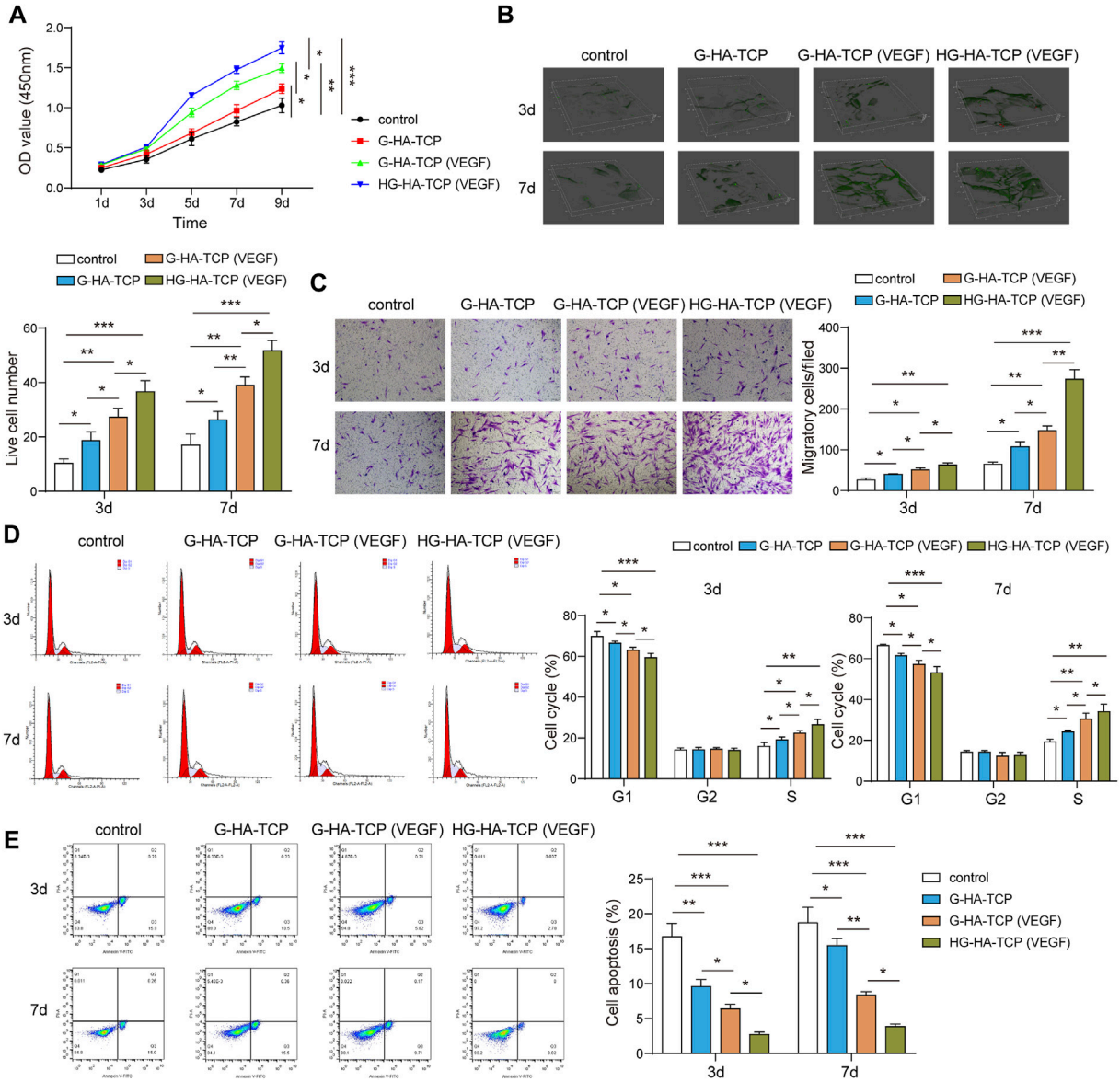

FIGURE 4 | Biocompatibility of scaffold materials. **(A)** Cell proliferation was detected using CCK-8 assay. **(B)** Cell survival was assessed usingLIVE/DEAD assay. **(C)** Transwell assay was performed to measure cell migration. **(D,E)** Flow cytometry was performedfor the detection of cell cycle and apoptosis $n = 3$. $^{*}p < 0.05$, $^{**}p < 0.01$, $^{***}p < 0.001$.

(VEGF) and G-HA-TCP scaffolds (**Figure 6A**). Results of cell invasion revealed that all three scaffold materials could promote cell invasion, and the HG-HA-TCP (VEGF) scaffold had a better promoting effect on cell invasion than G-HA- TCP (VEGF) and G-HA-TCP scaffolds (**Figure 6B**). In tube formation assay, the tube-forming effect of the G-HA-TCP (VEGF) group was slightly better than that of the G-HA-TCP group but was not as good as that of the HG-HA-TCP (VEGF) group (**Figure 6C**). Compared with the scaffold-free control group, VEGF expression wasincreased markedly in scaffold material groups. Among them, HG-HA-TCP (VEGF) group exhibited the highest amount, and the VEGF level in G-HA-TCP (VEGF) group was higher than that in the G-HA-TCP group (**Figure 6D**). These results revealed that HG-HA-TCP (VEGF) scaffolds could promote endothelial cell tubule formation, surpassing the efficacy of G-HA-TCP (VEGF) and G-HA-TCP scaffolds.

HG-HA-TCP (VEGF) Accelerates Bone Regeneration

After establishing a mouse model of bone defect, we first used micro-CT to observe the bone regeneration in each group of rats after implanting the scaffolds. Compared with the scaffold-free control group, the new bone in scaffold

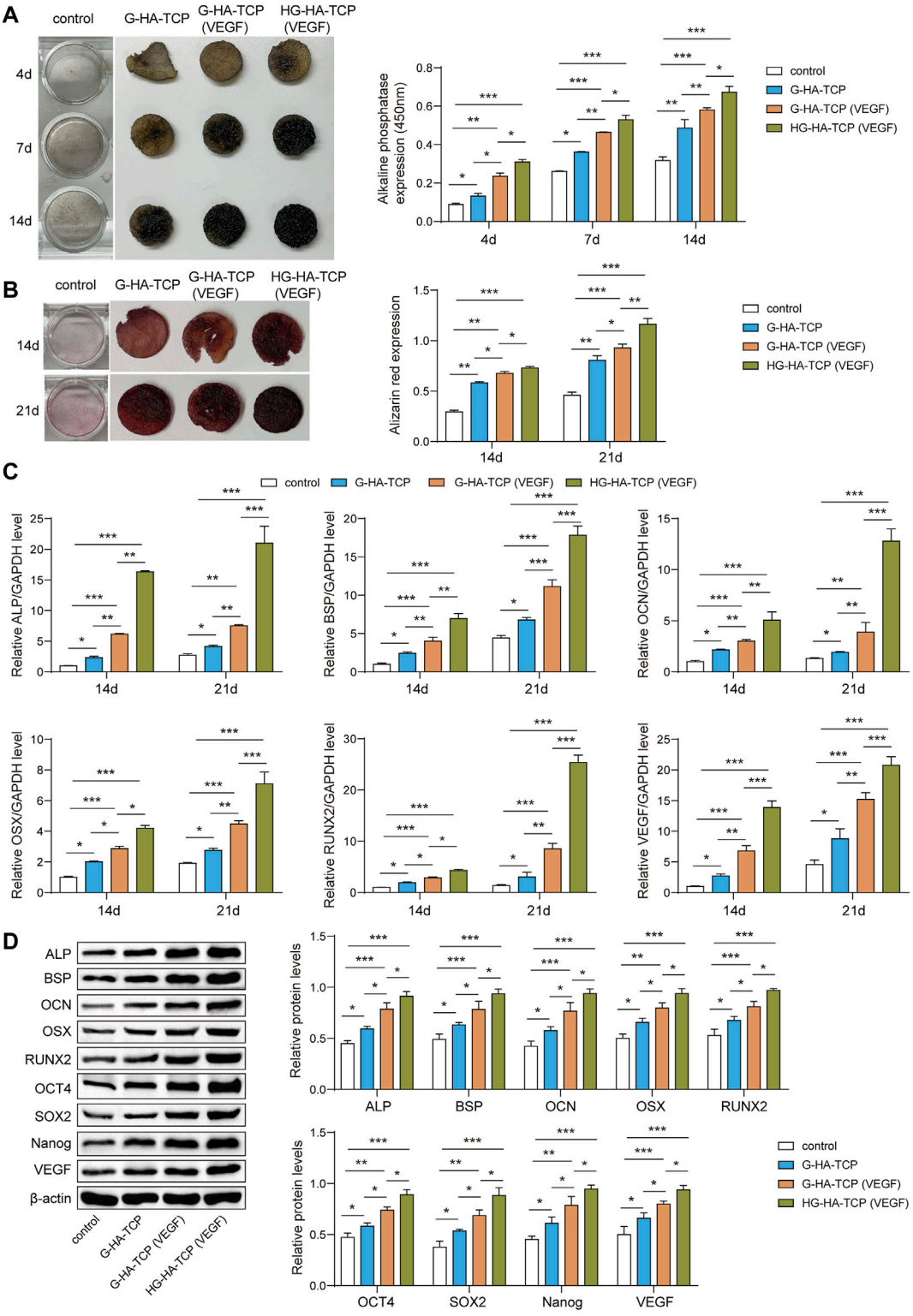

FIGURE 5 | HG-HA-TCP (VEGF) promotes the osteogenic differentiation of SHED. **(A)** ALP staining was performedto detect cell ALP activity. **(B)** Alizarin red S staining was performed to measure cell mineralisation. **(C)** qRT-PCR analysis of mRNA levelsof ALP, BSP, OCN, OSX, RUNX2, and VEGF. **(D)** Western blot analysis of protein expressions of ALP, BSP, OCN, OSX, RUNX2, OCT4, SOX2, Nanog, and VEGF () $n = 3$. $^{*}p < 0.05$, $^{**}p < 0.01$, $^{***}p < 0.001$.

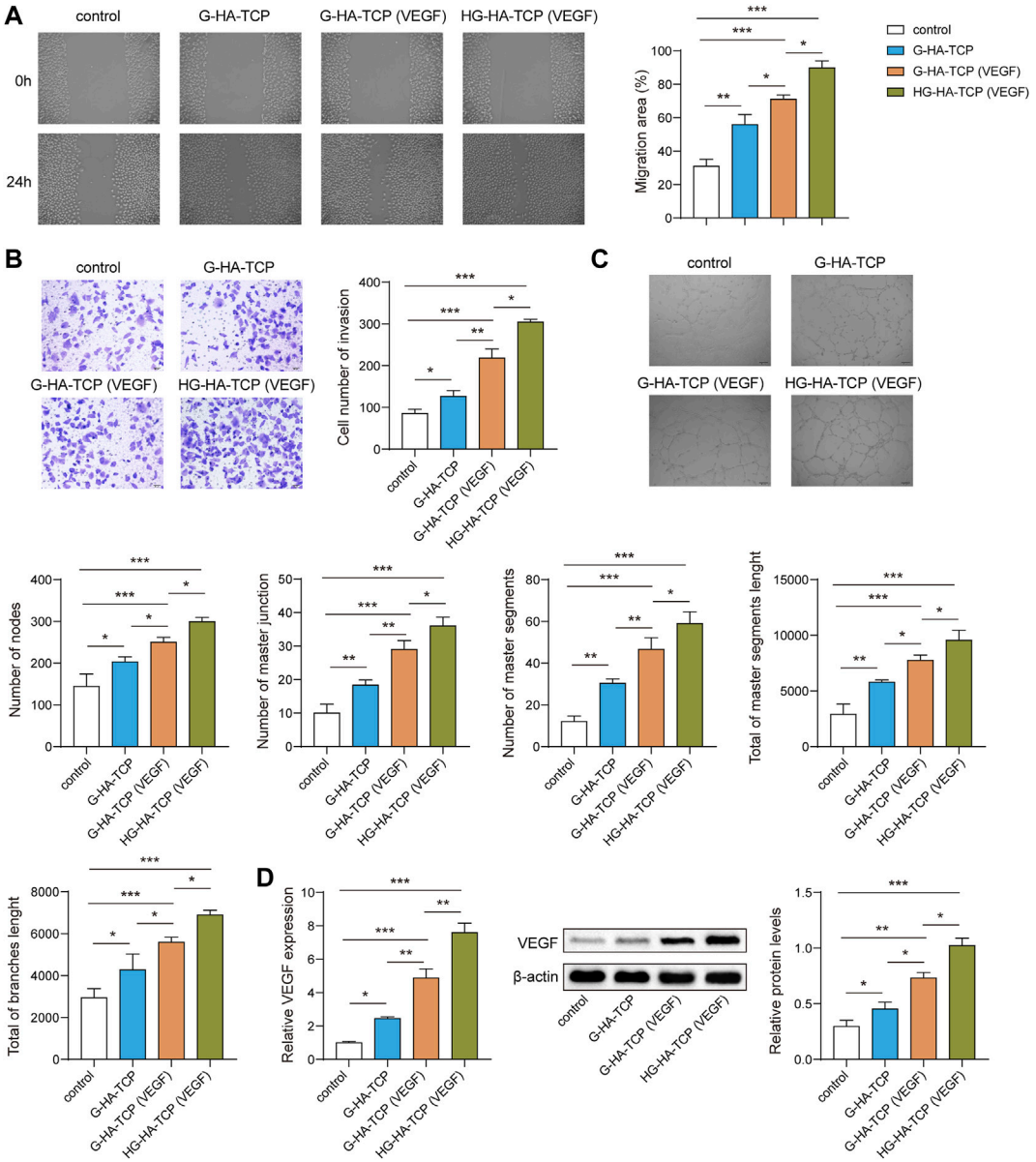

FIGURE 6 | HG-HA-TCP (VEGF) promotes endothelial cell angiogenesis. **(A)** Wound healing assay was performed to detect cell migration. **(B)** Transwell assay was performed for cell invasion measurement. **(C)** Tube formation assay was performed to assess angiogenesis *in vitro*. **(D)** VEGF expression was detected usingqRT-PCR and western blot $n = 3$. $^{*}p < 0.05$, $^{**}p < 0.01$, $^{***}p < 0.001$.

groups grew concentrically at 4, 8, and 12 weeks, with greater bone mass than that in the blank control group, and BMD and BV/TV increased markedly. In addition, the bone mass, BMD, and BV/TV in HG-HA-TCP (VEGF) group weregreater than thosein G--HA-TCP (VEGF) and G-HA-TCP groups (**Figure 7A**). Subsequently, H&E and Masson staining was performed for bone repair detection. A small but insignificant amount of new bone formed around the bone defect in a scaffold-free control group, whereasthe three scaffold groups exhibited theformation of a small numberof bone islands, new blood vessels, and fibrous tissue in the scaffold area. Compared with other groups, HG-HA-TCP (VEGF) group exhibited more new bone formation and fibrous tissue (**Figure 7B**). Further, the expressions of BMP2, CD31, RUNX2, and vWF in the bone tissue were detected using immunohistochemistry, revealing that the above indexes were expressed in a much higher amount in the bone tissue of rats in scaffold groups compared with that in the scaffold-free control group. Among which, HG-HA-TCP (VEGF) scaffold group performed notably better than G-HA-TCP (VEGF) and G-HA-TCP groups in terms of all proteins (**Figure 7C**).

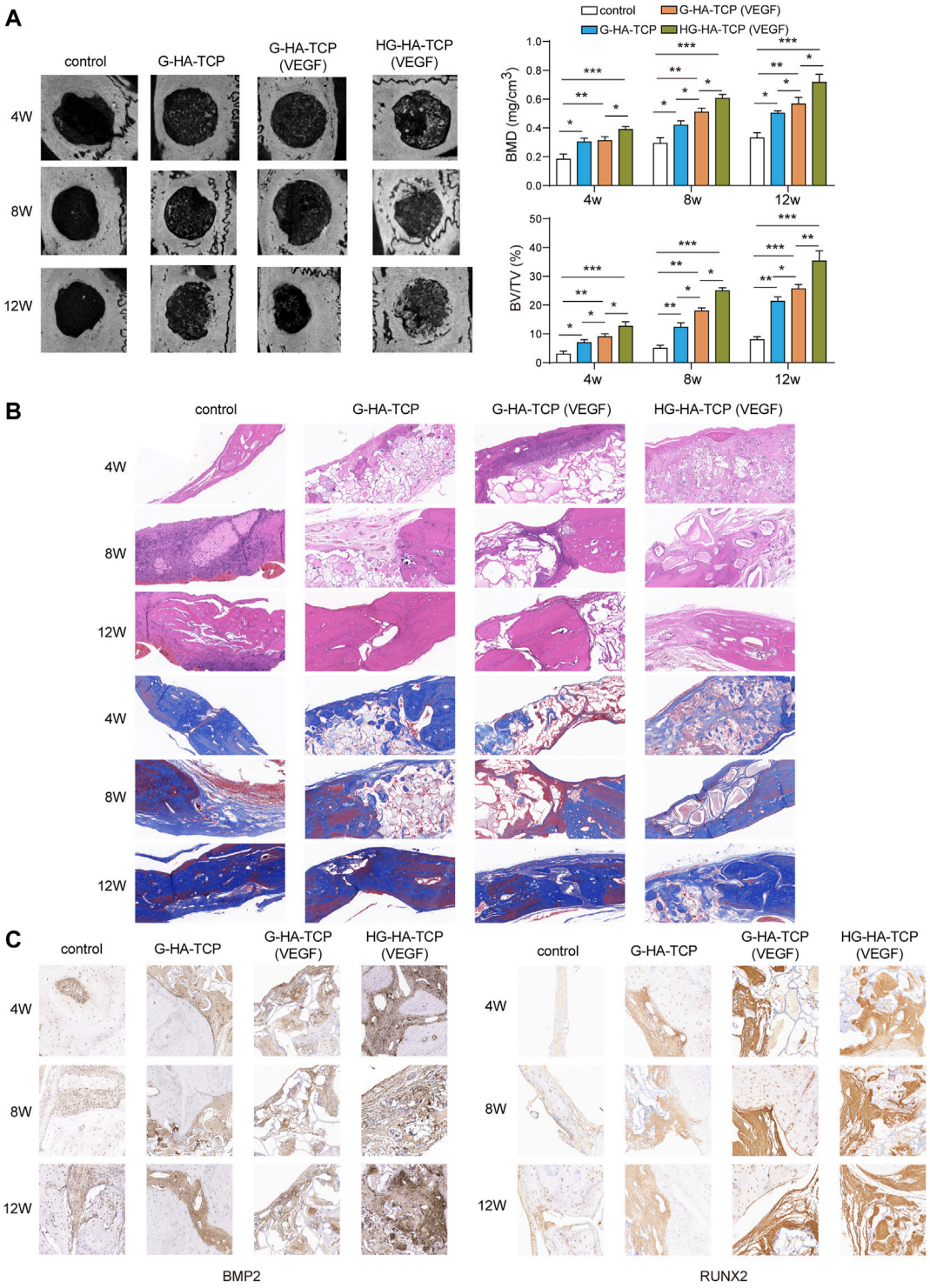

FIGURE 7 | *In vivo* experiments confirmed that HG-HA-TCP (VEGF) could accelerate bone regeneration. **(A)** Micro-CT observation of bone regeneration. **(B)** H&E and Massonstaining for the measurement of bone repair. **(C)** Immunohistochemical detection of BMP2, CD31, RUNX2, and vWF expressions $n = 6$. $^{*}p < 0.05$, $^{**}p < 0.01$, $^{***}p < 0.001$.

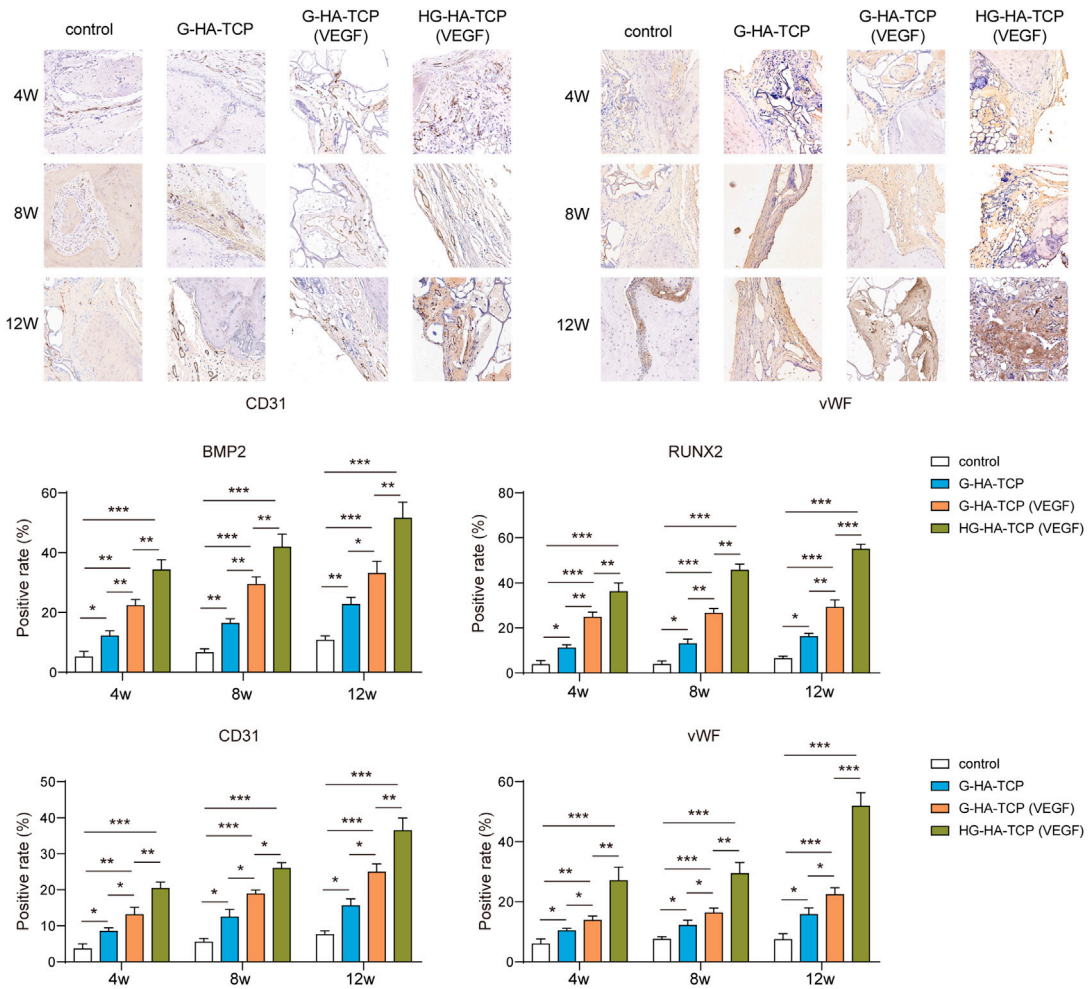

FIGURE 7 | (Continued).

The above results suggested that HG-HA-TCP (VEGF) scaffold accelerated bone regeneration by increasing the osteogenesis-angiogenesis coupling.

DISCUSSION

Large-scale defects of maxillofacial bone tissue can be caused by oral and maxillofacial trauma, tumours, and congenital deformities, etc., thus seriously affecting the masticatory function, pronunciation, and appearance of patients (Tatullo et al., 2015). Fortunately, defects of bone can be repaired to a favourable extent with tissue engineering technology (El-Rashidy et al., 2017), and ideal bioscaffold material applied in which should possess good biocompatibility, degradability, suitable degradation rate and biomechanical strength, good cell-interface relationship, and structure that is easy to process (Cui et al., 2018; Tian et al., 2021). In this study, it was observed that the porosity, pore size, and mechanical properties of HG-HA-TCP scaffold were similar to those of G-HA-TCP scaffold, which met the needs of bone tissue engineering. Moreover, it was of good biocompatibility and could effectively promote cell adhesion, proliferation, and migration after loading an appropriate amount of VEGF. AndVEGF-loaded HG-HA-TCP scaffolds could promote the expression of osteogenesis-related genes in SHED.

Studies have reported that the shape and size of scaffold pores of bioscaffold materials could affect the migration and growth of seed cells, and ideal pore size should be controlled between 100 and 400 μm (Deschamps et al., 2017). In this study, the pores of HG-HA-TCP scaffold were uniformly distributed; its internal morphology was analogous to that of natural cancellous bone with good integrity of pore wall. The diameter of the pores was 50–200 μm, which was conducive to the exchange of tissue nutrients and metabolic wastes and able to promote the effective growth of new tissue structures. G in scaffolds is a protein of natural origin, which can strengthen the mechanical properties of scaffold materials, make up for their rigidity

and is lack of elasticity. The elastic modulus of the scaffoldaresimilar to that of cancellous bone with a relatively flat stress-strain curve, and satisfy the requirements of mechanical properties (Echave et al., 2017; Wiria et al., 2007). As an ideal seed cell in tissue engineering, SHED poses strong proliferation ability, population multiplication rate, and convenience to its source. Itneither causes damage to the donor nor hasimmune rejection or ethical conflicts for autologous use. Combined with biological scaffolds, it can be applied to oral craniomaxillofacial tissue engineering, such as periodontal tissue regeneration and jaw defect repair (Nakamura et al., 2009; Tan et al., 2015). Thus, it was chosen to serve as seed cells in present study and was found that cells could express the mesenchymal stem cell markers CD44, CD90, and CD105, whereas the hematopoietic cell markers CD11b, CD34, CD45, and CD14 were negatively expressed (**Figure 2B**). Previous studies have also reported that SHED positively expressed the markers CD166, CD146, CD90, CD73, and CD29, but negatively expressed CD45, CD34, and CD14 (Huang et al., 2009; Rodríguez-Lozano et al., 2011), proving that SHED was successfully isolated in our study. Biocompatibility refers to possessing the ability to reproduce tissue, and to bolster cellular viability without causing any toxic action or immune responses from the host (Hussein et al., 2016). And an optimal bone scaffold must be osteoconductive to form new bone by recruiting progenitor cells, biomolecular signalling, and biocompatibility (Kharkar et al., 2013). Compatibility of biomaterials is critical for their biological functions and applications, for the host immune system is the first defender to respond during trauma or biomaterial implantation surgery (Anderson et al., 2008). Application of scaffolds unavoidably induces foreign body reactions, which is likely to cause damage to tissue regeneration and lead to fibrosis and scarring. However, immune responses to tissue damages can also accelerate the healing process to certain extent (Saleh and Bryant, 2018). To further confirm the biocompatibility of the scaffold materials, we conducted related analysis and revealed that HG-HA-TCP (VEGF) scaffold could promote cell proliferation, invasion and migration, and is featured withfavorable biocompatibility.

ALP secreted during osteoblast differentiation is an early bone formation and osteoblast marker, the activity of which can reflect the biological activity of osteoblasts (Siller and Whyte, 2018). And it was suggested from the results that ALP activity of HG-HA-TCP (VEGF) group was markedly greater than that of G-HA-TCP (VEGF) and G-HA-TCP groups on days 4, 7, and 14, suggesting that HG-HA-TCP (VEGF) functioned better in promoting osteogenic differentiation of SHED than that of G-HA-TCP (VEGF) scaffold. Previous study reported that HA can regulate the ALP expression in osteoblasts, that the formation of the mineralised nodule is a sign of late osteogenic differentiation (Yuan et al., 2017), and that Alizarin red S staining mainly uses Alizarin red S to react with calcium nodules deposited in osteogenic-induced extracellular, resulting in dark red-coloured compounds, which can reflect the osteogenic differentiation ability of cells. Results of our study indicated that the exudate of HG-HA-TCP (VEGF) group could significantly promote osteogenic differentiation of SHED and induce its mineralisation. Bone formation is a convoluted course, during the process of which *in vivo*, the expression of bone-related genes has a chronological order and the expression time is strictly controlled, which is essential for bone metabolism, formation, growth, and remodelling (Pan et al., 2017). ALP is produced early in cell development and is readily found on the cell surface and in stromal vesicles of bone and calcified cartilage (Lee et al., 2019). BSP, a marker in the middle and late stages of bone formation, was found in studies to be involved in the attachment and differentiation of fibroblasts, osteoblasts, and osteoclasts, as well as in the process of bone tissue mineralisation; it plays an essential role in periodontal tissue regeneration (Kasugai et al., 1992). RUNX2 can promote the immature differentiation of osteoblasts in early stage and is the earliest and most specific marker in bone formation (Ao et al., 2017). OSX is a negative regulator that is specifically expressed only in osteoblasts. Studies have suggested that overexpression of OSX inhibited the differentiation and maturation of osteoblasts, which revealed that only proper expression of OSX could stimulate bone formation (Yoshida et al., 2012). And results of present study suggested that mRNA levels of RALP, BSP, OCN, OSX, and RUNX2 were markedly elevated on the 14th day in SHED cultured on HG-HA-TCP (VEGF) scaffolds, suggesting that HG-HA-TCP (VEGF) scaffolds could promote SHED osteogenic differentiation at an early stage.

Bone is a highly vascularized connective tissue whose development, maturation, remodelling, and regeneration all depend on tight regulation of vascular supply (Dai and Rabie, 2007). Blood vessels not only supply oxygen or nutrients to the skeletal system and remove metabolites from the bone, but also supply the bone with specific hormones, growth factors, and neurotransmitters secreted by other tissues; they maintain bone cell survival and stimulate their activity (Filipowska et al., 2017). In our study, it was observed that compared with G-HA-TCP scaffold, HG-HA-TCP (VEGF) and G-HA-TCP (VEGF) scaffolds could promote angiogenic gene expression, in which HG-HA-TCP (VEGF) scaffold material had a stronger effect on promoting angiogenesis. This indicated that VEGF could regulate osteogenesis and angiogenesis through a certain signalling pathway. In addition, we observed that HG-HA-TCP (VEGF) scaffold had a stronger effect on the migration and invasion of SHED cells than the G-HA-TCP (VEGF) and G-HA-TCP groups, demonstrating that HG-HA-TCP (VEGF) scaffold material had stronger osteogenic effect than G-HA-TCP (VEGF) and G-HA-TCP groups.

Moreover, previous studies reported that VEGF was one of the most crucial regulators of angiogenesis and was essential for the development and regeneration of the bones (Schipani et al., 2009). VEGF played a dual role in the above processes, activating endothelial cells to accelerate their migration and proliferation and stimulating osteogenesis by regulating osteogenic growth factors (Hu and Olsen, 2016). It not only promoted vascular invasion and cartilage fragmentation tissue recruitment to hypertrophic cartilage but also was required for intramembranous ossification (Percival and Richtsmeier, 2013). Thus, angiogenesis and osteogenesis were tightly linked and must be tightly coupled for the physiological function of bone, as confirmed by our observations.

Previous studies demonstrated that intramembranous bone formation depended on the coupling relationship between angiogenesis and osteogenesis, and VEGF was essential in this coupling because both blood vessel and bone morphogenesis were VEGF-dependent (Tang et al., 2012). Angiogenesis and increased angiogenesis bring in bone-forming progenitor cells and

minerals, nutrients, and oxygen required for mineralisation. Moreover, vascular-released osteogenic factors, such as BMP2 accelerate osteoblast differentiation and mineralisation (Matsubara et al., 2012). The disadvantage of *in vitro* studies is that they cannot well-simulate the complex environment *in vivo*, so the osteogenic properties of scaffolds cannot be accurately reflected (Delgado-Ruiz et al., 2015). Therefore, we further evaluated the osteogenic ability of scaffolds through animal experiments. H&E and Masson staining indicated that VEGF-loaded scaffolds had better osteogenic ability, and HG-HA-TCP (VEGF) scaffolds better promoted new bone formation than G-HA-TCP (VEGF). This may be due to the stable loading of VEGF by heparin and its slow release, which expanded the time scale factor for slow-release growth; this, in turn, expanded the range of transportable growth factors for tissue repair and regeneration. A previous study reported that bolus injection of VEGF into the defect without scaffolds did not improve angiogenesis and bone formation, whereas VEGF bolus injection in a hydrogel, released at a relatively slow rate, successfully improved angiogenesis and osteogenesis (Kaigler et al., 2013). Above studies suggested that the release kinetics of VEGF were essential for the effect of biomaterials on bone formation and vascularisation. However, the release kinetics of VEGF in HG-HA-TCP scaffold still need further analysis.

CONCLUSION

The porosity, pore size, and mechanical properties of the HG-HA-TCP scaffold could meet the needs of bone tissue engineering with favourable biocompatibility. It could effectively promote cell adhesion, proliferation, and migration after loading an appropriate amount of VEGF. We confirmed that using HG-HA-TCP (VEGF) scaffold material could effectively promote the expression of osteogenesis-related genes in SHED and bone regeneration *in vivo*. The present study provided a theoretical basis for applying this new bone tissue engineering scaffold material in oral implants with insufficient bone mass, which is valuable in clinical practice. However, VEGF has its advantages and disadvantages, and only the appropriate concentration of VEGF can provide the best effect. Further experiments are required to identify a more precise concentration of VEGF, and the related mechanism of how VEGF promotes osteogenesis needs to be further studied.

DATA AVAILABILITY STATEMENT

The original contributions presented in the study are included in the article/supplementary material, further inquiries can be directed to the corresponding authors.

ETHICS STATEMENT

The animal study was reviewed and approved by the Ethics Committee of Beijing Stomatological Hospital.

AUTHOR CONTRIBUTIONS

D-LZ and KY designed the whole study work-flow. X-YC and C-YZ was in charge of the material synthesis and performance testing. XC and XH conducted in vitro experiments at the cellular level. C-YG and XC conducted *in vivo* experiments at the animal model level. XC, Y-YL, and C-YG summarized and analyzed the experimental data, and wrote the original version of this manuscript. KY and D-LZ reviewed and edited it. All coauthors authorized the submission of this manuscript.

FUNDING

This work was supported by the Beijing Science and Technology Achievement Transformation Coordination and Service Platform Construction Special Programme (No. SYGX202009); and the Beijing Hospitals Authority Youth Programme (No.QML20211401).

REFERENCES

Anderson, J. M., Rodriguez, A., and Chang, D. T. (2008). Foreign Body Reaction to Biomaterials. *Seminars Immunol.* 20 (2), 86–100. doi:10.1016/j.smim.2007.11.004

Ao, M., Chavez, M. B., Chu, E. Y., Hemstreet, K. C., Yin, Y., Yadav, M. C., et al. (2017). Overlapping Functions of Bone Sialoprotein and Pyrophosphate Regulators in Directing Cementogenesis. *Bone* 105, 134–147. doi:10.1016/j.bone.2017.08.027

Claassen, C., Sewald, L., Tovar, G., and Borchers, K. (2017). Controlled Release of Vascular Endothelial Growth Factor From Heparin-Functionalized Gelatin Type A and Albumin Hydrogels. *Gels* 3 (4), 35. doi:10.3390/gels3040035

Clark, D., Wang, X., Chang, S., Czajka-Jakubowska, A., Clarkson, B. H., and Liu, J. (2015). VEGF Promotes Osteogenic Differentiation of ASCs on Ordered Fluorapatite Surfaces. *J. Biomed. Mat. Res.* 103 (2), 639–645. doi:10.1002/jbm.a.35215

Cui, Y., Zhu, T., Li, A., Liu, B., Cui, Z., Qiao, Y., et al. (2018). Porous Particle-Reinforced Bioactive Gelatin Scaffold for Large Segmental Bone Defect Repairing. *ACS Appl. Mat. Interfaces* 10 (8), 6956–6964. doi:10.1021/acsami.7b19010

Dai, J., and Rabie, A. B. M. (2007). VEGF: an Essential Mediator of Both Angiogenesis and Endochondral Ossification. *J. Dent. Res.* 86 (10), 937–950. doi:10.1177/154405910708601006

Delgado-Ruiz, R. A., Calvo-Guirado, J. L., and Romanos, G. E. (2015). Critical Size Defects for Bone Regeneration Experiments in Rabbit Calvariae: Systematic Review and Quality Evaluation Using ARRIVE Guidelines. *Clin. Oral Impl. Res.* 26 (8), 915–930. doi:10.1111/clr.12406

Deschamps, I. S., Magrin, G. L., Magini, R. S., Fredel, M. C., Benfatti, C. A. M., and Souza, J. C. M. (2017). On the Synthesis and Characterization of β-Tricalcium Phosphate Scaffolds Coated with Collagen or Poly (D, L-Lactic Acid) for Alveolar Bone Augmentation. *Eur. J. Dent.* 11 (4), 496–502. doi:10.4103/ejd.ejd_4_17

Diomede, F., Marconi, G. D., Fonticoli, L., Pizzicanella, J., Merciaro, I., Bramanti, P., et al. (2020). Functional Relationship Between Osteogenesis and Angiogenesis in Tissue Regeneration. *Ijms* 21 (9), 3242. doi:10.3390/ijms21093242

Dorozhkin, S. V. (2010). Bioceramics of Calcium Orthophosphates. *Biomaterials* 31 (7), 1465–1485. doi:10.1016/j.biomaterials.2009.11.050

Echave, M. C., Burgo, L. S., Pedraz, J. L., and Orive, G. (2017). Gelatin as Biomaterial for Tissue Engineering. *Cpd* 23 (24), 3567–3584. doi:10.2174/0929867324666170511123101

El-Rashidy, A. A., Roether, J. A., Harhaus, L., Kneser, U., and Boccaccini, A. R. (2017). Regenerating Bone with Bioactive Glass Scaffolds: A Review of *In Vivo* Studies in Bone Defect Models. *Acta Biomater.* 62, 1–28. doi:10.1016/j.actbio.2017.08.030

Filipowska, J., Tomaszewski, K. A., Niedźwiedzki, Ł., Walocha, J. A., and Niedźwiedzki, T. (2017). The Role of Vasculature in Bone Development, Regeneration and Proper Systemic Functioning. *Angiogenesis* 20 (3), 291–302. doi:10.1007/s10456-017-9541-1

Fillingham, Y., and Jacobs, J. (2016). Bone Grafts and Their Substitutes. *Bone & Jt. J.* 98-B (1 Suppl. A), 6–9. doi:10.1302/0301-620X.98B.36350

Gu, X., Zha, Y., Li, Y., Chen, J., Liu, S., Du, Y., et al. (2022). Integrated Polycaprolactone Microsphere-Based Scaffolds with Biomimetic Hierarchy and Tunable Vascularization for Osteochondral Repair. *Acta Biomater.* 141, 190–197. doi:10.1016/j.actbio.2022.01.021

Gu, Y., Bai, Y., and Zhang, D. (2018). Osteogenic Stimulation of Human Dental Pulp Stem Cells with a Novel Gelatin-Hydroxyapatite-Tricalcium Phosphate Scaffold. *J. Biomed. Mat. Res.* 106 (7), 1851–1861. doi:10.1002/jbm.a.36388

Hu, K., and Olsen, B. R. (2016). The Roles of Vascular Endothelial Growth Factor in Bone Repair and Regeneration. *Bone* 91, 30–38. doi:10.1016/j.bone.2016.06.013

Huang, G. T.-J., Gronthos, S., and Shi, S. (2009). Mesenchymal Stem Cells Derived From Dental Tissuesvs. Those From Other Sources: Their Biology and Role in Regenerative Medicine. *J. Dent. Res.* 88 (9), 792–806. doi:10.1177/0022034509340867

Hussein, K. H., Park, K.-M., Kang, K.-S., and Woo, H.-M. (2016). Biocompatibility Evaluation of Tissue-Engineered Decellularized Scaffolds for Biomedical Application. *Mater. Sci. Eng. C* 67, 766–778. doi:10.1016/j.msec.2016.05.068

Kaigler, D., Silva, E. A., and Mooney, D. J. (2013). Guided Bone Regeneration Using Injectable Vascular Endothelial Growth Factor Delivery Gel. *J. Periodontology* 84 (2), 230–238. doi:10.1902/jop.2012.110684

Kasugai, S., Nagata, T., and Sodek, J. (1992). Temporal Studies on the Tissue Compartmentalization of Bone Sialoprotein (BSP), Osteopontin (OPN), and SPARC Protein During Bone Formation *In Vitro*. *J. Cell. Physiol.* 152 (3), 467–477. doi:10.1002/jcp.1041520305

Kharkar, P. M., Kiick, K. L., and Kloxin, A. M. (2013). Designing Degradable Hydrogels for Orthogonal Control of Cell Microenvironments. *Chem. Soc. Rev.* 42 (17), 7335–7372. doi:10.1039/c3cs60040h

Konovalenko, V. F., Ternovyi, N. K., Tuz, E. V., Protsenko, V. V., Solonitsyn, E. O., Abudayeh, A., et al. (2021). Experimental Substantiation of the Use of Hydroxyapatite - Tricalcium Phosphate Bioceramics for Replacing Bone Defects After Tumor Removal. *Exp. Oncol.* 43 (3), 237–241. doi:10.32471/exp-oncology.2312-8852

Lee, Y.-C., Chan, Y.-H., Hsieh, S.-C., Lew, W.-Z., and Feng, S.-W. (2019). Comparing the Osteogenic Potentials and Bone Regeneration Capacities of Bone Marrow and Dental Pulp Mesenchymal Stem Cells in a Rabbit Calvarial Bone Defect Model. *Ijms* 20 (20), 5015. doi:10.3390/ijms20205015

Marolt, D., Knezevic, M., and Vunjak-Novakovic, G. (2010). Bone Tissue Engineering with Human Stem Cells. *Stem Cell. Res. Ther.* 1 (2), 10. doi:10.1186/scrt10

Martino, M. l. M., Brkic, S., Bovo, E., Burger, M., Schaefer, D. J., Wolff, T., et al. (2015). Extracellular Matrix and Growth Factor Engineering for Controlled Angiogenesis in Regenerative Medicine. *Front. Bioeng. Biotechnol.* 3, 45. doi:10.3389/fbioe.2015.00045

Matsubara, H., Hogan, D. E., Morgan, E. F., Mortlock, D. P., Einhorn, T. A., and Gerstenfeld, L. C. (2012). Vascular Tissues Are a Primary Source of BMP2 Expression During Bone Formation Induced by Distraction Osteogenesis. *Bone* 51 (1), 168–180. doi:10.1016/j.bone.2012.02.017

Mistry, A. S., and Mikos, A. G. (2005). Tissue Engineering Strategies for Bone Regeneration. *Adv. Biochem. Eng. Biotechnol.* 94, 1–22. doi:10.1007/b99997

Nakamura, S., Yamada, Y., Katagiri, W., Sugito, T., Ito, K., and Ueda, M. (2009). Stem Cell Proliferation Pathways Comparison Between Human Exfoliated Deciduous Teeth and Dental Pulp Stem Cells by Gene Expression Profile from Promising Dental Pulp. *J. Endod.* 35 (11), 1536–1542. doi:10.1016/j.joen.2009.07.024

Novosel, E. C., Kleinhans, C., and Kluger, P. J. (2011). Vascularization Is the Key Challenge in Tissue Engineering. *Adv. Drug Deliv. Rev.* 63 (4-5), 300–311. doi:10.1016/j.addr.2011.03.004

Pan, J., He, S., Yin, X., Li, Y., Zhou, C., and Zou, S. (2017). Lithium Enhances Alveolar Bone Formation During Orthodontic Retention in Rats. *Orthod. Craniofac. Res.* 20 (3), 146–151. doi:10.1111/ocr.12190

Percival, C. J., and Richtsmeier, J. T. (2013). Angiogenesis and Intramembranous Osteogenesis. *Dev. Dyn.* 242 (8), 909–922. doi:10.1002/dvdy.23992

Roddy, E., DeBaun, M. R., Daoud-Gray, A., Yang, Y. P., and Gardner, M. J. (2018). Treatment of Critical-Sized Bone Defects: Clinical and Tissue Engineering Perspectives. *Eur. J. Orthop. Surg. Traumatol.* 28 (3), 351–362. doi:10.1007/s00590-017-2063-0

Rodríguez-Lozano, F. J., Bueno, C., Insausti, C. L., Meseguer, L., Ramírez, M. C., Blanquer, M., et al. (2011). Mesenchymal Stem Cells Derived From Dental Tissues. *Int. Endod. J.* 44 (9), 800–806. doi:10.1111/j.1365-2591.2011.01877.x

Saleh, L. S., and Bryant, S. J. (2018). The Host Response in Tissue Engineering: Crosstalk Between Immune Cells and Cell-Laden Scaffolds. *Curr. Opin. Biomed. Eng.* 6, 58–65. doi:10.1016/j.cobme.2018.03.006

Salehi, M., Naseri-Nosar, M., Ebrahimi-Barough, S., Nourani, M., Vaez, A., Farzamfar, S., et al. (2018). Regeneration of Sciatic Nerve Crush Injury by a Hydroxyapatite Nanoparticle-Containing Collagen Type I Hydrogel. *J. Physiol. Sci.* 68 (5), 579–587. doi:10.1007/s12576-017-0564-6

Schipani, E., Maes, C., Carmeliet, G., and Semenza, G. L. (2009). Regulation of Osteogenesis-Angiogenesis Coupling by HIFs and VEGF. *J. Bone Mineral Res.* 24 (8), 1347–1353. doi:10.1359/jbmr.090602

Siller, A. F., and Whyte, M. P. (2018). Alkaline Phosphatase: Discovery and Naming of Our Favorite Enzyme. *J. Bone Min. Res.* 33 (2), 362–364. doi:10.1002/jbmr.3225

Tan, J., Xu, X., Lin, J., Fan, L., Zheng, Y., and Kuang, W. (2015). Dental Stem Cell in Tooth Development and Advances of Adult Dental Stem Cell in Regenerative Therapies. *Cscr* 10 (5), 375–383. doi:10.2174/1574888x09666141110150634

Tang, W., Yang, F., Li, Y., de Crombrugghe, B., Jiao, H., Xiao, G., et al. (2012). Transcriptional Regulation of Vascular Endothelial Growth Factor (VEGF) by Osteoblast-Specific Transcription Factor Osterix (Osx) in Osteoblasts. *J. Biol. Chem.* 287 (3), 1671–1678. doi:10.1074/jbc.M111.288472

Tatullo, M., Marrelli, M., and Paduano, F. (2015). The Regenerative Medicine in Oral and Maxillofacial Surgery: The Most Important Innovations in the Clinical Application of Mesenchymal Stem Cells. *Int. J. Med. Sci.* 12 (1), 72–77. doi:10.7150/ijms.10706

Tian, B., Wang, N., Jiang, Q., Tian, L., Hu, L., and Zhang, Z. (2021). The Immunogenic Reaction and Bone Defect Repair Function of ε-Poly-L-Lysine (EPL)-Coated Nanoscale PCL/HA Scaffold in Rabbit Calvarial Bone Defect. *J. Mater. Sci. Mater. Med.* 32 (6), 63. doi:10.1007/s10856-021-06533-7

Wang, C., Yu, B., Fan, Y., Ormsby, R. W., McCarthy, H. O., Dunne, N., et al. (2019). Incorporation of Multi-Walled Carbon Nanotubes to PMMA Bone Cement Improves Cytocompatibility and Osseointegration. *Mater. Sci. Eng. C* 103, 109823. doi:10.1016/j.msec.2019.109823

Wiria, F. E., Leong, K. F., Chua, C. K., and Liu, Y. (2007). Poly-ε-Caprolactone/Hydroxyapatite for Tissue Engineering Scaffold Fabrication via Selective Laser Sintering. *Acta Biomater.* 3 (1), 1–12. doi:10.1016/j.actbio.2006.07.008

Wolters, W. J., Duncan, H. F., Tomson, P. L., Karim, I. E., McKenna, G., Dorri, M., et al. (2017). Minimally Invasive Endodontics: A New Diagnostic System for Assessing Pulpitis and Subsequent Treatment Needs. *Int. Endod. J.* 50 (9), 825–829. doi:10.1111/iej.12793

Wu, T., Liu, W., Huang, S., Chen, J., He, F., Wang, H., et al. (2021). Bioactive Strontium Ions/Ginsenoside Rg1-Incorporated Biodegradable Silk FIbroin-Gelatin Scaffold Promoted Challenging Osteoporotic Bone Regeneration. *Mater. Today Bio* 12, 100141. doi:10.1016/j.mtbio.2021.100141

Yoshida, C. A., Komori, H., Maruyama, Z., Miyazaki, T., Kawasaki, K., Furuichi, T., et al. (2012). SP7 Inhibits Osteoblast Differentiation at a Late Stage in Mice. *PLoS One* 7 (3), e32364. doi:10.1371/journal.pone.0032364

Yuan, J., Liu, X., Chen, Y., Zhao, Y., Liu, P., Zhao, L., et al. (2017). Effect of SOX2 on Osteogenic Differentiation of Dental Pulp Stem Cells. *Cell. Mol. Biol. (Noisy-le-grand)* 63 (1), 41–44. doi:10.14715/cmb/2017.63.1.8

Zha, Y., Li, Y., Lin, T., Chen, J., Zhang, S., and Wang, J. (2021). Progenitor Cell-Derived Exosomes Endowed with VEGF Plasmids Enhance Osteogenic Induction and Vascular Remodeling in Large Segmental Bone Defects. *Theranostics* 11 (1), 397–409. doi:10.7150/thno.50741

Zhu, Y., Cao, N., Zhang, Y., Cao, G., Hao, C., Liu, K., et al. (2022). The Ability and Mechanism of nHAC/CGF in Promoting Osteogenesis and Repairing Mandibular Defects. *Nanomaterials* 12 (2), 212. doi:10.3390/nano12020212

Zizzari, V. L., Zara, S., Tetè, G., Vinci, R., Gherlone, E., and Cataldi, A. (2016). Biologic and Clinical Aspects of Integration of Different Bone Substitutes in Oral Surgery: A Literature Review. *Oral Surg. Oral Med. Oral Pathology Oral Radiology* 122 (4), 392–402. doi:10.1016/j.oooo.2016.04.010

Conflict of Interest: The authors declare that the research was conducted in the absence of any commercial or financial relationships that could be construed as a potential conflict of interest.

Publisher's Note: All claims expressed in this article are solely those of the authors and do not necessarily represent those of their affiliated organizations, or those of the publisher, the editors and the reviewers. Any product that may be evaluated in this article, or claim that may be made by its manufacturer, is not guaranteed or endorsed by the publisher.

frontiers | Frontiers in Bioengineering and Biotechnology

REVIEW
published: 29 June 2022
doi: 10.3389/fbioe.2022.951513

Advanced Hydrogels With Nanoparticle Inclusion for Cartilage Tissue Engineering

Yunong Ao[1], En Zhang[2], Yangxi Liu[3], Liu Yang[1], Jun Li[1,2] and Fuyou Wang[1]**

[1]Center for Joint Surgery, Southwest Hospital, Third Military Medical University (Army Medical University), Chongqing, China, [2]Chongqing Institute for Food and Drug Control, Chongqing, China, [3]Institute of Life Sciences, Chongqing Medical University, Chongqing, China

Cartilage dysfunctions caused by congenital disease, trauma and osteoarthritis are still a serious threat to joint activity and quality of life, potentially leading to disability. The relatively well-established tissue engineering technology based on hydrogel is a promising strategy for cartilage defect repairing. However, several unmet challenges remain to be resolved before its wide application and clinical translation, such as weak mechanical property and compromised bioactivity. The development of nanomedicine has brought a new dawn to cartilage tissue engineering, and composite hydrogel containing nanoparticles can substantially mimic natural cartilage components with good histocompatibility, demonstrating unique biological effects. In this review, we summarize the different advanced nanoparticle hydrogels currently adopted in cartilage tissue engineering. In addition, we also discuss the various application scenarios including injection and fabrication strategies of nanocomposite hydrogel in the field of cartilage repair. Finally, the future application prospects and challenges of nanocomposite hydrogel are also highlighted.

Keywords: nanoparticles, composite hydrogels, tissue engineering, cartilage, repairing

OPEN ACCESS

Edited by:
Qian Feng,
Chongqing University, China

Reviewed by:
Zhong Li,
The Affiliated Hospital of Southwest Medical University, China
Xieping Dong,
Nanchang University, China
Bin Yang,
Peking University, China

****Correspondence:***
Jun Li
ljunzju@outlook.com
Fuyou Wang
wfy731023@163.com

Specialty section:
This article was submitted to Biomaterials, a section of the journal Frontiers in Bioengineering and Biotechnology

Received: *24 May 2022*
Accepted: *14 June 2022*
Published: *29 June 2022*

Citation:
Ao Y, Zhang E, Liu Y, Yang L, Li J and Wang F (2022) Advanced Hydrogels With Nanoparticle Inclusion for Cartilage Tissue Engineering. Front. Bioeng. Biotechnol. 10:951513. doi: 10.3389/fbioe.2022.951513

INTRODUCTION

Cartilage injury is a common orthopedic disease with pathogenic factors including sport trauma, arthritis and tumor resection, which mainly presents with joint pain, swelling deformity and dysfunction, seriously affecting the quality of patients' life (Ao et al., 2019). Articular cartilage belongs to hyaline cartilage, and is mainly composed of water, chondrocytes, type II collagen, and proteoglycans (Tang et al., 2016). Due to the lack of blood vessels, nerves, and lymph, cartilage has limited self-repair capacity after damage, and effective self-healing is not possible for large lesions, therefore the cartilage defect repair attracts a lot of attention in the field of orthopedics. Currently, the treatment for cartilage defects includes arthroscopic debridement, microfracture, cartilage transplantation, and chondrocyte transplantation (Advincula et al., 2021). However, there is still a mismatch between the structure and bio-function of the newly formed cartilage by these strategies and hyaline cartilage, as well as the mechanical properties (Zhang et al., 2016). In addition, for cartilage and chondrocyte transplantation, complications such as possibly harmful effects to the donor sites also limit their application. In the effects to repair cartilage defects effectively and safely, tissue engineering is today an extensively explored strategy due to its unlimited source and tunable physicochemical properties, and a variety of scaffold materials expand more possibilities (Yang et al., 2017).

Hydrogel is one of the promising materials for repairing cartilage due to the easy synthesis and bio-function, which can better simulate the microenvironment of hyaline cartilage, facilitating the proliferation and differentiation of progenitor cells (Miramini et al., 2020; Wang G et al., 2022). However, conventional hydrogel materials often have deficient physicochemical and biological performance in supporting cartilage regeneration. Therefore, an increasing number of studies have managed to combine nanoparticles with biomaterials to form nanocomposite hydrogel in order to improve their mechanical strength, stability and bio-functions (Farokhi et al., 2020; Kashte et al., 2021). In addition, the inclusion of nanoparticles can effectively promote cell attachment, stimulate cell growth and guide tissue regeneration (Li et al., 2016; Armiento et al., 2018). Because nanocomposites can facilitate hydrogels with enhanced mechanical properties, superior stability, and can be synergized with a variety of nanoparticles (NPs) with different preferred functions, they have received much attention since first reported in 2002 when Haraguchi and others introduced exfoliated clay into poly (N-isopropylacrylamide) to form a unique organic/inorganic network with elevated biomechanical properties (Haraguchi and Takehisa, 2002; Merino et al., 2015; Zhang et al., 2016; Zhao et al., 2020). The crosslinked structure between hydrogel polymer and nanoparticles is due to the unsaturated bonds or functional groups on the surface of nanoparticles, which form chemical crosslinking points to enhance the strength of materials and the nanoparticles perform their intrinsic bio-functions *in situ* or after release (Asadi et al., 2018; Niemczyk-Soczynska et al., 2019).

In this review, we focus on the recent research progress of nanocomposite hydrogels in the application of cartilage tissue engineering, summarize the different nanoparticles applied to composite hydrogels and corresponding fabrication strategies in order to promote the wide application of nanocomposite hydrogels in cartilage regeneration.

NANOPARTICLES APPLIED IN CARTILAGE REGENERATION

The innovative combination of NPs and hydrogels equips a variety of potential properties to hydrogels that were not present in conventional hydrogels, enhancing the cartilage repair capacity (Eftekhari et al., 2020; Keshvardoostchokami et al., 2021). Nanocomposite hydrogels with various structures and biological functions can be prepared by using different nanoparticles and cross-linking methods, which can be mainly divided into four categories according to their physical and chemical properties: metal and metal-oxide NPs, inorganic NPs, carbon-based NPs, and polymeric NPs (Thoniyot et al., 2015; Liu et al., 2021; Shi et al., 2021). The properties conferring to the composites depend on the incorporated nanoparticle types, such as enhancing cross-linking, improving mechanical strength and promoting cell proliferation. Different kind of nanoparticle hydrogel composites and their associated properties and applications are described below.

Metal and Metal-Oxide Nanoparticles

In previous studies, metal and its oxides have shown many unique physical and chemical properties, such as the surface plasmon resonance of gold nanoparticles and the broad-spectrum antibacterial properties of silver nanoparticles, and these characteristics can bring more great properties to nanocomposite hydrogels and expand their scope of application (Qiao et al., 2022). For instance, silver nanoparticles (Ag-NPs) have superior antibacterial properties and are widely used in anti-infection and implant surface coating (Barani et al., 2012). Ag-NPs are incorporated into traditional hydrogels to impart conductivity, which affected the swelling rate and conductivity of the hydrogels. The Ag concentration has a direct effect on the conductivity and swelling ratio, with higher concentrations of Ag ions bringing better conductivity, while also reducing the swelling rate and vice versa. Introduced Au nanorods-NIPAAm composite hydrogels and found that if the temperature was higher than the lower critical solution temperature of the gel matrix, the gel structure would collapse, resulting in on-demand burst release of the drug rather than diffusion-controlled release, which could be used in hydrogel drug delivery systems Shiotani et al. (2007). Cu has been studied as an inexpensive antibacterial agent to add to hydrogels, and Cometa and others fabricated an effective Cu-NPs poly (ethylene-glycol-diacrylate) hydrogel antibacterial coating, in which the high surface/volume ratio of Cu-NPs and charged quaternary ammonium salts conferred effective bactericidal capacity to nanocomposite hydrogels Cometa et al. (2013).

In addition to the many applications of metal nanoparticles in hydrogel fabrication, nanocomposite hydrogels prepared with metal oxides are also widely investigated in cartilage tissue engineering. Prepared nanocomposite hydrogels *via* mixing TiO_2 nanoparticles with chitosan, and the density, compressive resistance, and strength of the composite hydrogels were significantly improved compared with chitosan hydrogel scaffolds without TiO_2 Kumar (2018). In addition, their research also demonstrated that the addition of TiO_2 nanoparticles significantly delayed the degradation of hydrogel scaffolds, which can be beneficial for the balance of neo-cartilage formation and scaffold degradation in cartilage tissue engineering. Fe_3O_4 can promote the proliferation and chondrogenic differentiation of stem cells, and its nanocomposite hydrogel has been widely investigated to prepare porous scaffolds for cartilage repair. The inclusion of Fe_3O_4 in the hydrogel also provides a new strategy for *in situ* monitoring the degradation of the hydrogel scaffold. Combined pulsed electromagnetic fields with Fe_3O_4 embedded magnetic nanocomposite hydrogel, demonstrating that the nano hydrogel has good biocompatibility and pulsed electromagnetic field could effectively promote chondrogenic differentiation of seeded bone marrow stem cells (BMSCs) as well as the repair capacity of cartilage defects Huang et al. (2020). When combining ultra-small superparamagnetic iron oxide and cellulose nanocrystal/silk fibroin (SF), also showcased the possibility to monitor hydrogel degradation and cartilage regeneration process in rabbits Chen et al. (2018). Designed injectable dopamine-modified hydrogel microspheres with charge-guided composite

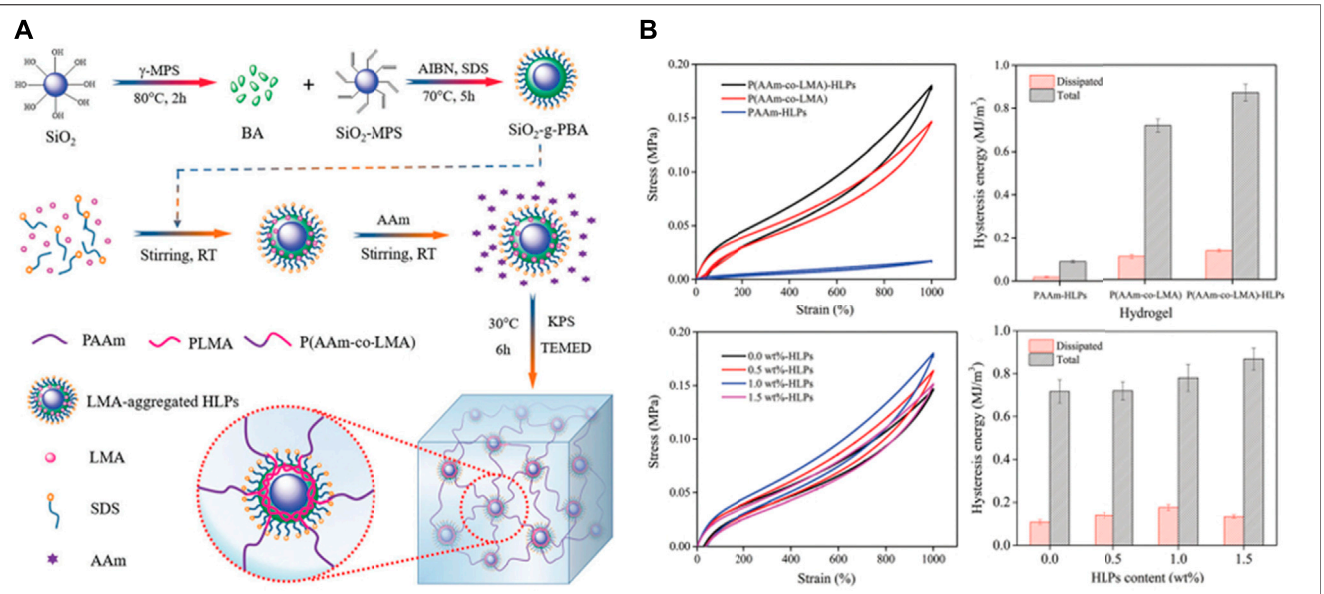

FIGURE 1 | (A) Schematic representation of nanocomposite hydrogels reinforced by core-shell SiO_2-g-PBA hybrid latex particles; **(B)** Loading–unloading cycle behaviors of SiO_2 incorporated nanocomposite hydrogels. Reproduced from Xia et al. (2017) with permission from Copyright 2017 Royal Society of Chemistry.

inclusion, wherein the modified surface helped the adhesion of spheres to cartilage surface and positively charged drug penetrated the cartilage matrix to target chondrocytes under the guidance of negatively charged cartilage matrix Lin et al. (2021). An efficient drug delivery system for cartilage adhesion, cartilage matrix penetration, and chondrocyte targeting was established, which solved the problem that drugs are difficult to penetrate cartilage matrix, significantly improved the utilization rate and efficacy, and effectively inhibited chondrocyte apoptosis. Metal-charged nanocomposite hydrogels showed good potential for medical applications for the regeneration of cartilage.

Although metal and metal-oxide NPs loaded hydrogels in cartilage regeneration have demonstrated promising results, however to date, there is no well-established preparation protocol or clinical practice to achieve these results, therefore, further comprehensive research is needed. Furthermore, the *in vivo* absorption and metabolism of introduced NPs through hydrogel implantation remains unexplored.

Inorganic Nanoparticles

In nanocomposite hydrogels, inorganic nanoparticles also present a wide variety of beneficial functions, such as increasing hydrogel hardness and maintaining a good porous structure of the hydrogel. At present, inorganic nanomaterials commonly used in the biomedical field mainly include silica, calcium phosphate and hydroxyapatite nanoparticles.

Si-NPs were often used as catalysts in previous studies, however the recent reports revealed their unique functions in nanocomposite hydrogel fabrication. Incorporated Si-NPs as cross-linkers into poly (acrylic acid) to fabricate nanocomposite gels, thus generating mechanical properties enhanced composite hydrogels Yang et al. (2013). Si-NPs composite hydrogels have also been shown to have a more sustained drug release profile when loaded with drugs such as doxorubicin. Alvarez and others prepared gentamicin-loaded Si-NPs hydrogel and found that the generated hydrogel could prolong the antibacterial effect through sustained gentamicin release from hydrogel Alvarez et al. (2014). In addition to Si-NPs, SiO_2 nanoparticles are also widely investigated in tissue engineering because of their large surface area and bio-functions. Reported that the composite hydrogel prepared with SiO_2 nano-emulsion particles can withstand larger external forces due to the rigid core of SiO_2, leading to enhanced mechanical properties (**Figure 1**) Xia et al. (2017). Besides, by incorporating mesoporous silica to modify gellan gum and Manuka honey mixed hydrogel, demonstrated the improved mechanical properties, superior cytocompatibility and antibacterial properties *in vitro* and *in vivo* Bonifacio et al. (2020). Furthermore, silica nanoparticles are also considered as great materials for toughening. Due to their advantages of high modulus, large specific surface area, and diverse functionalization as cross-linking agents in combination with hydrogels, silica nanoparticles have great potential in cartilage repair.

Nano-hydroxyapatite (nHA) is one of the most used nanomaterials currently, which has the advantages of good biological activity, great cytocompatibility and appropriate degradation ability, can enhance the formation of extracellular matrix mainly type I collagen in the calcified cartilage layer and subchondral bone area by inducing BMSCs to differentiate into osteoblasts, accelerating the formation of calcified cartilage layer and subchondral bone. At the same time, the degradation process of nHA does not produce harmful substances. Proposed composite hydrogels with nHA for the repair of cartilage defects in rabbits, and they found that composite hydrogels

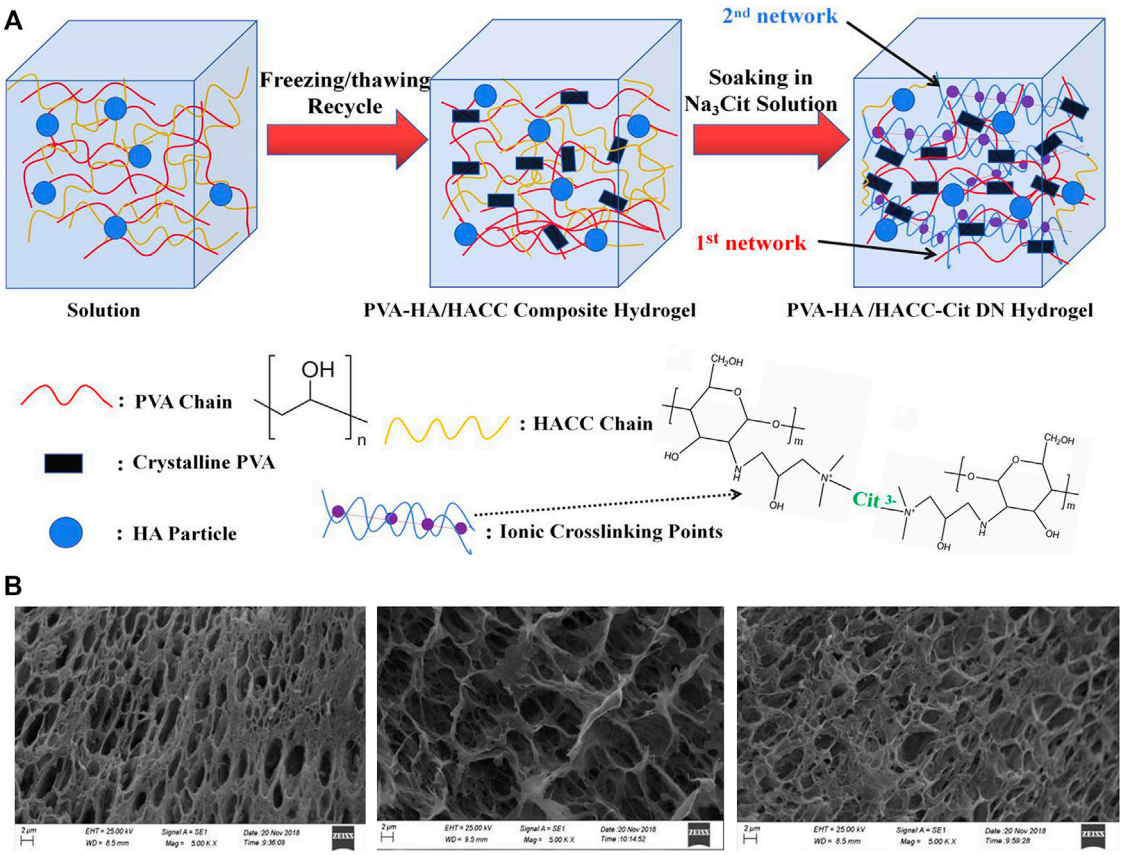

FIGURE 2 | (A) Preparation schematic diagram of the preparation of PVA-HA/HACC-Cit DN hydrogelr; **(B)** SEM images of the cross-section of composite hydrogels. Reproduced from Gan et al. (2020) with permission from Copyright 2020 Elsevier.

had elevated mechanical properties, and were conducive to the adhesion and proliferation of seeded rabbit chondrocytes, with promising potential for the repair of cartilage defects Su et al. (2019). Zhu and coworkers adopted nHA and polylactic acid to prepare cartilage scaffolds and used BMSCs as progenitor cells to repair rabbit full-thickness cartilage defects, the histological and immunohistochemical analyses showed that the cartilage defect was effectively repaired with a large amount of extracellular matrix produced Zhu et al. (2017). A similar repair capacity was also found by through developing composite hydrogels with nHA, adipose-derived stem cells and Kartogenin (KGN) in the rabbit cartilage defect model, and adipose-derived stem cells could maintain good biological morphology and proliferation ability in the composite hydrogels, supporting defect repair Wang Z et al. (2022). Fabricated double-grid nanocomposite hydrogels enhanced by nHA, which showed desirable fatigue resistance and consumption ability because of their unique double-physical cross-linked structure, and the presence of nano-hydroxyapatite helped the nanocomposite hydrogels achieve low friction coefficient, wear resistance, and cytocompatibility (**Figure 2**) Gan et al. (2020). Produced nanocomposite hydrogels by cryogel method with nHA and chitosan, and found that these nanocomposite hydrogels had interconnected porous structures with water content up to 92%, necessary for cell proliferation and differentiation, can be potentially used for cartilage defect repair Kaviani et al. (2019).

In order to achieve optimal mechanical and biological performance for cartilage repair hydrogels, different inorganic nanomaterials in nature have been investigated, focusing on the optimization of moduli, cytocompatibility and bio-functions. However, it is worth noting that the developed nanocomposite hydrogels are still far away from the natural cartilage in terms of physicochemical and structural geometry. How to adopt different organic hydrogel materials and inorganic nanoparticles to properly simulate the cartilage structure has emerged as a new challenge for tissue engineering. Moreover, there is a paucity of studies reporting the *in vivo* performance of newly developed "optimal" hydrogels based on different inorganic NPs, and further evaluation is required (Sultan and Mathew, 2019).

Carbon-Based Nanoparticles

Carbon-based nanomaterials applied in tissue engineering mainly include graphene, carbon nanomaterials, carbonized polymers, and carbon dots (CDs), which play a vital role in enhancing physical and chemical crosslinking in carbon-based nanocomposite hydrogels (Wang et al., 2019). CDs have many advantages including low photobleaching, red fluorescence, good uniformity and biocompatibility, which may be useful to study

the degradation of cartilage hydrogels *in vivo* or track the release and distribution of drugs (Xia C et al., 2018).

In addition to dispersing stress, articular cartilage also has the function of joint surface lubrication *in vivo*. The nanocomposite hydrogel prepared with CDs can be adopted to enhance the lubricity of tissue-engineered cartilage constructs. Applied carbon nanoparticles to prepare composite hydrogels, and CDs were tightly cross-linked to polymers through stable hydrogen bonds in the hydrogels, with stable physicochemical structures and improved lubricating properties Lu et al. (2018). The results showed that the storage modulus and loss modulus of the composite hydrogel were enhanced by the incorporation of CDs, and the nanocomposite hydrogel has a better shear force and higher viscosity, indicating its potential application for injection or bioprinting. In addition, the swelling rate and tensile strength of the composite hydrogel prepared by CDs were also significantly improved in comparison to those of hydrogel prepared conventionally, which was in line with the needs of cartilage tissue engineering. Carbon-based nanomaterials not only have the advantage of optimizing the physical and chemical properties of hydrogels, but also can stimulate cell proliferation, which is beneficial for the repair of cartilage defects. Demonstrated that multi-walled carbon nanotubes can concentrate more proteins and induce the expression of core-binding factor alpha-1 (CBFA1) and collagen type I alpha-1 (COLIA1), leading to promoted chondrogenic differentiation of human adipose-derived stem cells *in vitro*, this suggests their ability to regulate stem cell responses without exogenous growth factors Li et al. (2020). They also found that the incorporation of carbon nanofibers could improve mechanical and electrical properties, promoting cell proliferation and adhesion ability *in vitro*.

Graphene oxide (GO) is a derivative of graphene, which has many oxygen-containing functional groups on its surface that can be chemically modified (Gopinathan et al., 2017). Introduced graphene oxide into bioink that prepared by photo-crosslinked alginate with gelatin and chondroitin sulfate hydrogel, thereby improving biocompatibility and processability, and this nanocomposite hydrogel simulated cartilage extracellular matrix production and greatly improved the shape fidelity and resolution of the 3D printed scaffold Olate-Moya et al. (2020). The *in vitro* proliferation assay of adipose-derived stem cells showed that the nanocomposite hydrogel scaffold promoted seeded cell proliferation than pure alginate, and could induce cartilage differentiation in the absence of exogenous chondrogenic differentiation factors, which makes it very likely to be used in cartilage tissue engineering.

Polymeric Nanoparticles

Polymeric nanomaterials are widely used in cartilage tissue engineering mainly including dendrimers, core-shell particles, and liposomes etc. Because polymeric nanomaterials can be cross-linked by stable bonding, resulting in better regularity and mechanical strength, which have attracted special attention (Mohabatpour et al., 2016). At the beginning of this century, research on polymeric nanomaterials in the field of cartilage repair has been conducted. Dendrimers are hyperbranched polymers with external active functional groups that can combine with biomolecules to improve the solubility while effectively loading the drug into the core structure. Söntjens and others synthesized nano hydrogel scaffolds containing biological dendritic polymers for cartilage tissue repair wherein the hydrogel was a triblock copolymer prepared with PEG as the skeleton and dendritic poly (glycerol-succinic acid) as the terminal group Söntjens et al. (2006). The results illustrated that the addition of an appropriate concentration of dendritic polymers was beneficial to the maintenance of round morphology of encapsulated chondrocytes, and promoted the production of type II collagen and proteoglycans. Since then, they had synthesized several hydrogel materials for cartilage repair using PEG as the core and selectively combined with different dendritic macromolecules containing carbamates and ester bonds as terminal groups, illustrating that the compressive stiffness and viscoelasticity of carbamate-crosslinked dendritic polymer-based hydrogels can be comparable to natural articular cartilage through preparation adjusting. And this hydrogel can be injected into cartilage defect in the form of macromolecular monomer solution, followed by photo-crosslinking and can fit into the defect easily.

The spotlight of the dendritic polymer nanoparticles is that different functional groups can be selected and their concentrations are tailorable to match the desired physicochemical properties. Developed a polyamide-amine dendritic polymer (PAMAM) hydrogel to simulate extracellular matrix (ECM) Wang et al. (2014). Among them, the introduction of PAMAM is beneficial to increasing the crosslinking degree, limiting the expansion of hydrogels and improving their mechanical properties, in addition, the increased terminal groups can potentially be used to conjugate more functional groups. The fabricated scaffold promoted the proliferation and differentiation of mesenchymal stem cells without detectable cytotoxicity, which can be potentially applied in cartilage tissue engineering. In the research of Shen and others, they synthesized dopamine modified alginate (Alg-DA) by modifying alginate (Alg) with dopamine (DA), and polydopamine nanoparticles (PDA NPs) were introduced to generate hydrogel scaffold (Alg-DA/PDA). This nanocomposite hydrogel has high porosity, improved mechanical properties, desirable biocompatibility and appropriate degradation ratio. In addition, a novel nanocomposite hydrogel based on gelatin/polycaprolactone-polyethylene glycol-polycaprolactone (Gel/PCEC) was introduced in Asadi's group by incorporating PCL-PEG copolymer nanoparticles and transforming growth factor-β1 into gelatin hydrogel Asadi et al. (2019). The introduction of PCEC nanoparticles reduced the pore size of the hydrogel and improved the mechanical properties. The fabricated scaffold had good biocompatibility and cell adhesion, and the expression of cartilage-specific ECM genes such as type II collagen and aggrecan were effectively promoted by the designed scaffold. Developed an injectable 3D alginate saline gel including PCL-PEG-PCL (PCEC) microspheres as a carrier for calcium gluconate Liao et al. (2017). The released calcium gluconate promoted the conversion of chondrocyte/alginate suspension

and porous microspheres into gels, effectively mimicking the structure of cartilage. The results demonstrated that the nanocomposite hydrogels have properties preferred for cartilage regeneration including pore connectivity, high compressive modulus, good formability and degradation ratio, which can be used as a suitable matrix for cartilage tissue engineering.

Newly developed nanocomposite hydrogels represent a novel class of biomaterials that have the potential to enhance either mechanical or biological performance. While literature indicates an optimal mechanical property, *in vitro* and limited *in vivo* investigations are part of the dogma in the development of nanocomposite hydrogels and mechanisms for the physicochemical and biological properties promotion are not fully investigated systematically. Challenges lie in how to translate their unique properties into clinical applications. In any case, comprehensive *in vitro, in vivo* and long-term clinical characterization of NP biomaterials and implants are necessary.

FABRICATION STRATEGY

Nanoparticles significantly improve the properties of nanocomposite hydrogels, and their fabrication methods also profoundly affect the physicochemical properties of nanocomposite hydrogel scaffolds. Different fabrication strategy can meet various application requirements, and the main preparation methods of nanocomposite hydrogels include direct injection, electrospinning and 3D printing. In the fabrication process of nanocomposite hydrogels, according to the different timing of the introduction of nanoparticles, it can be mainly attributed to two categories. In the first one, nanoparticles and hydrogels form precast gels and further crosslinking, direct injection and 3D printing fall into this category. In another one, after the crosslinking of hydrogel, the nanoparticles are introduced in the hydrogel matrix, electrospinning falls into this category. The practical application of the different preparation methods and their properties are presented below.

Directing Injection

Injectable hydrogels allow *in situ* repair of cartilage defects by invasive techniques, wherein progenitor cells and growth factors can be delivered through hydrogel to enhance the clinical efficiency (Li et al., 2022; Luo et al., 2022). In comparison to rigid scaffold implantation, hydrogel injection has more advantages in tissue engineering due to its flexible traits in shape adaptability, which is more potential in clinical applications (Taymouri et al., 2021). In recent years, a large number of studies have been conducted to develop nanocomposite hydrogels for direct injection. For example, Obtained injectable hydrogel using polyethylene glycol-poly [L-alanine-poly (L-aspartic acid)] (PEG-PA-PD) triblock copolymers and layered double hydroxide (LDHs) nanocomposites, and performed *in vitro* experiments with tonsil-derived mesenchymal stem cells Lee et al. (2017). Compared with the traditional hydrogel system, the nanocomposite system was helpful to improve cell aggregation and significantly increased the expression of chondrogenic differentiation markers. In addition, the surface of LDHs can be modified by interaction with a variety of other bioactive molecules to design and prepare a variety of injectable nanocomposite hydrogels that can be used for cartilage repair.

However, in order to realize the clinical application of injectable hydrogels, it is necessary to fabricate hydrogel with similar biomechanical properties and composition to human cartilage. Generated silk fibroin-based injectable nanocomposite hydrogels, which have great gel morphology and porosity, and can improve mechanical properties, cell proliferation and nutrient exchange in cell-based therapy (**Figure 3**) Zheng et al. (2021). The results of the co-culture of injectable nano hydrogel with human fibroblasts and BMSCs showed that it had good biocompatibility. Boyer and coworkers prepared a nano-reinforcement clay reinforced hydrogel with an interpenetrating network, and verified that the injectable nanocomposite hydrogel can promote the secretion of glycosaminoglycans and enhance mechanical properties Boyer et al. (2018). Injectable hydrogels are an effective option that can be applied for cartilage repair, as also confirmed by results from animal experiments. Introduced an injectable hydrogel with Kartogenin-encapsulated nanoparticles for repairing porcine cartilage defects Yan et al. (2020). The results of macroscopic observation, micro-computed tomography and histologic revealed that this injectable nanocomposite hydrogel facilitated the repair of hyaline cartilage and subchondral bone in the porcine model. As a convenient and minimally invasive surgical approach, injectable nanohydrogels have important clinical application prospects.Electrospinning

Electrospinning is the preparation of one-dimensional nanoscale fibers by spraying polymer solutions, main electrospinning equipment is composed of a high-voltage power supply device, metal needle syringe and grounding device (Zhang et al., 2020). The preparation technique applied to electrospun nanofibers is relatively simple, and this method can deal with various natural materials or synthetic polymers. Choosing appropriate materials and parameters can easily control the properties of the prepared fibers and apply them in a variety of fields. Electrospun nanofibers have the potential for tissue engineering due to their high surface-to-volume ratio and high porosity (Song et al., 2021). The unique fibrous structure is able to withstand the stress experienced in various tissues, which is very much in line with the needs of cartilage scaffolds. For example, prepared PCL-based composite nanofiber scaffolds by incorporating different concentrations of GO and surface grafted PEG-modified GO-g-PEG through electrospinning, which have high mechanical strength and superior cytocompatibility and can be further used for cartilage repair Scaffaro et al. (2017). In order to obtain a three-dimensional porous nanofiber-reinforced hydrogel scaffold mimicking cartilage extracellular matrix, Gunes and others produced poly (3-hydroxybutyrate-co-3-hydroxyvalerate) nanofiber reinforced carboxymethyl chitosan-silk fibroin hydrogel *via* wet-electrospun Gunes et al. (2020). This composite scaffold obtained by dispersing wet electrospun nanofibers in a polymer matrix can maintain a stable

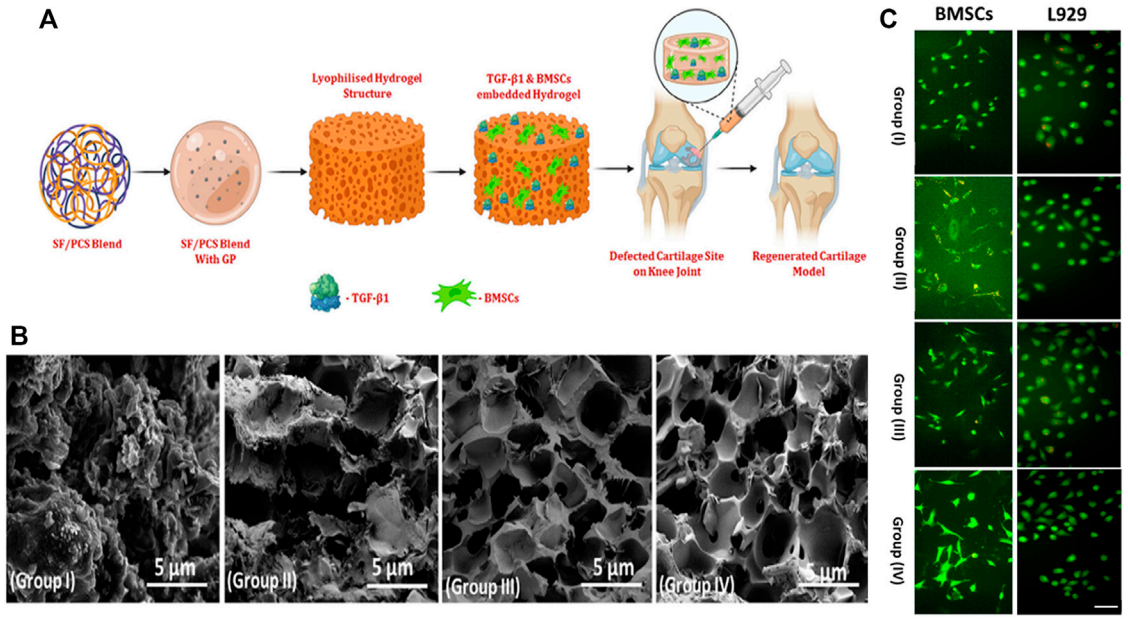

FIGURE 3 | (A) Schematic illustration of BMSCs and TGF-β1 encapsulated SF/PCS injectable hydrogel for cartilage repair; **(B)** The morphological of prepared hydrogel groups with different blending ratios were observed and visualized by SEM analysis; **(C)** Fluorescence microscopic observation of BMSCs and L929 seeded on different hydrogels after 24 h incubation. Reproduced from Zheng et al. (2021) with permission from Copyright 2022 Wiley.

interconnected microporous structure, which supported the differentiation of bone marrow stem cells. In the research of Hejazi's team, they fabricated three-dimensional nanofibrous scaffolds similar to the native cartilage structure, assuming that cells can grow under specific conditions and repair damaged tissue Hejazi et al. (2021). In this study, the gradient nanofiber scaffold was mainly composed of five layers and different materials were adopted according to unique tissue structures, including PCL, gelatin, nHA and chitosan. The multilayered scaffold structure exhibited better mechanical properties and promotes cell proliferation and has great potential in the treatment of cartilage defects. Generated nanocomposite hydrogels using highly negatively charged star-shaped poly (ethylene glycol)/heparin hydrogels (sPEG/Hep) as cartilage extracellular matrices *via* electrospinning technique, and the hydrogels combined with mPCL melt electrospun fiber networks showed mechanical morphology and internal structure similar to native cartilage, providing a suitable microenvironment for chondrocyte culture *in vitro* Bas et al. (2017). Subsequently, they also used finite element to build models to further simulate the deformation mechanism of the hydrogel structure and to predict the compressive modulus.

Electrospinning technology is also applied to drug sustained release and delivery systems because of its unique preparation technology, and the characteristics are also useful for the treatment of cartilage diseases. Applied coaxial electrospinning technology to encapsulate glucosamine sulfate (GAS) into the core of polycaprolactone (PCL) nanofibers, and this nanofiber structure can allow the continuous release of GAS over time. The results confirm that coaxial electrospinning can prepare GAS-loaded nanofibers with good tensile properties (Chen et al., 2020). *In vitro* experiments have shown that this nanofiber has a significant effect on the proliferation of rat articular chondrocytes, demonstrating its promise application in the field of cartilage tissue engineering. In another study, Zare and coworkers applied electrospinning to prepare composites synthesized from alginate, Kartogenin, and PLGA (**Figure 4**) Zare et al. (2021). As a scaffold/drug delivery system, the elastic modulus of this composite is significantly increased than that of the traditional hydrogels, and the results of resazurin test and Live/Dead staining confirmed that the composite can promote adipocyte mesenchymal stem cells to maintain better cell morphology and viability.

3D Printing

3D printing can fabricate a variety of customizable complex structures and has been widely used in many fields (Li P et al., 2021; Li Q et al., 2021). Among them, the application of 3D printing in the field of tissue engineering can endow the 3D structure fabrication, facilitating the incorporation of target cells and growth factors so as to construct biologically active tissue or organ analogs (Han et al., 2021; Wei et al., 2021). Previous studies have reported the preparation of hydrogel scaffolds *via* 3D printing. For example, used silk fibroin hydrogel modified with glycidyl methacrylate as bioink for 3D printing, and verified that it was a feasible strategy to form silk fibroin hydrogel scaffold with good biocompatibility and complex structures Kim et al. (2018). Introduced nanocomposite hydrogel constructs *via* 3D printing and post-photo-crosslinked, which achieved the regulation of macroscopic shape and internal pore structure, and regenerated mature cartilage with cartilage-specific ECM Xia H et al. (2018). Dutta

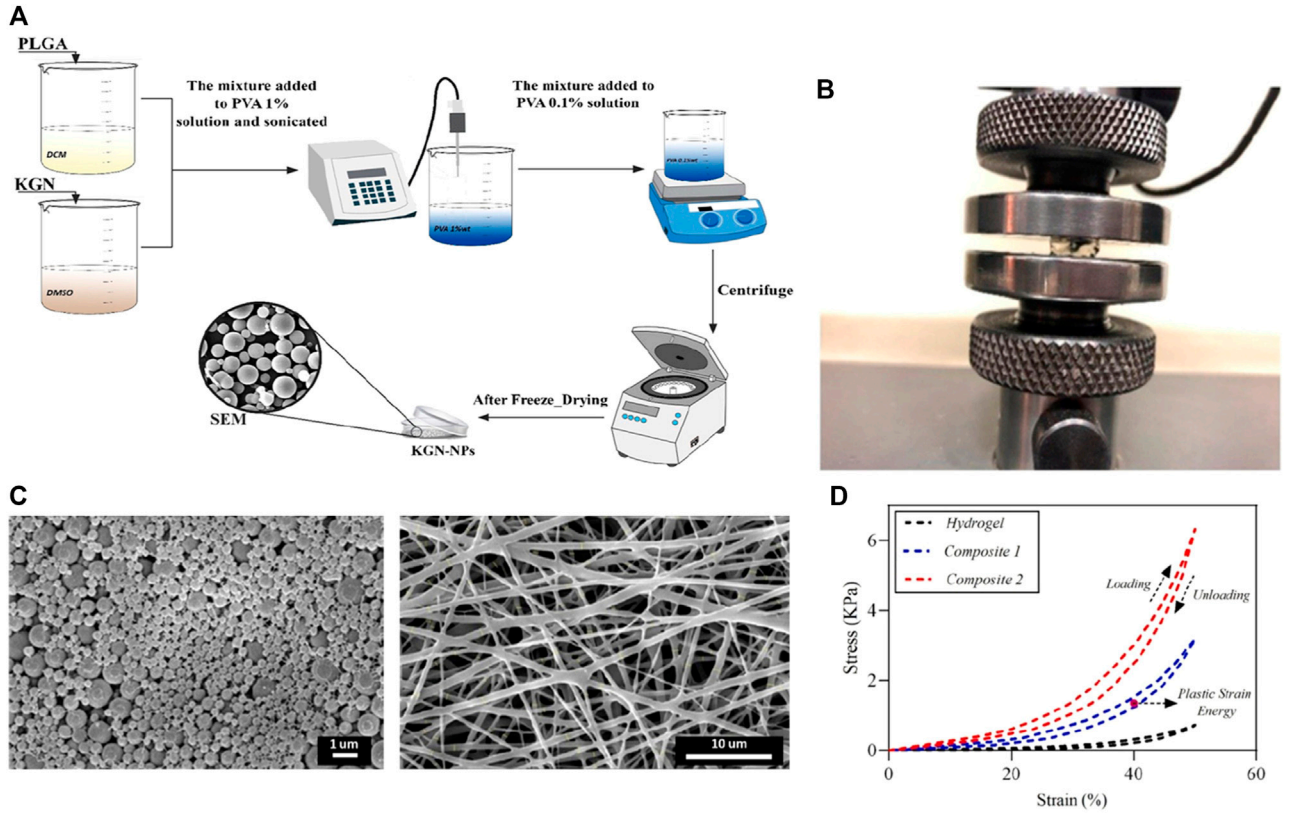

FIGURE 4 | (A) Schematic illustration of the synthesis of KGN-PLGA nanoparticles; **(B)** The mechanical test of fabricated samples; **(C)** The FESEM images of KGN-PLGA nanoparticles and Gelatin electrospun mat; **(D)** The results of hysteresis loop at 50% strain. Reproduced from Zare et al. (2021) with permission from Copyright 2021 Elsevier.

and others designed 3D-printable hybrid biodegradable hydrogels, which is composed of alginate, gelatin, and cellulose nanocrystals (**Figure 5**) Dutta et al. (2021). They demonstrated that the 3D printed scaffold can provide a favorable environment for cell proliferation, adhesion and nutrient exchange in tissue engineering applications.

3D printed cartilage scaffold with nanocomposite hydrogel can also promote cartilage repair by controlling the sustained release of incorporated growth factors. Reported two kinds of nanocomposite hydrogels that were prepared by introducing hydrothermally treated nHA and poly (lactic-co-glycolic acid) (PLGA) nanoparticles with nucleocapsid structure Castro et al. (2015). The results illustrated scaffolds fabricated with a composite hydrogel containing nHA were more conducive to the proliferation of MSCs than the PLGA hydrogel, while increased the compressive modulus as well. Nanocomposite hydrogel containing PLGA nanoparticles and TGF-β1 could achieve sustained release of TGF-β1 in fabricated cartilage scaffolds.

The natural cartilage has a gradient structure, and the artificial scaffolds are expected to have similar mechanical properties. There have been a large number of studies on joint cartilage, and 3D printing provides an effective way to better repair cartilage by preparing multilayer hydrogels with gradient hardness (Mancini et al., 2020). For instance, prepared cartilage repair scaffolds containing GO and HA nanoparticles *via* 3D printing. The designed scaffold had a specific structure with a smooth and flat surface, which was conducive to material load-bearing Meng et al. (2020). And the distance between the stents from top to bottom increased layer by layer, which was conducive to the formation of a firm connection between the material and the bone base, while there was no interface for the tight connection between each layer so as to prevent the loosening and shedding of the sample after implantation. In addition, it is concluded that the introduction of GO-HA can reduce the intermolecular hydrogen bonding and molecular entanglement density, and improve the dynamic viscosity of hydrogels. The solution shows obvious shear behavior in the range of printing shear rate, which can effectively avoid extrusion expansion, so improving the applicable range of sample printing and the condition parameters in the printing process. Reported a 3D printed nanocomposite scaffold to mimic the natural structure of artificial cartilage Liu et al. (2020). They firstly prepared PLGA electrospun nanofiber incorporated hydroxybutyl chitosan hydrogels and then injected it into PCL framework with an internal microchannel, which offered the nanocomposite hydrogel with preferable mechanical support and substance

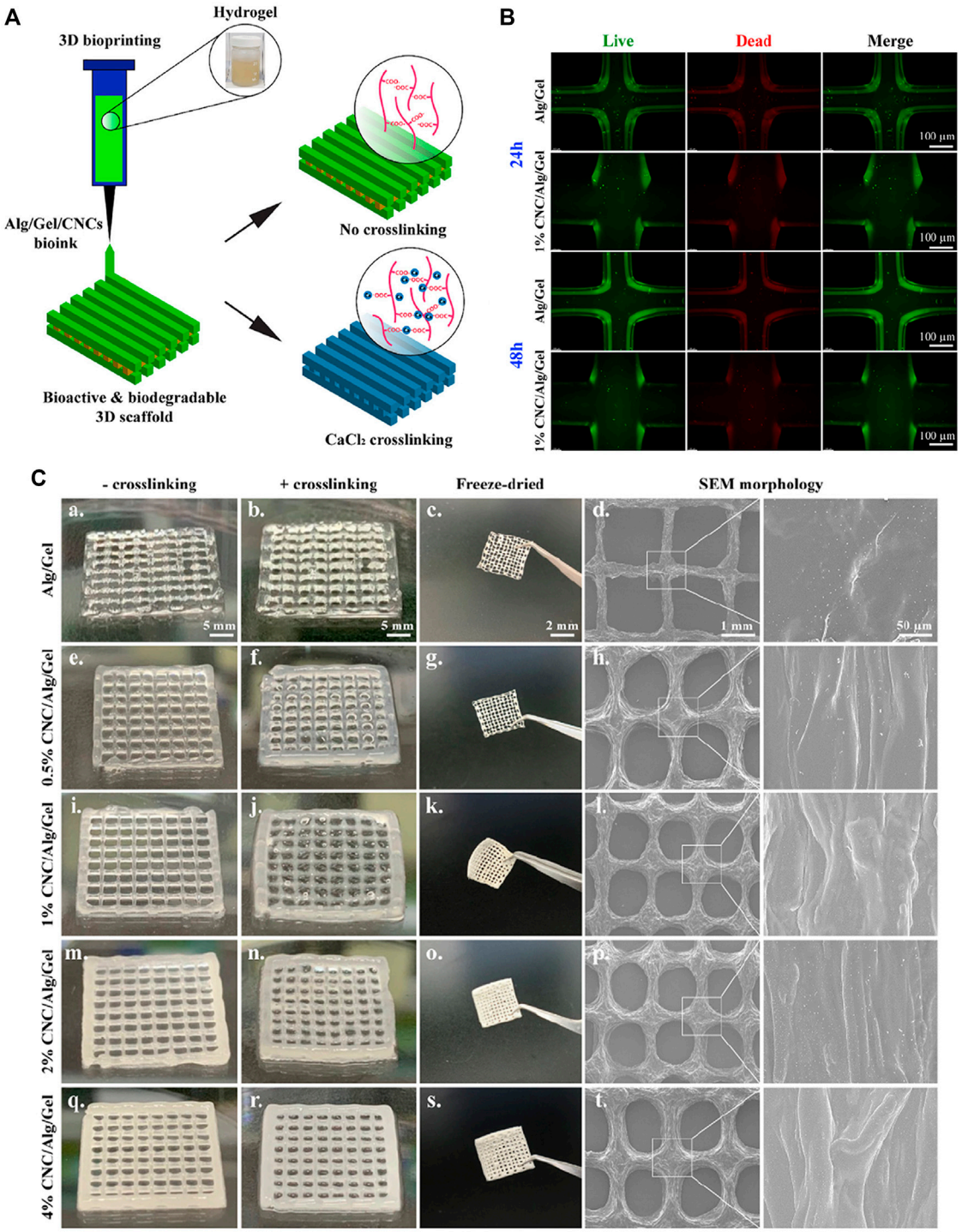

FIGURE 5 | (A) Schematic representation of 3D bioprinting using Alg/Gel/CNCs hydrogels for tissue engineering; **(B)** Images of Live/Dead assay of 3D bio-printed cell-laden constructs (Alg/Gel and 1% Alg/gel) at indicated time intervals; **(C)** Digital photographs showing the un-crosslinked, crosslinked, and fridge-dried scaffolds after 3D printing; SEM images showing the internal structure of printed scaffolds. Reproduced from Dutta et al. (2021) with permission from Copyright 2021 Elsevier.

exchange. Their research suggested that 3D printing is a feasible strategy to regulate the inner structure for providing an ideal biomimetic microenvironment for chondrogenic differentiation.

The properties of the material itself used for 3D printing also have a large impact on the scaffold performance, for example, prepared cell-free bilayer scaffolds by low-temperature deposition using GelMA as a matrix with HA incorporated into the

subchondral scaffold Gao et al. (2021). The effects of line spacing and line width of printed scaffolds on the cartilage regeneration in rabbits were evaluated, including the pore size, porosity, specific surface area and mechanical strength etc. Their results showed that with the increase of line spacing, the mechanical properties of the materials progressively decreased. The properly spaced scaffold presented cartilage regeneration with cartilage lacunae and subchondral bone formation. Therefore, the tractable rheological behavior of soft matter can be used to improve 3D printing, while bilayer hybrid scaffolds generated by continuous 3D printing are expected to be biomaterials for regenerating articular cartilage.

Cartilage tissue engineering aims to generate autologous cartilage-like grafts for defect therapy by defined positioning of growth factors, progenitor cells, and biomaterials in a 3D hierarchical manner, leading to the generation of mature cartilage tissue. Ongoing challenges toward functional cartilage regeneration, such as structural reconstruction, chemical simulation and cellular incorporation, are unlikely to be overcome by a single biomaterial and manufacturing technology. Advanced bio-fabrication strategies, through combining different nanocomposite hydrogels and manufacturing technologies are an emerging trend toward the recapitulation of the delicate and intricate structure of natural cartilage. However, following the current publications, it is still a challenge to speculate on how the optimal cartilage biomaterial/grafts should be developed to maximize regeneration capacity upon injection or implantation. Possibly, the revolution of new strategies that are capable of closely recapitulating the macro-/micro-structure of cartilage tissue and allowing the precise placement of different progenitor cells, growth factors, or bioactive elements will help achieve the desired biological functions.Conclusion and Future Perspectives.

Nanomedicine has been applied in different fields of biomedicine, including diagnosis, imaging, pharmaceutics and regenerative medicine, which also brings new directions for cartilage tissue engineering technology and contributes to cartilage regeneration and repair. Nanocomposite hydrogels change the physical and chemical function as well as biocompatibility of hydrogels based on the unique properties of nanoparticles, and the strong support of scaffold structure avoids the damage of hydrogels under compression *in vivo*, which has a promising application prospect in the field of cartilage tissue engineering. At present, although great progress has been made in the study of cartilage tissue engineering, it still faces many challenges and difficult problems. For example, whether the nanocomposite hydrogel can sustain good physicochemical properties under load-bearing conditions and provide strong support in cartilage defects. Degradability is also an important factor to be considered in the application of nanocomposite hydrogels in cartilage tissue engineering, and the degradation time should neither be too long nor too fast. On the one hand, it needs to provide physical and biochemical microenvironment support during tissue healing, and on the other hand, it also needs to have suitable degradability to reduce the adverse effects caused by the long-term residual of the scaffold material.

In this review, we introduce the relevant research progress of nanohydrogels for cartilage repair, and summarize the main nanomaterials currently applied in the preparation of nanocomposite hydrogels and related preparation techniques. Different fabrication techniques have their specific advantages, for example, 3D bio-printing fabricates hydrogel scaffolds with controllable porosity and internal structure, which is conducive to the transport of nutrients and the discharge of metabolites, and the characteristics can promote the migration, proliferation and differentiation of seeded cells in cartilage tissue engineering, which is of great significance for cartilage defect repair. However, the current materials science and engineering approach typically focus on the material design and scaffold geometry optimization concerning mechanical properties, geometry as well as unique bio-functions by means of *in vitro* testing or small animal evaluation. Many of them are yet to be evaluated by *in vivo* large animal studies and become the convention in clinical practice. Furthermore, *in vitro* and *in vivo* investigations to date typically emphasize biocompatibility and cartilage regeneration performance with a focus on very limited parameters in the short term. There is often little to no investigation in the longer term.

Promising future directions in nanocomposite hydrogel development for cartilage regeneration is the decoupling of different research in material development, scaffold design, fabrication optimization and adaptation of the implant following long-term cartilage remodeling. In the short term, nanocomposite hydrogels do not have subversive therapeutic effects on cartilage repair. There is still a long way to apply nanocomposite hydrogels in the clinical repair of cartilage, and different nanomaterials have their unique characteristics. How to combine these characteristics for cartilage repair in order to obtain the best repair effect remains unexplored.

AUTHOR CONTRIBUTIONS

YA and JL reviewed recent literature and drafted the present manuscript, EZ and YL made suggestions, FW and LY provided expert analysis and revised manuscript. All authors have read and agreed to the published version of the manuscript.

FUNDING

The authors acknowledge the funding provided by National Natural Science Foundation of China (No. 82172429), Department of Science and Technology of Chongqing Province (No. cstc2021jxjl130014).

REFERENCES

Advincula, R. C., Dizon, J. R. C., Caldona, E. B., Viers, R. A., Siacor, F. D. C., Maalihan, R. D., et al. (2021). On the Progress of 3D-Printed Hydrogels for Tissue Engineering. *MRS Commun.* 11 (5), 539–553. doi:10.1557/s43579-021-00069-1

Alvarez, G. S., Hélary, C., Mebert, A. M., Wang, X., Coradin, T., and Desimone, M. F. (2014). Antibiotic-loaded Silica Nanoparticle-Collagen Composite Hydrogels with Prolonged Antimicrobial Activity for Wound Infection Prevention. *J. Mat. Chem. B* 2 (29), 4660–4670. doi:10.1039/c4tb00327f

Ao, Y., Li, Z., You, Q., Zhang, C., Yang, L., and Duan, X. (2019). The Use of Particulated Juvenile Allograft Cartilage for the Repair of Porcine Articular Cartilage Defects. *Am. J. Sports Med.* 47 (10), 2308–2315. doi:10.1177/0363546519856346

Armiento, A. R., Stoddart, M. J., Alini, M., and Eglin, D. (2018). Biomaterials for Articular Cartilage Tissue Engineering: Learning from Biology. *Acta Biomater.* 65, 1–20. doi:10.1016/j.actbio.2017.11.021

Asadi, N., Alizadeh, E., Rahmani Del Bakhshayesh, A., Mostafavi, E., Akbarzadeh, A., and Davaran, S. (2019). Fabrication and *In Vitro* Evaluation of Nanocomposite Hydrogel Scaffolds Based on Gelatin/PCL-PEG-PCL for Cartilage Tissue Engineering. *ACS Omega* 4, 449–457. doi:10.1021/acsomega.8b02593

Asadi, N., Alizadeh, E., Salehi, R., Khalandi, B., Davaran, S., and Akbarzadeh, A. (2018). Nanocomposite Hydrogels for Cartilage Tissue Engineering: a Review. *Artif. Cells, Nanomedicine, Biotechnol.* 46 (3), 465–471. doi:10.1080/21691401.2017.1345924

Barani, H., Montazer, M., Samadi, N., and Toliyat, T. (2012). *In Situ* synthesis of Nano Silver/lecithin on Wool: Enhancing Nanoparticles Diffusion. *Colloids Surfaces B Biointerfaces* 92, 9–15. doi:10.1016/j.colsurfb.2011.10.062

Bas, O., De-Juan-Pardo, E. M., Meinert, C., D'Angella, D., Baldwin, J. G., Bray, L. J., et al. (2017). Biofabricated Soft Network Composites for Cartilage Tissue Engineering. *Biofabrication* 9 (2), 025014. doi:10.1088/1758-5090/aa6b15

Bonifacio, M. A., Cochis, A., Cometa, S., Scalzone, A., Gentile, P., Procino, G., et al. (2020). Advances in Cartilage Repair: The Influence of Inorganic Clays to Improve Mechanical and Healing Properties of Antibacterial Gellan Gum-Manuka Honey Hydrogels. *Mater. Sci. Eng. C* 108, 110444. doi:10.1016/j.msec.2019.110444

Boyer, C., Figueiredo, L., Pace, R., Lesoeur, J., Rouillon, T., Visage, C. L., et al. (2018). Laponite Nanoparticle-Associated Silated Hydroxypropylmethyl Cellulose as an Injectable Reinforced Interpenetrating Network Hydrogel for Cartilage Tissue Engineering. *Acta Biomater.* 65, 112–122. doi:10.1016/j.actbio.2017.11.027

Castro, N. J., O'brien, J., and Zhang, L. G. (2015). Integrating Biologically Inspired Nanomaterials and Table-Top Stereolithography for 3D Printed Biomimetic Osteochondral Scaffolds. *Nanoscale* 7 (33), 14010–14022. doi:10.1039/c5nr03425f

Chen, W., Wang, C., Gao, Y., Wu, Y., Wu, G., Shi, X., et al. (2020). Incorporating Chitin Derived Glucosamine Sulfate into Nanofibers via Coaxial Electrospinning for Cartilage Regeneration. *Carbohydr. Polym.* 229, 115544. doi:10.1016/j.carbpol.2019.115544

Chen, Z., Yan, C., Yan, S., Liu, Q., Hou, M., Xu, Y., et al. (2018). Non-invasive Monitoring of *In Vivo* Hydrogel Degradation and Cartilage Regeneration by Multiparametric MR Imaging. *Theranostics* 8 (4), 1146–1158. doi:10.7150/thno.22514

Cometa, S., Iatta, R., Ricci, M. A., Ferretti, C., and De Giglio, E. (2013). Analytical Characterization and Antimicrobial Properties of Novel Copper Nanoparticle-Loaded Electrosynthesized Hydrogel Coatings. *J. Bioact. Compatible Polym.* 28 (5), 508–522. doi:10.1177/0883911513498960

Dutta, S. D., Hexiu, J., Patel, D. K., Ganguly, K., and Lim, K.-T. (2021). 3D-printed Bioactive and Biodegradable Hydrogel Scaffolds of Alginate/gelatin/cellulose Nanocrystals for Tissue Engineering. *Int. J. Biol. Macromol.* 167, 644–658. doi:10.1016/j.ijbiomac.2020.12.011

Eftekhari, A., Maleki Dizaj, S., Sharifi, S., Salatin, S., Rahbar Saadat, Y., Zununi Vahed, S., et al. (2020). The Use of Nanomaterials in Tissue Engineering for Cartilage Regeneration; Current Approaches and Future Perspectives. *Int. J. Mol. Sci.* 21 (2), 536. doi:10.3390/ijms21020536

Farokhi, M., Jonidi Shariatzadeh, F., Solouk, A., and Mirzadeh, H. (2020). Alginate Based Scaffolds for Cartilage Tissue Engineering: A Review. *Int. J. Polym. Mater. Polym. Biomaterials* 69 (4), 230–247. doi:10.1080/00914037.2018.1562924

Gan, S., Lin, W., Zou, Y., Xu, B., Zhang, X., Zhao, J., et al. (2020). Nano-hydroxyapatite Enhanced Double Network Hydrogels with Excellent Mechanical Properties for Potential Application in Cartilage Repair. *Carbohydr. Polym.* 229, 115523. doi:10.1016/j.carbpol.2019.115523

Gao, J., Ding, X., Yu, X., Chen, X., Zhang, X., Cui, S., et al. (2021). Cell-Free Bilayered Porous Scaffolds for Osteochondral Regeneration Fabricated by Continuous 3D-Printing Using Nascent Physical Hydrogel as Ink. *Adv. Healthc. Mat.* 10 (3), 2001404. doi:10.1002/adhm.202001404

Gopinathan, J., Pillai, M. M., Sahanand, K. S., Rai, B. K. D., Selvakumar, R., and Bhattacharyya, A. (2017). Synergistic Effect of Electrical Conductivity and Biomolecules on Human Meniscal Cell Attachment, Growth, and Proliferation in Poly- ε -caprolactone Nanocomposite Scaffolds. *Biomed. Mat.* 12 (6), 065001. doi:10.1088/1748-605x/aa7f7b

Gunes, O. C., Albayrak, A. Z., Tasdemir, S., and Sendemir, A. (2020). Wet-electrospun PHBV Nanofiber Reinforced Carboxymethyl Chitosan-Silk Hydrogel Composite Scaffolds for Articular Cartilage Repair. *J. Biomater. Appl.* 35 (4-5), 515–531. doi:10.1177/0885328220930714

Han, X., Chang, S., Zhang, M., Bian, X., Li, C., and Li, D. (2021). Advances of Hydrogel-Based Bioprinting for Cartilage Tissue Engineering. *Front. Bioeng. Biotechnol.* 9, 746564. doi:10.3389/fbioe.2021.746564

Haraguchi, K., and Takehisa, T. (2002). Nanocomposite Hydrogels: A Unique Organic–Inorganic Network Structure with Extraordinary Mechanical, Optical, and Swelling/de-Swelling Properties. *Adv. Mat.* 14 (16), 1120–1124. doi:10.1002/1521-4095(20020816)14:16<1120::aid-adma1120>3.0.co;2-9

Hejazi, F., Bagheri-Khoulenjani, S., Olov, N., Zeini, D., Solouk, A., and Mirzadeh, H. (2021). Fabrication of Nanocomposite/nanofibrous Functionally Graded Biomimetic Scaffolds for Osteochondral Tissue Regeneration. *J. Biomed. Mater Res.* 109 (9), 1657–1669. doi:10.1002/jbm.a.37161

Huang, J., Jia, Z., Liang, Y., Huang, Z., Rong, Z., Xiong, J., et al. (2020). Pulse Electromagnetic Fields Enhance the Repair of Rabbit Articular Cartilage Defects with Magnetic Nano-Hydrogel. *RSC Adv.* 10 (1), 541–550. doi:10.1039/c9ra07874f

Kashte, S., Dhumal, R., Chaudhary, P., Sharma, R. K., Dighe, V., and Kadam, S. (2021). Bone Regeneration in Critical-Size Calvarial Defect Using Functional Biocompatible Osteoinductive Herbal Scaffolds and Human Umbilical Cord Wharton's Jelly-Derived Mesenchymal Stem Cells. *Mater. Today Commun.* 26, 102049. doi:10.1016/j.mtcomm.2021.102049

Kaviani, A., Zebarjad, S. M., Javadpour, S., Ayatollahi, M., and Bazargan-Lari, R. (2019). Fabrication and Characterization of Low-Cost Freeze-Gelated Chitosan/collagen/hydroxyapatite Hydrogel Nanocomposite Scaffold. *Int. J. Polym. Analysis Charact.* 24 (3), 191–203. doi:10.1080/1023666x.2018.1562477

Keshvardoostchokami, M., Majidi, S. S., Huo, P., Ramachandran, R., Chen, M., and Liu, B. (2021). Electrospun Nanofibers of Natural and Synthetic Polymers as Artificial Extracellular Matrix for Tissue Engineering. *Nanomaterials* 11 (1), 21. doi:10.3390/nano11010021

Kim, S. H., Yeon, Y. K., Lee, J. M., Chao, J. R., Lee, Y. J., Seo, Y. B., et al. (2018). Precisely Printable and Biocompatible Silk Fibroin Bioink for Digital Light Processing 3D Printing. *Nat. Commun.* 9 (1), 1620. doi:10.1038/s41467-018-03759-y

Kumar, P. (2018). Nano-TiO2 Doped Chitosan Scaffold for the Bone Tissue Engineering Applications. *Int. J. Biomater.* 2018, 6576157. doi:10.1155/2018/6576157

Lee, S. S., Choi, G. E., Lee, H. J., Kim, Y., Choy, J.-H., and Jeong, B. (2017). Layered Double Hydroxide and Polypeptide Thermogel Nanocomposite System for Chondrogenic Differentiation of Stem Cells. *ACS Appl. Mat. Interfaces* 9 (49), 42668–42675. doi:10.1021/acsami.7b17173

Li, P., Fu, L., Liao, Z., Peng, Y., Ning, C., Gao, C., et al. (2021). Chitosan hydrogel/3D-Printed Poly(ε-Caprolactone) Hybrid Scaffold Containing Synovial Mesenchymal Stem Cells for Cartilage Regeneration Based on Tetrahedral Framework Nucleic Acid Recruitment. *Biomaterials* 278, 121131. doi:10.1016/j.biomaterials.2021.121131

Li, Q., Xu, S., Feng, Q., Dai, Q., Yao, L., Zhang, Y., et al. (2021). 3D Printed Silk-Gelatin Hydrogel Scaffold with Different Porous Structure and Cell Seeding Strategy for Cartilage Regeneration. *Bioact. Mater.* 6 (10), 3396–3410. doi:10.1016/j.bioactmat.2021.03.013

Li, R., Zhou, C., Chen, J., Luo, H., Li, R., Chen, D., et al. (2022). Synergistic Osteogenic and Angiogenic Effects of KP and QK Peptides Incorporated with an Injectable and Self-Healing Hydrogel for Efficient Bone Regeneration. *Bioact. Mater.* 18, 267–283. doi:10.1016/j.bioactmat.2022.02.011

Li, X., Chen, S., Li, J., Wang, X., Zhang, J., Kawazoe, N., et al. (2016). 3d Culture of Chondrocytes in Gelatin Hydrogels with Different Stiffness. *Polymers* 8 (8), 269. doi:10.3390/polym8080269

Li, Y., Chen, M., Zhou, W., Gao, S., Luo, X., Peng, L., et al. (2020). Cell-free 3D Wet-Electrospun PCL/silk fibroin/Sr2+ Scaffold Promotes Successful Total Meniscus Regeneration in a Rabbit Model. *Acta Biomater.* 113, 196–209. doi:10.1016/j.actbio.2020.06.017

Liao, J., Wang, B., Huang, Y., Qu, Y., Peng, J., and Qian, Z. (2017). Injectable Alginate Hydrogel Cross-Linked by Calcium Gluconate-Loaded Porous Microspheres for Cartilage Tissue Engineering. *ACS Omega* 2 (2), 443–454. doi:10.1021/acsomega.6b00495

Lin, F., Wang, Z., Xiang, L., Deng, L., and Cui, W. (2021). Charge-Guided Micro/Nano-Hydrogel Microsphere for Penetrating Cartilage Matrix. *Adv. Funct. Mat.* 31 (49), 2107678. doi:10.1002/adfm.202107678

Liu, X., Song, S., Huang, J., Fu, H., Ning, X., He, Y., et al. (2020). HBC-nanofiber Hydrogel Scaffolds with 3D Printed Internal Microchannels for Enhanced Cartilage Differentiation. *J. Mat. Chem. B* 8 (28), 6115–6127. doi:10.1039/d0tb00616e

Liu, Y., Wang, M., Luo, Y., Liang, Q., Yu, Y., Chen, F., et al. (2021). Enhancing Stem Cell Therapy for Cartilage Repair in Osteoarthritis-A Hydrogel Focused Approach. *Gels* 7 (4), 263. doi:10.3390/gels7040263

Lu, H., Lv, L., Ma, J., Ban, W., Ren, S., Dong, G., et al. (2018). Carbon Dots Intensified Poly (Ethylene Glycol)/chitosan/sodium Glycerophosphate Hydrogel as Artificial Synovium Tissue with Slow-Release Lubricant. *J. Mech. Behav. Biomed. Mater.* 88, 261–269. doi:10.1016/j.jmbbm.2018.08.024

Luo, L., Gong, J., Wang, Z., Liu, Y., Cao, J., Qin, J., et al. (2022). Injectable Cartilage Matrix Hydrogel Loaded with Cartilage Endplate Stem Cells Engineered to Release Exosomes for Non-invasive Treatment of Intervertebral Disc Degeneration. *Bioact. Mater.* 15, 29–43. doi:10.1016/j.bioactmat.2021.12.007

Mancini, I. A. D., Schmidt, S., Brommer, H., Pouran, B., Schäfer, S., Tessmar, J., et al. (2020). A Composite hydrogel-3D Printed Thermoplast Osteochondral Anchor as Example for a Zonal Approach to Cartilage Repair: *In Vivo* Performance in a Long-Term Equine Model. *Biofabrication* 12 (3), 035028. doi:10.1088/1758-5090/ab94ce

Meng, Y., Cao, J., Chen, Y., Yu, Y., and Ye, L. (2020). 3D Printing of a Poly(vinyl Alcohol)-Based Nano-Composite Hydrogel as an Artificial Cartilage Replacement and the Improvement Mechanism of Printing Accuracy. *J. Mat. Chem. B* 8 (4), 677–690. doi:10.1039/c9tb02278c

Merino, S., Martín, C., Kostarelos, K., Prato, M., and Vázquez, E. (2015). Nanocomposite Hydrogels: 3D Polymer-Nanoparticle Synergies for On-Demand Drug Delivery. *ACS Nano* 9 (5), 4686–4697. doi:10.1021/acsnano.5b01433

Miramini, S., Fegan, K. L., Green, N. C., Espino, D. M., Zhang, L., and Thomas-Seale, L. E. J. (2020). The Status and Challenges of Replicating the Mechanical Properties of Connective Tissues Using Additive Manufacturing. *J. Mech. Behav. Biomed. Mater.* 103, 103544. doi:10.1016/j.jmbbm.2019.103544

Mohabatpour, F., Karkhaneh, A., and Sharifi, A. M. (2016). A Hydrogel/fiber Composite Scaffold for Chondrocyte Encapsulation in Cartilage Tissue Regeneration. *RSC Adv.* 6 (86), 83135–83145. doi:10.1039/c6ra15592h

Niemczyk-Soczynska, B., Gradys, A., Kolbuk, D., Krzton-Maziopa, A., and Sajkiewicz, P. (2019). Crosslinking Kinetics of Methylcellulose Aqueous Solution and its Potential as a Scaffold for Tissue Engineering. *Polym. (Basel)* 11 (11), 1772. doi:10.3390/polym11111772

Olate-Moya, F., Arens, L., Wilhelm, M., Mateos-Timoneda, M. A., Engel, E., and Palza, H. (2020). Chondroinductive Alginate-Based Hydrogels Having Graphene Oxide for 3d Printed Scaffold Fabrication. *ACS Appl. Mat. Interfaces* 12 (4), 4343–4357. doi:10.1021/acsami.9b22062

Qiao, K., Xu, L., Tang, J., Wang, Q., Lim, K. S., Hooper, G., et al. (2022). The Advances in Nanomedicine for Bone and Cartilage Repair. *J. Nanobiotechnol.* 20 (1), 141. doi:10.1186/s12951-022-01342-8

Scaffaro, R., Lopresti, F., Maio, A., Botta, L., Rigogliuso, S., and Ghersi, G. (2017). Electrospun PCL/GO-g-PEG Structures: Processing-Morphology-Properties Relationships. *Compos. Part A Appl. Sci. Manuf.* 92, 97–107. doi:10.1016/j.compositesa.2016.11.005

Shi, Z., Zhong, Q., Chen, Y., Gao, J., Pan, X., Lian, Q., et al. (2021). Nanohydroxyapatite, Nanosilicate-Reinforced Injectable, and Biomimetic Gelatin-Methacryloyl Hydrogel for Bone Tissue Engineering. *Int. J. Nanomed.* 16, 5603–5619. doi:10.2147/ijn.s321387

Shiotani, A., Mori, T., Niidome, T., Niidome, Y., and Katayama, Y. (2007). Stable Incorporation of Gold Nanorods into N-Isopropylacrylamide Hydrogels and Their Rapid Shrinkage Induced by Near-Infrared Laser Irradiation. *Langmuir* 23 (7), 4012–4018. doi:10.1021/la0627967

Song, J. Y., Ryu, H. I., Lee, J. M., Bae, S. H., Lee, J. W., Yi, C. C., et al. (2021). Conformal Fabrication of an Electrospun Nanofiber Mat on a 3d Ear Cartilage-Shaped Hydrogel Collector Based on Hydrogel-Assisted Electrospinning. *Nanoscale Res. Lett.* 16 (1), 116. doi:10.1186/s11671-021-03571-6

Söntjens, S. H., Nettles, D. L., Carnahan, M. A., Setton, L. A., and Grinstaff, M. W. (2006). Biodendrimer-based Hydrogel Scaffolds for Cartilage Tissue Repair. *Biomacromolecules* 7 (1), 310–316. doi:10.1021/bm050663e

Su, W., Hu, Y., Zeng, M., Li, M., Lin, S., Zhou, Y., et al. (2019). Design and Evaluation of Nano-Hydroxyapatite/poly(vinyl Alcohol) Hydrogels Coated with Poly(lactic-Co-Glycolic Acid)/nano-Hydroxyapatite/poly(vinyl Alcohol) Scaffolds for Cartilage Repair. *J. Orthop. Surg. Res.* 14 (1), 446. doi:10.1186/s13018-019-1450-0

Sultan, S., and Mathew, A. P. (2019). 3d Printed Porous Cellulose Nanocomposite Hydrogel Scaffolds. *J. Vis. Exp.* 146, e59401. doi:10.3791/59401

Tang, X., Wang, S., Zhan, S., Niu, J., Tao, K., Zhang, Y., et al. (2016). The Prevalence of Symptomatic Knee Osteoarthritis in china: Results from the china Health and Retirement Longitudinal Study. *Arthritis & Rheumatology* 68 (3), 648–653. doi:10.1002/art.39465

Taymouri, S., Amirkhani, S., and Mirian, M. (2021). Fabrication and Characterization of Injectable Thermosensitive Hydrogel Containing Dipyridamole Loaded Polycaprolactone Nanoparticles for Bone Tissue Engineering. *J. Drug Deliv. Sci. Technol.* 64, 102659. doi:10.1016/j.jddst.2021.102659

Thoniyot, P., Tan, M. J., Karim, A. A., Young, D. J., and Loh, X. J. (2015). Nanoparticle-hydrogel Composites: Concept, Design, and Applications of These Promising, Multi-Functional Materials. *Adv. Sci. (Weinh)* 2 (1-2), 1400010. doi:10.1002/advs.201400010

Wang, G., Zhang, X., Bu, X., An, Y., Bi, H., and Zhao, Z. (2022). The Application of Cartilage Tissue Engineering with Cell-Laden Hydrogel in Plastic Surgery: A Systematic Review. *Tissue. Eng. Regen. Med.* 19 (1), 1–9. doi:10.1007/s13770-021-00394-5

Wang, J., Cheng, Y., Chen, L., Zhu, T., Ye, K., Jia, C., et al. (2019). *In Vitro* and *In Vivo* Studies of Electroactive Reduced Graphene Oxide-Modified Nanofiber Scaffolds for Peripheral Nerve Regeneration. *Acta Biomater.* 84, 98–113. doi:10.1016/j.actbio.2018.11.032

Wang, Y., Zhao, Q., Zhang, H., Yang, S., and Jia, X. (2014). A Novel Poly(amido Amine)-Dendrimer-Based Hydrogel as a Mimic for the Extracellular Matrix. *Adv. Mat.* 26 (24), 4163–4167. doi:10.1002/adma.201400323

Wang, Z., Han, X., Song, Z., Gao, Z., Zhao, Y., and Wang, W. (2022). Treatment of Traumatic Cartilage Defects of Rabbit Knee Joint by Adipose Derived Stem Cells Combined with Kartogenin Hydroxyapatite Nano-Microsphere Complex. *J. Biomed. Nanotechnol.* 18 (1), 61–76. doi:10.1166/jbn.2022.3239

Wei, W., Ma, Y., Yao, X., Zhou, W., Wang, X., Li, C., et al. (2021). Advanced Hydrogels for the Repair of Cartilage Defects and Regeneration. *Bioact. Mater.* 6 (4), 998–1011. doi:10.1016/j.bioactmat.2020.09.030

Xia, C., Tao, S., Zhu, S., Song, Y., Feng, T., Zeng, Q., et al. (2018). Hydrothermal Addition Polymerization for Ultrahigh-Yield Carbonized Polymer Dots with Room Temperature Phosphorescence via Nanocomposite. *Chem. Eur. J.* 24 (44), 11303–11308. doi:10.1002/chem.201802712

Xia, H., Zhao, D., Zhu, H., Hua, Y., Xiao, K., Xu, Y., et al. (2018). Lyophilized Scaffolds Fabricated from 3d-Printed Photocurable Natural Hydrogel for Cartilage Regeneration. *ACS Appl. Mat. Interfaces* 10 (37), 31704–31715. doi:10.1021/acsami.8b10926

Xia, S., Song, S., Ren, X., and Gao, G. (2017). Highly Tough, Anti-fatigue and Rapidly Self-Recoverable Hydrogels Reinforced with Core-Shell Inorganic-Organic Hybrid Latex Particles. *Soft Matter* 13 (36), 6059–6067. doi:10.1039/c7sm01253e

Yan, W., Xu, X., Xu, Q., Sun, Z., Lv, Z., Wu, R., et al. (2020). An Injectable Hydrogel Scaffold with Kartogenin-Encapsulated Nanoparticles for Porcine Cartilage

Regeneration: A 12-month Follow-Up Study. *Am. J. Sports Med.* 48 (13), 3233–3244. doi:10.1177/0363546520957346

Yang, J., Han, C.-R., Duan, J.-F., Xu, F., and Sun, R.-C. (2013). Insitu Grafting Silica Nanoparticles Reinforced Nanocomposite Hydrogels. *Nanoscale* 5 (22), 10858–10863. doi:10.1039/c3nr04252a

Yang, J., Zhang, Y. S., Yue, K., and Khademhosseini, A. (2017). Cell-laden Hydrogels for Osteochondral and Cartilage Tissue Engineering. *Acta Biomater.* 57, 1–25. doi:10.1016/j.actbio.2017.01.036

Zare, P., Pezeshki-Modaress, M., Davachi, S. M., Zare, P., Yazdian, F., Simorgh, S., et al. (2021). Alginate Sulfate-Based Hydrogel/nanofiber Composite Scaffold with Controlled Kartogenin Delivery for Tissue Engineering. *Carbohydr. Polym.* 266, 118123. doi:10.1016/j.carbpol.2021.118123

Zhang, J., Yun, S., Du, Y., Zannettino, A. C. W., and Zhang, H. (2020). Fabrication of a Cartilage Patch by Fusing Hydrogel-Derived Cell Aggregates onto Electrospun Film. *Tissue Eng. Part A* 26 (15-16), 863–871. doi:10.1089/ten.TEA.2019.0318

Zhang, W., Ouyang, H., Dass, C. R., and Xu, J. (2016). Current Research on Pharmacologic and Regenerative Therapies for Osteoarthritis. *Bone Res.* 4 (1), 15040. doi:10.1038/boneres.2015.40

Zhao, H., Liu, M., Zhang, Y., Yin, J., and Pei, R. (2020). Nanocomposite Hydrogels for Tissue Engineering Applications. *Nanoscale* 12 (28), 14976–14995. doi:10.1039/d0nr03785k

Zheng, D., Chen, T., Han, L., Lv, S., Yin, J., Yang, K., et al. (2021). Synergetic Integrations of Bone Marrow Stem Cells and Transforming Growth Factor-B1 Loaded Chitosan Nanoparticles Blended Silk Fibroin Injectable Hydrogel to Enhance Repair and Regeneration Potential in Articular Cartilage Tissue. *Int. Wound. J.*, 1–16. doi:10.1111/iwj.13699

Zhu, W., Guo, D., Peng, L., Chen, Y. F., Cui, J., Xiong, J., et al. (2017). Repair of Rabbit Cartilage Defect Based on the Fusion of Rabbit Bone Marrow Stromal Cells and Nano-HA/PLLA Composite Material. *Artif. Cells, Nanomedicine, Biotechnol.* 45 (1), 115–119. doi:10.3109/21691401.2016.1138482

Conflict of Interest: The authors declare that the research was conducted in the absence of any commercial or financial relationships that could be construed as a potential conflict of interest.

Publisher's Note: All claims expressed in this article are solely those of the authors and do not necessarily represent those of their affiliated organizations, or those of the publisher, the editors and the reviewers. Any product that may be evaluated in this article, or claim that may be made by its manufacturer, is not guaranteed or endorsed by the publisher.

frontiers | Frontiers in Materials

TYPE Systematic Review
PUBLISHED 22 August 2022
DOI 10.3389/fmats.2022.929618

OPEN ACCESS

EDITED BY
Le Yu,
Ohio University, United States

REVIEWED BY
Chenghe Qin,
Guangdong Second Provincial General Hospital, China
Zhiwei Fang,
Johns Hopkins University, United States
Ganjun Feng,
West China Hospital, Sichuan University, China

*CORRESPONDENCE
Changfeng Fu,
fucf@jlu.edu.cn

SPECIALTY SECTION
This article was submitted to Biomaterials, a section of the journal Frontiers in Materials

RECEIVED 27 April 2022
ACCEPTED 07 July 2022
PUBLISHED 22 August 2022

CITATION
Xia Y, Wang H, Li Y and Fu C (2022), Engineered bone cement trigger bone defect regeneration.
Front. Mater. 9:929618.
doi: 10.3389/fmats.2022.929618

Engineered bone cement trigger bone defect regeneration

Yuanliang Xia, Hengyi Wang, Yuehong Li and Changfeng Fu*

Department of Spine Surgery, The First Hospital of Jilin University, Changchun, China

Bone defects, which can be caused by factors such as trauma, tumor, or osteomyelitis, are clinically common. They lessen the weight a bone is able to bear and cause severe pain to the patient. Although bone transplantation is the gold standard for treating bone defects, it is not suitable for all patients due to its poor availability, risk of spreading disease, and possibility of requiring a secondary surgery. Bone cement as a filler for bone defects can fill any shape of bone defect, and can quickly solidify when injected, providing mechanical strength sufficient for supporting the normal physiological activities of the bone. However, traditional bone cement lacks the ability to induce bone regeneration. Recently, various methods for enhancing the bone regeneration ability of bone cement have been developed, such as adding bone morphogenetic proteins, mesenchymal stem cells, and inorganic substances to bone cement. These methods not only ensure the original biological properties of the bone cement, but also improve the bone cement in terms of its mechanical strength and ability to induce bone regeneration. The aim of this review is to overview the process of bone regeneration, introduce improved bone cement formulations designed to promote bone regeneration, and discuss the clinical application of bone cement and its possibilities for future improvement.

KEYWORDS

bone regeneration, PMMA, calcium phosphate cement, osteoblasts, BMP-1

Introduction

Bone has a strong regenerative capacity under normal conditions. The repair potential of bone and its surrounding microenvironment, including inflammatory cells, endothelial cells, and Schwann cells, persists throughout adulthood, enabling damaged bone tissues to return to their homeostatic functional state (Schlundt et al., 2021). However, this self-healing method can only repair small bone defects. Infection, trauma, and bone tumor resection cause large bone defects; so, the normal physiological structure of the bone cannot be regained without medical intervention (Gillman and Jayasuriya, 2021). Autologous bone grafting, allogeneic bone grafting, and xenografting are the best ways to solve bone defects in clinic, among which autologous bone grafting is considered the gold standard for bone grafting (Schmidt, 2021). Since an autologous bone has the same function as the bone surrounding the defect, the success rate and fitting rate of autologous bone grafting are high; thus, autologous bone is an ideal filler for repairing bone defects. However, the availability of autologous bone for transplantation is

limited, and not everyone is a good candidate for autologous bone grafting. Moreover, infection and massive blood loss with autologous bone grafting can occur at the donor site (Myerson et al., 2019). These unfavorable factors limit the widespread application of autologous bone grafting. Bone allografts and xenografts, although widely available, are costly and difficult due to strict requirements for aseptic preservation and aseptic implantation. Furthermore, allografts and xenografts still pose a risk of disease transmission (Artas et al., 2018; P Baldwin et al., 2019; Hurle et al., 2021), and bone xenografts can even lead to immune rejection. Therefore, bone grafting methods are gradually moving toward the use of biomaterials to repair bone defects.

Biomaterials suitable to replace bone grafts need to have several properties (Elgali et al., 2017). The first is biological histocompatibility; that is, the material must be able to adapt to the injury environment in the local bone defect, and it must be compatible with the surrounding bone tissues and extracellular matrix so as to avoid damaging surrounding cells. A biocompatible scaffold can provide a favorable microenvironment for cell migration, proliferation, and differentiation, while possessing a degradation rate that matches bone repair and regeneration (García-Gareta et al., 2015; Zhu et al., 2021a). The second is pores conducive to the transport of nutrient metabolites and the inward regeneration of bone. Studies have shown that a small pore size is not conducive to cell infiltration and migration, and a large pore size cannot provide sufficient attachment area for bone regeneration (Zhu et al., 2021a). Excessive pore size is also not conducive to the stability of the filler. The third is mechanical tolerance; that is, the filler should locally adapt to the mechanical strength of the surrounding bone. This can be achieved through a phenomenon called mechanotransduction, in which cells respond to mechanical signals from their surroundings (Dupont et al., 2011). The fourth is being capable of inducing osteogenesis; bone cement can include bone morphogenetic proteins (BMPs) or other factors conducive to bone regeneration to achieve this (Li and Liu, 2017).

In recent years, many bio-tissue engineering materials for bone repair and regeneration have emerged, such as bone blocks (Chaushu et al., 2019), bone chips, bioglass (Duan et al., 2020), and implantable bandages for inducing osteogenic differentiation (Okuchi et al., 2021). These fillers are good substitutes for autologous bone and xenografts for bone defect repair. However, bone blocks need to be cut according to the shape and size of the defect during the operation, which increases the operation time and is not suitable for clinical application (Chaushu et al., 2019). Transplantable bandages induce bone regeneration but fail to compensate for mechanical strength in bone defects (Okuchi et al., 2021). The poor toughness of bioglass is also not conducive to topical application (Duan et al., 2020). Although 3D printing technology can be used to fabricate fillers with good mechanical strength, printing must be started a few days before surgery (Liaw and Guvendiren, 2017). Compared to these fillers, bone cement has unique advantages as a filler for small bone defects. Bone cement can fill the bone defect at the injection site and set quickly to provide good mechanical strength (Palmer et al., 2016). This can save operation time. Moreover, bone cement has good cytocompatibility and biocompatibility and can induce osteogenesis (Bimis et al., 2017). However, it has some serious potential complications, including bone cement implantation syndrome (BCIS) (Hines, 2018). BCIS can lead to severe cardiac arrhythmias, hypotensive shock, and even cardiac arrest. In addition, bone cement can leak into the surrounding environment, such as the venous system, which can lead to cardiac embolism (Song et al., 2020). Although the incidence of these adverse reactions is low, researchers still need to improve the setting properties of bone cement. The addition of natural organic substances such as alginate, chitosan, and gelatin to bone cement can improve the toughness, mechanical strength, and porosity of bone cement, thereby enhancing the ability of bone cement to induce bone regeneration and reducing its sequelae (Liu et al., 2021a; Wu et al., 2021). New bone formation is mainly caused by the joint action of osteoblasts, osteoclasts, and extracellular matrix at the site of injury (Katsimbri, 2017). Bone cement is relatively weak in regulating the osteogenic microenvironment. In recent years, platelet-rich plasma (PRP), an osteogenic growth factor, has been added to bone cement to promote bone repair (Hakimi et al., 2010; Shen et al., 2021; Tian et al., 2021). This new type of bone cement not only retains the mechanical strength and biocompatibility of the original bone cement but also provides growth factors for bone formation (Scheme 1; Table1, 2). In this review article, we introduce new types of bone cement developed to promote bone repair and regeneration, and we discuss the clinical

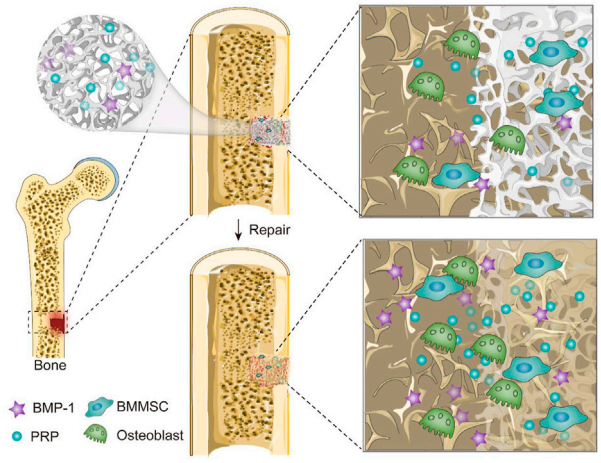

SCHRME 1
Schematic illustration of bone cement promotes bone regeneration in bone defect.

TABLE 1 Improved PMMA bone cement promotes bone regeneration.

Bone cement type	Supplementary materials	Components	Polymerization temperature	Result	References
PMMA	PEG	BMP-2	—	This system was capable of loading a model protein for BMP-2 at efficiencies of up to 100%	De Witte et al. (2020)
	mineralized collagen	—		MC-modified PMMA bone cement was associated with better vertebral height restoration in the long term	Zhu et al. (2021b)
	MgAl-layered double hydroxide (LDH)	—	88.2°C	PMMA&LDH boosts bone growth by 2.17- and 18.34-fold increments compared to the PMMA groups at 2 months	Wang et al. (2021)
	graphene oxide (GO)	—	72 ± 1°C	Thermal stability and enhanced mechanical properties have been achieved in nanohybrids vis-à-vis pure bone cement	Sharma et al. (2017)
	chitosan/graphene oxide	—	15.9% reduction	Cs/GO nanocomposite powder to the PMMA bone cement cause to increase the compressive strength by 16.2%, the compressive modulus by 69.1% and the bending strength by 24.0%	Tavakoli et al. (2020)
	MgO	—	—	It is of great interest to compare the bone repair effect using Mg2+versus other bioactive ions (such as Si or Sr ions53) in PMMA bone cements	Li et al. (2020b)
	Biphasic calcium Phosphate	—	—	The incorporation of BCP into PMMA-based bone cement would promote cell adhesion, proliferation, differentiation of BMSCs, and osteogenesis	Zhang et al. (2018)

application of bone cement, as well as possible directions for future improvement.

Bone regeneration

Bone regeneration is usually accomplished by the mutual regulation of osteoblasts, mesenchymal stem cells (MSCs) and extracellular matrix (ECM).

Osteoblasts

Osteoblasts are the only cells that can generate bone in vertebrates. Osteoblasts produce collagen to provide a scaffold for matrix mineralization. When the bone tissue matures, osteoblasts are embedded in the bone matrix and undergo structural changes to become osteocytes (Bonewald, 2011). After bone formation, active osteoblasts quiescent on the bone surface gradually evolve into bone lining cells. When a bone defect occurs, the quiescent bone lining cells on the bone surface turn into osteoblasts. Bone-lining cells are an important source of osteoblasts in adulthood (Mizoguchi and Ono, 2021). Osteoclasts, which are derived from hematopoietic stem cells, are capable of bone resorption. Under normal conditions, osteoblasts and osteoclasts are in relative balance *in vivo* to regulate osteogenesis and development (McDonald et al., 2021). When a bone defect occurs, the balance of osteoblasts and osteoclasts is disrupted. Induces bone mineral deposition through the regulation of calcium and phosphorus.

Mesenchymal stem cells

Stem cells have a strong ability to self-renew and differentiate into specific cells in the body. MSCs are the most commonly used stem cells for the treatment of bone diseases in preclinical research and clinical work (Saeed et al., 2016). MSCs in the bone marrow can differentiate into osteoblasts, adipocytes, or chondrocytes depending on the environment in which they exist. MSCs are considered precursors of osteoblasts and modulators of osteoclasts (Shang et al., 2020). The differentiation of MSCs into osteoblasts mainly depends on BMPs (Ponzetti and Rucci, 2021). BMPs have been reported to recruit bone marrow mesenchymal stromal/stem cells (BMMSCs) to the resorbed site during bone resorption to prevent bone resorption (Bal et al., 2020). MSCs reach the damaged site to generate a primary cartilaginous callus, which subsequently undergoes revascularization and calcification to gradually form normal bone tissues (Yorukoglu et al., 2017; Shang et al., 2020). Intramembranous osteogenesis and endochondral osteogenesis of bone regeneration depend on MSCs (Gresham et al., 2020).

Bone extracellular matrix

ECM is secreted by cells into the matrix and is mainly composed of hydroxyapatite, collagen fibers (type I in bone tissues and type II in cartilages), and trace elements (Gresham et al., 2020). As a scaffold for cell adhesion and proliferation, the ECM is primarily responsible for bone strength. Bone ECM dynamically interacts with osteoblasts and osteoclasts to regulate new bone formation during regeneration (Alcorta-Sevillano et al., 2020; Lin et al., 2020). In addition, studies

TABLE 2 Improve bone cement to promote bone defect regeneration.

Bone cement type	Supplementary materials	Components	Compressive strength	Porosity	Result	References
Calcium phosphate cement	MMSs	—	—	2–60 nm	MMSC provided space for more tissue ingrowth and induce anti-inflammatory M2 phenotype polarization of macrophages, angiogenesis and new bone formation	Tan et al. (2021)
	β-tricalcium phosphate	—	39.6 ± 3.8 MPa	—	The new CPC + 20%TCP possessed good cytocompatibility, acceptable injection force, higher compressive strength (increased by 63%), and greater odontogenic expression	Gu et al. (2021)
	PLGA	Alendronate	4–6 MPa	—	ALN-loaded CPC/PLGA presents clinically acceptable handling, suitable compressive strength, and a controlled ALN release	van Houdt et al. (2018)
	Calcium-deficient hydroxyl apatite Alginate	preosteoblast cells	—	—	α-TCP could be loaded with quercetin, which was released in a sustained manner throughout the entire 120 days testing period	Raja et al. (2021)
	PLGA	Si-Zn	45 MPa	20%–25%	PLGA microspheres and Si/Zn dual-elements incorporation within the CPC scaffolds synergistically enhanced bone regeneration	Liang et al. (2020)
	Brushite	Cu	27 MPa	—	Cu-loaded brushite cements showed good antibacterial properties and cell affinity	Li et al. (2021a)
	Collagen	BMP-1	11.7 MPa	175 μm	The presence of granules boosted both bone tissue growth as well as implant degradation behavior	Lee et al. (2017)
	Chitosan		12 MPa	56.80 ± 0.84%	CPC-complex system as a development for targeted localized drug or cell delivery for augmented bone regeneration	Lee et al. (2019)
	Alginate	BMMSCs PRP	—	267.43 ± 98.01) μm	The CPC scaffold is an effective alternative bone substitute for the management of critical size bone defects when used in combination with BMMSCs and PRP	Li et al. (2021b)
	SCPP fibers	Dopamine	—	—	D/SCPP fibers could effectively reinforce CPC cement and overcome some disadvantages of it	Wang et al. (2020)
Magnesium Phosphate Cement	O-CMC	—	33.8 MPa	13.8%	The Mg^{2+} release was related to the amount of O-CMC, which affected the degradation rate and the pH of the extracts of the OMPC samples	Gong et al. (2020)
	Citric acid		76 MPa	15%	The citric acid is possible to obtain composite cements which surpass the advantages of high compressive strength and bioactivity of its components	Wang et al. (2019)
	—	Chondroitin sulfate	29.67 ± 1.45 MPa	12.2%	CS-MPC had the highest compressive strength of 30 MPa, which was 58% higher than that of MPC.	Shi et al. (2021)
	CaMgP	—	13.4 MPa	9.2%	Bone healing with complete osseointegration of the CaMgP pastes into the bone defects and successive resorption of the materials depending on the calcium content	Ewald et al. (2019)
	Citric acid	—	—	—	Citrate elevating the osteogenic function of osteoblasts and angiogenic function of vascular endothelial cells depending on the dosage	Wu et al. (2020)

(Continued on following page)

TABLE 2 (*Continued*) Improve bone cement to promote bone defect regeneration.

Bone cement type	Supplementary materials	Components	Compressive strength	Porosity	Result	References
Portland Bone Cement	Magnesium glycerophosphate	—	30 MPa	—	The novel cements have a suitable self-setting time and the controllable degradation rare with the change of the content of MG.	Ding et al. (2018)
	Chitosan	—	—	—	APC-CT material exhibited satisfactory biocompatibility with SHED, maintaining favorable cell viability and attachment, and did not induce apoptotic cell death	Subhi et al. (2021)
	C3S	—	12.9 MPa	61%	3D-printed C3S bone cement scaffolds have excellent pore structure and high mechanical strength	Camilleri et al. (2014)
	C3S	MBG	12 MPa	70%	C3S/MBG30 scaffolds could induce new bone formation, but the C3S/ MBG30 scaffolds significantly improved the osteogenic capacity	Pei et al. (2016)
	C2S	—	19 ± 2 MPa	25–100 μm	C2S bone cement has good compressive strength and achieved the highest BIC and bone formation percentage on the 60th day	Zuleta et al. (2017)
	MBG	CSC	2.9 MPa	—	PSC/CS promote the fracture healing and reduce the postoperative complications	Zhu et al. (2017)
Borate Bone Cement	Chitosan	Sr	20 ± 1 MPa	—	The Sr-BBG cement showed a better capacity than the BBG cement to regenerate bone at the implant–bone interface	Shi et al. (2021)
	Chitosan	Sr	23.2 MPa	—	An increase in Sr substitution resulted in an increase in the injectability and setting time of the cement but little change in its compressive strength	Cui et al. (2020)

have found that ECM has a unique ability to induce osteogenesis through type I collagen (Komatsu et al., 2018). Hydroxyapatite is the main inorganic component of bone tissues with osteoinductive and osteoconductive properties. Angiogenesis precedes osteogenesis during bone regeneration (Oliveira et al., 2021). Various cytokines can be used in bone regeneration delivery technology to modulate the ECM to promote bone regeneration, such as platelet-derived growth factors (PDGFs), BMPs, insulin-like growth factors (IGFs), transforming growth factors (TGFs-ß), vascular endothelial growth factors (VEGFs), and osteoinductive GFs (Khojasteh et al., 2013). Therefore, the currently common bone cements that promote bone regeneration mainly regulate osteoblasts, MSCs and ECM. Next, we will introduce the currently commonly used bone cements to promote bone repair.

Improve bone cement

Polymethyl methacrylate bone cement

Polymethyl methacrylate (PMMA), a thermoplastic synthetic polymer synthesized by the polymerization of MMA monomers, has excellent properties, such as transparency and good tensile strength, mechanical properties, and processability (Forte et al., 2021). PMMA is widely used clinically in corneal transplantation (Talati et al., 2018), cranioplasty (Siracusa et al., 2021), denture repair (Tieh et al., 2021), vertebral fracture repair (Patel et al., 2021), and joint replacement (Rupp et al., 2021). However, PMMA bone cement hinders bone formation due to biological inertness, non-degradability, and potential cytotoxicity. High polymerization temperatures also lead to the death of surrounding osteoblasts and osteoblast-related cells, and the subsequent formation of a fibrous membrane hinders the osseointegration of PMMA cement to bone (Li et al., 2020a). Studies have found that bone tissue necrosis occurs within 1 min under conditions of more than 50° (Li et al., 2020a). In addition, free radicals from monomers after polymerization are a major source of adverse events (Saruta et al., 2021; Paz et al., 2019). Based on these unfavorable factors, PMMA cannot form biological bone tissues locally. Therefore, research on modified bone cement based on PMMA has been conducted in recent years (as Table1).

Bone morphogenetic protein-2 (BMP-2) is an important osteogenic growth factor in bone tissue regeneration. The technical difficulty encountered in using BMP-2 to repair bone defects is in delivering BMP-2 to the defect site while

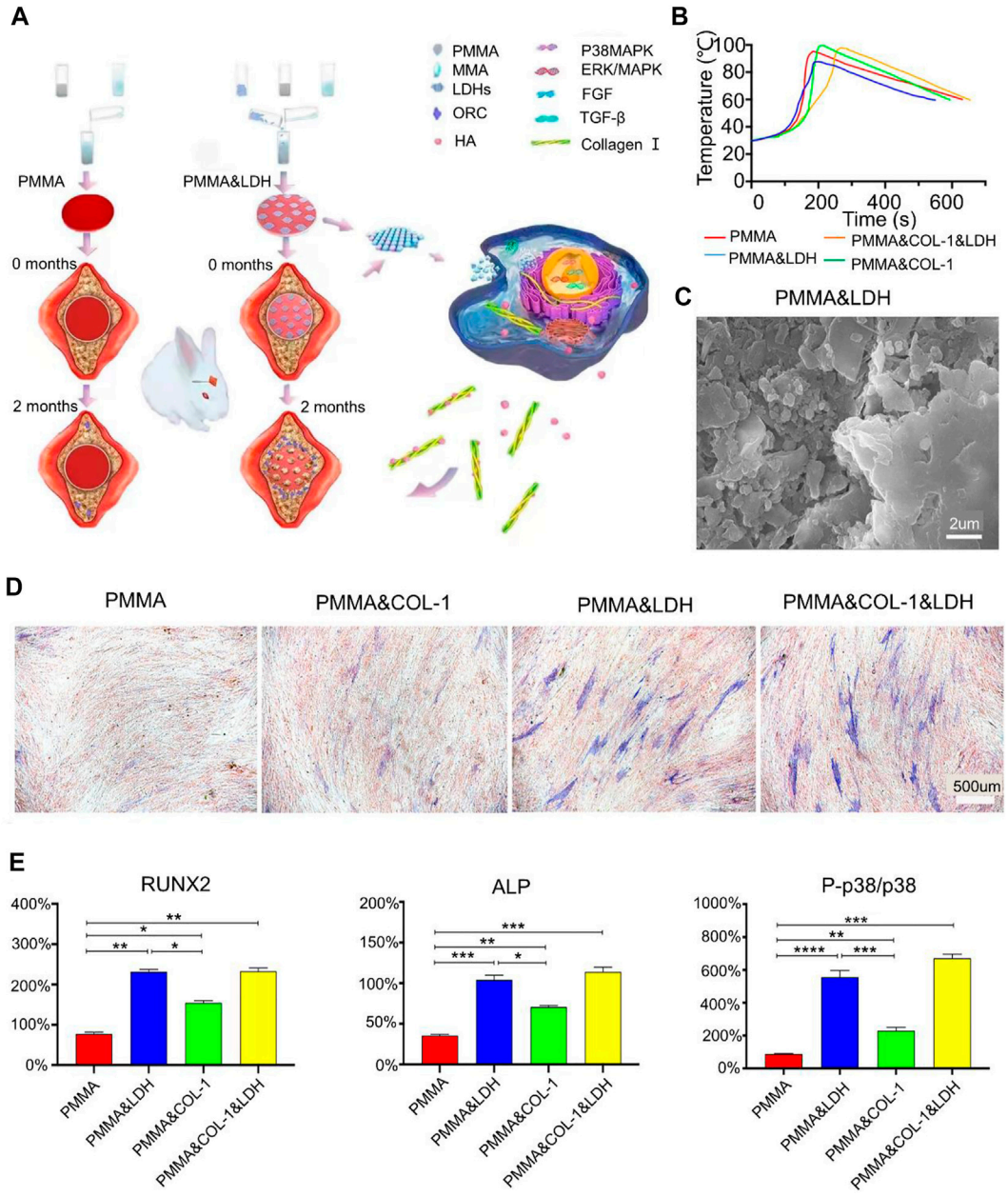

FIGURE 1
(A) Schematic illustration of layered double hydroxide-modified bone cement for promoting bone repair. **(B)** Temperature change during the reaction of the B polymer. **(C)** Scanning electron microscope image of PMMA and LDH. **(D)** Osteogenic differentiation ability was assessed by alkaline phosphatase (ALP) staining assay on day 14 of *in vitro* cell experiments (blue stained area represents alkaline phosphatase). **(E)** *In vivo* assay to assess osteogenic differentiation. Relative gene transcript levels of osteogenic markers (i.e., runt-related transcription factor 2 (Runx2), ALP, p38, and P-p38) in human bone marrow-derived mesenchymal stem cells on day 7. An increased ratio of P-p38 to p38 indicates the activation of the p38 MAPK signaling pathway. Reproduced with permission from (Wang et al., 2021).

maintaining its biological activity and local survival for a long time (Shen et al., 2021). De Witte et al. (2020) prepared degradable PMMA nanoparticles for the delivery of BMP-2. P (MMA-co-MAA) nanoparticles optimized for the controlled delivery of BMP-2. The hydrophobicity of PMMA and the hydroxyl groups on the surface of MMA increased the affinity of the nanoparticles for BMP-2. The addition of ester groups in the cross-linking increased the degradability of the nanoparticles and facilitated the release of BMP-2. This improved method not only promoted the degradation of PMMA but also increased the

delivery of BMP-2. The study confirmed that the nanoparticles had a 100% BMP-2 loading rate and had the potential to promote osteogenesis and angiogenesis to form vascularized bone (De Witte et al., 2020). Although nanoparticles can deliver BMP-2 to promote bone repair, they cannot change the unfavorable factors of PMMA bone cement itself, such as the lack of osseointegration and high elastic modulus (Rho et al., 2012). Mineralized collagen (MC) consists of type I collagen fibers and hydroxyapatite. The use of MC to improve PMMA in the treatment of osteoporotic pyramidal compression fractures has been reported (Hakimi et al., 2010). Zhu et al. (2021b) improved PMMA bone cement for the treatment of cone collapse using MC (Zhu et al., 2019). Compared with PMMA bone cement, MC-PMMA reduces the elastic modulus of the original PMMA bone cement and possesses biological activity more suitable for bone regeneration. Furthermore, it was found *via* computed tomography (CT) that the MC in MC-PMMA bone cement was replaced by new bone, and the new bone was more stable than PMMA. The incidence of re-fractures was also significantly reduced in patients after the application of MC-modified PMMA bone cement. However, not all mineralization improvements to bone cement can improve the performance of bone cement. For example, adding hydroxyapatite to improve PMMA reduces the compressive strength of bone cement (Kim et al., 2004). Wang et al. used magnesium-based polylactic acid microsheets to modify PMMA. This modification not only reduced the damage caused by PMMA to osteoblasts due to high polymerization temperature but also released magnesium ions to promote osteogenesis. In addition, the microsphere structure on the surface after lactate dehydrogenase degradation was also beneficial for bone formation (Figure 1) (Wang et al., 2021). In addition, Sharma et al. improved PMMA bone cement with amine group-functionalized graphene, which reduced cytotoxicity and improved the toughness of bone cement. Significant calcification was observed 20 days after bone injury (Saeed et al., 2016; Tavakoli et al., 2020). PMMA bone cement can also be improved by mixing it with magnesium oxide or calcium phosphate since these compounds promote bone formation (Zhang et al., 2018; Li et al., 2020b).

In conclusion, various inorganic materials can be mixed with PMMA bone cement to promote bone repair and regeneration. However, the porosity, biocompatibility, and mechanical strength obtained by mixing different ratios of PMMA with inorganic materials are different. In clinical practice, we can design bone cements with different characteristics according to the needs of different diseases for clinical selection.

Calcium phosphate cement

Calcium phosphate has unique biocompatibility, osteoconductivity, and bone-mineral-rich fractions that make it a promising bone-replacement material (Best et al., 2008). Calcium phosphate bone cement has plasticity and can be set into a suitable shape to fill bone defects as needed. However, calcium phosphate cement has a dense structure and poor biodegradability, which is not conducive to the ingrowth of living tissues. Additionally, its mechanical strength cannot meet the load-bearing capacity of the bone in the defect (Lobenhoffer et al., 2002; Liu et al., 2019). In recent years, researchers have optimized the properties of calcium phosphate bone cement to ensure that it has good biocompatibility and bone regeneration ability (as Table 2).

Tan et al. improved calcium phosphate bone cement using MgO (Tan et al., 2021). MgO is added to maintain the morphological structure after *in situ* curing. It was found that the addition of MgO reduced the temperature released during the curing process of bone cement, and released magnesium ions promoted the increase of M2 macrophages in the anti-inflammatory immune microenvironment (Gu et al., 2021). Macrophages persist at the site of injury for 2–3 weeks, providing a favorable environment for bone repair. At the same time, a large number of osteoblasts are present around the microspheres at the 12th week. Macrophages, as inflammatory and immune-related cells, can release growth factors and chemokines (such as BMP-2, BMP-4, and TGF-β1) in bone defects to promote the recruitment of fibroblasts to the defect (Yang and Liu, 2021). However, studies show that macrophages are not involved in the early stages of fracture healing (Schlundt et al., 2018).

Alendronate sodium, the most commonly used drug for the treatment of osteoporosis, increases bone mineral density (Vertesich et al., 2021). Hence, researchers have speculated whether the application of alendronate sodium can maintain the bone density of the bone defect in the early stage. In an animal study, mice treated with alendronate for 4 weeks exhibited a 139% increase in bone volume (Vertesich et al., 2021). In one study, alendronate was added to calcium phosphate bone cement, and poly (lactic-co-glycolic acid) (PLGA) was used to make porogen to promote the degradation of CPC/PLGA to release alendronate and form a porous structure. Although the calcium phosphate cement itself did not degrade, alendronate was released from the modified cement for up to 148 days. When alendronate sodium is clinically used for the treatment of osteoporosis patients, it promotes local bone formation. However, the alendronate released from the cement did not increase bone formation within the defect. Instead, new bone formation was detected around the defect area. Although there was no good explanation, the researchers speculated that it may have been due to the lack of alendronate sodium to induce the migration of preosteoblast cells to the center of the defect (van Houdt et al., 2018).

Raja et al. (2021) replaced alendronate with quercetin and used calcium-deficient hydroxyapatite-alginate to fabricate core-shell bone cement (Raja et al., 2021). Quercetin is to control the metabolism of bone tissue regeneration through sustained release

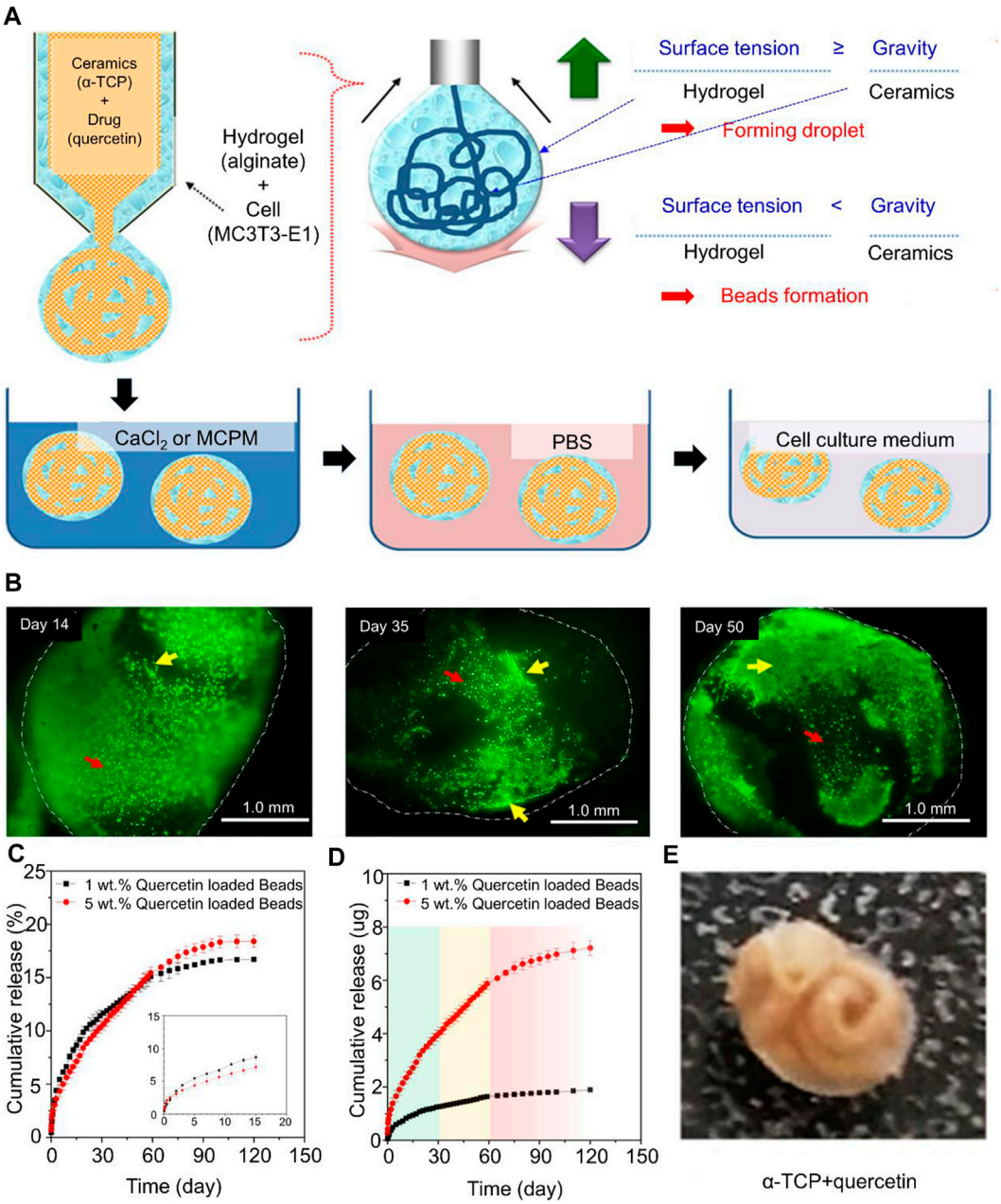

FIGURE 2
(A) Schematic of the processing of core–shell beads. **(B)** Fluorescence microscopy images of live/dead cells in core–shell beads (indicated with white dotted lines) cemented in PBS for 14, 35, and 50 days. Yellow arrows indicate cells showing growth and elongation, and red arrows indicate cells that retain their spherical shape in alginate. **(C)** Drug release profile from core–shell beads over the course of 120 days with different concentrations of quercetin. **(D)** Cumulative drug release at specific time points (in days). 0–30 days (green region): fast drug release, followed by decreased but stable release; 30–60 days (yellow region): constant and stable drug release; and 60–120 days (red region): declining drug release with time. **(E)** X-ray diffraction patterns of final core–shell beads after the addition of quercetin. Reproduced with permission from (Raja et al., 2021).

over a long period of time. Alginate is an anionic polysaccharide that changes shape when cross-linked. The purpose of the core-shell structure was to deliver preosteoblast cells to the site of bone injury. Cells were loaded on core-shell beads for 50 days (Figure 2). Cell growth was evident at the center of the nucleocapsid structure, but not in alginate. In addition, it was found that adding antibiotics could also control local infection, which is beneficial to bone formation (Liu et al., 2021a). Trace elements such as magnesium ions, zinc ions, strontium ions, and copper ions can also regulate the phenotype of macrophages and

promote bone repair and regeneration (Lin et al., 2019; Liang et al., 2020; Miao et al., 2020; Li et al., 2021a; Tao et al., 2021).

A simple bone cement material has insufficient pores in the middle, and osteocytes cannot grow toward the center of the bone cement; so, stable new bone cannot be formed. Degradable particles mixed with bone cement can remedy the lack of voids in bone cement. Biphasic calcium phosphate bone cements (BCPCs) composed of hydroxyapatite and tricalcium phosphate have good biodegradability (Gauthier et al., 2001; Rattanachan et al., 2020). Lee et al. prepared a bone substitute material (CPC-ccMCG-B) by adsorbing BMP-2 and porous particles to the surface of HAp through collagen fibers (Lee et al., 2017). The incorporation of porous particles facilitates the maintenance of the biocompatibility of the material. The study found that CPC-ccMCG-B provided sustained release of BMP-2 over 30 days. Compared with pure calcium phosphate cement, CPC-ccMCG-B can also significantly induce angiogenesis. Neovascularization helps osteoblasts recruit and form new bone in bone defects. A significant increase in the quantity of trabecular bone was observed within 4 weeks of implantation. However, the liquid-to-powder ratio (L/P) affected the compressive strength of CPC-ccMCG-B. The higher the L/P ratio, the greater the fluidity of the cementitious material and MCG, and the lower the compressive strength of CPC-ccMCG-B (Lee et al., 2017). Adding chitosan fiber as a reinforcing material to bone cement can improve the compressive strength of bone cement (Lee et al., 2019; Miao et al., 2020; Rattanachan et al., 2020).

MSCs have excellent inductive differentiation potential, which is conducive to promoting bone regeneration (Saeed et al., 2016). Li et al. cultured autologous BMMSCs for 7 days and encapsulated them in calcium phosphate bone cement in combination with PRP (Li et al., 2021b). PRP releases growth factors such as PDGF, TGF-β1, and VEGF, which benefit angiogenesis and macrophage activation, thereby stimulating host bone formation (Hakimi et al., 2010). This new bone cement has better mechanical properties and excellent biocompatibility than previous CPC. Although different implantation methods have certain negative effects on PRP-induced bone regeneration, the combination with stem cells is beneficial for bone healing (Li et al., 2021b). At 6 and 12 weeks after implantation, calcium phosphate cement mixed with BMMSCs and PRP had stronger osteogenic ability than calcium phosphate cement alone. Although the internal loading factors of bone cement can promote bone regeneration, the surface compatibility of calcium phosphate bone cement is still a problem. Dopamine-encapsulated strontium-doped calcium phosphate improves the mechanical properties of bone cement and enhances the cytocompatibility of the cement surface with surrounding bone tissues (Wang et al., 2020).

In conclusion, calcium phosphate bone cement is currently the most commonly used inorganic bone substitute material, and it still has great untapped potential. Thus far, it has been demonstrated that chitosan, alginate, and inorganic ions can be used to improve the mechanical strength and porosity of calcium phosphate bone cement. However, a major technical difficulty remaining to be solved is in delivering growth factors to the defect site and in increasing the duration of action while ensuring their survival rate in order to enhance bone defect repair.

Magnesium phosphate cement

Magnesium phosphate bone cement is known for its rapid setting, high strength, and rapid biodegradation capabilities (Mestres and Ginebra, 2011). In the process of bone repair, the ability of magnesium ions to promote the proliferation and differentiation of osteoblasts gives magnesium phosphate bone cement unique advantages over other types of bone cements (Wang et al., 2014). Although not as rich in bone minerals as calcium phosphate bone cement, magnesium phosphate bone cement can still have a wide range of applications due to the magnesium ions. However, under humid conditions in the body, the phosphate in the magnesium phosphate cement matrix will dissolve, resulting in changes in the surrounding pH and a decrease in the mechanical strength of the cement (Liu et al., 2019). This is undesirable since mechanical strength is an important factor for bone defect repair. Moreover, magnesium phosphate bone cement will generate a lot of heat before setting, and this heat will damage the cells around the defect, causing these cells to lose their ability to repair bone (Ostrowski et al., 2016). Therefore, magnesium phosphate cement alone is not a good material for local filling in bone repair. Reducing the changes to pH caused by magnesium phosphate bone cement is a relatively difficult work; so, there have been few studies on improving magnesium phosphate bone cement.

Magnesium phosphate and ammonium ions can form struvite with high absorbability under neutral conditions (Fuchs et al., 2021). Struvite has high mechanical strength, which can, to a certain extent, compensate for the decrease in mechanical strength caused by pH changes. However, the synthesis of struvite results in amine emissions (Wenisch et al., 2003), which is a difficult problem to solve. Gong et al. (2020) used potassium dihydrogen phosphate (KH_2PO_4) as a source of phosphate to solve the problem of amine emissions and simultaneously synthesized K-struvite. They also introduced non-toxic and degradable natural oxy-carboxymethyl chitosan (O-CMC) into magnesium phosphate cement (MPC), denoting the product as OMPC, to improve the cement's compressive strength. The addition of oxygen-carboxymethyl chitosan enhances the mechanical properties and cytocompatibility of potassium MPC. The study confirmed that the improvement in compressive

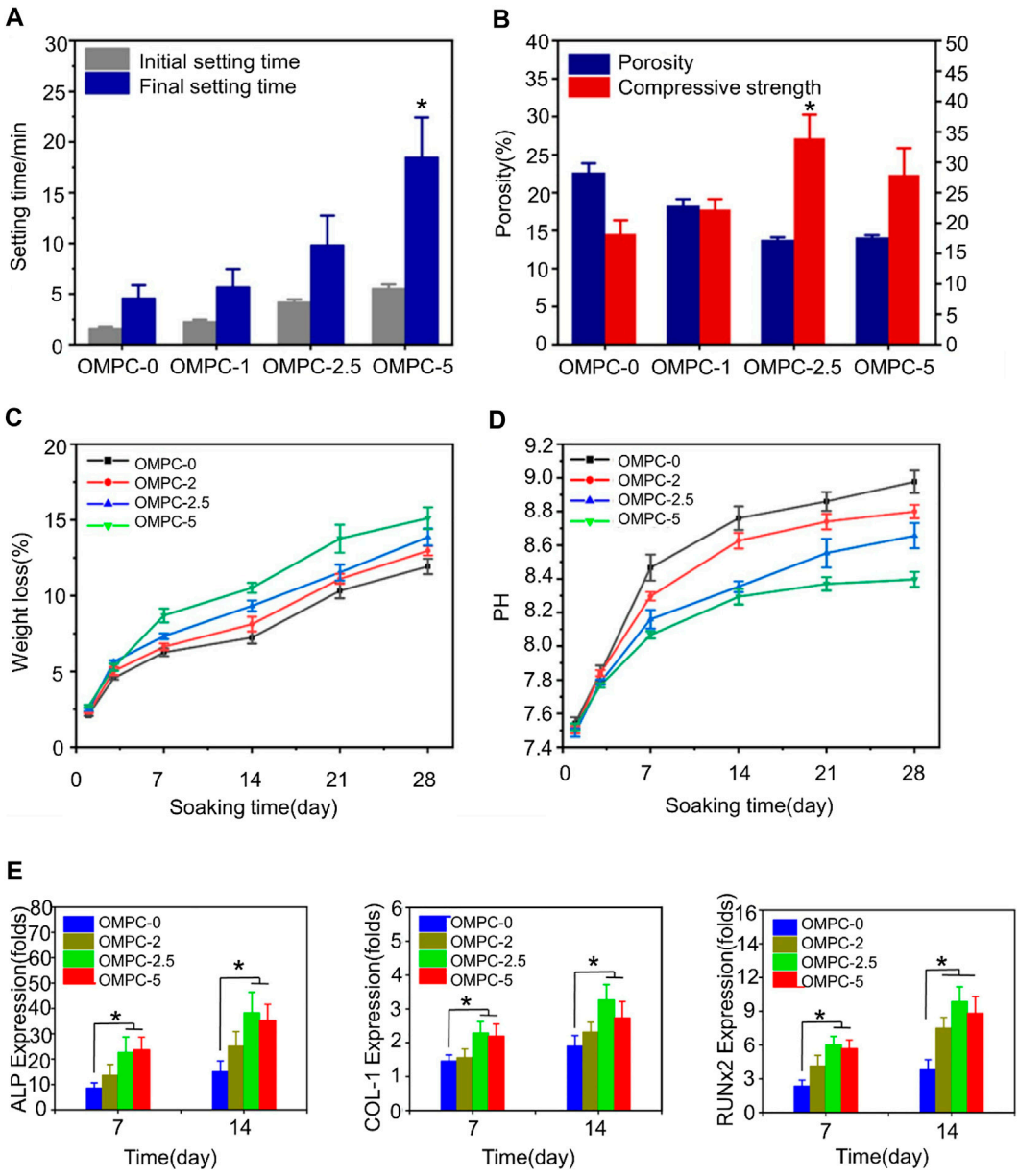

FIGURE 3
(A) Clotting time of OMPC scaffolds. **(B)** Porosity and compressive strength of OMPC scaffolds. **(C)** *In vitro* degradation of OMPC scaffolds. *In vitro* weight loss rate of OMPC scaffolds immersed in Tris-HCl solution. The first 3 days had the fastest degradation rate, with a loss of about 5% of the total weight of all OMPC groups. On day 28, the weight reduction rate of OMPC-5 reached 15.11 wt%. **(D)** pH values for all OMPC groups. The incorporation of O-CMC slightly lowered the final pH of OMPC. **(E)** Osteogenic differentiation results of MC3T3-E1 cells cultured on OMPC scaffolds. The expression levels of osteogenic differentiation-related genes were measured on days 7 and 14. Reproduced with permission from (Gong et al., 2020).

strength was related to the added O-CMC. The porosity of the OMPC-2.5% group is the lowest at 13.8%, while the compressive strength reaches the maximum value of 33.8 MPa. The study also demonstrated that OMPC released magnesium ions to promote cell proliferation and bone repair. Furthermore, O-CMC reduced the pH value of the solution, which made up for the decrease in bone cement strength caused by phosphate dissolution (Figure 3) (Gong et al., 2020).

Although potassium magnesium phosphate bone cement has many advantages, its short clotting time is not conducive to clinical application (Wang et al., 2019). Shi mixed different proportions of chondroitin sulfate (CS) with MPC to

synthesize new CS-MPC composites (Shi et al., 2021). CS promotes calcium deposition in the extracellular matrix and osteogenic differentiation of BMMSCs (Manton et al., 2007). It was found that 2.5% CS-MPC had the highest compressive strength, at 29.67 ± 1.45 MPa, and the lowest porosity, at 12.2%. Cells on CS-MPCs were detected on days 3 and 5, and it was found that the expression levels of osteogenesis-related genes COL1, RUNX2, and OCN were also higher than those in the MPC group. In addition, magnesium phosphate powder was added to calcium phosphate bone cement to prepare premixed cement $Ca_xMg_{(3-x)}(PO_4)_2$ (x = 0.25 and 0.75) (Ewald et al., 2019). It was found that the porosity of premixed bone cement in PBS *in vitro* increased to 16%–25% after 30 days without a consequent decrease in compressive strength. This may be related to the release of the oil phase. In addition, citrate can inhibit hydration and improve the mechanical strength of bone cement, and it can also regulate the energy metabolism pathway of MSCs to induce osteogenic differentiation and angiogenesis of MSCs (Ma et al., 2018; Binu et al., 2013; Hurle et al., 2018). Wu et al. loaded citrate into magnesium phosphate bone cement and found that it not only improved the curing time, compressive strength, and cytocompatibility of bone cement but also promoted peripheral vascular and osteogenic differentiation (Wu et al., 2020).

In conclusion, although magnesium phosphate bone cement has its unique advantages, it is difficult to improve and has significant negative effects. Hence, little research on improving magnesium phosphate bone cement has been conducted. Although natural bioactive substances can make up for certain drawbacks, magnesium phosphate bone cement is still rarely used clinically. Some researchers have mixed calcium phosphate cement with magnesium phosphate cement to prepare a new type of cement. This new type of bone cement has certain minerals and mechanical strength, but it is difficult to manufacture. Different ratios of calcium phosphate and magnesium phosphate will need to be comprehensively assessed in order to guide the development of new bone cements that meet specific needs. Overall, magnesium phosphate bone cement still requires much development before it becomes suitable for clinical application.

Portland bone cement

Portland cement is widely used in the treatment of dental pulp, and its main components are tricalcium silicate (C3S) and Dicalcium silicate (C2S) (Kaur et al., 2017). C3S and C2S can stimulate the proliferation and osteogenic differentiation of bone, and they both have good biocompatibility. However, Portland cement has low resistance to early compression and a long setting time, which do not meet the clinical requirements of bone defect repair (Wu et al., 2015). When C2S and C3S come in contact with water, silicic acid and calcium hydroxide are immediately produced. Phosphate and calcium hydroxide form hydroxyapatite (Sharma et al., 2020). Ding et al. (2018) mixed magnesium glycerophosphate (MG) with Portland cement to synthesize a new type of bone cement. MG can not only promote the degradation of bone cement to release phosphate but can also release magnesium necessary for bone regeneration. Glycerol phosphate is the basic substance of metabolism throughout the life cycle. The study showed that the compressive strength of bone cement reached 30 MPa on the 7th day, and hydroxyapatite was formed on the surface, which provided a good foundation for new bone formation (Ding et al., 2018). In addition, studies have shown that chitosan can induce silicate bone cement to upregulate osteogenic markers and induce matrix mineralization (Subhi et al., 2021). However, Portland cement is hydraulically hard and reduces porosity over time (Camilleri et al., 2014). Once the porosity is reduced, it is not conducive to cell growth and nutrient metabolism. A possible solution is to use 3D printed scaffolds to tune pore morphology and porosity as needed (Pei et al., 2016). Yang et al. (2017) used silicate bone cement to prepare scaffolds to enhance bone repair and regeneration (Figure 4). The formation of nano-needle-like structures on the surface of scaffold pores was conducive to the attachment and diffusion of bone marrow stem cells. The scaffolds had a maximum compressive strength of 12.9 MPa and a porosity of 61%. This porosity is too high, which is a common problem among 3D printed scaffolds. Although larger porosity is beneficial for cell growth, it leads to a decrease in compressive strength (Yang et al., 2017). Studies have shown that although the compressive strength of this 3D-printed scaffold is not as good as that of calcium phosphate cement, it has exceeded that reported in other literature (0.9–8.7 MPa) (Camilleri et al., 2014; Zuleta et al., 2017). This type of scaffold is only suitable for the repair of non-load-bearing bones.

Mesoporous bioactive glasses (MBGs), most of which are silicates, have excellent biocompatibility and tunable surface porosity (Wu and Chang, 2012). In bone regeneration, MBGs can promote the expression of osteogenesis-related genes (Wu et al., 2010). However, MBGs are brittle at low sintering temperatures, leading to rapid collapse of the porous structure (Ghamor-Amegavi et al., 2020). Gou et al. developed yolk-shell granule-like bone cement with silicate and MBG for promoting bone regeneration (Ghamor-Amegavi et al., 2020). This bidirectional calcium phosphate bone cement rapidly degraded and released MBGs in rabbits. The highest bone volume fractions (BV/TV) were shown at 8–12 weeks post-implantation. Bone fragility caused by osteoporosis was also lessened (Wang et al., 2014). In another study, MBG was mixed with calcium sulfate to form a high BG content injectable BG/calcium sulfate composite cement. The composite bone cement degraded slowly, and the mass loss of calcium sulfate cement reached 52% after soaking in simulated body fluid (SBF) for 4 weeks. Although its compressive strength is not high, it satisfies the bone repair of vertebral body compression fractures (Zhu et al., 2017). As previously mentioned, metal ions can improve the biological properties of Portland cement. Copper ions, for example, can induce bone marrow mesenchymal cells to release

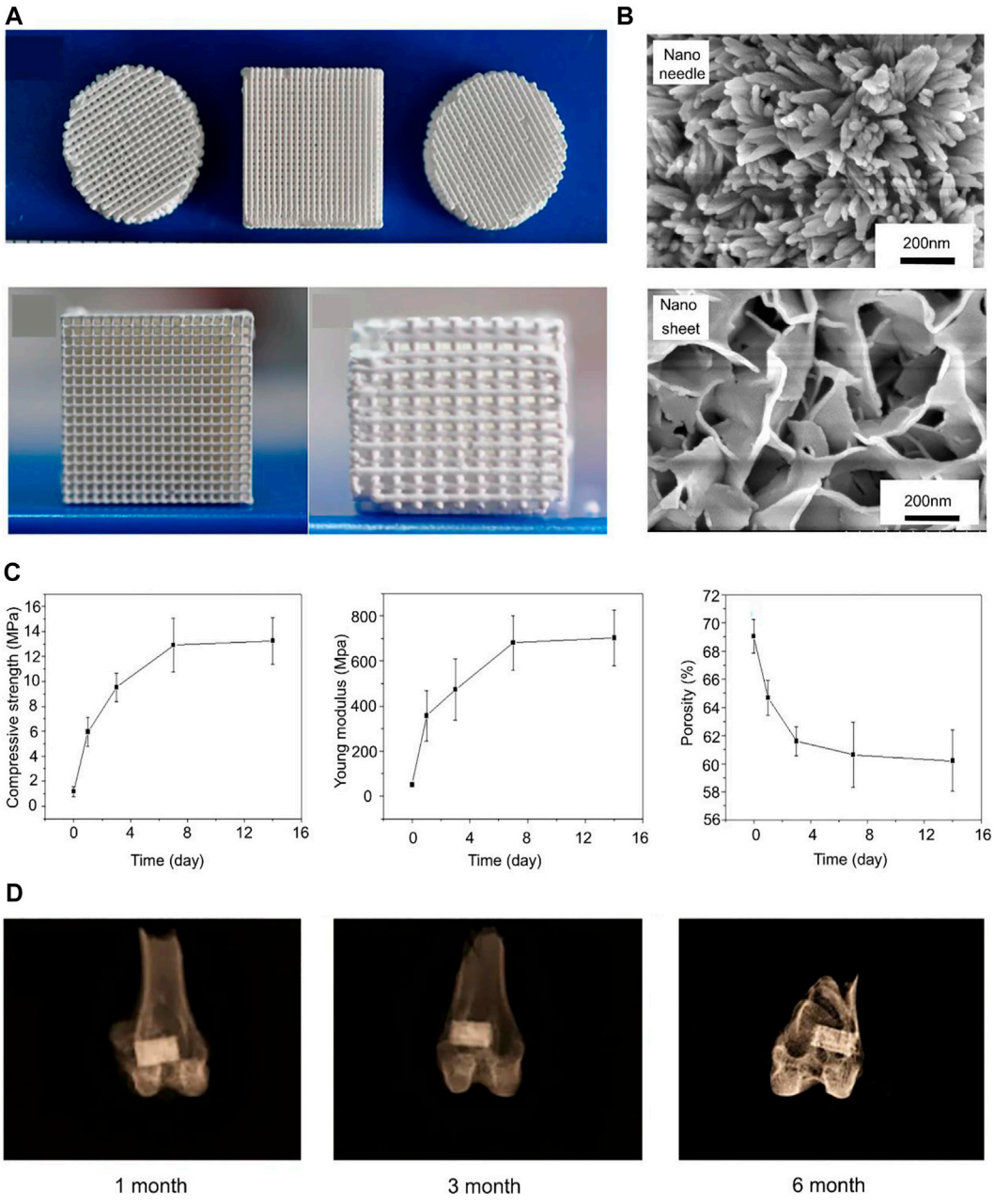

FIGURE 4
(A) 3D printed C3S bone cements with different shapes. **(B)** Nanoneedle and nanosheet structures formed by C3S bone cement scaffolds in Na_2HPO_4 aqueous solution and $(NH_4)_2HPO_4$ aqueous solution. **(C)** Compressive strength, Young's modulus, and porosity of C3S scaffolds at different curing times (0, 1, 3, 7, 14 days). **(D)** X-rays of C3S–NN scaffolds after being implanted for 1 month, 3 months, and 6 months. Reproduced with permission from (Yang et al., 2017).

hypoxia-inducible factor and vascular endothelial growth factor, which contribute to the revascularization of bone defects (Bejarano et al., 2017). Copper ion-doped hydroxyapatite exhibits antibacterial activity and promotes bone regeneration (Zhang et al., 2020).

Portland cement is not as widely used as calcium phosphate cement. However, for small bone defects, such as those in teeth, Portland cement still has a certain application value. Due to its low compressive strength, Portland cement cannot be used for the defect repair of limb bones. Improved Portland cement can be used to repair vertebral fractures, but its application is currently limited to animals. Additionally, silicate bone cement needs to be further improved to expand its clinical applicability.

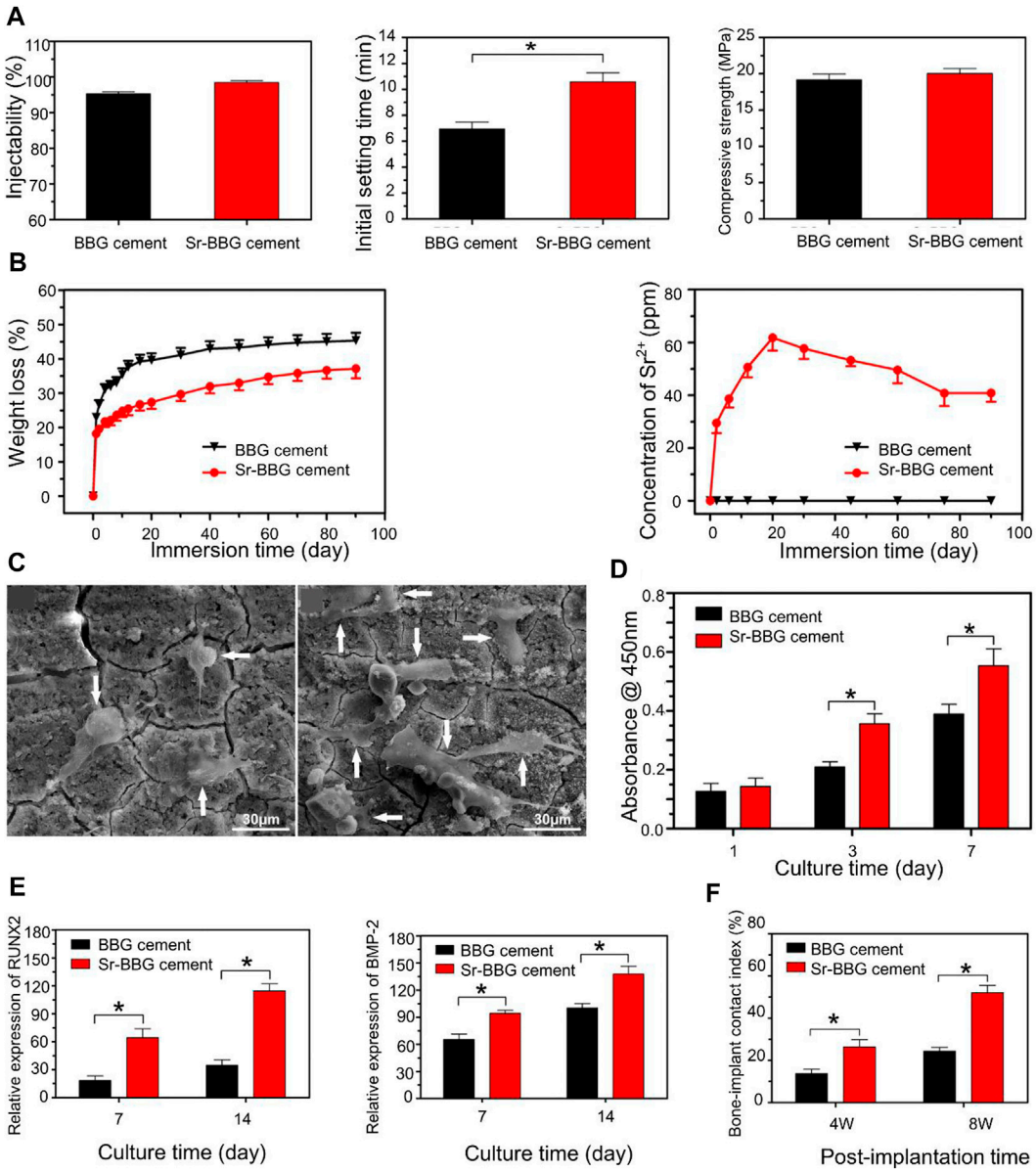

FIGURE 5
(A) Physical properties of BBG and Sr-BBG cements: injectability, initial setting time, and compressive strength. **(B)** Weight loss of BBG and Sr-BBG cement, and the amount of Sr^{2+} ions released from the Sr-BBG cement into the SBF. **(C)** SEM images showing the attachment of human bone marrow-derived mesenchymal stem cells (hBMSCs) on BBG and Sr-BBG cement after culturing for 3 days. **(D)** CCK8 proliferation experiments on days 1, 3, and 7: hBMSCs cultured on BBG and Sr-BBG cement. **(E)** The expression levels of osteogenic differentiation-related genes were measured on days 7 and 14. **(F)** Newly formed bone and bone-implant contact (BIC) index of BBG and Sr-BBG cement implanted at 4 and 8 weeks in critical-sized rabbit femoral condyle defects. Reproduced with permission from (Zhang et al., 2015).

Borate/borosilicate bone cement

Borate bone cement is a kind of bioactive glass made by partially or totally replacing SiO_2 with B_2O_3 (Huang et al., 2006). The degradation rate can be regulated by changing the ratio of B_2O_3 and SiO_2. Boron can reduce the hydration temperature and delay the solidification reaction. Borate cement with vancomycin can repair 87% of bone defects in the treatment of osteomyelitis (Cui et al., 2014). Strontium (Sr) can stimulate the expression of the MSC solid gene and inhibit the activity of osteoclasts to promote bone regeneration (Zhang et al., 2015). Zhang developed an injectable glass bone cement (Sr-BBG) by mixing strontium and chitosan with borate bone cement (Figure 5) (Zhang et al., 2015). Bone cement has good biological activity, osteogenesis capacity and the release of Sr in a controlled manner. The setting time of Sr-BBG bone cement

was 10.6 ± 1.2 min. The expression of osteogenesis-related genes could be detected within 7 days *in vivo*. Increasing the proportion of strontium resulted in longer setting times but did not affect the compressive strength. In addition, the new bone formation and implant contact index of Sr-BBG were significantly better than those of BBG (Cui et al., 2020). In view of the rapid setting of magnesium phosphate bone cement, Li et al. incorporated magnesium phosphate into borosilicate bone cement to prepare a composite bone cement (MPC-BG). The study found that the coagulation time of magnesium phosphate bone cement was delayed after adding BG. However, the compressive strength was affected when the MPC/BG ratio exceeded 3:1 (Li et al., 2020a).

Although borosilicate-loaded growth factors have achieved certain success in promoting bone repair, their inherent stability is poor. Most borate cements are used to improve the mechanical strength of PMMA cements (Cui et al., 2017; Funk et al., 2018; Cole et al., 2020), since it is still difficult to use borosilicate bone cement alone in clinical practice.

Calcium aluminate bone cement

Calcium aluminate cement has higher mechanical properties and a lower curing temperature than calcium phosphate cement (Oh et al., 2004). However, this kind of bone cement has a long setting time, which is not conducive to clinical application. A study found that the addition of lithium chloride can reduce the setting time of calcium aluminate cement without affecting the compressive strength of the cement (Acuña-Gutiérrez et al., 2017). *In vivo* experiments also confirmed the absence of cytotoxicity after the addition of lithium chloride. However, this modification method cannot ensure that there are sufficient calcium ions around the cement to promote bone repair. Calcium chloride modified calcium aluminate bone cement can ensure that calcium aluminate bone cement releases calcium ions for 84 h (Castro-Raucci et al., 2018). Nonetheless, calcium aluminate cements are not as useful as other types of cements, possibly due to their inferior fabrication methods and biohistocompatibility compared to other types of bone cements. Among the few calcium aluminate cements that have been studied, most have been used to improve other types of bone cements.

Inorganic nanohybrid bone cement

In addition to the above-mentioned bone cements commonly used in clinical practice, polymer bone cements also have unique advantages. Unlike traditional bone cements, the crosslinking and stabilization of these polymers depend on thienyl groups and double bonds (Liu et al., 2021b). In order to speed up the formation of chemical bonds, it is often necessary to use catalysts to speed up the reaction process. However, most of the catalysts contain aromatic groups or heavy metal ions that are harmful to the body. Strain-promoted alkyne-azide cycloaddition (SPAAC) click chemistry is a mild and fast click reaction (Gordon et al., 2012). This reaction can be accomplished without the addition of initiators and catalysts. Liu et al. developed an organic-inorganic nanohybrid (click-ON) injectable bone cement system using SPAAC technology. The hybrid was mainly composed of propylene glycol fumarate and esters. Studies have shown that with different ratios of the two substances, the gelation time of the hybrid varies from a few minutes to 30 min. *In vivo* experiments indicated that on the 21st day, the content of MSCs and osteogenic markers was significantly increased. Significant osteogenesis was observed 4 weeks after the scaffold was injected. Compared with PMMA bone cement, the hybrid has low toxicity, strong degradability, and can promote the proliferation and differentiation of MSCs.

Polymer bone cement has the advantages of low toxicity and easy availability, which traditional bone cement does not have, and it also has advantages for *in vivo* osteogenesis (Tang et al., 2021). Whether it can provide compressive strength around the bone defect is questionable since no studies have reported on this topic. We speculate that polymer bone cement probably has lower strength compared to traditional bone cement. Therefore, polymer bone cement needs to be further improved to promote its clinical application.

Challenges and limitations

To date, PMMA, calcium phosphate, and magnesium phosphate bone cements have been widely used in the field of orthopedics. However, these traditional bone cements have drawbacks that limit their clinical application. The regeneration of bone into normal bone tissue is a complex process. Traditional bone cements provide support for bone regeneration, but they do not promote the induction of bone regeneration. Today, biomaterials have made great breakthroughs in tissue engineering. Traditional bone cements can be improved by natural bioactive substances such as chitosan and alginate to form new types of bone cements that are more stable and that have greater mechanical strength while retaining the other mechanical properties of bone cement. Improved bone cement with the ability to induce bone regeneration can also be developed. Loading osteogenic growth factor on bone cement can form a microenvironment favorable for bone formation *in situ*. Appropriate porosity not only satisfies the compressive strength of new bone but also facilitates the inward formation of new bone. Better osteogenic properties of new types of bone cements have been observed in animal models. Therefore, new bone cements have great promise for clinical application in bone repair.

Future perspective and conclusion

However, the optimal mixing ratios of conventional bone cements and natural active substances remain unknown. The mechanical strength and porosity provided by mixtures of different proportions are different, and the characteristics of bone cement required for repairing various bone defects are also different. There is an urgent need for a new type of bone cement suitable for repairing most bone defects in clinical practice. To date, Improved bone cements have only been validated in animals. Furthermore, new types of bone cements can repair small bone defects, but it remains unclear whether they can repair large bone defects. For large bone defects, the repair time after bone cement filling is long, and patients may need a second operation or even autologous bone implantation, which is troubling for both patients and clinicians. At present, for large bone defects, only 3D printing stent technology can provide a good basis for treatment. Therefore, there is still an urgent need for bone cement suitable for repairing large bone defects.

Data availability statement

The original contributions presented in the study are included in the article/supplementary material, further inquiries can be directed to the corresponding author.

Author contributions

All authors read and approved the final manuscript. YX wrote the initial manuscript. CF and YX contributed new ideas. HW created the figures. YL and HW created Table 1. YX, HY, and YL revised the manuscript and approved the final version.

Funding

This work was supported by the National Natural Science Foundation of China (Grant Nos. 82071391), the Science and Technology Development Program of Jilin Province (Grant No. 20200404182YY), the Provincial Health Special Project of Jilin Province (Grant No. JLSWSRCZX 2020-104), the "13th Five-Year" Science and Technology Research Planning Project of Jilin Province (Grant No. JLKHJJKH20190042KJ), and the Achievement Transformation Fund of the First Hospital of Jilin University (Grant No. JDYYZH-2102052).

Acknowledgments

We would like to express our appreciation to everyone who was involved in the drafting and preparation of the manuscript.

Conflict of interest

The authors declare that the research was conducted in the absence of any commercial or financial relationships that could be construed as a potential conflict of interest.

Publisher's note

References

Acuña-Gutiérrez, I. O., Escobedo-Bocardo, J. C., Almanza-Robles, J., Cortes-Hernandez, D., Saldivar-Ramirez, M., Resendiz-Hernandez, P., et al. (2017). Development of LiCl-containing calcium aluminate cement for bone repair and remodeling applications. *Mater. Sci. Eng. C* 70, 357–363. doi:10.1016/j.msec.2016.09.022

Alcorta-Sevillano, N., Macías, I., Infante, A., and Rodríguez, C. I. (2020). Deciphering the relevance of bone ECM signaling. *Cells* 9 (12), 2630. doi:10.3390/cells9122630

Artas, G., Gul, M., Acikan, I., Kirtay, M., Bozoglan, A., Simsek, S., et al. (2018). A comparison of different bone graft materials in peri-implant guided bone regeneration. *Braz. oral Res.* 32, e59. doi:10.1590/1807-3107bor-2018.vol32.0059

Bal, Z., Kushioka, J., Kodama, J., Kaito, T., Yoshikawa, H., Korkusuz, P., et al. (2020). BMP and TGFβ use and release in bone regeneration. *Turk. J. Med. Sci.* 50 (SI-2), 1707–1722. doi:10.3906/sag-2003-127

Bejarano, J., Detsch, R., Boccaccini, A. R., and Palza, H. (2017). PDLLA scaffolds with Cu- and Zn-doped bioactive glasses having multifunctional properties for bone regeneration. *J. Biomed. Mat. Res. A* 105 (3), 746–756. doi:10.1002/jbm.a.35952

Best, S. M., Porter, A. E., Thian, E. S., and Huang, J. (2008). Bioceramics: Past, present and for the future. *J. Eur. Ceram. Soc.* 28 (7), 1319–1327. doi:10.1016/j.jeurceramsoc.2007.12.001

Bimis, A., Canal, L. P., Karalekas, D., and Botsis, J. (2017). On the mechanical characteristics of a self-setting calcium phosphate cement. *J. Mech. Behav. Biomed. Mat.* 68, 296–302. doi:10.1016/j.jmbbm.2017.02.017

Binu, S., Soumya, S. J., and Sudhakaran, P. R. (2013). Metabolite control of angiogenesis: Angiogenic effect of citrate. *J. Physiol. Biochem.* 69 (3), 383–395. doi:10.1007/s13105-012-0220-9

Bonewald, L. F. (2011). The amazing osteocyte. *J. Bone Min. Res.* 26 (2), 229–238. doi:10.1002/jbmr.320

Camilleri, J., Laurent, P., and About, I. (2014). Hydration of Biodentine, Theracal LC, and a prototype tricalcium silicate-based dentin replacement material after pulp capping in entire tooth cultures. *J. Endod.* 40 (11), 1846–1854. doi:10.1016/j.joen.2014.06.018

Castro-Raucci, L. M. S., Teixeira, L. N., Barbosa, A. F. S., Fernandes, R. R., Raucci-Neto, W., Jacobovitz, M., et al. (2018). Calcium chloride-enriched calcium aluminate cement promotes *in vitro* osteogenesis. *Int. Endod. J.* 51 (6), 674–683. doi:10.1111/iej.12883

Chaushu, L., Chaushu, G., Kolerman, R., Vered, M., Naishlos, S., and Nissan, J. (2019). Anterior atrophic mandible restoration using cancellous bone block allograft. *Clin. Implant Dent. Relat. Res.* 21 (5), 903–909. doi:10.1111/cid.12744

Cole, K. A., Funk, G. A., Rahaman, M. N., and McIff, T. E. (2020). Mechanical and degradation properties of poly(methyl methacrylate) cement/borate bioactive glass composites. *J. Biomed. Mat. Res.* 108 (7), 2765–2775. doi:10.1002/jbm.b.34606

Cui, X., Huang, C., Zhang, M., Ruan, C., Peng, S., Li, L., et al. (2017). Enhanced osteointegration of poly(methylmethacrylate) bone cements by incorporating strontium-containing borate bioactive glass. *J. R. Soc. Interface* 14 (131), 20161057. doi:10.1098/rsif.2016.1057

Cui, X., Zhang, Y., Wang, J., Huang, C., Wang, Y., Yang, H., et al. (2020). Strontium modulates osteogenic activity of bone cement composed of bioactive borosilicate glass particles by activating Wnt/β-catenin signaling pathway. *Bioact. Mater.* 5 (2), 334–347. doi:10.1016/j.bioactmat.2020.02.016

Cui, X., Zhao, C., Gu, Y., Li, L., Wang, H., Huang, W., et al. (2014). A novel injectable borate bioactive glass cement for local delivery of vancomycin to cure osteomyelitis and regenerate bone. *J. Mat. Sci. Mat. Med.* 25 (3), 733–745. doi:10.1007/s10856-013-5122-z

De Witte, T. M., Wagner, A. M., Fratila-Apachitei, L. E., Zadpoor, A. A., and Peppas, N. A. (2020). Degradable poly(methyl methacrylate)-co-methacrylic acid nanoparticles for controlled delivery of growth factors for bone regeneration. *Tissue Eng. Part A* 26 (23-24), 1226–1242. doi:10.1089/ten.tea.2020.0010

Ding, Z., Li, H., Wei, J., Li, R., and Yan, Y. (2018). Developing a novel magnesium glycerophosphate/silicate-based organic-inorganic composite cement for bone repair. *Mater. Sci. Eng. C* 87, 104–111. doi:10.1016/j.msec.2018.03.001

Duan, H., Cao, C., Wang, X., Tao, J., Li, C., Xin, H., et al. (2020). Magnesium-alloy rods reinforced bioglass bone cement composite scaffolds with cortical bone-matching mechanical properties and excellent osteoconductivity for load-bearing bone *in vivo* regeneration. *Sci. Rep.* 10 (1), 18193. doi:10.1038/s41598-020-75328-7

Dupont, S., Morsut, L., Aragona, M., Enzo, E., Giulitti, S., Cordenonsi, M., et al. (2011). Role of YAP/TAZ in mechanotransduction. *Nature* 474 (7350), 179–183. doi:10.1038/nature10137

Elgali, I., Omar, O., Dahlin, C., and Thomsen, P. (2017). Guided bone regeneration: Materials and biological mechanisms revisited. *Eur. J. Oral Sci.* 125 (5), 315–337. doi:10.1111/eos.12364

Ewald, A., Kreczy, D., Bruckner, T., Gbureck, U., Bengel, M., Hoess, A., et al. (2019). Development and bone regeneration capacity of premixed magnesium phosphate cement pastes. *Mater. (Basel, Switz.* 12 (13), 2119. doi:10.3390/ma12132119

Forte, M. A., Silva, R. M., Tavares, C. J., and E Silva, R. F. (2021). Is poly(methyl methacrylate) (PMMA) a suitable substrate for ALD? *Polym. (Basel).* 13 (8), 1346. doi:10.3390/polym13081346

Fuchs, A., Kreczy, D., Bruckner, T., Gbureck, U., Stahlhut, P., Bengel, M., et al. (2021). Bone regeneration capacity of newly developed spherical magnesium phosphate cement granules. *Clin. Oral Investig.* 26, 2619–2633. doi:10.1007/s00784-021-04231-w

Funk, G. A., Burkes, J. C., Cole, K. A., Rahaman, M. N., and McIff, T. E. (2018). Antibiotic elution and mechanical strength of PMMA bone cement loaded with borate bioactive glass. *J. Bone Jt. Infect.* 3 (4), 187–196. doi:10.7150/jbji.27348

García-Gareta, E., Coathup, M. J., and Blunn, G. W. (2015). Osteoinduction of bone grafting materials for bone repair and regeneration. *Bone* 81, 112–121. doi:10.1016/j.bone.2015.07.007

Gauthier, O., Goyenvalle, E., Bouler, J. M., Guicheux, J., Pilet, P., Weiss, P., et al. (2001). Macroporous biphasic calcium phosphate ceramics versus injectable bone substitute: A comparative study 3 and 8 weeks after implantation in rabbit bone. *J. Mat. Sci. Mat. Med.* 12 (5), 385–390. doi:10.1023/a:1011284517429

Ghamor-Amegavi, E. P., Yang, X., Qiu, J., Xie, L., Pan, Z., Wang, J., et al. (2020). Composition control in biphasic silicate microspheres on stimulating new bone regeneration and repair of osteoporotic femoral bone defect. *J. Biomed. Mat. Res.* 108 (2), 377–390. doi:10.1002/jbm.b.34396

Gillman, C. E., and Jayasuriya, A. C. (2021). FDA-approved bone grafts and bone graft substitute devices in bone regeneration. *Mater. Sci. Eng. C* 130, 112466. doi:10.1016/j.msec.2021.112466

Gong, C., Fang, S., Xia, K., Chen, J., Guo, L., and Guo, W. (2020). Enhancing the mechanical properties and cytocompatibility of magnesium potassium phosphate cement by incorporating oxygen-carboxymethyl chitosan. *Regen. Biomater.* 8 (1), rbaa048. doi:10.1093/rb/rbaa048

Gordon, C. G., Mackey, J. L., Jewett, J. C., Sletten, E. M., Houk, K. N., and Bertozzi, C. R. (2012). Reactivity of biarylazacyclooctynones in copper-free click chemistry. *J. Am. Chem. Soc.* 134 (22), 9199–9208. doi:10.1021/ja3000936

Gu, Y., Xie, X., Zhuang, R., Weir, M. D., Oates, T. W., Bai, Y., et al. (2021). A biphasic calcium phosphate cement enhances dentin regeneration by dental pulp stem cells and promotes macrophages M2 phenotype *in vitro*. *Tissue Eng. Part A* 27 (17-18), 1113–1127. doi:10.1089/ten.tea.2020.0257

H Gresham, R. C., Bahney, C. S., and Leach, J. K. (2020). Growth factor delivery using extracellular matrix-mimicking substrates for musculoskeletal tissue engineering and repair. *Bioact. Mater.* 6 (7), 1945–1956. doi:10.1016/j.bioactmat.2020.12.012

Hakimi, M., Jungbluth, P., Sager, M., Betsch, M., Herten, M., Becker, J., et al. (2010). Combined use of platelet-rich plasma and autologous bone grafts in the treatment of long bone defects in mini-pigs. *Injury* 41 (7), 717–723. doi:10.1016/j.injury.2009.12.005

Hines, C. B. (2018). Understanding bone cement implantation syndrome. *Aana J.* 86 (6), 433–441.

Huang, W., Day, D. E., Kittiratanapiboon, K., and Rahaman, M. N. (2006). Kinetics and mechanisms of the conversion of silicate (45S5), borate, and borosilicate glasses to hydroxyapatite in dilute phosphate solutions. *J. Mat. Sci. Mat. Med.* 17 (7), 583–596. doi:10.1007/s10856-006-9220-z

Hurle, K., Oliveira, J. M., Reis, R. L., Pina, S., and Goetz-Neunhoeffer, F. (2021). Ion-doped brushite cements for bone regeneration. *Acta Biomater.* 123, 51–71. doi:10.1016/j.actbio.2021.01.004

Hurle, K., Weichhold, J., Brueckner, M., Gbureck, U., Brueckner, T., and Goetz-Neunhoeffer, F. (2018). Hydration mechanism of a calcium phosphate cement modified with phytic acid. *Acta Biomater.* 80, 378–389. doi:10.1016/j.actbio.2018.09.002

Katsimbri, P. (2017). The biology of normal bone remodelling. *Eur. J. Cancer Care (Engl).* 26 (6), e12740. doi:10.1111/ecc.12740

Kaur, M., Singh, H., Dhillon, J. S., Batra, M., and Saini, M. (2017). MTA versus biodentine: Review of literature with a comparative analysis. *J. Clin. Diagn. Res.* 11 (8), ZG01–ZG05. doi:10.7860/JCDR/2017/25840.10374

Khojasteh, A., Behnia, H., Naghdi, N., Esmaeelinejad, M., Alikhassy, Z., and Stevens, M. (2013). Effects of different growth factors and carriers on bone regeneration: A systematic review. *Oral Surg. Oral Med. Oral Pathology Oral Radiology* 116 (6), e405–e423. doi:10.1016/j.oooo.2012.01.044

Kim, S. B., Kim, Y. J., Yoon, T. L., Park, S. A., Cho, I. H., et al. (2004). The characteristics of a hydroxyapatite–chitosan–PMMA bone cement. *Biomaterials* 25 (26), 5715–5723. doi:10.1016/j.biomaterials.2004.01.022

Komatsu, N., Kajiya, M., Motoike, S., Takewaki, M., Horikoshi, S., Iwata, T., et al. (2018). Type I collagen deposition via osteoinduction ameliorates YAP/TAZ activity in 3D floating culture clumps of mesenchymal stem cell/extracellular matrix complexes. *Stem Cell. Res. Ther.* 9 (1), 342. doi:10.1186/s13287-018-1085-9

Lee, G. H., Makkar, P., Paul, K., and Lee, B. (2017). Incorporation of BMP-2 loaded collagen conjugated BCP granules in calcium phosphate cement based injectable bone substitutes for improved bone regeneration. *Mater. Sci. Eng. C* 77, 713–724. doi:10.1016/j.msec.2017.03.296

Lee, H. J., Kim, B., Padalhin, A. R., and Lee, B. T. (2019). Incorporation of chitosan-alginate complex into injectable calcium phosphate cement system as a bone graft material. *Mater. Sci. Eng. C* 94, 385–392. doi:10.1016/j.msec.2018.09.039

Li, C., Sun, J., Shi, K., Long, J., Li, L., Lai, Y., et al. (2020b). Preparation and evaluation of osteogenic nano-MgO/PMMA bone cement for bone healing in a rat critical size calvarial defect. *J. Mat. Chem. B* 8 (21), 4575–4586. doi:10.1039/d0tb00074d

Li, W. H., Hao, W., Wu, C., Tao, J., Ai, F., Xin, H., et al. (2020a). Injectable and bioactive bone cement with moderate setting time and temperature using borosilicate bio-glass-incorporated magnesium phosphate. *Biomed. Mat.* 15 (4), 045015. doi:10.1088/1748-605x/ab633f

Li, G., Shen, W., Tang, X., Mo, G., Yao, L., and Wang, J. (2021). Combined use of calcium phosphate cement, mesenchymal stem cells and platelet-rich plasma for bone regeneration in critical-size defect of the femoral condyle in mini-pigs. *Regen. Med.* 16 (5), 451–464. doi:10.2217/rme-2020-0099

Li, X., Li, G., Zhang, K., Pei, Z., Zhao, S., and Li, J. (2021). Cu-loaded Brushite bone cements with good antibacterial activity and operability. *J. Biomed. Mat. Res.* 109 (6), 877–889. doi:10.1002/jbm.b.34752

Li, Y., and Liu, C. (2017). Nanomaterial-based bone regeneration. *Nanoscale* 9 (15), 4862–4874. doi:10.1039/c7nr00835j

Liang, W., Gao, M., Lou, J., Bai, Y., Zhang, J., Lu, T., et al. (2020). Integrating silicon/zinc dual elements with PLGA microspheres in calcium phosphate cement scaffolds synergistically enhances bone regeneration. *J. Mat. Chem. B* 8 (15), 3038–3049. doi:10.1039/c9tb02901j

Liaw, C. Y., and Guvendiren, M. (2017). Current and emerging applications of 3D printing in medicine. *Biofabrication* 9 (2), 024102. doi:10.1088/1758-5090/aa7279

Lin, S. H., Zhang, W. J., and Jiang, X. Q. (2019). Applications of bioactive ions in bone regeneration. *Chin. J. Dent. Res.* 22 (2), 93–104. doi:10.3290/j.cjdr.a42513

Lin, X., Patil, S., Gao, Y-G., and Qian, A. (2020). The bone extracellular matrix in bone formation and regeneration. *Front. Pharmacol.* 11, 757. doi:10.3389/fphar.2020.00757

Liu, J., Liao, J., Li, Y., Yang, Z., Ying, Q., Xie, Y., et al. (2019). Bioactive tetracalcium phosphate/magnesium phosphate composite bone cement for bone repair. *J. Biomater. Appl.* 34 (2), 239–249. doi:10.1177/0885328219845597

Liu, S. M., Chen, W. C., Ko, C. L., Chang, H. T., Chen, Y. S., Haung, S. M., et al. (2021a). *In vitro* evaluation of calcium phosphate bone cement composite hydrogel beads of cross-linked gelatin-alginate with gentamicin-impregnated porous scaffold. *Pharm. (Basel)* 14 (10), 1000. doi:10.3390/ph14101000

Liu, X., Camilleri, E. T., Li, L., Gaihre, B., Rezaei, A., Park, S., et al. (2021b). Injectable catalyst-free "click" organic-inorganic nanohybrid (click-ON) cement for minimally invasive *in vivo* bone repair. *Biomaterials* 276, 121014. doi:10.1016/j.biomaterials.2021.121014

Lobenhoffer, P., Gerich, T., Witte, F., and Tscherne, H. (2002). Use of an injectable calcium phosphate bone cement in the treatment of tibial plateau fractures: A prospective study of twenty-six cases with twenty-month mean follow-up. *J. Orthop. Trauma* 16 (3), 143–149. doi:10.1097/00005131-200203000-00001

Ma, C., Tian, X., Kim, J. P., Xie, D., Ao, X., Shan, D., et al. (2018). Citrate-based materials fuel human stem cells by metabonegenic regulation. *Proc. Natl. Acad. Sci. U. S. A.* 115 (50), E11741–E11750. doi:10.1073/pnas.1813000115

Manton, K. J., Leong, D. F., Cool, S. M., and Nurcombe, V. (2007). Disruption of heparan and chondroitin sulfate signaling enhances mesenchymal stem cell-derived osteogenic differentiation via bone morphogenetic protein signaling pathways. *Stem Cells* 25 (11), 2845–2854. doi:10.1634/stemcells.2007-0065

McDonald, M. M., Kim, A. S., Mulholland, B. S., and Rauner, M. (2021). New insights into osteoclast biology. *JBMR plus* 5 (9), e10539. doi:10.1002/jbm4.10539

Mestres, G., and Ginebra, M. P. (2011). Novel magnesium phosphate cements with high early strength and antibacterial properties. *Acta Biomater.* 7 (4), 1853–1861. doi:10.1016/j.actbio.2010.12.008

Miao, Q., Yang, S., Ding, H., and Liu, J. (2020). Controlled degradation of chitosan-coated strontium-doped calcium sulfate hemihydrate composite cement promotes bone defect repair in osteoporosis rats. *Biomed. Mat.* 15 (5), 055039. doi:10.1088/1748-605x/ab9fcf

Mizoguchi, T., and Ono, N. (2021). The diverse origin of bone-forming osteoblasts. *J. Bone Min. Res.* 36 (8), 1432–1447. doi:10.1002/jbmr.4410

Myerson, C. L., Myerson, M. S., Coetzee, J. C., McGaver, R. Stone, and Giveans, M. R. (2019). Subtalar arthrodesis with use of adipose-derived cellular bone matrix compared with autologous bone graft: A multicenter, randomized controlled trial. *J. Bone Jt. Surg.* 101 (21), 1904–1911. doi:10.2106/jbjs.18.01300

Oh, S. H., Finones, R., Jin, S., Choi, S. Y., and Kim, K. N. (2004). Influence of tricalcium aluminate phase on *in vitro* biocompatibility and bioactivity of calcium aluminate bone cement. *J. Mat. Res.* 19 (4), 1062–1067. doi:10.1557/jmr.2004.0139

Okuchi, Y., Reeves, J., Ng, S. S., Doro, D. H., Junyent, S., Liu, K. J., et al. (2021). Wnt-modified materials mediate asymmetric stem cell division to direct human osteogenic tissue formation for bone repair. *Nat. Mat.* 20 (1), 108–118. doi:10.1038/s41563-020-0786-5

Oliveira, É. R., Nie, L., Podstawczyk, D., Allahbakhsh, A., Ratnayake, J., Brasil, D. L., et al. (2021). Advances in growth factor delivery for bone tissue engineering. *Int. J. Mol. Sci.* 22 (2), 903. doi:10.3390/ijms22020903

Ostrowski, N., Roy, A., and Kumta, P. N. (2016). Magnesium phosphate cement systems for hard tissue applications: A review. *ACS Biomater. Sci. Eng.* 2 (7), 1067–1083. doi:10.1021/acsbiomaterials.6b00056

P Baldwin, D. J. Li, Li, D. J., Auston, D. A., Mir, H. S., Yoon, R. S., and Koval, K. J. (2019). Autograft, allograft, and bone graft substitutes: Clinical evidence and indications for use in the setting of orthopaedic trauma surgery. *J. Orthop. Trauma* 33 (4), 203–213. doi:10.1097/bot.0000000000001420

Palmer, I., Nelson, J., Schatton, W., Dunne, N. J., Buchanan, F., and Clarke, S. A. (2016). Biocompatibility of calcium phosphate bone cement with optimised mechanical properties: An *in vivo* study. *J. Mat. Sci. Mat. Med.* 27 (12), 191. doi:10.1007/s10856-016-5806-2

Patel, A., Petrone, B., and Carter, K. R. (2021). "Percutaneous vertebroplasty and kyphoplasty," in *StatPearls* (Treasure Island (FL): StatPearls Publishing).

Paz, E., Ballesteros, Y., Abenojar, J., Del Real, J. C., and Dunne, N. J. (2019). Graphene oxide and graphene reinforced PMMA bone cements: Evaluation of thermal properties and biocompatibility. *Mater. (Basel)* 12 (19), 3146. doi:10.3390/ma12193146

Pei, P., Qi, X., Du, X., Zhu, M., Zhao, S., and Zhu, Y. (2016). Three-dimensional printing of tricalcium silicate/mesoporous bioactive glass cement scaffolds for bone regeneration. *J. Mat. Chem. B* 4 (46), 7452–7463. doi:10.1039/c6tb02055k

Ponzetti, M., and Rucci, N. (2021). Osteoblast differentiation and signaling: Established concepts and emerging topics. *Int. J. Mol. Sci.* 22 (13), 6651. doi:10.3390/ijms22136651

Raja, N., Park, H., Choi, Y-J., and Yun, H-s. (2021). Multifunctional calcium-deficient hydroxyl apatite–alginate core–shell-structured bone substitutes as cell and drug delivery vehicles for bone tissue regeneration. *ACS Biomater. Sci. Eng.* 7 (3), 1123–1133. doi:10.1021/acsbiomaterials.0c01341

Rattanachan, S. T., Srakaew, N. L., Thaitalay, P., Thongsri, O., Dangviriyakul, R., Srisuwan, S., et al. (2020). Development of injectable chitosan/biphasic calcium phosphate bone cement and *in vitro* and *in vivo* evaluation. *Biomed. Mat.* 15 (5), 055038. doi:10.1088/1748-605x/ab8441

Rho, Y. J., Choe, W. J., and Chun, Y. I. (2012). Risk factors predicting the new symptomatic vertebral compression fractures after percutaneous vertebroplasty or kyphoplasty. *Eur. Spine J.* 21 (5), 905–911. doi:10.1007/s00586-011-2099-5

Rupp, M. N. Walter, Ismat, A., and Alt, V. (2021). Polymethyl methacrylate cement coating of intramedullary implants : A new technique for revision surgery with the example of a temporary knee arthrodesis. Video article. *Orthopade* 50 (9), 758–762. doi:10.1007/s00132-021-04111-x

Saeed, H., Ahsan, M., Saleem, Z., Iqtedar, M., Islam, M., Danish, Z., et al. (2016). Mesenchymal stem cells (MSCs) as skeletal therapeutics - an update. *J. Biomed. Sci.* 23, 41. doi:10.1186/s12929-016-0254-3

Saruta, J., Ozawa, R., Hamajima, K., Saita, M., Sato, N., Ishijima, M., et al. (2021). Prolonged post-polymerization biocompatibility of polymethylmethacrylate-tri-n-butylborane (PMMA-TBB) bone cement. *Mater. (Basel)* 14 (5), 1289. doi:10.3390/ma14051289

Schlundt, C., El Khassawna, T., Serra, A., Dienelt, A., Wendler, S., Schell, H., et al. (2018). Macrophages in bone fracture healing: Their essential role in endochondral ossification. *Bone* 106, 78–89. doi:10.1016/j.bone.2015.10.019

Schlundt, C., Fischer, H., Bucher, C. H., Rendenbach, C., Duda, G. N., and Schmidt-Bleek, K. (2021). The multifaceted roles of macrophages in bone regeneration: A story of polarization, activation and time. *Acta Biomater.* 133, 46–57. doi:10.1016/j.actbio.2021.04.052

Schmidt, A. H. (2021). Autologous bone graft: Is it still the gold standard? *Injury* 52 (2), S18–s22. doi:10.1016/j.injury.2021.01.043

Shang, F., Yu, Y., Liu, S., Ming, L., Zhang, Y., Zhou, Z., et al. (2020). Advancing application of mesenchymal stem cell-based bone tissue regeneration. *Bioact. Mater.* 6 (3), 666–683. doi:10.1016/j.bioactmat.2020.08.014

Sharma, K., Sharma, S., Thapa, S., Bhagat, M., Kumar, V., and Sharma, V. (2020). Nanohydroxyapatite-Gelatin-and acrylic acid-based novel dental restorative material. *ACS Omega* 5 (43), 27886–27895. doi:10.1021/acsomega.0c03125

Sharma, R., Kapusetti, G., Bhong, S. Y., Roy, P., Singh, S. K., Singh, S., et al. (2017). Osteoconductive amine-functionalized graphene–poly(methyl methacrylate) bone cement composite with controlled exothermic polymerization. *Bioconjug. Chem.* 28 (9), 2254–2265. doi:10.1021/acs.bioconjchem.7b00241

Shen, H., Zhi, Y., Zhu, F., Si, J., Shi, J., and Shen, S. G. (2021). Experimental and clinical evaluation of BMP2-CPC graft versus deproteinized bovine bone graft for guided bone regeneration: A pilot study. *Dent. Mat. J.* 40 (1), 191–201. doi:10.4012/dmj.2019-437

Shi, Y. L. Yu, Yu, L., Gong, C., Li, W., Zhao, Y., and Guo, W. (2021). A bioactive magnesium phosphate cement incorporating chondroitin sulfate for bone regeneration. *Biomed. Mat.* 16 (3), 035034. doi:10.1088/1748-605x/abf5c4

Siracusa, V., Maimone, G., and Antonelli, V. (2021). State-of-Art of standard and innovative materials used in cranioplasty. *Polym. (Basel)* 13 (9), 1452. doi:10.3390/polym13091452

Song, Y., Huang, X., and Wu, L. (2020). Removal of intracardiac bone cement embolism after percutaneous kyphoplasty: A case report. *Med. Baltim.* 99 (11), e19354. doi:10.1097/md.0000000000019354

Subhi, H., Husein, A., Mohamad, D., Nik Abdul Ghani, N. R., and Nurul, A-A. (2021). Chitosan-based accelerated Portland cement promotes dentinogenic/osteogenic differentiation and mineralization activity of SHED. *Polymers* 13 (19), 3358. doi:10.3390/polym13193358

Talati, R. K., Hallak, J. A., Karas, F. I., de la Cruz, J., and Cortina, M. S. (2018). Retroprosthetic membrane formation in boston keratoprosthesis: A case-control-matched comparison of titanium versus PMMA backplate. *Cornea* 37 (2), 145–150. doi:10.1097/ico.0000000000001462

Tan, S., Wang, Y., Du, Y., Xiao, Y., and Zhang, S. (2021). Injectable bone cement with magnesium-containing microspheres enhances osteogenesis via anti-inflammatory immunoregulation. *Bioact. Mater.* 6 (10), 3411–3423. doi:10.1016/j.bioactmat.2021.03.006

Tang, G., Liu, Z., Liu, Y., Yu, J., Wang, X., Tan, Z., et al. (2021). Recent trends in the development of bone regenerative biomaterials. *Front. Cell. Dev. Biol.* 9, 665813. doi:10.3389/fcell.2021.665813

Tao, Z. S., Zhou, W. S., Zhang, R. T., Li, Y., Xu, H. G., Wei, S., et al. (2021). Co-modification of calcium phosphate cement to achieve rapid bone regeneration in osteoporotic femoral condyle defect with lithium and aspirin. *Am. J. Transl. Res.* 13 (3), 952–966.

Tavakoli, M., Bakhtiari, S. S. E., and Karbasi, S. (2020). Incorporation of chitosan/graphene oxide nanocomposite in to the PMMA bone cement: Physical, mechanical and biological evaluation. *Int. J. Biol. Macromol.* 149, 783–793. doi:10.1016/j.ijbiomac.2020.01.300

Tian, Y., Liu, J., et al. (2021). Clinical study of calcium phosphate cement loaded with recombinant human bone morphogenetic protein 2 combined with calcium phosphate cement loaded with antibiotic for chronic osteomyelitis with bone defect. *Zhongguo Xiu Fu Chong Jian Wai Ke Za Zhi* 35 (5), 573–578.

Tieh, M. T., Waddell, J. N., and Choi, J. J. E. (2021). Optical properties and color stability of denture teeth-A systematic review. *J. Prosthodont.* 31, 385–398. doi:10.1111/jopr.13429

van Houdt, C. I. A., Gabbai-Armelin, P. R., Lopez-Perez, P. M., Ulrich, D. J. O., Jansen, J. A., Renno, A. C. M., et al. (2018). Alendronate release from calcium phosphate cement for bone regeneration in osteoporotic conditions. *Sci. Rep.* 8 (1), 15398. doi:10.1038/s41598-018-33692-5

Vertesich, K., Sosa, B. R., Niu, Y, Ji, G, Suhardi, V, Turajane, K, et al. (2021). Alendronate enhances osseointegration in a murine implant model, *J. Orthop. Res.* 39, 719–726. doi:10.1002/jor.24853

Wang, G., Li, J., Zhang, W., Xu, L., Pan, H., Wen, J., et al. (2014). Magnesium ion implantation on a micro/nanostructured titanium surface promotes its bioactivity and osteogenic differentiation function. *Int. J. Nanomedicine* 9, 2387–2398. doi:10.2147/ijn.s58357

Wang, S., Xu, C., Yu, S., Wu, X., Jie, Z., and Dai, H. (2019). Citric acid enhances the physical properties, cytocompatibility and osteogenesis of magnesium calcium phosphate cement. *J. Mech. Behav. Biomed. Mat.* 94, 42–50. doi:10.1016/j.jmbbm.2019.02.026

Wang, X., Peng, X., Yue, P., Qi, H., Liu, J., Li, L., et al. (2020). A novel CPC composite cement reinforced by dopamine coated SCPP fibers with improved physicochemical and biological properties. *Mater. Sci. Eng. C* 109, 110544. doi:10.1016/j.msec.2019.110544

Wang, Y., Shen, S., Hu, T., Williams, G. R., Bian, Y., Feng, B., et al. (2021). Layered double hydroxide modified bone cement promoting osseointegration via multiple osteogenic signal pathways. *ACS Nano* 15 (6), 9732–9745. doi:10.1021/acsnano.1c00461

Wenisch, S., Stahl, J. P., Horas, U., Heiss, C., Kilian, O., Trinkaus, K., et al. (2003). *In vivo* mechanisms of hydroxyapatite ceramic degradation by osteoclasts: Fine structural microscopy. *J. Biomed. Mat. Res.* 67A (3), 713–718. doi:10.1002/jbm.a.10091

Wu, C., and Chang, J. (2012). Mesoporous bioactive glasses: Structure characteristics, drug/growth factor delivery and bone regeneration application. *Interface Focus* 2 (3), 292–306. doi:10.1098/rsfs.2011.0121

Wu, C., Zhang, Y., Zhu, Y., Friis, T., and Xiao, Y. (2010). Structure-property relationships of silk-modified mesoporous bioglass scaffolds. *Biomaterials* 31 (13), 3429–3438. doi:10.1016/j.biomaterials.2010.01.061

Wu, S., Lei, L., Bao, C., Liu, J., Weir, M. D., Ren, K., et al. (2021). An injectable and antibacterial calcium phosphate scaffold inhibiting *Staphylococcus aureus* and supporting stem cells for bone regeneration. *Mater. Sci. Eng. C* 120, 111688. doi:10.1016/j.msec.2020.111688

Wu, X., Dai, H., Yu, S., Zhao, Y., Long, Y., Li, W., et al. (2020). Magnesium calcium phosphate cement incorporating citrate for vascularized bone regeneration. *ACS Biomater. Sci. Eng.* 6 (11), 6299–6308. doi:10.1021/acsbiomaterials.0c00929

Wu, Y., Tang, X., Chen, J., Tang, T., Guo, H., Tang, S., et al. (2015). Improvement of bioactivity, degradability, and cytocompatibility of biocement by addition of mesoporous magnesium silicate into sodium-magnesium phosphate cement. *J. Mat. Sci. Mat. Med.* 26 (9), 238. doi:10.1007/s10856-015-5579-z

Yang, C., Wang, X., Ma, B., Zhu, H., Huan, Z., Ma, N., et al. (2017). 3D-Printed bioactive Ca(3)SiO(5) bone cement scaffolds with nano surface structure for bone regeneration. *ACS Appl. Mat. Interfaces* 9 (7), 5757–5767. doi:10.1021/acsami.6b14297

Yang, N., and Liu, Y. (2021). The role of the immune microenvironment in bone regeneration. *Int. J. Med. Sci.* 18 (16), 3697–3707. doi:10.7150/ijms.61080

Yorukoglu, A. C., Kiter, A. E., Akkaya, S., Satiroglu-Tufan, N. L., and Tufan, A. C. (2017). A concise review on the use of mesenchymal stem cells in cell sheet-based tissue engineering with special emphasis on bone tissue regeneration. *Stem cells Int.*, 2374161–2374213. doi:10.1155/2017/2374161

Zhang, F., Zhou, M., Gu, W., Shen, Z., Ma, X., Lu, F., et al. (2020). Zinc-/copper-substituted dicalcium silicate cement: Advanced biomaterials with enhanced osteogenesis and long-term antibacterial properties. *J. Mat. Chem. B* 8 (5), 1060–1070. doi:10.1039/c9tb02691f

Zhang, X., Kang, T., Liang, P., Tang, Y., and Quan, C. (2018). Biological activity of an injectable biphasic calcium phosphate/PMMA bone cement for induced osteogensis in rabbit model. *Macromol. Biosci.* 18 (3), 1700331. doi:10.1002/mabi.201700331

Zhang, Y., Cui, X., Zhao, S., Wang, H., Rahaman, M. N., Liu, Z., et al. (2015). Evaluation of injectable strontium-containing borate bioactive glass cement with enhanced osteogenic capacity in a critical-sized rabbit femoral condyle defect model. *ACS Appl. Mat. Interfaces* 7 (4), 2393–2403. doi:10.1021/am507008z

Zhu, J., Yang, S., Yang, Y., Yao, T., Liu, G., Fan, S., et al. (2021). Modified poly(methyl methacrylate) bone cement in the treatment of Kümmell disease. *Regen. Biomater.* 8 (1), rbaa051. doi:10.1093/rb/rbaa051

Zhu, J., Zhang, K., Luo, K., Qiu, Z., Yang, S., Cui, F., et al. Mineralized collagen modified polymethyl methacrylate bone cement for osteoporotic compression vertebral fracture at 1-year follow-up. Spine 1976), 2019. 44(12): p. 827–838. doi:10.1097/brs.0000000000002971

Zhu, T., Ren, H., Li, A., Liu, B., cui, C., Dong, Y., et al. (2017). Novel bioactive glass based injectable bone cement with improved osteoinductivity and its *in vivo* evaluation. *Sci. Rep.* 7 (1), 3622. doi:10.1038/s41598-017-03207-9

Zhu, Y., Goh, C., and Shrestha, A. (2021). Biomaterial properties modulating bone regeneration. *Macromol. Biosci.* 21 (4), e2000365. doi:10.1002/mabi.202000365

Zuleta, F., Murciano, A., Gehrke, S., Mate-Sanchez de Val, J., Calvo-Guirado, J., and De Aza, P. (2017). A new biphasic dicalcium silicate bone cement implant. *Mater. (Basel, Switz.* 10 (7), 758. doi:10.3390/ma10070758

frontiers | Frontiers in Bioengineering and Biotechnology

TYPE Original Research
PUBLISHED 23 August 2022
DOI 10.3389/fbioe.2022.971294

OPEN ACCESS

EDITED BY
Chen Yang,
University of Chinese Academy of Sciences, China

REVIEWED BY
Zhiwei Fang,
Johns Hopkins University, United States
Sneh Gautam,
G. B. Pant University of Agriculture and Technology, India
Adeleh Gholipour-Kanani,
Islamic Azad University, Iran

*CORRESPONDENCE
Mantas Malinauskas,
mantas.malinauskas@lsmuni.lt

SPECIALTY SECTION
This article was submitted to Biomaterials, a section of the journal Frontiers in Bioengineering and Biotechnology

RECEIVED 16 June 2022
ACCEPTED 19 July 2022
PUBLISHED 23 August 2022

CITATION
Malinauskas M, Jankauskaite L, Aukstikalne L, Dabasinskaite L, Rimkunas A, Mickevicius T, Pockevicius A, Krugly E, Martuzevicius D, Ciuzas D, Baniukaitiene O and Usas A (2022), Cartilage regeneration using improved surface electrospun bilayer polycaprolactone scaffolds loaded with transforming growth factor-beta 3 and rabbit muscle-derived stem cells. *Front. Bioeng. Biotechnol.* 10:971294. doi: 10.3389/fbioe.2022.971294

Cartilage regeneration using improved surface electrospun bilayer polycaprolactone scaffolds loaded with transforming growth factor-beta 3 and rabbit muscle-derived stem cells

Mantas Malinauskas[1]*, Lina Jankauskaite[1], Lauryna Aukstikalne[1], Lauryna Dabasinskaite[2], Augustinas Rimkunas[1], Tomas Mickevicius[1], Alius Pockevicius[3], Edvinas Krugly[2], Dainius Martuzevicius[2], Darius Ciuzas[2], Odeta Baniukaitiene[2] and Arvydas Usas[1]

[1]Institute of Physiology and Pharmacology, Lithuanian University of Health Sciences, Kaunas, Lithuania, [2]Faculty of Chemical Technology, Kaunas University of Technology, Kaunas, Lithuania, [3]Department of Veterinary Pathobiology, Veterinary Academy, Lithuanian University of Health Sciences, Kaunas, Lithuania

Polycaprolactone (PCL) has recently received significant attention due to its mechanical strength, low immunogenicity, elasticity, and biodegradability. Therefore, it is perfectly suitable for cartilage tissue engineering. PCL is relatively hydrophobic in nature, so its hydrophilicity needs to be enhanced before its use in scaffolding. In our study, first, we aimed to improve the hydrophilicity properties after the network of the bilayer scaffold was formed by electrospinning. Electrospun bilayer PCL scaffolds were treated with ozone and further loaded with transforming growth factor-beta 3 (TGFβ3). *In vitro* studies were performed to determine the rabbit muscle-derived stem cells' (rMDSCs) potential to differentiate into chondrocytes after the cells were seeded onto the scaffolds. Statistically significant results indicated that ozonated (O) scaffolds create a better environment for rMDSCs because collagen-II (Coll2) concentrations at day 21 were higher than non-ozonated (NO) scaffolds. In *in vivo* studies, we aimed to determine the cartilage regeneration outcomes by macroscopical and microscopical/histological evaluations at 3- and 6-month time-points. The Oswestry Arthroscopy Score (OAS) was the highest at both mentioned time-points using the scaffold loaded with TGFβ3 and rMDSCs. Evaluation of cartilage electromechanical quantitative parameters (QPs) showed significantly better results in cell-treated scaffolds at both 3 and 6 months. Safranin O staining indicated similar results as in macroscopical evaluations—cell-treated scaffolds revealed greater staining with safranin, although an empty defect also showed better results than non-cell-treated scaffolds. The scaffold with chondrocytes

represented the best score when the scaffolds were evaluated with the Mankin histological grading scale. However, as in previous *in vivo* evaluations, cell-treated scaffolds showed better results than non-cell-treated scaffolds. In conclusion, we have investigated that an ozone-treated scaffold containing TGFβ3 with rMDSC is a proper combination and could be a promising scaffold for cartilage regeneration.

KEYWORDS

cartilage regeneration, PCL scaffolds, ozone treatment, transforming growth factor-beta 3, rabbit MDSCs, cell-scaffold construct

1 Introduction

The subsequent healing of articular cartilage remains a significant clinical problem. Adult human articular cartilage is approximately 2–4 mm and serves as a cushion for joints against a physiological load (Hunziker et al., 2002). Because cartilage lacks nerves, blood vessels, and lymphatics, its ability to regenerate itself is restricted (Li et al., 2022). Thus, cartilage degradation can quickly lead to gradual tissue deterioration, persistent joint pain, dysfunction, and finally to the degenerative disease, osteoarthritis (OA) (Borrelli et al., 2019). To protect the cartilage from further degradation, it is necessary to apply the appropriate treatment. For many years, orthopedic surgeons treating articular cartilage injuries sought to achieve stable fixation of the articular cartilage surface restoration of limb alignment and joint stability (Borrelli et al., 2019). However, such treatment is not fully effective in cartilage preservation as it is also important to emphasize that there is an ongoing cellular response that needs to be controlled (Li et al., 2022). Following initial cartilage damage, local cells release inflammatory factors into the synovial fluid, which surrounds the cartilage (Sokolove and Lepus, 2013). These inflammatory factors, such as interleukin-1 or/and 6 (IL-1, IL-6), and tumor necrosis factor-alpha (TNF-α) inhibit chondrogenesis (Choukair et al., 2014). To improve neo-tissue formation, the impact of inflammation on cartilage tissue should be considered. A variety of techniques exist in articular cartilage repair and regeneration, each with its own advantages and drawbacks (Makris et al., 2015). The microfracture technique has limitations in chondrogenesis as this technique results in fibrocartilage formation, that is, biochemically and biomechanically inadequate for hyaline articular cartilage (Bae et al., 2006). Tissue engineering approaches using a variety of cell sources including autologous, allogenic, and xenogeneic stem cells have resulted in the repair of tissues with hyaline-like properties (Jelodari et al., 2022). Cartilage engineering by embedding relevant cells like articular chondrocytes or mesenchymal stem cells (MSCs) and growth factors, particularly transforming growth factor beta (TGFβ) (Wang et al., 2014), into scaffolds support chondrocyte growth and proliferation (Francis et al., 2018). In addition, MSCs scaffolding together with loaded differentiation factors, TGFβ1 or TGFβ3, may enhance articular cartilage formation because of their anti-inflammatory potential (Yoshimura et al., 2010; Stewart et al., 2018). MSCs are multipotent progenitor cells that can self-renew and differentiate into cartilage (Gomez-Salazar et al., 2020), while the most commonly used adult source tissue for human MSCs are bone marrow, muscle, and adipose tissue (Pittenger et al., 2019). Muscle-derived stem cells (MDSCs) have clonogenicity and growth kinetics superior to bone-derived stem cells (Čamernik et al., 2019). The necessity for a biomaterial scaffold to stimulate cell attachment, spreading, migration, proliferation, and differentiation for successful tissue regeneration is a fundamental challenge in tissue engineering in 3D microenvironments (Mohammadinejad et al., 2020). Biomaterials should be biodegradable and should have the same mechanical properties as native cartilage. However, no single best material is available that would be the gold standard for tissue engineering. Polycaprolactone (PCL) has recently received significant attention due to its mechanical strength, low immunogenicity, elasticity, biodegradability, and biocompatibility (Theodoridis et al., 2019). PCL scaffolds can promote stem cell differentiation and proliferation, while their hydrophobic profile inhibits cellular attachment, limiting their suitability in tissue engineering (Sousa et al., 2014). However, the surface of porous 3D PCL scaffold modification improves the hydrophilic properties and growth factor release (Qin et al., 2022). Treatment with ultraviolet irradiation and ozone (O_3) increases the surface hydrophilicity of PCL scaffolds for effective cell attachment and proliferation (Samsudin et al., 2017).

In this study, we aimed to evaluate the formation of cartilage tissue using rabbit muscle-derived stem cells (rMDSCs) on electrospun bilayer PCL ozone-treated scaffolds with loaded TGFβ3. The latter has been developed and validated *in vitro* during our earlier investigations (Dabasinskaite et al., 2022; Jankauskaite et al., 2022). First, we investigated the scaffold's potential *in vitro* to provide and maintain a microenvironment for rMDSC proliferation and differentiation into chondrocytes. In addition, to elucidate the advantages of ozone-treated (O) over non-ozonated (NO) scaffolds in order to select a more suitable scaffold variant for *in vivo* studies, we hypothesized that PCL ozone-treated scaffolds with loaded TGFβ3 and rMDSCs would outperform other groups and will show similar results to the control group—scaffolds with chondrocytes in the *in vivo* rabbit model for supporting neocartilage formation. Such

demonstration of this type of scaffold has not been described earlier.

2 Materials and methods

2.1 Polycaprolactone scaffold characteristics

The scaffold was formed from a two-layer composite of fibrous matrixes, each having variations in composition and processing. The chondral layer polymer solution was composed of poly(e)caprolactone (PCL, IUPAC name: (Hunziker et al., 2002; Bae et al., 2006):-polyoxepan-2-one, CAS: 24980–41–4, Mn—80 kDa, Cat. No: 440744) dissolved with cellulose and cellulose acetate (CA, 39.7% acetyl content, Mn–50 kDa, CAS: 9004-35-7). The subchondral layer polymer solution was prepared similarly to the chondral layer, except that hydroxyapatite (HA, <15 μm particle size, CAS: 1306-06-5) powder was added. The fabrication procedure of both layers and electrospinning and ozonation techniques (treatment with O_3) were described previously (Dabasinskaite et al., 2021; Dabasinskaite et al., 2022). PCL pellets and CA powder (2:1, w/w) were dissolved in acetone and N.N-dimethylformamide mixture at 2:3 (v/v) to obtain 30% (w/v) polymer solution. The mixing process was carried out at 40°C on the magnetic stirrer. The scaffolds were fabricated by using a cryo-electrospinning setup (voltage 26–28 kV, temperature 35°C, and RH 30%). The scaffolds were post-treated to convert cellulose acetate to cellulose and to introduce functional groups for the binding of the growth factor. The fabricated fibrous mats were cut into scaffold specimens (6 mm in diameter and a weight of 0.50 g). The scaffolds were placed in a glass reactor containing water (20°C) and treated by bubbling O_3 from an *ex situ* generator into the reactor at a mass flow of 400 mg/h. Subsequently, the samples were stored in a vacuum dryer at 21°C for 12 h. Before *in vitro* and *in vivo* experiments, scaffolds were sterilized with ethylene oxide. The scaffold was cut into 6 mm diameter and 1 mm height sample discs for *in vitro* and *in vivo* studies.

2.2 Transforming growth factor-beta 3 loading on bilayer polycaprolactone scaffolds

Dosage and timing of TGFβ3 (Thermo Fisher Scientific, United States) loading on PCL were selected, as previously described (Jankauskaite et al., 2022). In brief, scaffolds were incubated with 10 ng/ml TGFβ3. After the most efficient binding duration was clarified, samples for *in vitro* and *in vivo* experiments were covered with 100 μl of 10 ng/ml TGFβ3 for 24 h, providing sufficient time for protein binding to unmodified and modified scaffolds (Dabasinskaite et al., 2022). Subsequently, the unbound protein was washed with PBS, and scaffolds were submitted for further experiments.

2.3 Ethics in animal experimentation

Tissue collection for rMDSC and rabbit chondrocyte (rCh) isolation and further *in vivo* studies in rabbits were approved by the Ethics Committee of the State Food and Veterinary Service (No G2-133).

2.4 Isolation, differentiation, and characterization of rabbit muscle-derived stem cells

Biopsies of skeletal muscles of New Zealand rabbits (n = 4) were collected, and rMDSCs were isolated using a pre-plating technique with some modifications (Lavasani et al., 2013). After washing, dissecting from residual tendon, fat, and connective tissue, and mechanical digestion, minced muscle tissue was submitted for enzymatic digestion with 0.2% of collagenase type XI and kept with gentle continuous rocking at 37°C for 1.5 h. Furthermore, the previously described protocol was followed with an adjusted centrifugation speed of 1,400 rpm for 5 min (Lavasani et al., 2013). Obtained cells were cultivated in a monolayer on the collagen-coated surface using Dulbecco's modified Eagle's medium (DMEM) with 4.5 g glucose/L (Gibco, United Kingdom), supplemented with 10% fetal bovine serum (FBS) (Gibco, United Kingdom), 10% horse serum (HS) (Gibco, United Kingdom), 0.5% chicken embryo extract (LSP, United Kingdom), and 1% penicillin/streptomycin [Penicillin/Streptomycin (10000 U/l) (P/S), Gibco, United Kingdom] at 37°C in a 5% CO_2 humidified incubator. The medium for rMDSCs was changed every 3 days. Passages 5 up to 10 were used for further experiments.

First, the morphology of cells was evaluated *via* light microscopy. The lineage of isolated rMDSCs was identified by flow cytometry for strain biomarkers and by differentiation ability. Also, the sixth passage of rMDSCs was tested for CD45, CD44, and CD105 (Invitrogen, United States) by flow cytometry [FACSMelody (BD)]. Multipotent differentiation capacity was proven by induced, adipogenic, osteogenic, and myogenic differentiation in a monolayer and chondrogenic differentiation in pellet culture. Adipogenesis was induced with an adipogenesis differentiation medium (Gibco, United Kingdom). After 14 days of cultivation, adipogenic cultures were stained with Oil Red O (Sigma-Aldrich, United States) for microscopic visualization of lipid droplets. Osteogenesis was evaluated *via* microscopy when cultures were stained with alizarin red (Sigma-Aldrich, United States) and after 14 days of incubation with an osteogenesis differentiation medium (Gibco, United Kingdom). The chondrogenic

capacity was proved by successful chondrogenic pellet formation after 21 days of incubation with chondrogenesis differentiation medium (Gibco, United Kingdom) and stained with safranin O (Sigma-Aldrich, United States) and toluidine blue (Sigma-Aldrich, United States). Myogenesis was analyzed by muscle-specific desmin protein detection with immunohistochemistry using rabbit anti-desmin antibodies (Sigma-Aldrich, United States), and cell nuclei were highlighted by DAPI fluoroshield (Sigma-Aldrich, United States).

After differentiation, rMDSCs were fixed with 1% PFA and stained, as previously described. Fixed differentiated rMDSCs were evaluated *via* microscopy (Olympus BX63, Japan).

2.5 Isolation and monoculture of rabbit chondrocytes

Each biopsy sample of rabbit articular cartilage was taken from the intercondylar notch and immersed in a 50-ml conical sterile polypropylene centrifuge tube (TPP, Switzerland) containing a total of 15 ml transport medium with 12 ml of DMEM, 3 ml of fetal bovine serum (FBS) (Gibco, United Kingdom), and 15 µl of 0.1% gentamycin (Gibco, United Kingdom). The biopsy was transported immediately to the laboratory for further chondrocyte isolation procedure. The sample of articular cartilage was three times washed with Hams/F12 (Gibco, United Kingdom) containing 1% penicillin/streptomycin [penicillin/streptomycin (10000 U/l), Gibco, United Kingdom]. The cartilage was then minced with a sterile scalpel blade into small pieces in a petri dish containing 2 ml of protease (type XIV, >3.5 U/mg, Sigma-Aldrich, United States) solution. The minced cartilage was transferred into the tube with 8 ml of protease solution and left for digestion for 60 min at 37°C, with 5% CO2. After 60 min, the protease solution was changed to 10 ml of collagenase (type A > 150 U/mg, Worthington Biochemical, United States) solution, and cartilage pieces were digested for 16 h at 37°C and 5% CO_2. The enzymatic reaction was neutralized with 10 ml of DMEM supplemented with 10% FBS and 0.1% gentamycin (medium) and then filtered through a 70-µm cell strainer (Falcon, United Kingdom) into a 50-ml tube and centrifuged at x 300 g (4°C) for 10 min. The supernatant was carefully discarded, and the cell pellet was filled with a fresh 1 ml of medium. The mixture was resuspended, and the cell count and viability were determined by the trypan blue dye exclusion test. The cells were plated in tissue culture flasks at a density of 2×10^3 cell/cm^2. The morphology of the cells was examined regularly, and the image was taken with a microscope. When the cells reached 80%–90% confluence, they were trypsinized by TrypLE-Express enzyme (x1) and phenol red (Gibco, United Kingdom), and chondrocytes [passage 0 (P0)] were harvested, centrifuged, and resuspended in a culture medium. The culture medium was changed every 3 days. Cells were replated at a density of 2–6 × 10^3 cm^2.

2.6 Pellet culture

rMDSC and rCh pellets were established in microcentrifuge tubes by suspension of 2×10^5 cells in 400 µl of the medium. The tubes were centrifuged at x 300 g (4°C) for 6 min. The tops of the tubes were perforated with an 18-gauge needle after centrifugation to permit gaseous exchange. After 72 h, corresponding to the first time, the medium was changed, and the pellets were gently detached from the bottom. This procedure was repeated every 3 days until the 21-day pellet-culturing time-point was reached. The rMDSC pellet was cultured in a chondrogenesis differentiation medium (Gibco, United Kingdom). Control pellets containing rMDSC cells were cultured using an identical cell culture medium described in Section 2.5. The triplets of both pellets including rMDSC and control were formed.

2.7 Cell proliferation assay

Unstained cell-scaffold complexes were cultivated in 96-well plates. Briefly, cells were seeded on scaffolds at a density of 50,000 cells per scaffold. Three replicates were set up for each group. Cell proliferation was examined at the following time-points: days 1, 3, 7, 14, and 21. On each day, 10 µl of the CCK-8 (Abcam, United States) solution was added to each well with the cell-scaffold complex. After 3–4 h incubation, the medium was collected into separate 96-well plates, and the absorbance of each well was measured using a microplate reader (Thermo Fisher Scientific, Finland).

2.8 Enzyme-linked immunosorbent assay

TGFβ3 and collagen 2 (Coll2) concentrations in the supernatants during culturing were quantified using ELISA kits. The cell culture medium from TGFβ3-loaded NO or O scaffolds and non-TGFβ3-loaded NO or O scaffolds, both rMDSC and hCh were aspirated on days 1, 3, 7, 14, 21, and 28, frozen at −80°C, and kept until needed (less than one month). TGFβ3 and Coll2 were measured according to the protocols of commercially available ELISA kits: TGFβ3 (Assay Biotech, United States) and Coll2 (Cloud-Clone Corp., United States). Absorption at 450 nm was measured using a microplate reader (Multiskan GO 1.00.40 (Thermo Fisher Scientific)).

2.9 Animal surgery and scaffold preparation

Twenty-three male 3–4-month-old New-Zeeland White rabbits were used for the study. Each knee was randomly assigned to one of the following treatment groups. There were

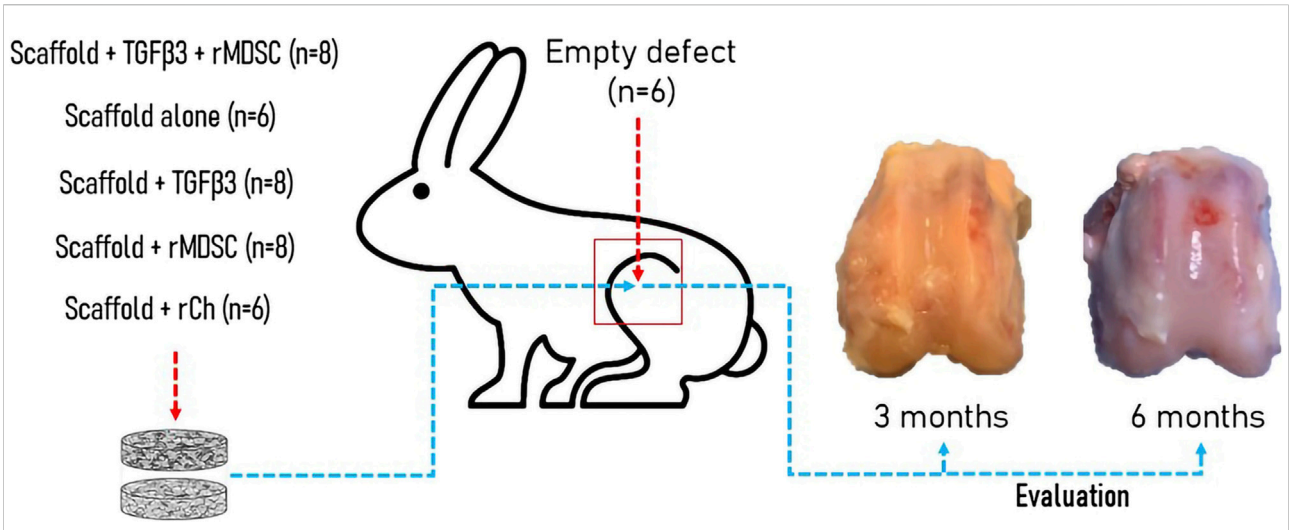

FIGURE 1
Experimental *in vivo* rabbit model. Different groups were formed according to the type of implant into the cartilage defect. Evaluation of cartilage repair including macroscopic, electromechanical, and histological analyses was performed after 3 and 6 months. TGFβ3, transforming growth factor-beta 3; rMDSCs, rabbit muscle-derived stem cells; rCh, rabbit chondrocyte.

six experimental groups according to the treatment and bilayer scaffold preparation for implantation into cartilage defect (Figure 1). There were the following groups: empty defect (E, $n = 6$), scaffold alone (cell-free and growth factor free) (S, $n = 6$), TGFβ3-loaded scaffold (St, $n = 8$), TGFβ3-loaded scaffold + rMDSC (Stm, $n = 8$), scaffold with rMDSC (Sm, $n = 8$), and scaffold with rabbit chondrocyte (rCh) (Sc, $n = 6$) groups. Ozonated scaffolds were used in all groups. Rabbits were euthanized 3 and 6 months after surgery. Two animals did not survive until the end of the designated time-point and were excluded from the study.

2.10 Surgical procedure

Under general isoflurane (Vetpharma Animal Health, Barcelona, Spain) anesthesia, following shaving and sterile preparation of both legs, a 3-cm medial parapatellar incision was made in each knee, exposing the patellofemoral groove. Using slow-speed dental trephine under constant irrigation with saline, an osteochondral defect, measuring 4.5 mm in diameter and 4–5 mm deep, was created in a trochlear groove in both knees. Defects were filled with a two-layer scaffold that consisted of the chondral layer made of poly(*e*)caprolactone and cellulose (PCL-CEL) at the top prepared in different ways and the subchondral layer made of PCL-CEL-HA at the bottom. Scaffolds were press-fitted into the cartilage defect and sealed with fibrin glue (Tisseel Lyo, Baxter, Switzerland). Following wound closure, the knee was moved through a full range of motion to ensure normal patellar tracking. After surgery, all animals were allowed to move freely in the cages and provided with food and water *ad libitum*.

2.11 Macroscopic evaluation and grading of the cartilage repair site

Thereafter, 3 and 6 months after implantation, animals were euthanized, and the articular cartilage defect repair site was evaluated macroscopically and assessed using a modified Oswestry Arthroscopy Score (OAS) by two independent researchers. According to this scoring system, the score was based on a point system with a total of 8 points, representing healthy cartilage. Repair tissue surface level, integration with surrounding cartilage, appearance, and color of the repair tissue surface were assessed. Stiffness on probing was excluded in our study because repaired cartilage properties were evaluated electromechanically by using an Arthro-BST device (Biomomentum Inc., Laval, Quebec, Canada).

2.12 Electromechanical evaluation

Electromechanical properties of cartilage were evaluated using an Arthro-BST device 3 and 6 months after transplantation, as described elsewhere (Mickevicius et al., 2015). Briefly, positively charged mobile ions in the cartilage stroma are displaced, with respect to the fixed and negatively charged proteoglycan molecules during cartilage compression. The probe of the device registers streaming potentials after

compression, and with the assistance of software, it generates quantitative parameters (QPs) in numeric values from 0 to 36. The high QP parameter is a digital reflection of extracellular matrix disintegration, weak electromechanical properties, and inferior load-bearing capacity of the cartilage, while low QP indicates strong electromechanical properties and superior load-bearing capacity. QP measurements in each repair site were recorded four to five times to obtain median values.

2.13 Histological evaluation and grading

After macroscopic and QP examination, distal femurs of the rabbits were dissected, fixed in 10% neutral buffered formalin, decalcified, and embedded in paraffin. Then, 5-F06DM thick sagittal sections were stained with safranin O/fast green, as previously described (Mickevicius et al., 2015). Light microscopy images of the repair site were taken at x 40 magnification with an Olympus BX61 microscope equipped with an Olympus DP72 CCD camera by cellSens Dimension imaging software (Olympus, Japan). A total of 30 snap pictures of the entire implantation site were combined into one final picture using the manual stitched image acquisition function of the software. The quality of the repaired cartilage was blindly evaluated by two investigators using the Mankin histological grading score, as described in Pearson et al. (2011). According to the Mankin grading system, healthy cartilage is rated with 0 points. The articular surface is rated 0–4 from smooth to cracked or completely disorganized, respectively. Chondrocyte morphology and proliferation are assessed from 0 (normal cell distribution) to 3 points (zones without cells). The extent of safranin-O staining is assessed from 0 to 4 points (not stained). With a maximum of 11 points, the cartilage is estimated as fully damaged.

2.14 Statistical analysis

Statistical analysis was accomplished by IBM SPSS 28.0 software (SPSS Inc., Chicago, IL, United States) for Windows. All the quantitative data were expressed as mean ± standard deviation (SD). Kruskal–Wallis and Mann–Whitney U tests were used to analyze the differences. A p-value of <0.05 was considered significant.

3 Results

3.1 Isolation, differentiation, and characterization of rabbit muscle-derived stem cells

Rabbit MDSCs were isolated from a few rabbits and analyzed by flow cytometry. FACS analysis showed the expressions of rabbit stem cell surface markers (CD44 and CD105) and lack of the hematopoietic marker (CD45) on pp6 (Figure 2A). Isolated cells excelled by homogeneity and rapid proliferation after pre-plate 6 cells were expanded (Figure 2B). Pp6 cells demonstrated adipogenic differentiation capacity after 14 days of cultivation in an adipogenic induction medium (Figure 2C, adipogenesis). The myogenic potential was determined by finding desmin-positive cells after 18 days of incubation with a low-serum myogenic medium (Figure 2C, myogenesis). After 14 days, rabbit MDSCs differentiated into osteocytes, and after 21 days, they formed a chondrogenic pallet which stained positive for safranin and toluidine blue, as shown in Figure 2C.

3.2 Rabbit muscle-derived stem cell proliferation and differentiation into chondrocytes

At the initial time-points (D1–D7), there was a significantly lower proliferation rate of rMDSCs on NO scaffolds than NO loaded with TGFβ3, as well as O with or without a TGFβ3 ($p < 0.01$) (Figure 3A). On day 14, NO showed a significant increase in rMDSC growth compared to NO loaded with TGFβ3. However, there were no significant cell growth changes when compared to the other two scaffolds. We analyzed the TGFβ3 protein release but observed no difference between the NO and O scaffolds loaded with TGFβ3 ($p > 0.05$) (Figure 3B). In addition, untreated scaffolds were tested to assess if rMDSCs produced TGFβ3; however, no protein was identified (data not shown).

Nevertheless, on day 21, ozonated TGFβ3-loaded PCL scaffolds showed increased Coll2 production, suggesting rMDSC differentiation into chondrocytes ($p < 0.001$) (Figure 3C).

3.3 Macroscopic evaluation and grading of the cartilage repair site

Considering that ozonated scaffolds provided a better environment in our *in vitro* studies and based on our previous research (Jankauskaite et al., 2022), they were further submitted for *in vivo* experiments.

The macroscopic images of the rabbit femoral condyles at 3 and 6 months after transplantation are depicted in Figure 4A. The mean Oswestry Arthroscopy Score (OAS) values in each experimental group are shown in Figure 4B.

Stm and Sm demonstrated better results 3 months after transplantation (mean score—7.50 ± 0.58 and 7.25 ± 0.5, respectively). Stm and Sm had significantly higher scores than E, S, St, or Sc. Sc showed significantly higher scores (mean score 6.38 ± 0.63) than S but significantly lower scores than Stm and Sm. Overall, E, S, and St had lower scores (5.38 ± 1.38, 4.88 ± 0.25, and 5.38 ± 0.48, respectively).

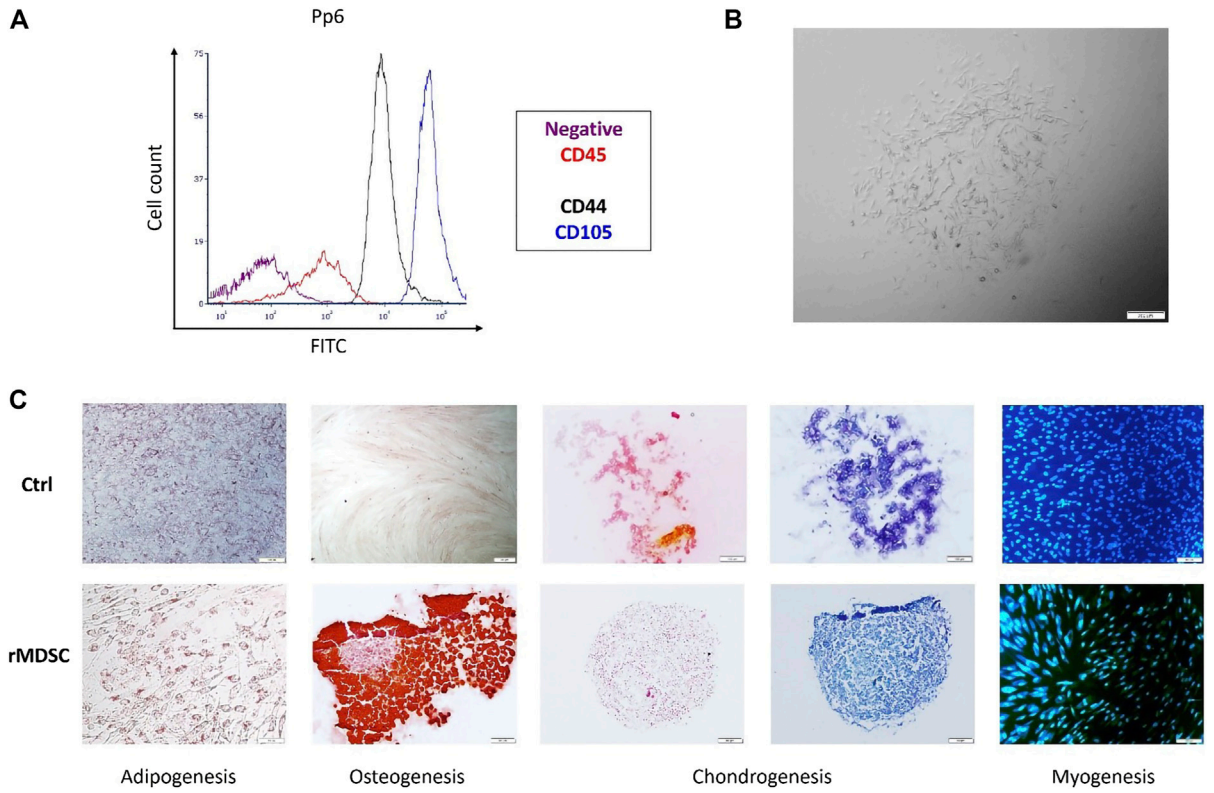

FIGURE 2
Characterization of isolated rMDSCs. The expression of specific stem-cell markers of preplate 6 (pp6) was tested *via* FACS **(A)**. Pp6 was differentiated into adipocytes, osteocytes, chondrocytes, and myocytes **(C)**. Isolated cell (preplate 6; passage 5) morphology was identified *via* microscopy **(B)**. **(A)** purple color—negative control, red—CD45, black—CD44, and blue—CD105; **(C)** adipogenesis—Oil Red O staining; osteogenesis—Alizarin red staining; chondrogenesis—safranin O (orange-red) and toluidine blue (blue) staining; myogenesis—DAPI (blue) and desmin (Fitc). CD, cluster of difference; pp6, preplate 6; rMDSCs, rabbit muscle-derived stem cells; ctrl, undifferentiated rMDSCs. Scale bar –100 μm.

At 6 months post-transplantation, Stm scored a high score (7.0 ± 0.82), and Sm and Sc scores were significantly higher than E, S, and St, but no difference was found between these groups. Sc was superior to E, S, and St ($p < 0.05$) (Figure 4B).

Overall, during the period from 3 to 6 months, results tended to show slight macroscopic score deterioration. Defects filled with S and Sc had statistically lower scores at 6 months than at 3 months, while scores of E, St, Stm, and Sm were similar between the time-points.

3.4 Electromechanical evaluation

Greater electromechanical quantitative parameter (QP) values represent greater degenerative changes in the cartilage (Figure 4C). After 3 months post-transplantation, the highest QP values were observed in the empty defect € and defect filled with scaffold alone (S) (10.85 ± 1.1 and 12.5 ± 3.87, respectively) compared to defects filled with St, Stm, and Sc scaffolds which had significantly lower QP values $p < 0.05$. St-, Stm-, and Sm-treated groups revealed similar results to Sc. Overall, Stm demonstrated the best QP value (5.95 ± 1.42); however, it was not significant compared to St, Sm, and Sc.

We observed similar tendencies 6 months post-transplantation. Worst QP values were registered in the E and S groups (14.15 ± 1.46 and 15.69 ± 1.46, respectively). In contrast to 3 months, at 6 months post-transplantation, S and St had significantly worse results than scaffolds with cells ($p < 0.05$). The best electromechanical values were attributed to Stm- and Sc-treated groups (7.05 ± 1 and 7.30 ± 2.04, respectively).

Comparing degenerative processes between 3 and 6 months post-transplantation, scaffolds without cells demonstrated clearly worse results than cellular scaffolds. The worst electromechanical measurements were found in empty defects and S scaffolds (Figure 4C). However, no statistical cartilage deterioration was observed in all cellular scaffolds after 6 months.

3.5 Histological evaluation and grading

Images of histological sections stained with safranin-O/fast green are presented in Figure 5A. Mankin histological grading

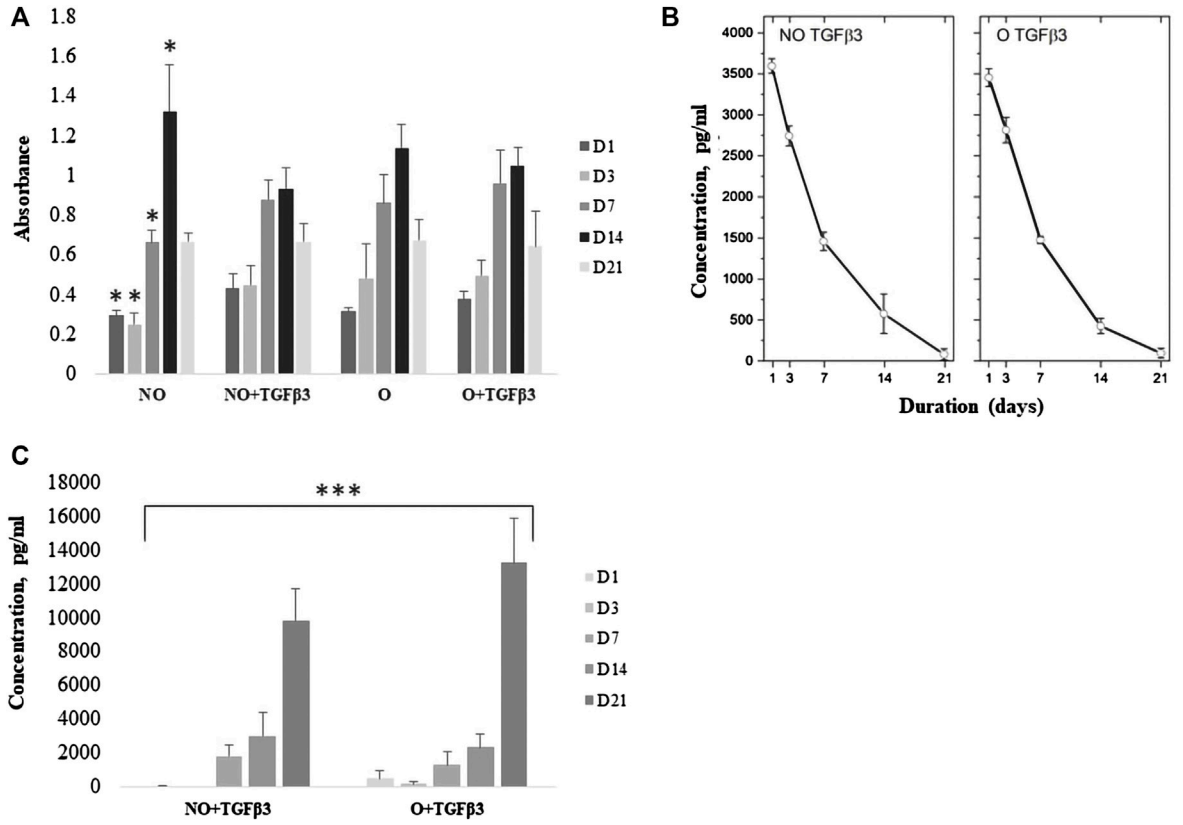

FIGURE 3
Cell proliferation within scaffolds **(A)**, TGFβ3 release from scaffolds with rMDSCs **(B)** and collagen-II (Coll2) protein production from ozone-treated and untreated scaffolds with loaded TGFβ3 **(C)**. The cell proliferation rate was tested on days **(D)** 1, 3, 7, 14, and, 21 *via* CCK-8. TGFβ3 and collagen-II protein levels were tested at the same time-points *via* ELISA. Results are presented as mean ± standard deviation. * represents p-value <0.01 comparing NO at D1, 3, and 7 to NO loaded with TGFβ3 and O with or without TGFβ3. p-value <0.01 also belongs to NO D14 compared with NO loaded with TGFβ3 **(A)**. *** represents <0.001 p-value; the Kruskal–Wallis test showed a significant difference between multiple time-points (D1–D21) compared to NO and O scaffolds loaded with TGFβ3 in Coll2 protein analyses **(C)**. NO-untreated; O, ozone-treated; TGFβ3, transforming growth factor-beta 3; pg/ml, picograms per milliliter.

scores in each experimental group are summarized in Figure 5B. At 3 months postoperatively, the repaired tissue was consistently well organized in all groups. Membranes were partially bonded to the adjacent cartilage and the subchondral bone, and little clustering was detected at the border of native cartilage. Active integration with adjacent cartilage was less evident. All grafts exhibited hyaline cartilage morphology (scarcity of safranin-O staining). Sc scaffolds demonstrated the best results after 3 months (3.0 ± 0.41). Stm and Sm had similar scores and were significantly better than S and St scaffolds (4.25 ± 1.26 and 4.5 ± 0.58, respectively). Interestingly, inferior results were observed in S (9.0 ± 1.83) and St scaffolds (7.25 ± 1.5) compared to cellular scaffolds ($p < 0.05$). Remarkably, empty defects had significantly better scores than S and St scaffolds and significantly worse scores than Sc scaffolds ($p < 0.05$), but no difference was observed with Stm and Sm scaffolds.

We observed similar results after 6 months. E, St, Stm, and Sm scores were similar. The worst results were observed in S and St scaffold groups (10.63 ± 0.75 and 7.75 ± 1.5, respectively), and it was clearly inferior to all other treatment groups ($p < 0.05$).

4 Discussion

With an increased life expectancy, there is an augmentation in degenerative conditions affecting cartilage tissue; thus, articular cartilage repair *via* different regenerative techniques is highly investigated. Recently, a focus has been set on engineering a biomimetic cellular microenvironment for the regeneration of a cartilaginous tissue, which has no potential to rejuvenate by itself. In our study, we aimed to examine the properties of an electrospun PCL bilayer scaffold consisting of a chondral layer with or without TGFβ3 and seeded with rMDSC and a subchondral layer supplemented with HA. To the best of our knowledge, this is the first study demonstrating that the PCL scaffold created a proper microenvironment for rabbit MDSCs

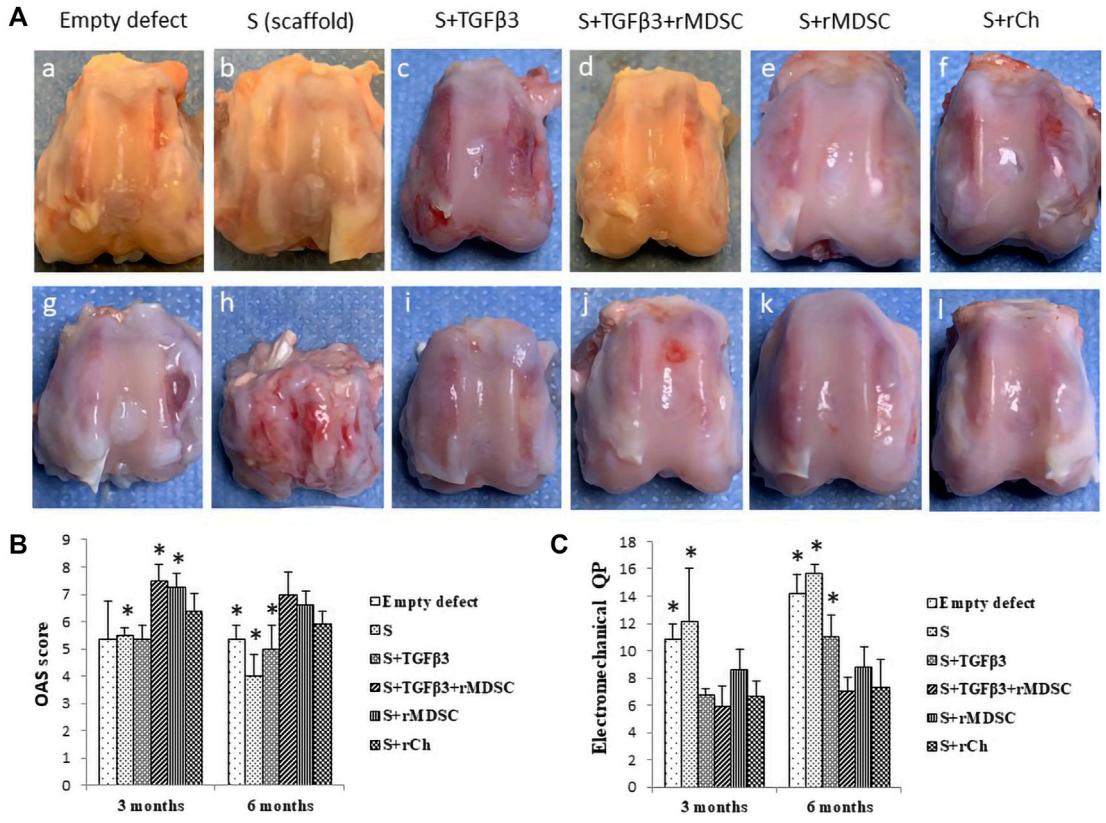

FIGURE 4
Healing of cartilage defects with different scaffolds after 3 **(A–F)** and 6 (g, h, i, j, k, and l) months **(A)**. Macroscopic evaluation of cartilage defect healing according to the Oswestry Arthroscopy Score (OAS) **(B)**. Evaluation of cartilage electromechanical quantitative parameters (QPs) by using the Arthro-BST device **(C)**. Results are presented as mean ± standard deviation. * represents *p*-value <0.05 compared to Sc with other scaffolds—S, Stm, and Sm at 3 months. In addition, the *p*-value <0.05 represents the difference compared to Sc with E, S, and St at 6 months **(B)**. *p*-value <0.05 showed as * indicates significant differences between Sc and E or S scaffolds at 3 months, also comparing Sc with E, S, and St scaffolds at 6 months **(C)**. S, scaffold; TGFβ3, transforming growth factor-beta 3; rMDSCs, rabbit muscle-derived stem cells; rCh, rabbit chondrocyte. Abbreviations of the scaffolds (E, S, St, Stm, Sm, and Sc) are described in Section 2.9.

and showed highly promising results toward neocartilage formation *in vitro* and *in vivo*.

Cells and their microenvironment are highly important in the regenerative process. First, such elements as chemical properties, technical composition, and mechanics are associated with cell behavior, e.g., their migration, proliferation, or differentiation (Demoor et al., 2014; Girão et al., 2020; Abpeikar et al., 2021). For our scaffold production, we selected PCL, a highly biodegradable, elastic, and low cytotoxic material used in the electrospinning process, which provided a porous structure for our scaffolds. The porosity of the chondral layer was 90.7%; the mean pore diameter was 171 μm. For the subchondral layer, porosity was 94.4%, and the mean pore diameter was 240 μm. To improve its properties, scaffolds underwent ozone treatment and were further modified by supplementation of TGFβ3 protein. Ozone treatment has been already analyzed and shown to impact cell adhesion and proliferation (Rediguieri et al., 2017; Samsudin et al., 2018). In addition, this process can improve attachment of growth factors such as insulin growth factor-1 (Dabasinskaite et al., 2021) necessary to increase required differentiation toward chondrocytes, while the present study did not show an obvious impact on better TGFβ3 attachment than non-ozonated scaffolds. As we used rMDSCs, we selected TGFβ3 as the additional factor which is a confirmed factor in stimulating stem cells to undergo the chondrogenesis process (Grafe et al., 2018; Music et al., 2020). This material and technique already examined in different studies created a proper environment for our cells—rabbit MDSCs and chondrocytes. We did show its potential in the previous experimental study as well (Jankauskaite et al., 2022). The proliferation capacity was increased within the first 14 days. Ozonation and protein loading gave clear advancement as rMDSCs proliferated significantly more in three scaffolds (NO + TGFβ3, O, and O + TGFβ3) and provided a superior environment for the cells. Even though we could not detect

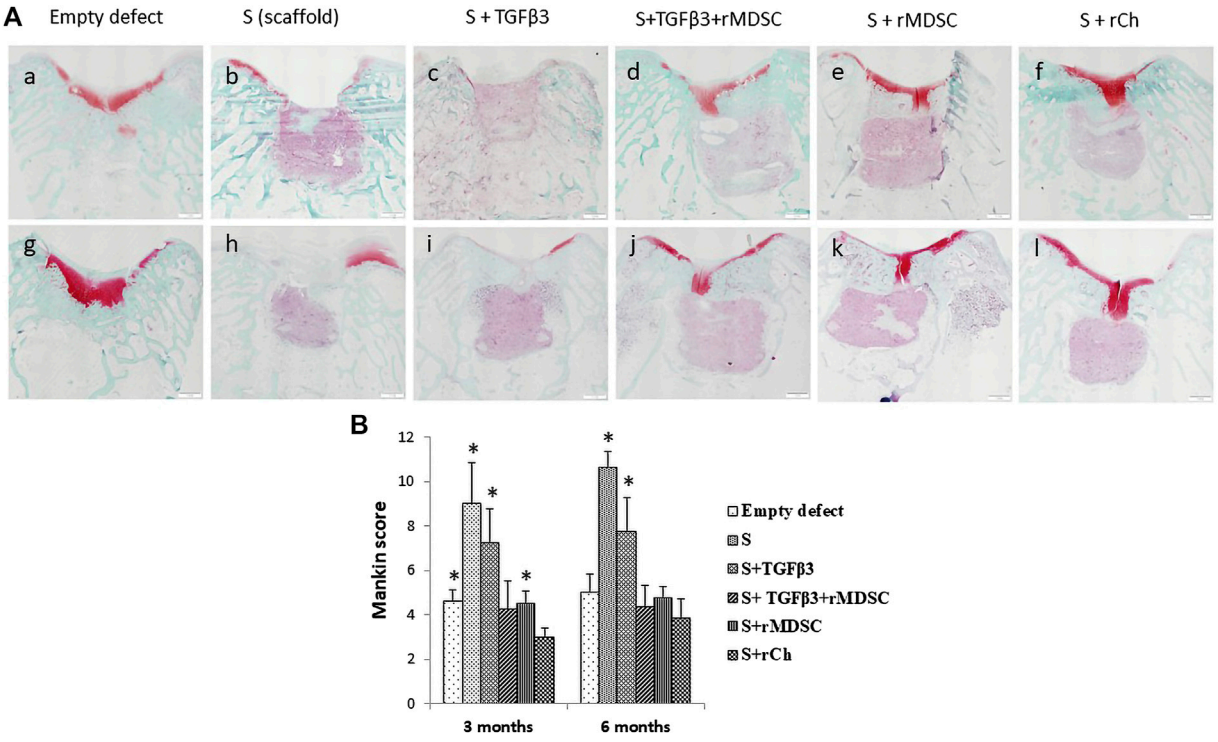

FIGURE 5
Safranin O staining of cartilage defects in different treatment groups after 3 **(A–F)** and 6 (g, h, i, j, k, and l) months **(A)**. Evaluation of cartilage healing according to the Mankin histological grading scale **(B)**. Scale bar-1 mm. Results are presented as mean ± standard deviation. * represents *p*-value <0.05 Sc with other scaffolds, E, S, St, and Sm scaffolds at 3 months. In addition, the *p*-value <0.05 represents a statistically significant difference compared to Sc with S and St scaffolds at 6 months. S, scaffold; TGFβ3, transforming growth factor-beta 3; rMDSCs, rabbit muscle-derived stem cells; rCh, rabbit chondrocyte. Abbreviations of the scaffolds (E, S, St, Stm, Sm, and Sc) are described in Section 2.9.

differences in TGFβ3 amounts between NO and O loaded with protein, ozone-treated protein-loaded PCL scaffolds demonstrated to provide a superior environment regarding neocartilage formation *in vitro*. The environment influencing and inducing proliferation is important, but differentiation toward chondrocytes is obligatory. Our scaffolds met those two requirements; moreover, cells were viable for 21 days, and differentiation into chondrocytes was observed starting on day 7. Interestingly, ozonated scaffolds loaded with TGFβ3 stimulated chondrogenesis earlier—starting on day 1 (after seeding).

At 3 months, the histological defect filled with the scaffold loaded with TGFβ3 and seeded with rMDSC had statistically comparable regeneration to the control group—the scaffold with chondrocytes. When scaffold-containing rMDSC was compared to a scaffold loaded with TGFβ3, the previous scaffold showed better regeneration. It suggests that rMDSCs, in the presence of TGFβ3, provide superior conditions for cartilage regeneration than using scaffolds only with cells. The positive effect of TGFβ3 in promoting chondrogenesis has been shown in the literature with other stem cells (Sun et al., 2018; Li et al., 2020). Moreover, we observed better macroscopic healing results after 3 months post-transplantation in animals treated with scaffolds containing rMDSC and TGFβ3 compared to scaffolds with chondrocytes alone. After 6 months, scaffolds with rMDSC and scaffolds containing TGFβ3 had comparable histological and macroscopic results. The findings indicate the TGFβ3 effect on the rMDSC ability to regenerate cartilage tissue for up to 3 months. On the contrary, after 6 months, scaffolds with TGFβ3 had significantly better outcomes than scaffolds alone. The findings suggest that scaffolds with the addition of TGFβ3 may stimulate surrounding host cells for up to 6 months. Various studies proved the beneficial effect of TGFβ3 on cartilage regeneration using different cell types and constructs (Sun et al., 2018; Li et al., 2020; Barati et al., 2020). As our scaffold is well biodegradable, the supplementation of TGFβ3 in the scaffold can promote differentiation and proliferation of remaining tissue chondrocytes in the scenario of cartilage injury (Li et al., 2022). In addition, it is possible that TGFβ3 can engage other types of cells circulating in the synovial fluid including fibroblasts (Denu et al., 2016), MSCs (Barati et al., 2020), or even fat cells (Li et al., 2020) to form new cartilage. At 6 months, a scaffold with TGFβ3 and rMDSCs showed comparable electromechanical,

macroscopic, and histological outcomes to the golden standard scaffold in our study called "control scaffold"—the scaffold embedded with chondrocytes. Chondrocyte-scaffold constructs are already widely applied in cartilage regeneration (Nam et al., 2009; Kon et al., 2011; Anders et al., 2012), having in mind the side effects of stem cells (overgrowth, tumor formation, need for specific conditions for specific tissue formation, etc.). However, the use of chondrocytes has its drawbacks because it can lead to the dedifferentiation of these cells (Mayne et al., 1976; Harrison et al., 2000; Stokes et al., 2001). This can result in further loss of tissue, increase inflammation, and cause progressing loss of the function of the joint. Therefore, another promising technique may be the use of MSCs and growth factors with optimally selected cell count and concentration of growth factor, as well as the selection of biomaterial and its appropriate fabrication to ensure the proper environment for seeded cells. In our study, over the 6-month period, the worsening results of the overall non-cellular groups were determined to show non-endurant properties of the regenerated tissue. Most of the cellular scaffolds demonstrated similar results between the same time-points. Sm and Stm scaffolds had comparable results between 3 and 6 months macroscopically, histologically, and electromechanically, indicating regenerated cartilage tissue-endurant properties over a 3-month period.

In summary, the present study showed the potential of the bilayer PCL scaffold, which was ozonated and loaded with TGFβ3 to stimulate rMDSC differentiation into cartilage tissue *in vitro* and *in vivo* in the rabbit model. This is the first study showing promising results of the combination of different factors (use of two differently prepared layers of the scaffold, ozone treatment, and embedding of stem cells) on articular cartilage regeneration. However, in order to translate the use of our developed scaffold into clinical studies, additional *in vitro* studies should be completed to eliminate the limitations of this scaffold. In addition, more *in vitro* studies should be performed to analyze the selection of the most appropriate concentration of TGFβ3 and the duration when scaffolds are incubated with the growth factor. Repeated *in vivo* studies are required if the results of *in vitro* studies will be significantly inferior/superior to those presented in our experiments. Adding, a longer *in vivo* study with regard to the articular joint function should be accomplished.

Data availability statement

The original contributions presented in the study are included in the article/Supplementary Material; further inquiries can be directed to the corresponding author.

Ethics statement

The animal study was reviewed and approved by the Ethics Committee of the State Food and Veterinary Service (G2-133).

Author contributions

AU—study conceptualization and design; LD, EK, DM, DC, and OB—scaffold production and testing; LJ—rMDSC isolation; MM—rCh isolation; LJ and LA—FACS, microscopy, *in vitro* cell experiments, protein binding, and data analysis; LJ and MM—protein analysis and data analysis; TM, AR, and AU—*in vivo* experiments and data analysis; AP—histology and microscopical *in vivo* tissue analysis; LJ and MM—manuscript drafting; LJ, MM, and AU—manuscript editing. All authors approved the final version of the manuscript.

Funding

This project has received funding from the European Regional Development Fund (project No 01.2.2-LMT-K-718-01-0078) under a grant agreement with the Research Council of Lithuania (LMTLT).

Acknowledgments

The authors kindly thank Prof. J. Kupcinskas' lab for providing access to FACS. They also thank all the patients who contributed to this research. Additionally, they thank Prof. V. Borutaite and her lab for access to the ELISA reader. The authors are grateful to our technician Laurencija Stroliene for all the support and laboratory administration.

Conflict of interest

The authors declare that the research was conducted in the absence of any commercial or financial relationships that could be construed as a potential conflict of interest.

Publisher's note

References

Abpeikar, Z., Milan, P. B., Moradi, L., Anjomshoa, M., and Asadpour, S. (2021). Influence of pore sizes in 3D-scaffolds on mechanical properties of scaffolds and survival, distribution, and proliferation of human chondrocytes. *Mech. Adv. Mater. Struct.* doi:10.1080/15376494.2021.1943077

Anders, S., Goetz, J., Schubert, T., Grifka, J., and Schaumburger, J. (2012). Treatment of deep articular talus lesions by matrix associated autologous chondrocyte implantation - results at five years. *Int. Orthop.* 36 (11), 2279–2285. doi:10.1007/s00264-012-1635-1

Bae, D. K., Yoon, K. H., and Song, S. J. (2006). Cartilage healing after microfracture in osteoarthritic knees. *Arthrosc. J. Arthrosc. Relat. Surg.* 22 (4), 367–374. doi:10.1016/j.arthro.2006.01.015

Barati, D., Gegg, C., and Yang, F. (2020). Nanoparticle-mediated TGF-β release from microribbon-based hydrogels accelerates stem cell-based cartilage formation *in vivo*. *Ann. Biomed. Eng.* 48 (7), 1971–1981. doi:10.1007/s10439-020-02522-z

Borrelli, J., Olson, S. A., Godbout, C., Schemitsch, E. H., Stannard, J. P., and Giannoudis, P. v. (2019). Understanding articular cartilage injury and potential treatments. *J. Orthop. Trauma* 33, S6–S12. doi:10.1097/bot.0000000000001472

Čamernik, K., Mihelič, A., Mihalič, R., Marolt Presen, D., Janež, A., Trebše, R., et al. (2019). Skeletal-muscle-derived mesenchymal stem/stromal cells from patients with osteoarthritis show superior biological properties compared to bone-derived cells. *Stem Cell Res.* 38, 101465. doi:10.1016/j.scr.2019.101465

Choukair, D., Hügel, U., Sander, A., Uhlmann, L., and Tönshoff, B. (2014). Inhibition of IGF-I-related intracellular signaling pathways by proinflammatory cytokines in growth plate chondrocytes. *Pediatr. Res.* 76 (3), 245–251. doi:10.1038/pr.2014.84

Dabasinskaite, L., Krugly, E., Baniukaitiene, O., Ciuzas, D., Martuzevicius, D., Jankauskaite, L., et al. (2022). Design and fabrication method of bi-layered fibrous scaffold for cartilage regeneration. *Biochem. Eng. J.* 182, 108413. doi:10.1016/j.bej.2022.108413

Dabasinskaite, L., Krugly, E., Baniukaitiene, O., Martuzevicius, D., Ciuzas, D., Jankauskaite, L., et al. (2021). The effect of ozone treatment on the physicochemical properties and biocompatibility of electrospun poly(ε)caprolactone scaffolds. *Pharmaceutics* 13 (8), 1288. doi:10.3390/pharmaceutics13081288

Demoor, M., Ollitrault, D., Gomez-Leduc, T., Bouyoucef, M., Hervieu, M., Fabre, H., et al. (2014). Cartilage tissue engineering: Molecular control of chondrocyte differentiation for proper cartilage matrix reconstruction. *Biochimica Biophysica Acta (BBA) - General Subj.* 1840 (8), 2414–2440. doi:10.1016/j.bbagen.2014.02.030

Denu, R. A., Nemcek, S., Bloom, D. D., Goodrich, A. D., Kim, J., Mosher, D. F., et al. (2016). Fibroblasts and mesenchymal stromal/stem cells are phenotypically indistinguishable. *Acta Haematol.* 136 (2), 85–97. doi:10.1159/000445096

Francis, S. L., di Bella, C., Wallace, G. G., and Choong, P. F. M. (2018). Cartilage tissue engineering using stem cells and bioprinting technology—barriers to clinical translation. *Front. Surg.* 5, 70. doi:10.3389/fsurg.2018.00070

Girão, A. F., Semitela, Â., Pereira, A. L., Completo, A., and Marques, P. A. A. P. (2020). Microfabrication of a biomimetic arcade-like electrospun scaffold for cartilage tissue engineering applications. *J. Mat. Sci. Mat. Med.* 31 (8), 69–9. doi:10.1007/s10856-020-06407-4

Gomez-Salazar, M., Gonzalez-Galofre, Z. N., Casamitjana, J., Crisan, M., James, A. W., and Péault, B. (2020). Five decades later, are mesenchymal stem cells still relevant? *Front. Bioeng. Biotechnol.* 8, 148. doi:10.3389/fbioe.2020.00148

Grafe, I., Alexander, S., Peterson, J. R., Snider, T. N., Levi, B., Lee, B., et al. (2018). TGF-B family signaling in mesenchymal differentiation. *Cold Spring Harb. Perspect. Biol.* 10 (5), a022202. doi:10.1101/cshperspect.a022202

Harrison, P. E., Ashton, I. K., Johnson, W. E. B., Turner, S. L., Richardson, J. B., and Ashton, B. A. (2000). The *in vitro* growth of human chondrocytes. *Cell Tissue Bank.* 1 (4), 255–260. doi:10.1023/a:1010131729208

Hunziker, E. B., Quinn, T. M., and Häuselmann, H. J. (2002). Quantitative structural organization of normal adult human articular cartilage. *Osteoarthr. Cartil.* 10 (7), 564–572. doi:10.1053/joca.2002.0814

Jankauskaite, L., Malinauskas, M., Aukstikalne, L., Dabasinskaite, L., Rimkunas, A., Mickevicius, T., et al. (2022). Functionalized electrospun scaffold-human-muscle-derived stem cell construct promotes *in vivo* neocartilage formation. *Polym. (Basel)* 14 (12), 2498. doi:10.3390/polym14122498

Jelodari, S., Ebrahimi Sadrabadi, A., Zarei, F., Jahangir, S., Azami, M., Sheykhhasan, M., et al. (2022). New insights into cartilage tissue engineering: Improvement of tissue-scaffold integration to enhance cartilage regeneration. *BioMed Res. Int.* 2022, 1–13. doi:10.1155/2022/7638245

Kon, E., Filardo, G., Berruto, M., Benazzo, F., Zanon, G., della Villa, S., et al. (2011). Articular cartilage treatment in high-level male soccer players: A prospective comparative study of arthroscopic second-generation autologous chondrocyte implantation versus microfracture. *Am. J. Sports Med.* 39 (12), 2549–2557. doi:10.1177/0363546511420688

Lavasani, M., Lu, A., Thompson, S. D., Robbins, P. D., Huard, J., and Niedernhofer, L. J. (2013). Isolation of muscle-derived stem/progenitor cells based on adhesion characteristics to collagen-coated surfaces. *Methods Mol. Biol.* 976, 53–65. doi:10.1007/978-1-62703-317-6_5

Li, D., Ma, X., and Zhao, T. (2020). Mechanism of TGF-β 3 promoting chondrogenesis in human fat stem cells. *Biochem. Biophys. Res. Commun.* 530 (4), 725–731. doi:10.1016/j.bbrc.2020.06.147

Li, M., Yin, H., Yan, Z., Li, H., Wu, J., Wang, Y., et al. (2022). The immune microenvironment in cartilage injury and repair. *Acta Biomater.* 140, 23–42. doi:10.1016/j.actbio.2021.12.006

Makris, E. A., Gomoll, A. H., Malizos, K. N., Hu, J. C., and Athanasiou, K. A. (2015). Repair and tissue engineering techniques for articular cartilage. *Nat. Rev. Rheumatol.* 11 (1), 21–34. doi:10.1038/nrrheum.2014.157

Mayne, R., Vail, M. S., Mayne, P. M., and Miller, E. J. (1976). Changes in type of collagen synthesized as clones of chick chondrocytes grow and eventually lose division capacity. *Proc. Natl. Acad. Sci. U. S. A.* 73 (5), 1674–1678. doi:10.1073/pnas.73.5.1674

Mickevicius, T., Pockevicius, A., Kucinskas, A., Gudas, R., MacIulaitis, J., Noreikaite, A., et al. (2015). Impact of storage conditions on electromechanical, histological and histochemical properties of osteochondral allografts. *BMC Musculoskelet. Disord.* 16 (1), 314. doi:10.1186/s12891-015-0776-y

Mohammadinejad, R., Kumar, A., Ranjbar-Mohammadi, M., Ashrafizadeh, M., Han, S. S., Khang, G., et al. (2020). Recent advances in natural gum-based biomaterials for tissue engineering and regenerative medicine: A review. *Polym. (Basel)* 12 (1), 176. doi:10.3390/polym12010176

Music, E., Klein, T. J., Lott, W. B., and Doran, M. R. (2020). Transforming growth factor-beta stimulates human bone marrow-derived mesenchymal stem/stromal cell chondrogenesis more so than kartogenin. *Sci. Rep.* 10 (1), 8340. doi:10.1038/s41598-020-65283-8

Nam, E. K., Ferkel, R. D., and Applegate, G. R. (2009). Autologous chondrocyte implantation of the ankle: A 2- to 5-year follow-up. *Am. J. Sports Med.* 37 (2), 274–284. doi:10.1177/0363546508325670

Pearson, R. G., Kurien, T., Shu, K. S. S., and Scammell, B. E. (2011). Histopathology grading systems for characterisation of human knee osteoarthritis--reproducibility, variability, reliability, correlation, and validity. *Osteoarthr. Cartil.* 19 (3), 324–331. doi:10.1016/j.joca.2010.12.005

Pittenger, M. F., Discher, D. E., Péault, B. M., Phinney, D. G., Hare, J. M., and Caplan, A. I. (2019). Mesenchymal stem cell perspective: Cell biology to clinical progress. *npj Regen. Med.* 4 (1), 22–15. doi:10.1038/s41536-019-0083-6

Qin, X., Wu, Y., Liu, S., Yang, L., Yuan, H., Cai, S., et al. (2022). Surface modification of polycaprolactone scaffold with improved biocompatibility and controlled growth factor release for enhanced stem cell differentiation. *Front. Bioeng. Biotechnol.* 9, 802311. doi:10.3389/fbioe.2021.802311

Rediguieri, C. F., de Bank, P. A., Zanin, M. H. A., Leo, P., Cerize, N. N. P., de Oliveira, A. M., et al. (2017). The effect of ozone gas sterilization on the properties and cell compatibility of electrospun polycaprolactone scaffolds. *J. Biomaterials Sci. Polym. Ed.* 28 (16), 1918–1934. doi:10.1080/09205063.2017.1358549

Samsudin, N., Hashim, Y. Z. H. Y., Arifin, M. A., Mel, M., Salleh, H. M., Sopyan, I., et al. (2017). Optimization of ultraviolet ozone treatment process for improvement of polycaprolactone (PCL) microcarrier performance. *Cytotechnology* 69 (4), 601–616. doi:10.1007/s10616-017-0071-x

Samsudin, N., Hashim, Y. Z. H., Arifin, M. A., Mel, M., Mohd Salleh, H., Sopyan, I., et al. (2018). Surface modification of Polycaprolactone (PCL) microcarrier for performance improvement of human skin fibroblast cell culture. *IOP Conf. Ser. Mat. Sci. Eng.* 290 (1), 012016. doi:10.1088/1757-899x/290/1/012016

Sokolove, J., and Lepus, C. M. (2013). Role of inflammation in the pathogenesis of osteoarthritis: Latest findings and interpretations. *Ther. Adv. Musculoskelet. Dis.* 5 (2), 77–94. doi:10.1177/1759720x12467868

Sousa, I., Mendes, A., Pereira, R. F., and Bártolo, P. J. (2014). Collagen surface modified poly(ε-caprolactone) scaffolds with improved hydrophilicity and cell adhesion properties. *Mater. Lett.* 134, 263–267. doi:10.1016/j.matlet.2014.06.132

Stewart, A. G., Thomas, B., and Koff, J. (2018). TGF-β: Master regulator of inflammation and fibrosis. *Respirology* 23 (12), 1096–1097. doi:10.1111/resp.13415

Stokes, D. G., Liu, G., Dharmavaram, R., Hawkins, D., Piera-Velazquez, S., and Jimenez, S. A. (2001). Regulation of type-II collagen gene expression during human chondrocyte de-differentiation and recovery of chondrocyte-specific phenotype in culture involves Sry-type high-mobility-group box (SOX) transcription factors. *Biochem. J.* 360 (2), 461–470. doi:10.1042/bj3600461

Sun, Q., Zhang, L., Xu, T., Ying, J., Xia, B., Jing, H., et al. (2018). Combined use of adipose derived stem cells and TGF-β3 microspheres promotes articular cartilage regeneration *in vivo*. *Biotech. Histochem.* 93 (3), 168–176. doi:10.1080/10520295.2017.1401663

Theodoridis, K., Aggelidou, E., Manthou, M., Demiri, E., Bakopoulou, A., and Kritis, A. (2019). Assessment of cartilage regeneration on 3D collagen-polycaprolactone scaffolds: Evaluation of growth media in static and in perfusion bioreactor dynamic culture. *Colloids Surfaces B Biointerfaces* 183, 110403. doi:10.1016/j.colsurfb.2019.110403

Wang, W., Rigueur, D., and Lyons, K. M. (2014). TGFβ signaling in cartilage development and maintenance. *Birth Defect. Res. C* 102 (1), 37–51. doi:10.1002/bdrc.21058

Yoshimura, A., Wakabayashi, Y., and Mori, T. (2010). Cellular and molecular basis for the regulation of inflammation by TGF- . *J. Biochem.* 147 (6), 781–792. doi:10.1093/jb/mvq043

frontiers | Frontiers in Bioengineering and Biotechnology

TYPE Original Research
PUBLISHED 26 August 2022
DOI 10.3389/fbioe.2022.990507

OPEN ACCESS

EDITED BY
Le Yu,
Ohio University, United States

REVIEWED BY
Jiang Wu,
The Fourth Military Medical University, China
Liwei Zheng,
Sichuan University, China

*CORRESPONDENCE
Kaili Lin,
lklecnu@aliyun.com
Jiaqiang Liu,
liujqmj@163.com
Jianyong Wu,
wujianyong@xinhuamed.com.cn

†These authors share first authorship

SPECIALTY SECTION
This article was submitted to Biomaterials, a section of the journal Frontiers in Bioengineering and Biotechnology

RECEIVED 10 July 2022
ACCEPTED 27 July 2022
PUBLISHED 26 August 2022

CITATION
Lao A, Chen Y, Sun Y, Wang T, Lin K, Liu J and Wu J (2022), Transcriptomic analysis provides a new insight: Oleuropein reverses high glucose-induced osteogenic inhibition in bone marrow mesenchymal stem cells via Wnt10b activation.
Front. Bioeng. Biotechnol. 10:990507.
doi: 10.3389/fbioe.2022.990507

Transcriptomic analysis provides a new insight: Oleuropein reverses high glucose-induced osteogenic inhibition in bone marrow mesenchymal stem cells *via* Wnt10b activation

An Lao[1†], Yu Chen[2†], Yiting Sun[2], Tiange Wang[2], Kaili Lin[2*], Jiaqiang Liu[2*] and Jianyong Wu[1*]

[1]Department of Stomatology, Xin Hua Hospital, Shanghai Jiao Tong University School of Medicine, Shanghai, China, [2]Shanghai Key Laboratory of Stomatology, National Center for Stomatology, National Clinical Research Center for Oral Diseases, Department of Oral and Cranio-maxillofacial Surgery, Shanghai Jiao Tong University School of Medicine, College of Stomatology, Shanghai Ninth People's Hospital, Shanghai Jiao Tong University, Shanghai, China

Adverse events of diabetes mellitus (DM) include bone damages, such as the increased incidence of osteoporosis and bone fractures, which are known as diabetic osteopathy. The pathogenic mechanism of diabetic osteopathy is complex, and hyperglycemia is a vital cause involved in it. Bone marrow mesenchymal stem cells (BMSCs) exert a significant effect on bone formation. Therefore, in this paper, transcriptomic changes of BMSCs cultured in high glucose (35 mM) for 30 days are mainly investigated. In addition, 794 up-regulated genes and 1,162 down-regulated genes were identified. Then, biological functions of the differentially expressed genes in the high glucose microenvironment were investigated by two kinds of functional analyses. Gene Set Enrichment Analysis was also applied to focus on the significant gene sets and it is found that Wnt10b expression witnessed a remarkable decrease in BMSCs under the high glucose microenvironment. At last, *in vitro* experiments revealed that oleuropein effectively reversed high glucose-induced osteogenic inhibition *via* activating Wnt10b in BMSCs.

KEYWORDS

transcriptome sequencing, BMSCs, high glucose microenvironment, Wnt10b, oleuropein

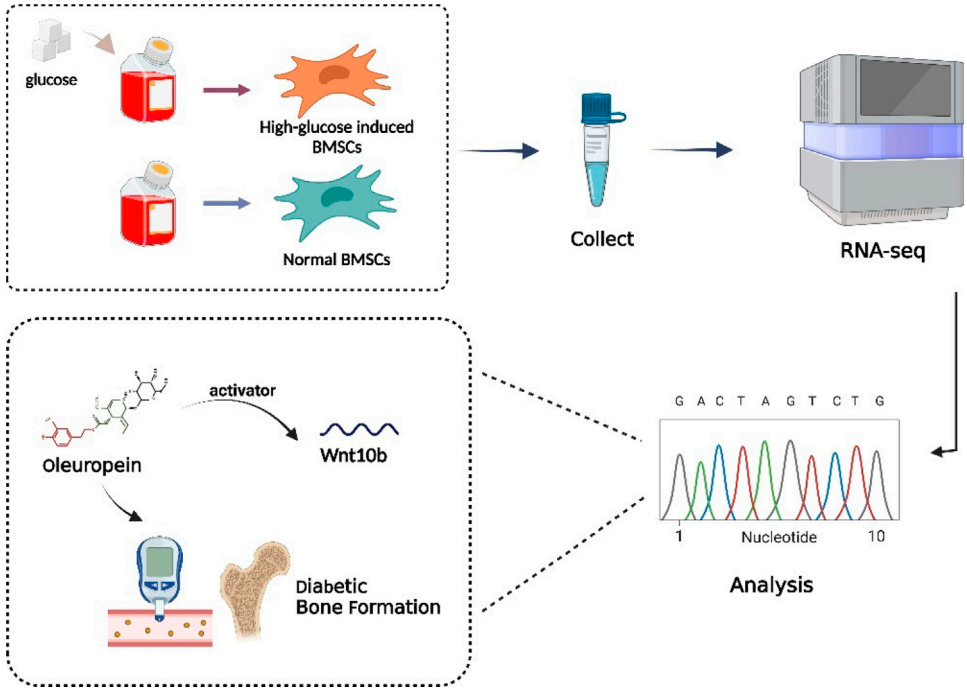

GRAPHICAL ABSTRACT

Highlights

Transcriptomic analysis indicates potential genes or pathways of influencing diabetic bone formation, which also providing a potential medicine—oleuropein. And we proved oleuropein reverses high glucose-induced osteogenic inhibition *via* wnt10b activation.

Introduction

DM is a common metabolic disease characterized by chronic hyperglycemia (Magliano et al., 2020), with an increasing prevalence worldwide (Zimmet et al., 2016). Its chronic complications exert negative effects on various organs, including bones, resulting in osteoporosis and fragility fractures, which are called "diabetic osteopathy". With a high morbidity and mortality, diabetic osteopathy is usually associated with high health-care costs (Hamann et al., 2012; Napoli et al., 2017). Diabetic osteopathy has complex underlying mechanisms, and is a result of the interaction of several factors, including a high glucose level and bone metabolism (Epstein et al., 2016; Chen et al., 2022).

Osteoblasts derived from mesenchymal stem cells control bone formation and osteoclasts stemmed from hematopoietic stem cells contribute to bone absorption. These dynamic processes are the key to the balance of bone metabolism (Rachner et al., 2011). If bone resorption and formation are out of balance, metabolic bone diseases such as age-related osteoporosis arise (Tencerova and Kassem, 2016). In the recent years, researchers have paid increasing attention to the biology of bone marrow, which is a chamber of bones and regulates bone homeostasis (Vandoorne et al., 2018; Zhou et al., 2019). Abnormalities of bone marrow microenvironment dynamics can also lead to metabolic bone diseases. Diabetes mellitus can cause various abnormalities of bone marrow microenvironment, the most intuitive of it is high glucose, which may contribute to the skeletal complications.

BMSCs are multipotent stem cells that exist in bone marrow stroma and can differentiate into osteoblasts (Guan et al., 2012; Tencerova and Kassem, 2016; Wei et al., 2022). It has been reported that there are reduced bone mass and inhibited osteogenesis in the condition of diabetes mellitus (Gilbert and Pratley, 2015), suggesting that an abnormal differentiation of BMSCs under high glucose microenvironment may be a possible pathogenetic mechanism, but it remained to be further investigated.

Several researches have been reported to explore the gene transcripts of BMSCs. Ao Zhou et al. (2016) investigated the effects of lipopolysaccharide (LPS) treatment on the changes of whole genome splicing pattern in mouse BMSCs, revealing that splicing patterns of 197 exons were changed by LPS. Serena Rubina Baglio et al. (2015) made small RNA sequencing analysis of exosomes secreted by mesenchymal stem cells of the adult

derived from two different sources: adipose and bone marrow. There is a lack of the sequencing analysis of BMSCs in a high glucose microenvironment, which requires further exploration and study.

RNA-seq analysis was carried out in this paper to characterize the transcriptomic changes of BMSCs in the high glucose microenvironment. Besides, whether a high glucose level led to BMSCs dysfunction and how it was regulated by a number of factors were explored. On the basis of RNA-seq results, we found that oleuropein may be the potential molecular compound to reverse high glucose-induced osteogenic inhibition. It may provide new insights and treatment methods into diabetic osteopathy.

Materials and methods

Animals and cell culture

4-week-old male C57BL/6 mice were bought from the Laboratory Animal Center of the 9th People's Hospital, affiliated to Shanghai Jiao Tong University School of Medicine. All the experiments of this study were approved by the Shanghai Jiao Tong University Animal Care and Use Committee. Metaphysis of mice femurs and tibias isolated from adherent soft tissue was cut out, and the marrow was rinsed with 10 ml Minimum Essential Medium Alpha (αMEM) containing 10% fetal bovine serum (FBS) and 1% penicillin and streptomycin (Gibco) and then cultured in a humid environment at 5% CO_2 and 37°C. On third day, the medium was changed to a new αMEM medium containing 5.5 mM or 35 mM glucose (Sigma-Aldrich, Shanghai, China), and the cells were cultured for another 30 days.

Flow cytometry

Before exposure to the high glucose microenvironment, flow cytometry was applied to verify the cells were stem cells. Mouse mesenchymal stem cell detection kit (MUXMX-09011, Cyagen, China) was used according to the instruction. The stained cells were detected by flow cytometer (NovoCyte™ 2060R, ACEA Biosciences, China).

RNA extraction, library construction, and sequencing.

After culturing for 30 days, total RNA was extracted from each group (containing three parallel samples) using RNAiso Plus reagent (Takara) following the instruction. A sequencing library was generated using the TruSeq RNA Sample Preparation Kit (Illumina). Then, mRNA was isolated and purified from the total RNA by magnetic beads with poly-T oligonucleotide attached. The divalent cations in Illumina's proprietary fragmenting buffer played the dominant part in fragmentation at high temperatures. Random oligonucleotides combined with SuperScript II produced the first strand cDNA, followed by the generation of the second strand cDNA by DNA polymerase I and RNase H. Under the action of exonucleases and polymerases, the rest overhangs were transformed to blunt ends and then removed. After treating the 3′ ends of the DNA fragments by adenylation, the Illumina PE adapter oligonucleotides were bound together for hybridization. The AMPure XP system (Beckman Coulter) was used to purify the library fragments, so as to pick out 200 bp-long cDNA fragments. In a PCR reaction with 15 cycles, the DNA fragments attached with adapter molecules at both ends were selectively enriched by Illumina PCR Primer Cocktail. AMPure XP system was used to purify the products before a high sensitivity DNA assay was conducted to quantify the products on a Bioanalyzer 2,100 system (Agilent). Finally, a HiSeq platform (Illumina) was used to sequence the library.

Transcriptome assembly and gene annotation

After sample sequencing, image files were obtained, which were then converted into FASTQ format data (Raw Data). The sequencing data were screened by the Cutadapt (v1.15) software to obtain sequences with good quality (Clean Data). HISAT2 (http://ccb.jhu.edu/software/hisat2/index.shtml) was used to the filtered reads to input into the reference genome, and the comparative region distribution of mapped reading fragments was calculated. Firstly, each gene's count values read were compared as the initial expression of the gene by using HTSeq (0.9.1) statistics, and then the expression was standardized by FPKM. Secondly, DESeq (1.30.0) was used to analyze the DEGs under the screened conditions of expression difference multiple $|\log2FoldChange| > 1$ as well as significant p-value < 0.05. At the same time, the two-way cluster analysis of all the genes differentially expressed in samples was conducted using R language Pheatmap (1.0.8) software package. The distance was calculated by the Euclidean method and the heat map was obtained by using the complete linkage method based on the expression of the same gene in various samples and distinct genes in the same sample. Next, we counted the number of genes differentially enriched in each Term after all genes were input into Terms of the Gene Ontology (GO) database. Terms significantly enriched by DEGs were summarized by the hypergeometric distribution method on the basis of the whole genome, in order to

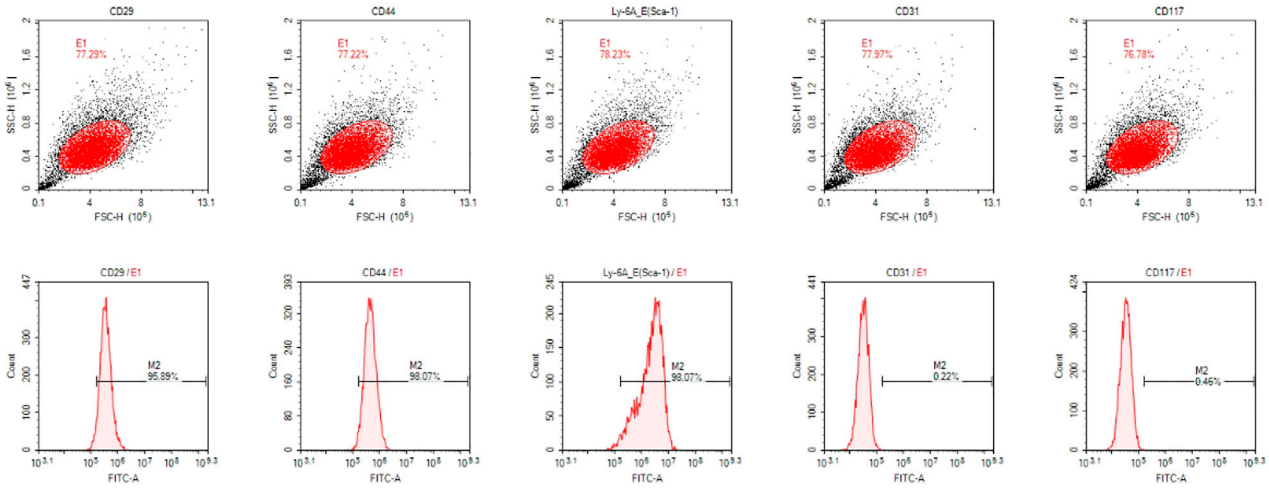

FIGURE 1
The results of flow cytometry.

TABLE 1 Primer sequences used in this study.

Primer	Primer sequences
Runx2	F: GACTGTGGTTACCGTCATGGC
	R: ACTTGGTTTTTCATAACAGCGGA
Osterix	F: CCTTCCCTCACTCATTTCCTGG
	R: TGTTGCCTGGACCTGGTGAGAT
OCN	F: GCAGGAGGGCAATAAGGTAGT
	R: GCGGTCTTCAAGCCATACTG
β-tubulin	F: CTGCTCATCAGCAAGATCAGAG
	R: GCATTATAGGGCTCCACCACAG
Wnt10b	F: GCGGGTCTCCTGTTCTTGG
	R: CCGGGAAGTTTAAGGCCCAG

reveal possible functions of these genes in samples. We also numbered genes differentially expressed in KEGG pathway at distinct levels, and the metabolic and signaling pathways involving DEGs were identified. Moreover, GSEA of all detected genes was conducted by GSEA software (version 3.0), which is on the basis of gene sets to analyze different biological functions between two groups.

Gene expression data sets

The GSE26168 dataset was obtained from the public Gene Expression Omnibus (GEO) database (http://www.ncbi.nlm.nih.gov/geo) and normalized using Robust Multichip Average (RMA). The student *t*-test was performed to compare differences between the experimental group and the control group. A *p*-value of 0.05 indicated statistical significance. IBM SPSS Statistics 20.0 was used for statistical analysis.

Cell proliferation assay

After cell culture in normal or high glucose medium (αMEM with 5.6 mM or 35 mM glucose) for 30 days, BMSCs were seeded at a density of 5×10^3 cells/well in a 96-well plate and induced with different concentrations of oleuropein for 1, 3, 7 days respectively. BMSCs proliferation was assessed using a cell counting kit-8 (CCK-8, Sangon, China). The absorbance at the wavelength of 450 nm was measured with a universal microplate spectrophotometer (Thermo LabSystems, Beverly, MA, United States).

Alkaline phosphatase assay

After cultured in normal or high glucose medium (αMEM with 5.6 mM or 35 mM glucose) for 30 days, BMSCs were seeded in a 48-well dish at a density of 2×10^4 cells/well. After adhered, the cells were cultured in osteogenic medium (Cyagen, China) with normal glucose (5.6 mM, LG group) and high glucose (35 mM, HG group), which were then induced with different concentrations of oleuropein (0, 3.125, 6.25, 12.5, 25, and 50 μM) (MCE, China) for another 7 days. ALP staining was performed in accordance with the instructions of BCIP/NBT Alkaline Phosphatase Kit (Beyotime, China), and the semi-quantitative analysis of ALP activity was operated based on the protocol of Alkaline Phosphatase Assay Kit (Nanjing Jiancheng, China).

10.3389/fbioe.2022.990507

TABLE 2 RNASeq Map statistics.

Sample	Clean reads	Total mapped	Multiple mapped	Uniquely mapped
HG_a	51040814	49525914 (97.03%)	1971785 (3.98%)	47554129 (96.02%)
HG_b	40477830	39400235 (97.34%)	1562007 (3.96%)	37838228 (96.04%)
HG_c	43331230	42167765 (97.31%)	1672053 (3.97%)	40495712 (96.03%)
LG_A	4365278	42250986 (96.78%)	1591466 (3.77%)	40659520 (96.23%)
LG_B	53030162	51361031 (96.85%)	2061740 (4.01%)	49299291 (95.99%)
LG_C	42047404	40707117 (96.81%)	1616699 (3.97%)	39090418 (96.03%)

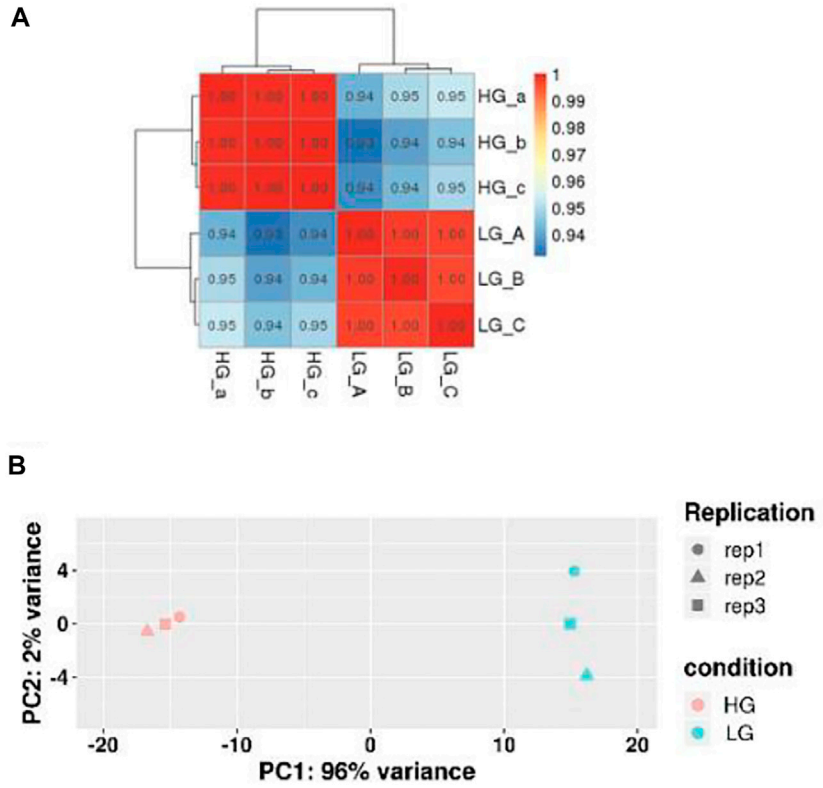

FIGURE 2
Correlation of gene expression levels between samples. **(A)** Sample Correlation Test. The closer the correlation coefficient was to one, the more similar the expression patterns between samples were. **(B)** Principal Components Analysis. The closer the samples, the higher the degree of similarity.

Quantitative real-time PCR

After 7 days of osteogenesis induction, RNAiso Plus (Takaro, Japan) was used to extract total RNA of different groups according to the manufacturer's instructions. Applying PrimeScript™ RT Master Mix kit (Perfect Real Time) (Takara, Japan) to reverse transcription. qPCR was performed *via* the TB Green Premix Ex Taq™ kit (Tli RNaseH Plus) (Takara) in LightCycler@ 96 Instrument (Roche). β-tubulin was standardized as the internal reference. Primer sequences used in this study were listed in Table 1.Each sample was assayed in triplicate. Data analysis adopted $2^{-\Delta\Delta CT}$ calculation method.

Data analysis

The Student *t*-test was performed to compare differences between two groups. One-way analysis of variance was used for comparison among multiple groups, followed by a stepwise comparison between groups. $\alpha = 0.05$, $p < 0.05$ considered as

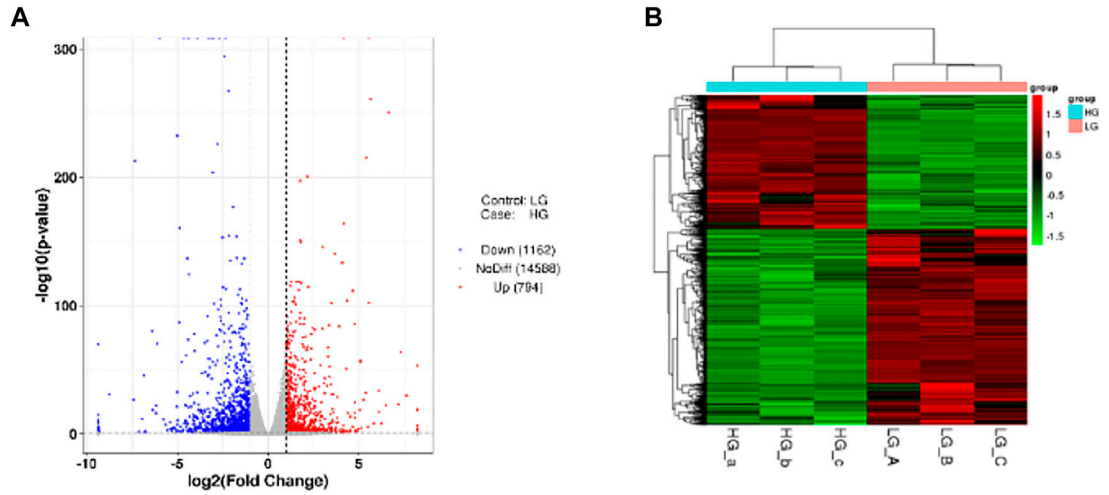

FIGURE 3
DEGs among the two groups. **(A)** The Volcano plot. The two vertical dashed lines mean 2 times the expression difference threshold. The dashed horizontal line stand for the threshold value of p-value = 0.05. The red dots are the upregulated genes HG group vs. LG group, while the blue dots are the downregulated genes, and the gray dots stand for the genes that are not significantly differentially expressed. **(B)** Cluster of differentially expressed genes. Red and green colors represent highly expressed genes and lowly expressed genes, respectively.

statistically significant. In the chart, statistical differences are indicated by "*", "*" means $p < 0.05$, "**"means $p < 0.01$, and "***"means $p < 0.001$. IBM SPSS Statistics 20.0 was used for statistical analysis.

Results

Flow cytometry results

The results of flow cytometry were shown in Figure 1. The positive expression rates of surface markers CD29, CD44, and Sca-1 of mesenchymal stem cells were 95.89%, 98.07%, and 98.07% respectively, while the positive expression rates of CD31 and CD117 were only 0.22% and 0.46% respectivley. These results indicated that the cells we extracted were identified as stem cells for their highly expressed surface markers of mesenchymal stem cells.

Sequencing, *de novo* assembly, and functional annotation

RNA-seq analysis of three parallel samples was carried out (three control samples and three experimental samples). We collected equal quantities of total RNA from the three replicates of the control and experimental groups to minimize the errors caused by individual differences. The assembled transcriptomes of BMSCs had a good quality (Table 2). Pearson correlation coefficient was employed to represent the correlation of gene expression levels between samples (Figure 2A). The expression patterns of the parallel samples from two groups were quite similar. Principal Components Analysis (PCA) also showed very similar results between samples (Figure 2B).

Differentially expressed genes

In order to study the gene expression in a high glucose environment, DESeq was used for differential analysis of genes expression. DEGs were screened under the conditions of $|\log2FoldChange| > 1$ with significant p-value <0.05 of all DEGs, we identified that 794 genes were upregulated while 1,162 were downregulated when BMSCs were exposed to high glucose environment (Figure 3A). The cluster of differentially expressed genes was shown in Figure 3B.

Functional analysis of DEGs

DEGs significantly enriched to GO terms or metabolic pathways were identified by the functional GO and KEGG enrichment analysis. As can be seen from the GO database, DEGs mainly included the following potential functions, namely, cellular component (CC), molecular function (MF) and biological process (BP). In each GO category, the top 10 GO term items with the smallest p-value have the most significant enrichment (Figure 4A). According to the GO enrichment results, the degree of enrichment was measured by the values of rich factor, FDR and the number of genes enriched to this GO Term. The top 20 GO

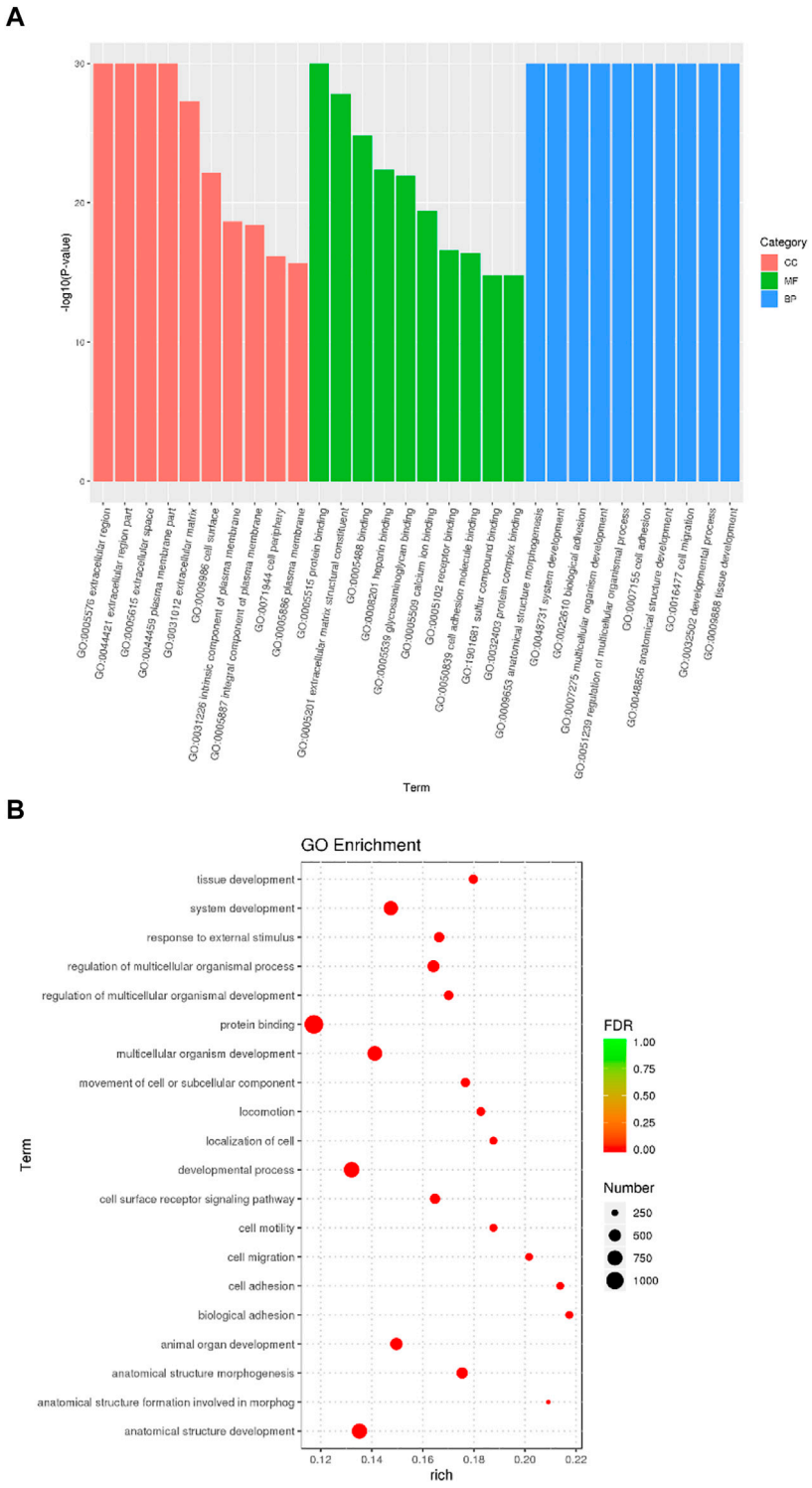

FIGURE 4
GO enrichment analysis of DEGs from BMSCs in high glucose microenvironment at 35 mM concentration for 30 days. **(A)** GO enrichment analysis histogram. **(B)** GO enrichment analysis bubble map.

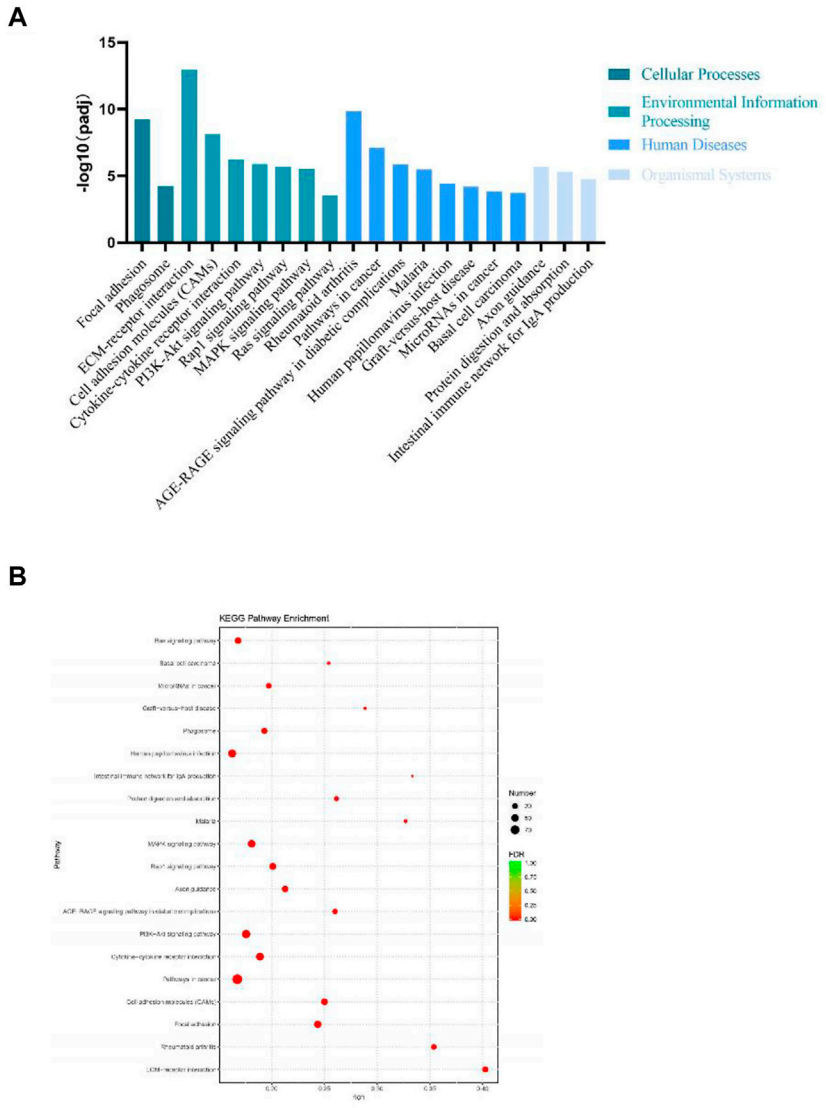

FIGURE 5
KEGG enrichment analysis of DEGs from BMSCs in high glucose microenvironment at 35 mM concentration for 30 days. **(A)** KEGG pathway enrichment analysis histogram. **(B)** KEGG enrichment analysis bubble map.

Term items with the least FDR value have the most significant enrichments (Figure 4B). It is worth noting that the potential function functions of DEGs related to cell activities such as motility, migration and adhesion, as well as to the development of system, multicellular organism, anatomical structure and tissue. All the annotated KEGG pathways were grouped into four major types: cellular processes, environmental information, human diseases and organismal systems. The top 20 GO pathways with the smallest *p* value and enriched by most genes are shown in Figure 5A. Interestingly, we found our results verified some ideas in the field of diabetic suppression of bone formation. Just as Figure 5A illustrated, high glucose microenvironment influences biological process of stem cells such as migration, adhesion, which may be one of the main reasons why the diabetic condition proved to be detrimental for osteogenesis (Gilbert, 2013; Chen et al., 2021). Figure 5B shows the top 20 KEGG Term items having the most significant enrichment, including PI3K-Akt, Rap1, MAPK, Ras, and TGF-beta signaling pathways. PI3K-AKT pathways and MAPK pathways are both classical pathways that related to osteogenesis. Also, PI3K-AKT, Ras, and TGF-beta signaling pathways implied inflammation or reactive oxygen species (ROS) would be crucial to diabetic bone formation (Sanchez-de-Diego et al., 2019; Yuchen et al., 2020; Dawei et al., 2021; Zhang et al., 2021). Interestingly, two signaling pathways were found to be related to diabetes mellitus, i.e., AGE-RAGE pathway in diabetic complications and Type 1 diabetes mellitus. Activation of advanced glycation end

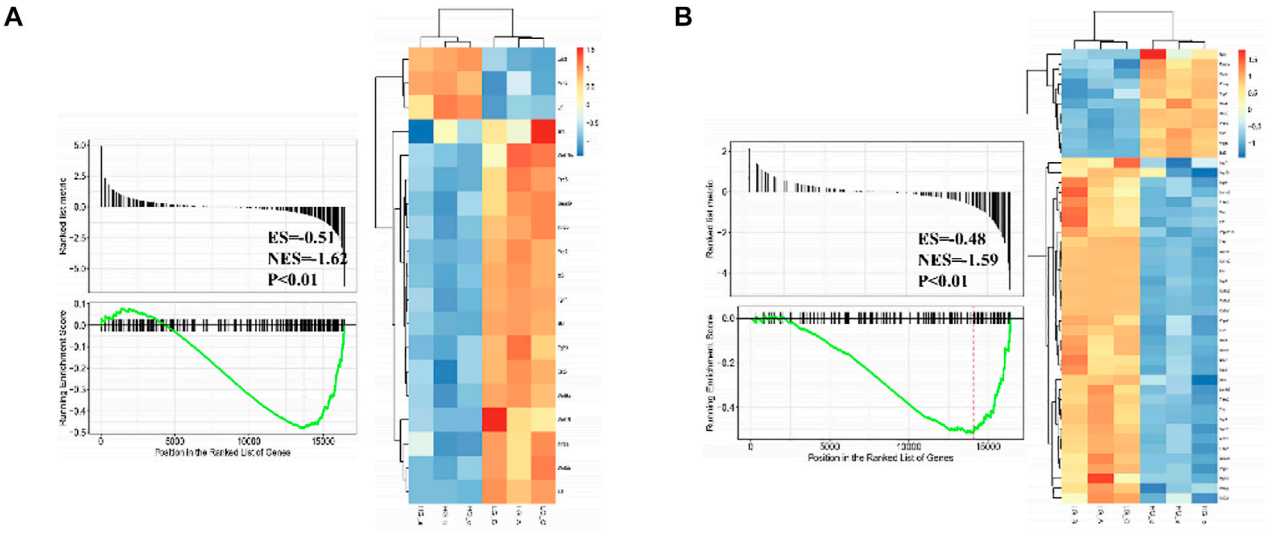

FIGURE 6
GSEA plot showing most enriched gene sets of all detected genes from BMSCs in high glucose microenvironment at 35 mM concentration for 30 days.

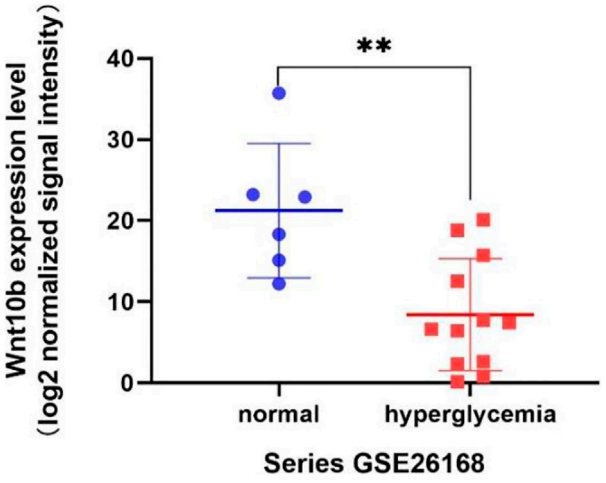

FIGURE 7
Wnt10b expression level from the GEO data sets (GSE26168).

products (AGEs) receptor by the high glucose enhanced the expression of inflammatory cytokines and contributed to chronic inflammation (Napoli et al., 2017).

GSEA findings

Differentially expressed gene sets between normal glucose and high glucose microenvironment were identified using with FDR < 0.25 and p-value < 0.001. The top two gene sets that were negatively related to high glucose condition were enriched in focal adhesion and signaling pathways regulating pluripotency of stem cells. DEGs related to these two gene sets were shown in Figure 6.

Wnt10b was significantly downregulated in DM

According to the result of GSEA, genes associated with pluripotency regulation of stem cells were significantly down-regulated under a high glucose microenvironment, including Wnt10b. Through searching the public Gene Expression Omnibus (GEO) database, a previous study (GSE26168) analyzed the blood samples of male pre-diabetes and Type 2 Diabetes mellitus (T2DM) patients after an overnight fasting (Karolina et al., 2011). Then we reanalyzed the GSE26168 dataset and consistently found the down-regulated expression of Wnt10b in blood samples of people with impaired fasting glucose and DM (Figure 7).

Oleuropein reversed the osteogenic suppression of BMSCs under the high glucose microenvironment *via* Wnt10b activation

To further verity the function of Wnt10b in osteogenic activity of BMSCs, cells cultured with high-glucose medium were dealt with oleuropein, which proved to be an activator of Wnt10b (Park

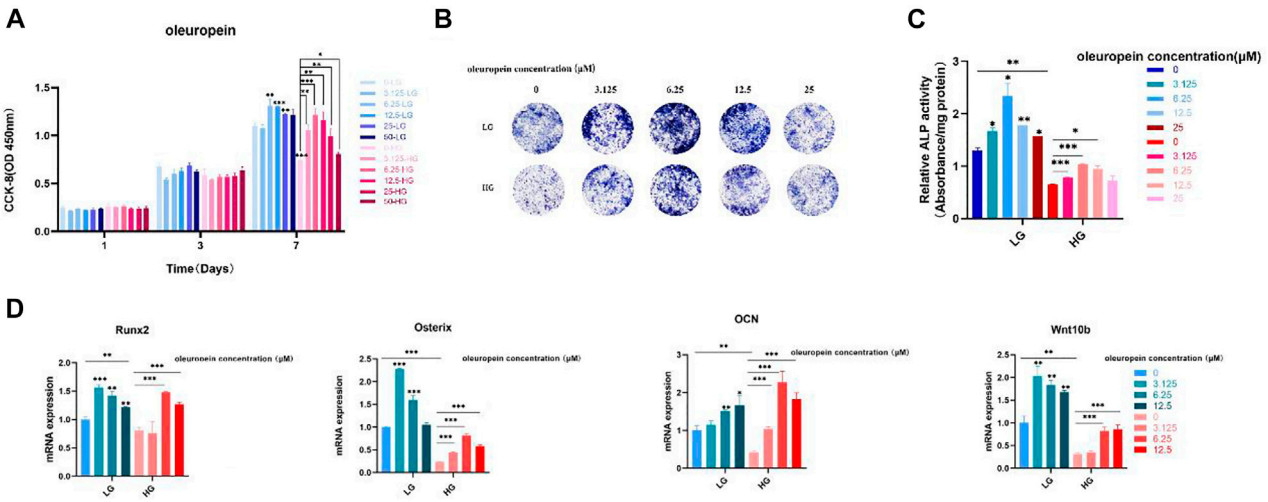

FIGURE 8
Oleuropein reverses the osteogenic suppression of BMSCs under the high glucose microenvironment. **(A)** CCK-8 analysis. **(B)** ALP staining. **(C)** Semi-quantitative analysis of ALP. **(D)** PCR analysis.

et al., 2011; Santiago-Mora et al., 2011; Kuem et al., 2014; Tong et al., 2015; Ahamad et al., 2019). The results of CCK-8 showed that the proliferation of BMSCs was suppressed under the high glucose microenvironment and 3.125 μM–25 μM oleuropein induction could promote the cell proliferation effectively (Figure 8A). ALP staining demonstrated that high glucose microenvironment results in significant osteo-inhibition, which was reversed by 3.125 μM–12.5 μM oleuropein induction (Figure 8B). Additionally, semi-quantitative analysis of ALP also confirmed these findings (Figure 8C). According to CCK-8 and ALP experiments' results, we chosen 6.25 μM–12.5 μM concentration of oleuropein that appeared better abilities of promoting cell proliferation and osteogenesis for further exploring. qRT-PCR results have shown the down-regulated mRNA levels of osteogenesis-associated genes, including Runx2, Osterix and OCN in BMSCs cultured with high glucose medium for 7 days, and their levels were up-regulated by 6.25 μM–12.5 μM oleuropein induction, as well as the mRNA level of Wnt10b (Figure 8D).

Discussions

Elevated blood glucose level is the major characteristic of DM, leading to the high glucose microenvironment in which various tissues are affected and then a series of complications occur. Osseous tissues are composed of multiple types of cells, including osteoblasts, osteoclast, osteocytes and BMSCs that suffer from the change of bone microenvironment (Shahen et al., 2020). BMSCs are featured by the differentiation potential to multi-lineage cells, including osteoblasts, and they play a critical in bone metabolism. Transcriptional control is necessary for differentiation of BMSCs. However, the transcriptional change of BMSCs under high glucose microenvironment is largely unknown. In this paper, mouse BMSCs were exposed to a 35 mM-glucose microenvironment for continuous 30 days to simulate the uncontrolled chronic high glucose environment (Li et al., 2019; Chen et al., 2022). Through the whole transcriptional sequencing, a total of 794 up-regulated genes and 1,162 down-regulated genes were preliminarily identified.

BMSCs osteogenesis is driven by various signaling pathways, such as the Hedgehog pathway (Tu et al., 2012), the Notch pathway (Canalis et al., 2016), the Wnt/β-catenin pathway (Wang et al., 2012), etc. The influence of signaling pathways on the high glucose microenvironment has been rarely reported. Jyoti Shrestha Takanche et al. (2020) suggested that gomisin A could regulate osteoblast differentiation under the oxidative stress condition induced by high glucose (25 mM D-glucose companied with 5 mU/ml glucose oxidase) through upregulating HO-1 and maintaining mitochondrial homeostasis. Xiaozhou Ying et al. (2015) confirmed that high glucose (30 mM) suppresses osteogenic differentiation of human BMSCs, but the activated PI3K/Akt signaling pathway by silibinin induction can reverse the osteogenic dysfunctions. Zhuling Jiang et al. (2019) reported that high glucose (4,500 mg/l glucose) results in osteoblastic dysfunctions, which, however, can be reversed by the activation of Shh signaling pathway. According to the functional analysis of EDGs, we targeted a few signaling pathways that deserved to be further tapped, including the PI3K-Akt, Rap1, MAPK, Ras, TGF-β and AGE-RAGE signaling pathways.

From the GSEA result, two significant gene sets related to high glucose exposure were discovered, including the Focal adhesion and Signaling pathways regulating pluripotency of

stem cells. Multitude of genes associated to pluripotency regulation of stem cells significantly witnessed a significant drop under the high glucose microenvironment, including Wnt10b. To further vertify the connection between Wnt10b expression and DM, we searched in public Gene Expression Omnibus (GEO) database and found a previous study (GSE26168) that analyze the blood samples from male pre-diabetes and T2DM patients (Karolina et al., 2011). Consistently, we revealed that there is also a decrease in the expression of Wnt10b in the blood samples after reanalysis. Several studies have proven that the expression of Wnt10b is inhibited in DM patients (Abiola et al., 2009; Janssen et al., 2020). Wendy et al. suggested that mice with acitvated Wnt10b present decreased bone loss, obesity inhibition, increasing insulin sensitivity and glucose tolerance (Wright et al., 2007). Besides, Wnt10b plays a vital role in driving osteogenesis and inhibiting adipogenesis (Collins et al., 2017). Bennett et al. (2002) Bennett et al. (2005) have validated that Wnt10b$^{-/-}$ mice presents a significant decrease in osteoblasts, while Wnt10b promoter drives bone formation. Previous researches also demonstrated that Wnt10b is a crucial regulator of the mesenchymal progenitor fate, mainly through changing bone formation rather than bone resorption (Wend et al., 2012).

To further verify the function of Wnt10b in high glucose-induced osteogenesis inhibition, BMSCs were induced with varying concentrations of oleuropein, which has been validated as Wnt10b activator (Park et al., 2011; Kuem et al., 2014). Oleuropein is acquired from leaves and fruit oil, which is the most active phenolic compound in olive oil and regarded as one of the most beneficial compound of it (Drira et al., 2011; Ahamad et al., 2019). It has been strongly validated that oleuropein is functional in anti-oxidant, anti-inflammation, anti-diabetic, cardioprotective, anticancer and hepatoprotective actions (Ahamad et al., 2019). Nowadays, the biological function of oleurpein in bone regeneration has been well concerned (Puel et al., 2006; Santiago-Mora et al., 2011). A previous study discovered that oleuropein can regulate stem cells differentiation, prevent bone loss or osteoporosis (Santiago-Mora et al., 2011). In our research, we validated the outstanding effect of oleuropein in promoting the proliferation and differentiation of BMSCs under a high glucose microenvironment through CCK-8 and ALP analysis respectively. qRT-PCR also proved that oleuropein up-regulated Wnt10b, as well as the osteogenesis-related genes Runx2、Osterix and OCN.

In conclusion, the results of RNA-seq showed that the high glucose microenvironment could significantly influence the cell adhesion and pluripotency regulation of BMSCs. Wnt10b has been discovered as a potential biomarker and therapeutic target to reverse high glucose-induced osteogenic suppression, and oleuropein might be an effective drug in the treatment of diabetic osteopathy. Other potential transcriptional factors and signal molecules involved in the osteogenesis of BMSCs should be further investigated in the future, and their molecular mechanisms, thus more clearly clarifying the transcriptional regulation of the dynamic changes in osteogenesis under the high glucose microenvironment. Our results may provide new insight into diabetic osteopathy.

Data availability statement

The data presented in the study are deposited in the NCBI repository, accession number PRJNA861406.

Ethics statement

The animal study was reviewed and approved by all the experiments of this study were approved by the Shanghai Jiao Tong University Animal Care and Use Committee.

Author contributions

AL and YC performed the experiments and wrote the original draft. YS and TW helped part of experiments and statistical analysis. KL, JL, and JW led the conceptualization and project administration, also supervised the writing and editing. All authors contributed to the article and approved the submitted version.

Fuding

We acknowledge support by the Natural Science Foundation of China (No. 82071081), Special Project of Clinical Research in Health Industry of Shanghai Municipal Health Commission (Excellence Program) (No.20224Z0010) and Clinical Research and Key Support Project of Shanghai ShenKang Hospital Development Center (No. SHDC2020CR5015).

Acknowledgments

Thanks to BioRender.com for helping us to create the graphic abstract.

Conflict of interest

The authors declare that the research was conducted in the absence of any commercial or financial relationships that could be construed as a potential conflict of interest.

Publisher's note

References

Abiola, M., Favier, M., Christodoulou-Vafeiadou, E., Pichard, A., Martelly, I., and Guillet-Deniau, I. (2009). Activation of wnt/β-catenin signaling increases insulin sensitivity through a reciprocal regulation of Wnt10b and SREBP-1c in skeletal muscle cells. *PloS one* 4, e8509. doi:10.1371/journal.pone.0008509

Ahamad, J., Toufeeq, I., Khan, M., Ameen, M., Anwer, E., Uthirapathy, S., et al. (2019). Oleuropein: A natural antioxidant molecule in the treatment of metabolic syndrome. *Phytotherapy Res.* 33, 3112–3128. doi:10.1002/ptr.6511

Baglio, S. R., Rooijers, K., Koppers-Lalic, D., Verweij, F. J., Perez Lanzon, M., Zini, N., et al. (2015). Human bone marrow- and adipose-mesenchymal stem cells secrete exosomes enriched in distinctive miRNA and tRNA species. *Stem Cell. Res. Ther.* 6, 127. doi:10.1186/s13287-015-0116-z

Bennett, C., Longo, K., Wright, W., Suva, L., Lane, T., Hankenson, K., et al. (2005). Regulation of osteoblastogenesis and bone mass by Wnt10b. *Proc. Natl. Acad. Sci. U. S. A.* 102, 3324–3329. doi:10.1073/pnas.0408742102

Bennett, C., Ross, S., Longo, K., Bajnok, L., Hemati, N., Johnson, K., et al. (2002). Regulation of Wnt signaling during adipogenesis. *J. Biol. Chem.* 277, 30998–31004. doi:10.1074/jbc.m204527200

Canalis, E., Bridgewater, D., Schilling, L., and Zanotti, S. (2016). Canonical Notch activation in osteocytes causes osteopetrosis. *Am. J. Physiology-Endocrinology Metabolism* 310, E171–E182. doi:10.1152/ajpendo.00395.2015

Chen, Y., Chen, L., Huang, R. Y., Yang, W. Y., Chen, S. Y., Lin, K. L., et al. (2021). Investigation for GSK3 beta expression in diabetic osteoporosis and negative osteogenic effects of GSK3 beta on bone marrow mesenchymal stem cells under a high glucose microenvironment. *Biochem. Biophysical Res. Commun.* 534, 727–733. doi:10.1016/j.bbrc.2020.11.010

Chen, Y., Chen, L., Wang, Y. T., Lin, K. L., and Liu, J. Q. (2022). Lithium-containing bioactive glasses enhanced 3D-printed PLGA scaffolds for bone regeneration in diabetes. *Compos. Part B Eng.* 230, 109550. doi:10.1016/j.compositesb.2021.109550

Collins, F., Rios-Arce, N., McCabe, L., and Parameswaran, N. (2017). Cytokine and hormonal regulation of bone marrow immune cell Wnt10b expression. *PloS one* 12, e0181979. doi:10.1371/journal.pone.0181979

Dawei, Z., Liyuan, Z., Hongliang, L., and Zuolin, W. (2021). Titanium modified with ZnO nanofilm and fibronectin: Preventing peri-implantitis and biocompatibility. *J. Inorg. Mater.* 36, 125–1322. doi:10.15541/jim202100125

Drira, R., Chen, S., and Sakamoto, K. (2011). Oleuropein and hydroxytyrosol inhibit adipocyte differentiation in 3 T3-L1 cells. *Life Sci.* 89, 708–716. doi:10.1016/j.lfs.2011.08.012

Epstein, S., Defeudis, G., Manfrini, S., Napoli, N., and Pozzilli, P. (2016). Scientific committee of the first international symposium on D, bone: **Diabetes and disordered bone metabolism (diabetic osteodystrophy): Time for recognition**. *Osteoporos. Int.* 27, 1931–1951. doi:10.1007/s00198-015-3454-x

Gilbert, M. P., and Pratley, R. E. (2015). The impact of diabetes and diabetes medications on bone health. *Endocr. Rev.* 36, 194–213. doi:10.1210/er.2012-1042

Gilbert, R. E. (2013). Augmenting endothelial repair in diabetes: Role of bone marrow-derived cells. *Can. J. Diabetes* 37, 315–318. doi:10.1016/j.jcjd.2013.06.009

Guan, M., Yao, W., Liu, R., Lam, K. S., Nolta, J., Jia, J., et al. (2012). Directing mesenchymal stem cells to bone to augment bone formation and increase bone mass. *Nat. Med.* 18, 456–462. doi:10.1038/nm.2665

Hamann, C., Kirschner, S., Gunther, K. P., and Hofbauer, L. C. (2012). Bone, sweet bone--osteoporotic fractures in diabetes mellitus. *Nat. Rev. Endocrinol.* 8, 297–305. doi:10.1038/nrendo.2011.233

Janssen, L., Van Dam, A., Hanssen, M., Kooijman, S., Nahon, K., Reinders, H., et al. (2020). Higher plasma sclerostin and lower wnt signaling gene expression in white adipose tissue of prediabetic south asian men compared with white caucasian men. *Diabetes Metab. J.* 44, 326–335. doi:10.4093/dmj.2019.0031

Jiang, Z. L., Jin, H., Liu, Z. S., Liu, M. Y., Cao, X. F., Jiang, Y. Y., et al. (2019). Lentiviralmediated Shh reverses the adverse effects of high glucose on osteoblast function and promotes bone formation *via* Sonic hedgehog signaling. *Mol. Med. Rep.* 20, 3265–3275. doi:10.3892/mmr.2019.10540

Karolina, D. S., Armugam, A., Tavintharan, S., Wong, M. T., Lim, S. C., Sum, C. F., et al. (2011). MicroRNA 144 impairs insulin signaling by inhibiting the expression of insulin receptor substrate 1 in type 2 diabetes mellitus. *PLoS One* 6, e22839. doi:10.1371/journal.pone.0022839

Kuem, N., Song, S., Yu, R., Yun, J., and Park, T. (2014). Oleuropein attenuates visceral adiposity in high-fat diet-induced obese mice through the modulation of WNT10b- and galanin-mediated signalings. *Mol. Nutr. Food Res.* 58, 2166–2176. doi:10.1002/mnfr.201400159

Li, X., Li, Z., Li, B., Zhu, X., and Lai, X. (2019). Klotho improves diabetic cardiomyopathy by suppressing the NLRP3 inflammasome pathway. *Life Sci.* 234, 116773. doi:10.1016/j.lfs.2019.116773

Magliano, D. J., Sacre, J. W., Harding, J. L., Gregg, E. W., Zimmet, P. Z., and Shaw, J. E. (2020). Young-onset type 2 diabetes mellitus - implications for morbidity and mortality. *Nat. Rev. Endocrinol.* 16, 321–331. doi:10.1038/s41574-020-0334-z

Napoli, N., Chandran, M., Pierroz, D. D., Abrahamsen, B., Schwartz, A. V., Ferrari, S. L., et al. (2017). Mechanisms of diabetes mellitus-induced bone fragility. *Nat. Rev. Endocrinol.* 13, 208–219. doi:10.1038/nrendo.2016.153

Park, S., Choi, Y., Um, S., Yoon, S., and Park, T. (2011). Oleuropein attenuates hepatic steatosis induced by high-fat diet in mice. *J. hepatology* 54, 984–993. doi:10.1016/j.jhep.2010.08.019

Puel, C., Mathey, J., Agalias, A., Kati-Coulibaly, S., Mardon, J., Obled, C., et al. (2006). Dose-response study of effect of oleuropein, an olive oil polyphenol, in an ovariectomy/inflammation experimental model of bone loss in the rat. *Clin. Nutr. Edinb. Scotl.* 25, 859–868. doi:10.1016/j.clnu.2006.03.009

Rachner, T. D., Khosla, S., and Hofbauer, L. C. (2011). Osteoporosis: Now and the future. *Lancet* 377, 1276–1287. doi:10.1016/s0140-6736(10)62349-5

Sanchez-de-Diego, C., Valer, J. A., Pimenta-Lopes, C., Rosa, J. L., and Ventura, F. (2019). Interplay between BMPs and reactive oxygen species in cell signaling and pathology. *Biomolecules* 9, 534. doi:10.3390/biom9100534

Santiago-Mora, R., Casado-Díaz, A., De Castro, M., and Quesada-Gómez, J. (2011). Oleuropein enhances osteoblastogenesis and inhibits adipogenesis: The effect on differentiation in stem cells derived from bone marrow. *Osteoporos. Int.* 22, 675–684. doi:10.1007/s00198-010-1270-x

Shahen, V. A., Gerbaix, M., Koeppenkastrop, S., Lim, S. F., McFarlane, K. E., Nguyen, A. N. L., et al. (2020). Multifactorial effects of hyperglycaemia, hyperinsulinemia and inflammation on bone remodelling in type 2 diabetes mellitus. *Cytokine Growth Factor Rev.* 55, 109–118. doi:10.1016/j.cytogfr.2020.04.001

Takanche, J. S., Kim, J. E., Han, S. H., and Yi, H. K. (2020). Effect of gomisin A on osteoblast differentiation in high glucose-mediated oxidative stress. *Phytomedicine* 66, 153107. doi:10.1016/j.phymed.2019.153107

Tencerova, M., and Kassem, M. (2016). The bone marrow-derived stromal cells: Commitment and regulation of adipogenesis. *Front. Endocrinol.* 7, 127. doi:10.3389/fendo.2016.00127

Tong, T., Kim, N., and Park, T. (2015). Topical application of oleuropein induces anagen hair growth in telogen mouse skin. *PloS one* 10, e0129578. doi:10.1371/journal.pone.0129578

Tu, X., Joeng, K. S., and Long, F. (2012). Indian hedgehog requires additional effectors besides Runx2 to induce osteoblast differentiation. *Dev. Biol.* 362, 76–82. (N. Y. 1985). doi:10.1016/j.ydbio.2011.11.013

Vandoorne, K., Rohde, D., Kim, H. Y., Courties, G., Wojtkiewicz, G., Honold, L., et al. (2018). Imaging the vascular bone marrow niche during inflammatory stress. *Circ. Res.* 123, 415–427. doi:10.1161/circresaha.118.313302

Wang, J., Sinha, T., and Wynshaw-Boris, A. (2012). Wnt signaling in mammalian development: Lessons from mouse genetics. *Cold Spring Harb. Perspect. Biol.* 4, a007963. doi:10.1101/cshperspect.a007963

Wei, H., Cui, J., Lin, K., Xie, J., and Wang, X. (2022). Recent advances in smart stimuli-responsive biomaterials for bone therapeutics and regeneration. *Bone Res.* 10, 17. doi:10.1038/s41413-021-00180-y

Wend, P., Wend, K., Krum, S., and Miranda-Carboni, G. (2012). The role of WNT10B in physiology and disease. *Acta physiol. Oxf. Engl.* 204, 34–51. doi:10.1111/j.1748-1716.2011.02296.x

Wright, W., Longo, K., Dolinsky, V., Gerin, I., Kang, S., Bennett, C., et al. (2007). Wnt10b inhibits obesity in ob/ob and agouti mice. *Diabetes* 56, 295–303. doi:10.2337/db06-1339

Ying, X., Chen, X., Liu, H., Nie, P., Shui, X., Shen, Y., et al. (2015). Silibinin alleviates high glucose-suppressed osteogenic differentiation of human bone marrow stromal cells via antioxidant effect and PI3K/Akt signaling. *Eur. J. Pharmacol.* 765, 394–401. doi:10.1016/j.ejphar.2015.09.005

Yuchen, C., Ziyang, L., Xin, X., Zhangfan, W., Aihua, Y., Song, Y., et al. (2020). An injectable composite bone cement based on mesoporous borosilicate bioactive glass spheres. *J. Inorg. Mater.* 35, 1398–1406. doi:10.15541/jim20200140

Zhang, S. Y., Dai, Q. Q., Zhang, B., Liu, S. Y., Wang, Y., Zhang, Y. X., et al. (2021). Syngeneic bone marrow transplantation in combination with PI3K inhibitor reversed hyperglycemia in later-stage streptozotocin-induced diabetes. *Ann. Transl. Med.* 9, 1642. doi:10.21037/atm-21-3329

Zhou, A., Li, M., He, B., Feng, W., Huang, F., Xu, B., et al. (2016). Lipopolysaccharide treatment induces genome-wide pre-mRNA splicing pattern changes in mouse bone marrow stromal stem cells. *BMC Genomics* 17 (7), 509. doi:10.1186/s12864-016-2898-5

Zhou, Q., Xie, F., Zhou, B., Wang, J., Wu, B., Li, L., et al. (2019). Differentially expressed proteins identified by TMT proteomics analysis in bone marrow microenvironment of osteoporotic patients. *Osteoporos. Int.* 30, 1089–1098. doi:10.1007/s00198-019-04884-0

Zimmet, P., Alberti, K. G., Magliano, D. J., and Bennett, P. H. (2016). Diabetes mellitus statistics on prevalence and mortality: Facts and fallacies. *Nat. Rev. Endocrinol.* 12, 616–622. doi:10.1038/nrendo.2016.105

frontiers | Frontiers in Bioengineering and Biotechnology

TYPE Original Research
PUBLISHED 15 September 2022
DOI 10.3389/fbioe.2022.1011482

OPEN ACCESS

EDITED BY
Le Yu,
Ohio University, United States

REVIEWED BY
Zhihong Dong,
Chengdu University, China
Changchun Zhou,
Sichuan University, China

*CORRESPONDENCE
Penglai Wang,
wpl0771@163.com
Changyong Yuan,
yuanchangyong1983@foxmail.com

†These authors have contributed equally to this work.

SPECIALTY SECTION
This article was submitted to Biomaterials, a section of the journal Frontiers in Bioengineering and Biotechnology

RECEIVED 04 August 2022
ACCEPTED 19 August 2022
PUBLISHED 15 September 2022

CITATION
Geng T, Wang Y, Lin K, Zhang C, Wang J, Liu Y, Yuan C and Wang P (2022), Strontium-doping promotes bone bonding of titanium implants in osteoporotic microenvironment. *Front. Bioeng. Biotechnol.* 10:1011482. doi: 10.3389/fbioe.2022.1011482

Strontium-doping promotes bone bonding of titanium implants in osteoporotic microenvironment

Tengyu Geng[1,2†], Yiru Wang[1,2†], Kaili Lin[3], Cheng Zhang[1], Jing Wang[1], Ya Liu[1], Changyong Yuan[1,2*] and Penglai Wang[1,2*]

[1]School of Stomatology, Xuzhou Medical University, Xuzhou, China, [2]Department of Dental Implant, The Affiliated Stomatological Hospital of Xuzhou Medical University, Xuzhou, China, [3]Department of Oral & Cranio-Maxillofacial Surgery, Shanghai Ninth People's Hospital, Shanghai Jiao Tong University School of Medicine, Shanghai Key Laboratory of Stomatology, Shanghai Research Institute of Stomatology, Shanghai, China

Osteoporosis is a major challenge to oral implants, and this study focused on improving the osseointegration ability of titanium (Ti) implants in osteoporosis environment *via* surface modification, including doping of strontium ion and preparation of nanoscale surface feature. Our previous studies have shown that strontium (Sr) ions can enhance osteogenic activity. Therefore, we aimed to comprehensively evaluate the effect of hydrothermal treatment of Sr-doped titanium implant coating on bone-binding properties in the microenvironment of osteoporosis in this study. We fabricated Sr-doped nanocoating (AHT-Sr) onto the surface of titanium implants *via* hydrothermal reaction. The rough Sr-doping had good biological functions and could apparently promote osteogenic differentiation of osteoporotic bone marrow mesenchymal stem cells (OVX-BMSCs). Most importantly, AHT-Sr significantly promoted bone integration in the osteoporosis environment. This study provides an effective approach to implant surface modification for better osseointegration in an osteoporotic environment.

KEYWORDS

titanium implants, surface modification, osteoporosis, strontium, osseointegration

Introduction

Titanium (Ti) implants have been extensively utilized in the field of oral implant based on their good mechanical properties, bone-binding ability, and biocompatibility (Huang et al., 2004; Spriano et al., 2018). However, some factors may increase the risk of implant failure such as osteoporosis, diabetes, cancer, and smoking (Holahan et al., 2008; Chen

Abbreviations: Ti, titanium; Sr, Strontium; BMSCs, Bone marrow-derived mesenchymal stem cells; AHT, alkali-heat treated titanium; FE-SEM, field-emission scanning electron microscopy; EDS, energy-dispersive spectrometry; ICP-MS, inductively coupled plasma atomic emission spectroscopy; PBS, phosphate buffered saline; OVX, ovariectomies surgery; RT, room temperature; ALP, Alkaline phosphatase; SD, standard deviation.

et al., 2016; de Oliveira et al., 2020; Naseri et al., 2020; Zhang et al., 2021; Wei et al., 2022). Osteoporosis is a systemic bone metabolic disease caused by an imbalance between osteogenesis and osteoclast, which is often accompanied by a significant decrease in bone mineral density (Park et al., 2014; Takahashi et al., 2016; Russow et al., 2018). Osteoporosis can result in inadequate bone-implant contact, severely disrupting initial implant stability and bone integration (Du et al., 2016; Wang et al., 2021c). Osteoporosis is a challenge to the success of oral implants. There are significant changes of hormones and cytokines in bone marrows for patients with osteoporosis (Du et al., 2016). The pathological environment disrupts differentiation, proliferation, and intercellular communication of bone marrow stem cells in osteoporosis patients (Alghamdi et al., 2013; Dudeck et al., 2014). Therefore, titanium implants need to be biologically active to undergo bone integration in osteoporosis environment.

Several studies have shown the positive effects of strontium (Sr), tantalum, gallium, and zinc on osteogenic differentiation (Lin et al., 2013; Bonifacio et al., 2017; Zhao et al., 2019; Wang et al., 2021d). Sr is an important component of bone. It plays a key role in bone integration by promoting osteoblast differentiation and accelerating bone formation, while inhibiting osteoclast differentiation and reducing bone resorption (Choudhary et al., 2007; Bonnelye et al., 2008; Montagna et al., 2020). Sr-containing drugs play an active role in clinical application for anti-osteoporosis. However, oral Sr-containing drugs have low utilization rate and can cause systemic adverse reactions (Kolodziejska et al., 2021). Extensive efforts have focused on the construction of Sr-containing implant coatings for long-term and stable release. of Sr (Xing et al., 2020; Kuo et al., 2022). Bone marrow-derived mesenchymal stem cells (BMSCs), the precursors of osteoblastic-lineage cells, play a central role in bone formation (Bianco et al., 2011; Fu et al., 2022). Previous studies have demonstrated that Sr can promote MSCs differentiation in an normal physiological environment (Wang et al., 2020). However, the effect and underlying mechanism of strontium ion on MSCs in an osteoporotic environment remains unknown. Alkali heat treatment is a simple and stable method to construct Sr-containing coating on the surface of titanium implants, which leads to formation of nano-scale surface structures (Wang et al., 2018; Wang et al., 2020; Okuzu et al., 2021). Nanoscale surface features increase protein adsorption, stimulate osteoblast migration, and accelerate integration of bone and implants (Ding et al., 2020; Shu et al., 2020; Wang et al., 2022). By adjusting reaction conditions, the synergy of the two strategies provide a new idea for promoting osteoporotic bone bonding.

In this study, Sr-doped nanocoating was constructed on the implant surface by alkali heat treatment. BMSCs from osteoporotic rats were isolated and cultured and their biological properties, such as cell proliferation, cell morphology, and osteogenic differentiation, were estimated after AHT-Sr treatment. In addition, the osseointegration ability of titanium implants containing Sr-doped coating was evaluated *in vivo* in osteoporosis rats.

Materials and methods

Preparation of the materials

Titanium plates with dimensions of 10 mm × 10 mm × 1 mm and cylindrical implants consisting of titanium (2 mm × 4 mm) were employed in *vitro* and *in vivo* studies, respectively. The samples were polished to 2,000 grit with SiC sandpaper and cleaned by ultrasonic with acetone, ethanol, and deionized water. The samples were immersed in 5 M NaOH solution and subjected to hydrothermal treatment at 80°C for 6 h to form a rough surface, thoroughly ultrasonically cleaned in deionized water, and then wet-oxidized in deionized water at 200°C for 4 h. After thorough ultrasonic cleaning in deionized water, the samples were immersed in deionized water and 0.04 M $SrCl_2$. The samples before alkali heat treatment (AHT) were labeled as Ti. The obtained samples treated with water and $SrCl_2$ were labeled AHT and AHT-Sr, respectively.

Surface characterization

The surface topography of the three groups of Ti plates was examined using field-emission scanning electron microscopy (FE-SEM; FEI Teneo VS, United States). X-ray energy-dispersive spectrometry (EDS; S4800, Hitachi) was used to observe the elemental composition above the three surfaces. Contact angle measurement (JY-82B Kruss DSA, Germany) was used to study and measure the wetting properties of the surface. The amount of Sr^{2+} leached was assessed by inductively coupled plasma atomic emission spectroscopy (ICP-MS; PerkinElmer NexION 300X, United States). The samples were placed in 10 ml of phosphate buffered saline (PBS) solution at 37°C and without stirring for various durations (1, 2, 3, 5, 7, 14 21, and 28 days).

Cell culture

Forty 12-week-old female Sprague Dawley rats (average weight: 250 g) were used in this study. Thirty rats were randomly selected for bilateral ovariectomies surgery (OVX) to obtain osteoporotic condition. The remaining 10 rats were assigned to the control group and subjected to sham surgery. Twelve weeks later, the femurs of the two groups were taken for micro-CT to verify whether the model was successfully constructed. Meanwhile, BMSCs obtained from healthy rats (H-BMSCs) and OVX rats (OVX-BMSCs) were collected from the bone marrow of the tibia as well as femora of two rat groups as previously described. *In vitro* experiments were performed using cells from the third to fifth passages. H-BMCSs were seeded on Ti surfaces (Ctrl) while OVX-BMSCs were seed onto different Ti disk surfaces (Ti, AHT, and AHT-Sr). Animal experiments

were performed under the authorization of the ethical committee of Xuzhou Medical University.

Cell proliferation

BMSCs at a cell density of about 2×10^4 cells/ml were seeded onto titanium surfaces and then cultured for 1, 4, or 7 days. At each time point, cell proliferation was assessed by the CCK-8 assay. After rinsing thrice with PBS, the cells were incubated in 400 µl of fresh culture medium (supplemented with 10% CCK-8 solution) at 37°C in the dark. After 2 h, 100 µl/well of the supernatant was transferred to a 96-well plate and absorbance at a wavelength of 450 mm was determined using a microplate reader (Thermo Fisher Scientific, Waltham, MA, United States).

Initial cell adhesion

The BMSCs at a cell density of ~2×10^4 cells/ml were seeded onto titanium surfaces for 24 h. At various time points, the cells were washed thrice with PBS and then fixed with 4% PFA for 10 min at room temperature (RT). The samples were permeabilized using 0.1% Triton™ X-100 in PBS for 15 min. The samples were then stained with FITC-phalloidin and with DAPI for another 5 min in the dark following the manufacturer's instructions. Cytoskeletal F-actin (red fluorescence) and cell nuclei (blue fluorescence) were assessed under an inverted fluorescence microscope (Olympus, IX73, Japan).

Cell migration

BMSCs (cell density: 5,000 cells/well) were seeded onto the Ti substrate for 24 h, and a straight wound was made on the cell layer using a 1-ml pipette tip. After culturing for another 24 h, the cells were fixed with 4% PFA and stained with FITC-phalloidin and DAPI, then observed under fluorescence optics. Cell migration capacity was evaluated by measuring the width of the cell wound.

Alkaline phosphatase staining

BMCSs were seeded at a density of about 2×10^4 cells/ml and cultured in osteogenic induction media after adhering supplemented with 100 µg/ml ascorbic acid, 2 mmol/L β-glycerophosphate, and 10 nmol/L dexamethasone. Alkaline phosphatase (ALP) staining was conducted using a BCIP/NBT ALP kit (Beyotime, Shanghai, China) on days 4 and 7 of the cell culture following the manufacturer's instructions.

Quantitative Real-time PCR

BMSCs were seeded onto each sample at a density of 2×10^5 cells/well. After culturing for 4 and 7 days, total RNA was extracted using TRIzol reagent (Takara Bio, Japan). A PrimeScript RT reagent kit (Takara Bio, Shiga, Japan) was used in reverse transcription of total RNA to cDNA. Real-time RT-PCR was conducted using a Quantitative SYBR Green Kit (Takara Bio, Shiga, Japan) and was detected by LightCycler480 System (Roche Diagnostics, Rotkreuz, Switzerland). Table 1 shows the primer sequences. The PCR conditions were as follows: 1) initial denaturation at 95°C for 30 s; 2) PCR: 95°C, 5 s; 60°C, 20 s, for 40 cycles; 3) melting: 95°C, 5 s; 60°C, 1 min; 95°C, for 1 cycle; and 4) cooling: 50°C, 30 s for 1 cycle. β-actin was used as control. The results were calculated using the $2^{-\Delta\Delta CT}$ method.

Animal implant surgery

Twelve weeks post bilateral ovariectomy, the 20 OVX Sprague Dawley rats were randomly assigned to two groups (10 each), namely, AHT implants and AHT-Sr implants. After inducing general anesthesia using 10% sterile chloral hydrate solution, we made 1.8-mm-diameter implant holes in the femoral metaphysis (approximately 7 mm above the knee joint). A single implant was randomly placed into each femur. At 2 and 4 weeks after surgery, five rats in each group were sacrificed. We collected the femora and removed adherent tissues, and fixed these in 4% paraformaldehyde at RT for subsequent analysis.

Micro-CT analysis of femora

The rats were sacrificed, and their femora were fixed with 4% phosphate buffered PFA. The samples were scanned using a SCANCO µCT 100 system (SCANCO Medical AG, Brüttisellen, Zurich, Switzerland) at a 4-µm resolution, 160 µA tube current, and 50 kV tube voltage. Regions of interest were selected within the 0.5–4.5 mm area below the growth plate at the distal ends of each femur.

Statistical analysis

Data were expressed as the mean ± standard deviation (SD). Statistical analysis was performed using the IBM SPSS ver. 18.0. We assessed statistical differences using the two-way analysis of variance. Differences with a $p < 0.05$ were considered statistically significant.

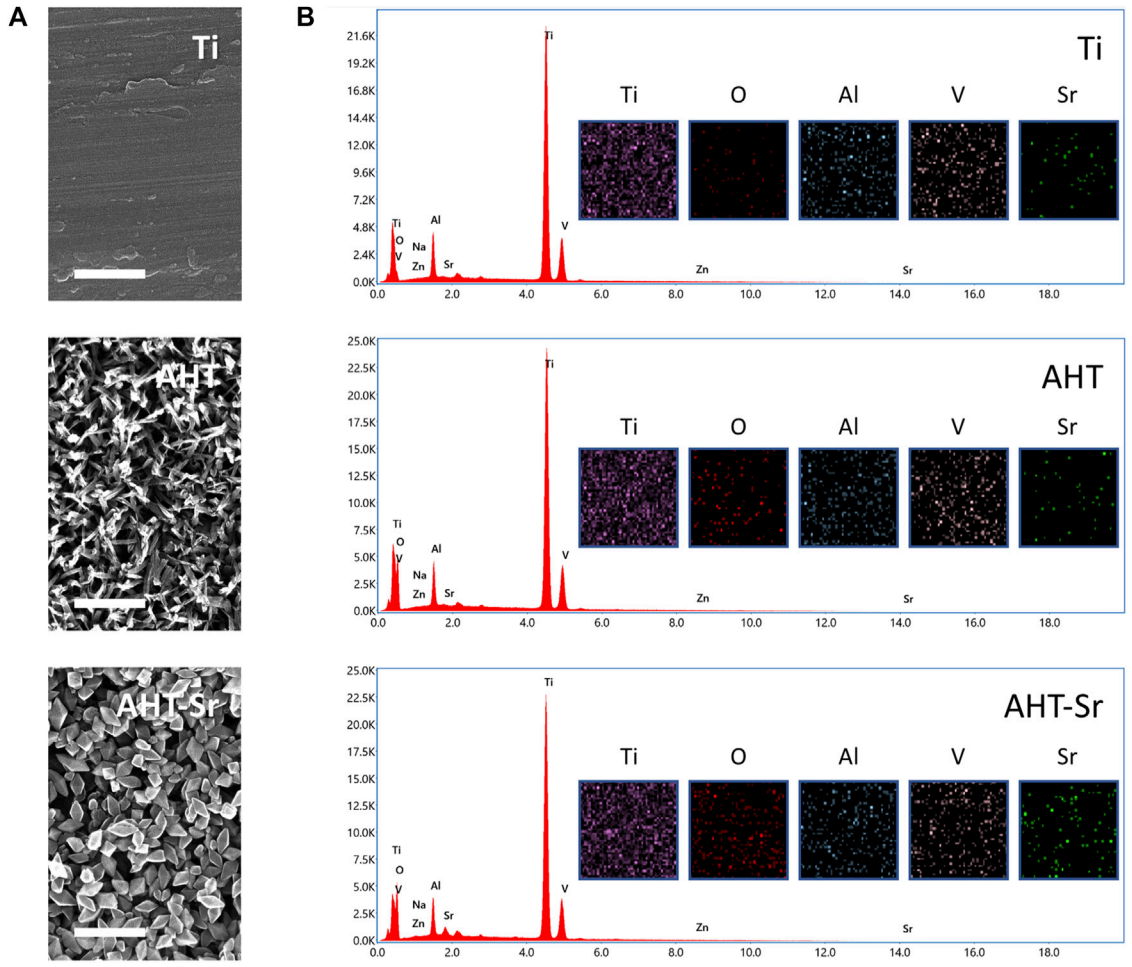

FIGURE 1
Surface characterizations of Ti, AHT, and AHT-Sr. **(A)** Representative SEM images showing the rough surface of Ti, AHT, and AHT-Sr. Scale bars: 500 nm. **(B)** EDS spectra and mappings of Ti, AHT, and AHT-Sr substrates.

Results

Characterization of Sr-doped nanocoating surface

Figure 1A Shows the SEM micrographs of samples with different coating parameters. The surface of Ti groups showed obvious polishing scratches. The AHT groups were characterized with a sponge network structure that was similar to our previous findings. Evenly distributed nanoscale (Ø 200–300 nm) particles could be found on AHT-Sr specimens. The EDS spectrum of AHT-Sr is shown in Figure 1B. The main elements of the AHT-Sr coating included Ti, O, Al, V, and Sr. Relative to the other two groups, Sr content increased in AHT-Sr, indicating that we had successfully Sr-doped the coating. The elemental composition of various samples as determined by EDS are shown in Table 2.

In addition, the hydrophilic/hydrophobic ability of multiple samples were evaluated by water contact angle measurement (Figure 2A). The contact angle on the Ti and AHT was around 76.05° ± 0.47° and 46.32° ± 1.00°, respectively. However, the contact angle was 13.77° ± 0.73° on the AHT-Sr, indicating a high degree of hydrophilicity. This phenomenon may be attributable to the increase in surface roughness. Previous studies have indicated that osseointegration is influenced by the response of osteoblast cells to surface roughness and alteration in wettability. Protein adsorption test showed that AHT-Sr surface adsorbed more protein than Ti surface (Figure 2B). Figure 2C shows Sr ion release from AHT-Sr for 28 days. The accumulation concentration over the full 28 days was 260 μg/L.

TABLE 1 Primers used in qRT-PCR.

RNA	Sequence, 5′-3′
β-actin	Forward: GTAAAGACCTCTATGCCAACA
	Reverse: GGACTCATCGTACTCCTGCT
ALP	Forward: TATGTCTGGAACCGCACTGAAC
	Reverse: CACTAGCAAGAAGAAGCCTTTGG
BMP-2	Forward: GAAGCCAGGTGTCTCCAAGAG
	Reverse: GTGGATGTCCTTTACCGTCGT
BSP	Forward: AGAAAGAGCAGCACGGTTGAGT
	Reverse: GACCCTCGTAGCCTTCATAGCC
COL-I	Forward: GCCTCCCAGAACATCACCTA
	Reverse: GCAGGGACTTCTTGAGGTTG
OCN	Forward: GCCCTGACTGCATTCTGCCTCT
	Reverse: TCACCACCTTACTGCCCTCCTG
OPN	Forward: CCAAGCGTGGAAACACACAGCC
	Reverse: GGCTTTGGAACTCGCCTGACTG

Establishment of osteoporotic conditions

OVX, a time-honored model to obtain osteoporotic condition, was used in this study. Here, bone conditions were evaluated by animal micro-computed tomography after 12 weeks of post-surgery to confirm whether our *in vivo* model of osteoporosis was established after OVX. Three-dimensional reconstruction showed a decline in bone level after OVX (Figure 3A). Twelve weeks after OVX, the volume of new bone and the thickness and number of trabecular bones significantly decreased, while the trabecular space significantly increased (Figure 3B).

Cell attachment and proliferation on Titanium, AHT, and Sr-doped nanocoating samples

With cell proliferation, the number of OVX-BMSCs steadily increased over time. Similar proliferation rates of cells cultured on Ti, AHT, and AHT-Sr surfaces were observed for 7 days (Figure 4A). A scratch experiment was performed to assess MSC migration capacity (Figure 4B). After 12 h, the wound closure condition of OVX-BMSCs grown on an AHT or AHT-Sr surface was better compared to the Ti surface. Immunofluorescence staining of F-actin and nuclei were performed to evaluate initial cell attachment 4 h after cell seeding. OVX-BMSCs grown on the AHT and AHT-Sr surface showed clear

TABLE 2 Element contents on the surface of Ti, AHT, and AHT-Sr samples determined by EDS.

	Ti (wt%)	O (wt%)	Al (wt%)	V (wt%)	Sr (wt%)
Ti	86.3	1.5	5.7	4.9	0.6
AHT	73.5	16.2	4.4	4.4	0.6
AHT-Sr	71.8	17.6	4.0	3.7	1.9

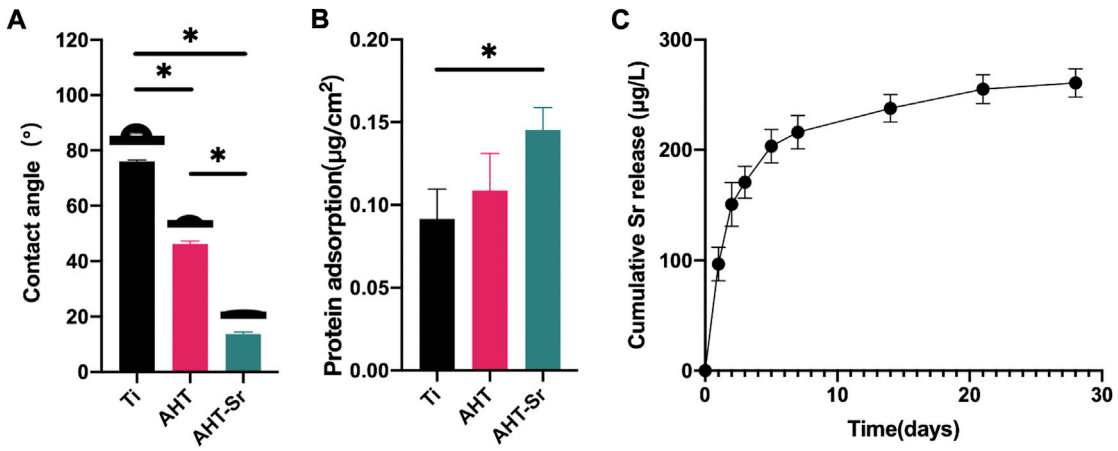

FIGURE 2
Surface physicochemical properties of Ti, AHT, and AHT-Sr. **(A)** Measurement of water contact angles in various specimens (n = 3). **(B)** Protein adsorption assay. **(C)** Cumulative release profile of Sr^{2+} ions from AHT-Sr within 28 days after incubation in PBS. The results are presented as the mean ± SD, n = 3, *p < 0.05.

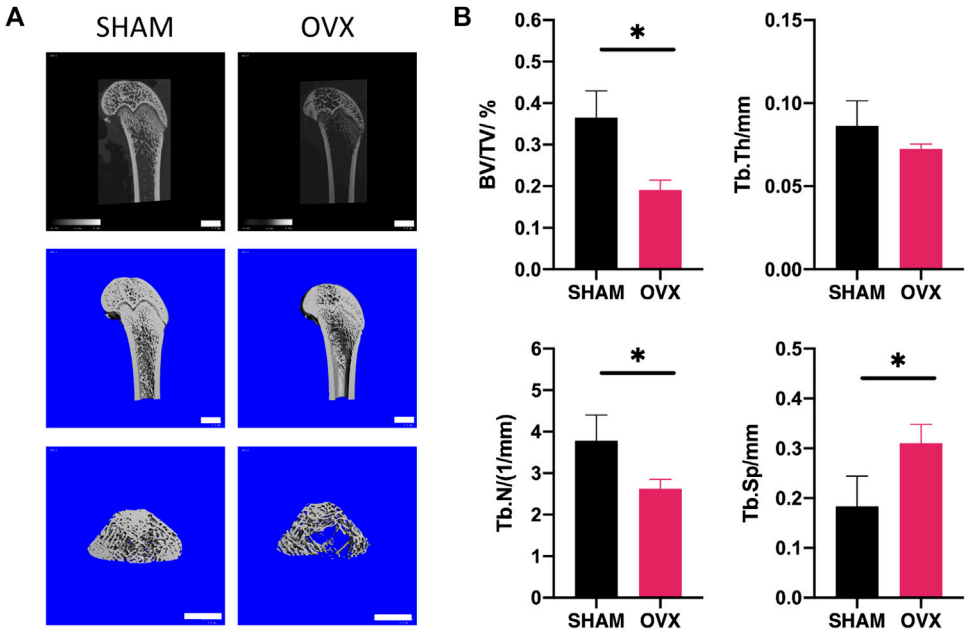

FIGURE 3
Establishment of OVX rat model for osteoporosis. OVX was performed at 12 weeks using micro-CT scanning to validate bone conditions. **(A)** 3D representative micro-CT micrographs of femoral condyles in the OVX and sham groups. Scale bars: 2 mm. **(B)** Quantitative parameters used to assess morphological bone alterations such as trabecular bone volume percentage (BV/TV), trabecular thickness (Tb.Th), trabecular number (Tp.N) and trabecular separation (Tb.Sp) (n = 6). Asterisks represent significant differences among groups (*p < 0.05).

filopodia extensions (Figure 4B). However, no significant differences in the initial adherent cell number on the Ti, AHT, and AHT-Sr samples were observed.

Sr-doped nanocoating promotes osteogenic differentiation of osteoporotic bone marrow mesenchymal stem cells osteogenic differentiation in *vitro*

ALP activity and osteogenic gene expression of OVX-BMSCs were assessed to investigate osteogenic differentiation of OVX-BMSCs *in vitro*. First, ALP activity was detected by ALP staining after 4 and 7 days as a representative marker of early stage of osteogenic differentiation. According to Figure 5A, the cells cultured on the AHT-Sr surface showed darker purple dye effect compared to those cultured on the AHT coatings. Second, we assessed the expression of osteogenic markers using RT-PCT after culturing for four and 7 days. Compared with our findings from OVX-BMSCs cultured on AHT, the OVX-BMSCs grown on AHT-Sr exhibited upregulated ALP, BMP-2, COL-1, OCN, OPN, and BSP expression (Figure 5B). These results suggest that AHT-Sr, with released Sr^{2+} ions, facilitates early osteogenesis of OVX-BMSCs.

Sr-doped nanocoating implant osseointegration in *vivo*

Previous studies have shown that AHT implants can enhance their osteogenic activity compared to Ti implants with smooth surface (Zhang et al., 2020; Wang et al., 2021). And treated implants with hydrophilic surfaces have been widely used in clinic. Therefore, we selected AHT as the control group *in vivo* experiments. Micro-CT was performed to analyze primary bone healing. Figure 6A shows the schematic diagram of 3D reconstruction including associated parameters. Significantly higher osteogenesis of AHT-Sr implants was observed relative to AHT implants after 2 and 4 weeks (Figure 6B). The volume of the newly formed bone and thickness and number of trabecular bones around the AHT-Sr implant were significantly higher than the AHT implants while trabecular space was significantly lower (Figure 6C).

Discussion

Dysfunctional BMSCs result in bone formation defects in osteoporosis that in turn may cause implant failure (Du et al., 2016). In previous studies, coating with Sr ions on the implant

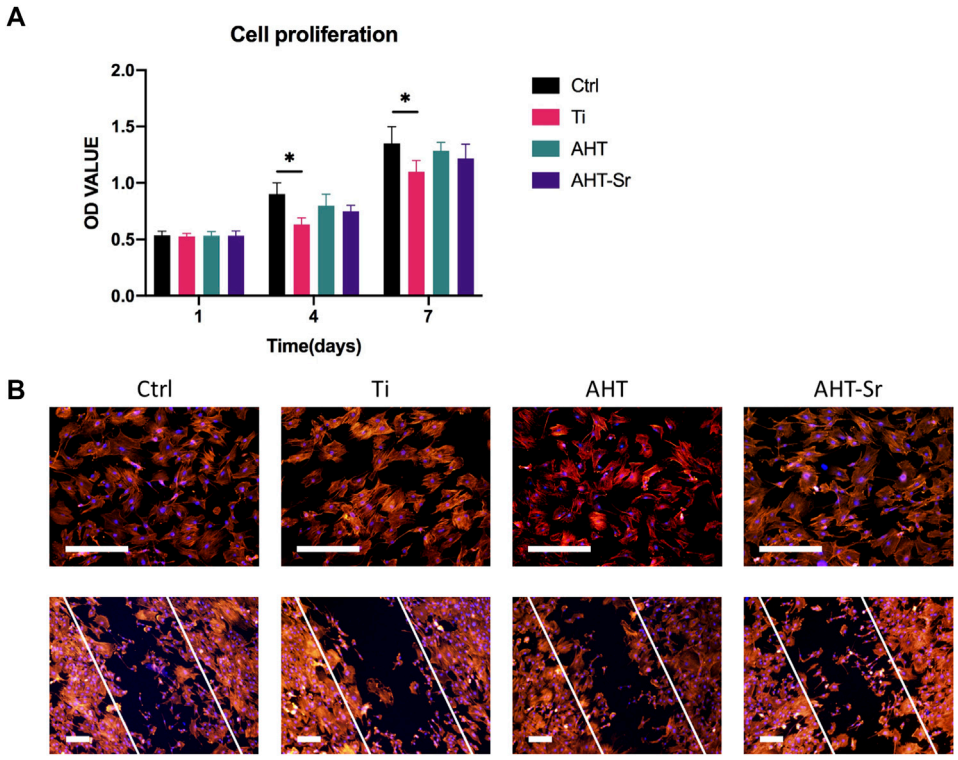

FIGURE 4
Biocompatibility studies on Ti disks. **(A)** Proliferation of H-BMSCs grown on Ti surfaces and OVX-BMSCs grown on different Ti disk surfaces. **(B)** F-actin immunostaining images of H-BMSCs and OVX-BMSCs grown on Ti, AHT, and AHT-Sr. Representative images of three separate experiments. Scale bars: 100 μm. Error bars indicate the SD of three separate experiments.

surface can achieve better osteogenesis effect in health model (Zhao et al., 2019). However, the quantitative effect of AHT-Sr coatings on the osteoporosis model remains unclear. It would be of great significance to comprehensively evaluate the osseointegration following AHT-Sr implantation *in vivo*. Therefore, in this study, we successfully established an osteoporosis rat model. In addition, we coated nanoscale Sr onto AHT surfaces and found that in the osteoporosis model, AHT-Sr exhibited great osteogenic activity both *in vitro* and *in vivo*.

OVX rat models have been used in many studies for postmenopausal osteoporosis (Tao et al., 2015; Tao et al., 2016). In the present study, the trabecular bone volume of OVX rats markedly decreased in the distal femur 12 weeks after surgery, and BV/TV calculated by Micro-CT was significantly lower, which indicates that an osteoporosis model had been successfully established. Compared with H-BMSCs, VOX-BMSCs had decreased osteogenic differentiation ability and were used in *in vitro* studies.

As stated in the *in vitro* tests, OVX-BMSCs on AHT and AHT-Sr exhibited highly branched pseudopods extending into the microstructures of the coating (Figure 5). This result may be related to the roughness and good wettability of AHT-Sr surface. Previous studies have shown that that Ti implants with rough surfaces enhance osteoblast adhesion and extension compared to those with smooth surfaces (Gittens et al., 2014; Salou et al., 2015). The micro/nanotopography structures generated by hydrothermal treatment in this study were similar to those described in other studies (Kim et al., 2016). These micro/nanoscale structures observed through SEM on the AHT-Sr implant surface may enhance bone formation. In addition, osteoblast attachment could be promoted by implants with higher surface hydrophilicity (Le et al., 2021). Kubo et al. (2009) have reported that uniformly distributed 300-nm nano surface structures significantly enhance ALP activity, mRNA expression of Col1, and Ocn, and total calcium deposition in BMSCs. After alkali heat treatment, AHT-Sr induced VOX-BMSC differentiation *in vitro* with microstructures of approximately 300 nm in size that were randomly distributed. Surface wettability also influences implant osseointegration. Wilson et al. have shown that hydrophilic surfaces improve binding of adhesive proteins onto the osteoblast surface and promote their growth (Wilson et al., 2005; Deng et al., 2010). Moreover, greater surface wettability can speed healing and early

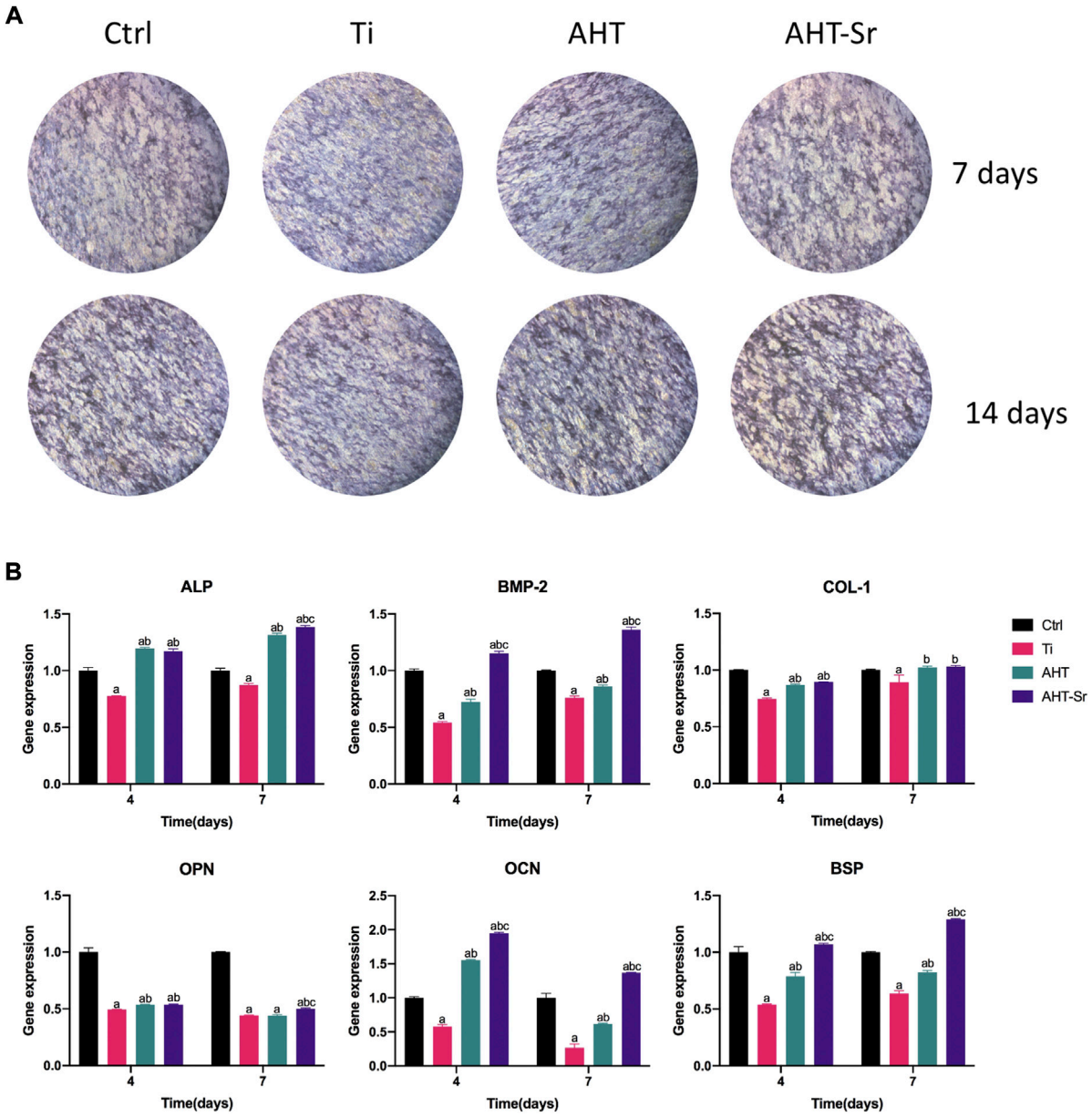

FIGURE 5
AHT-Sr promoted osteogenic differentiation of OVX-BMSCs. **(A)** ALP staining of H-BMSCs and OVX-BMSCs cultured on Ti, AHT and AHT-Sr disks for 4 and 7 days. Representative images of three separate experiments. **(B)** mRNA expression of selected osteogenic markers in H-BMSCs and OVX-BMSCs that were cultured on different Ti disks for 4 and 7 days. Error bars indicate the SD of three separate experiment. *$p < 0.05$.

bone bonding. We assumed an alike increase in osteogenic activity as wettability gradually increased from Ti and AHT to AHT-Sr (Figure 2).

As expected, the AHT-Sr had better osseointegration than the AHT considering Sr release. The chemical composition of coating is an important factor affecting the adhesion and attachment of osteoblasts (Wang et al., 2020). The release of Sr ions can alter local pH, increase cell microenvironment basicity, modify cell transmembrane protein structure, and improve the binding of cells onto proteins adsorbed on the AHT-Sr surface to promote adhesion (Zhang et al., 2014; Zhang et al., 2016; Schmidt et al., 2020). Over the years, in various experimental studies and clinical trials, a large number of studies have shown that stable Sr ions can promote bone formation and reduce bone resorption (Alghamdi and Jansen, 2013; Zhang et al., 2021).

Clinically, early osteogenesis has a significant impact on the success of implants. The degree of early osteogenesis relies on the

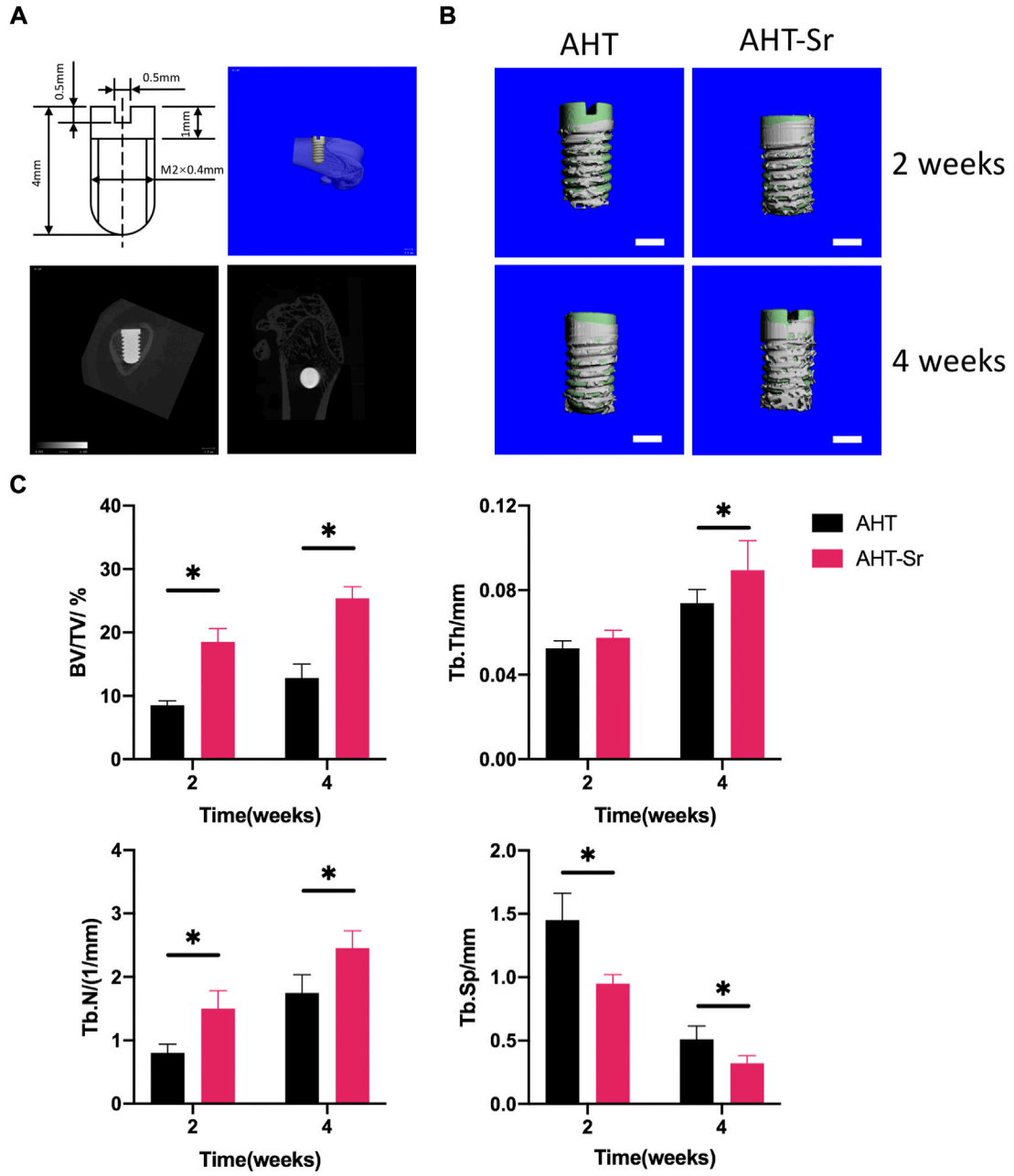

FIGURE 6
Osseointegration of AHT and AHT-Sr implants was measured by micro-CT. **(A)** Schematic of the surgery. **(B)** Reconstructed pictures of AHT implants (Control) and AHT-Sr implants at 2 and 4 weeks post surgery. Scale bar representing 1 mm; $n = 5$ per group. **(C)** BV/TV, Tb.Th, Tb.N, and Tb. Sp were measured. $n = 5$. $^*p < 0.05$.

ability of osteoblasts to generate new bone, which is controlled by related genes and proteins. ALP, COL-1, BMP-2, OCN, OPN, and BSP are indicators of osteoblast differentiation and mineralization and thus were assessed in this study (Figure 5B). ALP and COL-1 genes are early markers of osteoblast differentiation (Ding et al., 2016; Sun et al., 2021). OPN can adjust cell adhesion, migration, and mineral deposition as a multifunctional extracellular matrix protein (He et al., 2018). BMP-2 has an important role in activate osteoblasts and promote bone formation (Wang et al., 2021). OCN influences late differentiation of osteoblasts, which mainly occurs in the mineralization stage (Wan et al., 2022; Yu et al., 2022). *In vitro* RT-PCR analysis showed that the expression levels of these genes in cells cultured on AHT-Sr were significantly higher than those cultured on AHT. In addition, compared with AHT, ALP

protein secretion, which promotes the mineralization of collagen matrix, was enhanced both *in vitro* and *in vivo* (Figure 5A). These findings suggest that AHT-Sr coating induces osteogenesis *in vitro* and *in vivo* by simultaneously maintaining bone regeneration and disrupting bone resorption. However, despite its beneficial effects, the mechanism by which Sr ions induce bone formation remains unclear. Sr can activate the CaSR and NFATc/Wnt signaling pathways and regulate OPG/RANKL and other mechanisms (Cui et al., 2020). Therefore, Sr imparts different effects on osteoclasts and osteoblasts, thereby resulting in increased bone mass, bone strength, and bone structure. Furthermore, Sr also influences the ras-MAPK signaling pathway. Peng et al. (2009) have reported that Sr upregulates Runx2 transcription and increases phosphorylation levels in human bone mesenchymal stem cells *via* the Ras-MAPK pathway, resulting in the upregulation of OCN, COL2A, OPN, and other genes that in turn enhances osteoblast differentiation. Zhang et al. (2018) found that micro structures and Sr ions could synergistically promote osteogenic differentiation by activating ERK1/2 and p38 MAPK signaling pathway. However, the mechanism of Sr ion induced bone formation remains unclear, and further studies are needed to clarify its underlying molecular mechanism.

The impact of AHT-Sr on osseointegration was assessed by histological analysis of micro-CT images for its potential clinical application. The results of this investigation showed that AHT-Sr coatings enhanced implant osseointegration and improved implant trabecular microstructure, thereby enhancing early implant osseointegration.

Conclusion

In this study, we simulated the osteoporotic environment *in vitro* by culturing BMSCs isolated from the bone marrow of OVX Sprague Dawley rats to evaluate the therapeutic effect of AHT-Sr. After alkali heat treatment, AHT-Sr exhibited a rough surface with low contact angle and steadily released Sr ions. Based on our results, we showed that Sr-incorporated surfaces treated *via* hydrothermal reactions enhanced osteogenesic differentiation and early bone osseointegration using osteoporotic models and thus may potentially be used as a surface modification method for implant surfaces.

Data availability statement

The raw data supporting the conclusion of this article will be made available by the authors, without undue reservation.

Ethics statement

The animal study was reviewed and approved by the Animal experiments were performed under the authorization of the ethical committee of Xuzhou Medical University.

Author contributions

TG caried out the experiments and drafted the original manuscript. YW carried out the statistical analyses. KL contributed to the conceptualization and experimental designs. CZ assisted in the experiment and data collection. JW and YL performed cell culture. CY and PW led the conceptualization and project administration, and supervised the writing and editing of the manuscript. All authors approved the final version of the manuscript.

Funding

The Program of Xuzhou Science and Technology (Nos. KC21151 and KC21236) supported this study.

Acknowledgments

We thank Zhiwei Liu in public Experimental Research Center, Xuzhou Medical University for his technical assistance on Scanning Electron Microscope.

Conflict of interest

The authors declare that the research was conducted in the absence of any commercial or financial relationships that could be construed as a potential conflict of interest.

Publisher's note

All claims expressed in this article are solely those of the authors and do not necessarily represent those of their affiliated organizations, or those of the publisher, the editors and the reviewers. Any product that may be evaluated in this article, or claim that may be made by its manufacturer, is not guaranteed or endorsed by the publisher.

References

Alghamdi, H. S., Bosco, R., van den Beucken, J. J., Walboomers, X. F., and Jansen, J. A. (2013). Osteogenicity of titanium implants coated with calcium phosphate or collagen type-I in osteoporotic rats. *Biomaterials* 34 (15), 3747–3757. doi:10.1016/j.biomaterials.2013.02.033

Alghamdi, H. S., and Jansen, J. A. (2013). Bone regeneration associated with nontherapeutic and therapeutic surface coatings for dental implants in osteoporosis. *Tissue Eng. Part B Rev.* 19 (3), 233–253. doi:10.1089/ten.TEB.2012.0400

Bianco, P., Sacchetti, B., and Riminucci, M. (2011). Stem cells in skeletal physiology and endocrine diseases of bone. *Endocr. Dev.* 21, 91–101. doi:10.1159/000328138

Bonifacio, M. A., Cometa, S., Dicarlo, M., Baruzzi, F., de Candia, S., Gloria, A., et al. (2017). Gallium-modified chitosan/poly(acrylic acid) bilayer coatings for improved titanium implant performances. *Carbohydr. Polym.* 166, 348–357. doi:10.1016/j.carbpol.2017.03.009

Bonnelye, E., Chabadel, A., Saltel, F., and Jurdic, P. (2008). Dual effect of strontium ranelate: Stimulation of osteoblast differentiation and inhibition of osteoclast formation and resorption *in vitro*. *Bone* 42 (1), 129–138. doi:10.1016/j.bone.2007.08.043

Chen, Y., Chen, X. Y., Shen, J. W., He, F. M., and Liu, W. (2016). The characterization and osteogenic activity of nanostructured strontium-containing oxide layers on titanium surfaces. *Int. J. Oral Maxillofac. Implants* 31 (4), e102–e115. doi:10.11607/jomi.4415

Choudhary, S., Halbout, P., Alander, C., Raisz, L., and Pilbeam, C. (2007). Strontium ranelate promotes osteoblastic differentiation and mineralization of murine bone marrow stromal cells: Involvement of prostaglandins. *J. Bone Min. Res.* 22 (7), 1002–1010. doi:10.1359/jbmr.070321

Cui, X., Zhang, Y., Wang, J., Huang, C., Wang, Y., Yang, H., et al. (2020). Strontium modulates osteogenic activity of bone cement composed of bioactive borosilicate glass particles by activating Wnt/β-catenin signaling pathway. *Bioact. Mater.* 5 (2), 334–347. doi:10.1016/j.bioactmat.2020.02.016

de Oliveira, P., Bonfante, E. A., Bergamo, E. T. P., de Souza, S. L. S., Riella, L., Torroni, A., et al. (2020). Obesity/metabolic syndrome and diabetes mellitus on peri-implantitis. *Trends Endocrinol. Metabolism* 31 (8), 596–610. doi:10.1016/j.tem.2020.05.005

Deng, Y., Morrissey, S., Gathergood, N., Delort, A. M., Husson, P., and Costa Gomes, M. F. (2010). The presence of functional groups key for biodegradation in ionic liquids: Effect on gas solubility. *ChemSusChem* 3 (3), 377–385. doi:10.1002/cssc.200900241

Ding, Q., Cui, J., Shen, H., He, C., Wang, X., Shen, S. G. F., et al. (2020). Advances of nanomaterial applications in oral and maxillofacial tissue regeneration and disease treatment. *WIREs Nanomed Nanobiotechnol* 13, e1669. doi:10.1002/wnan.1669

Ding, Y. F., Li, R. W., Nakai, M., Majumdar, T., Zhang, D. H., Niinomi, M., et al. (2016). Osteoanabolic implant materials for orthopedic treatment. *Adv. Healthc. Mater.* 5 (14), 1740–1752. doi:10.1002/adhm.201600074

Du, Z., Xiao, Y., Hashimi, S., Hamlet, S. M., and Ivanovski, S. (2016). The effects of implant topography on osseointegration under estrogen deficiency induced osteoporotic conditions: Histomorphometric, transcriptional and ultrastructural analysis. *Acta Biomater.* 42, 351–363. doi:10.1016/j.actbio.2016.06.035

Dudeck, J., Rehberg, S., Bernhardt, R., Schneiders, W., Zierau, O., Inderchand, M., et al. (2014). Increased bone remodelling around titanium implants coated with chondroitin sulfate in ovariectomized rats. *Acta Biomater.* 10 (6), 2855–2865. doi:10.1016/j.actbio.2014.01.034

Fu, Z., Zhuang, Y., Cui, J., Sheng, R., Tomás, H., Rodrigues, J., et al. (2022). Development and challenges of cells-and materials-based tooth regeneration. *Eng. Regen.* doi:10.1016/j.engreg.2022.04.003

Gittens, R. A., Scheideler, L., Rupp, F., Hyzy, S. L., Geis-Gerstorfer, J., Schwartz, Z., et al. (2014). A review on the wettability of dental implant surfaces II: Biological and clinical aspects. *Acta Biomater.* 10 (7), 2907–2918. doi:10.1016/j.actbio.2014.03.032

He, Y., Mu, C., Shen, X., Yuan, Z., Liu, J., Chen, W., et al. (2018). Peptide LL-37 coating on micro-structured titanium implants to facilitate bone formation *in vivo* via mesenchymal stem cell recruitment. *Acta Biomater.* 80, 412–424. doi:10.1016/j.actbio.2018.09.036

Holahan, C. M., Koka, S., Kennel, K. A., Weaver, A. L., Assad, D. A., Regennitter, F. J., et al. (2008). Effect of osteoporotic status on the survival of titanium dental implants. *Int. J. Oral Maxillofac. Implants* 23 (5), 905–910.

Huang, P., Zhang, Y., Xu, K., and Han, Y. (2004). Surface modification of titanium implant by microarc oxidation and hydrothermal treatment. *J. Biomed. Mat. Res.* 70B (2), 187–190. doi:10.1002/jbm.b.30009

Kim, H. S., Kim, Y. J., Jang, J. H., and Park, J. W. (2016). Surface engineering of nanostructured titanium implants with bioactive ions. *J. Dent. Res.* 95 (5), 558–565. doi:10.1177/0022034516638026

Kołodziejska, B., Stępień, N., and Kolmas, J. (2021). The influence of strontium on bone tissue metabolism and its application in osteoporosis treatment. *Ijms* 22 (12), 6564. doi:10.3390/ijms22126564

Kubo, K., Tsukimura, N., Iwasa, F., Ueno, T., Saruwatari, L., Aita, H., et al. (2009). Cellular behavior on TiO2 nanonodular structures in a micro-to-nanoscale hierarchy model. *Biomaterials* 30 (29), 5319–5329. doi:10.1016/j.biomaterials.2009.06.021

Kuo, Y. J., Chen, C. H., Dash, P., Lin, Y. C., Hsu, C. W., Shih, S. J., et al. (2022). Angiogenesis, osseointegration, and antibacterial applications of polyelectrolyte multilayer coatings incorporated with silver/strontium containing mesoporous bioactive glass on 316L stainless steel. *Front. Bioeng. Biotechnol.* 10, 818137. doi:10.3389/fbioe.2022.818137

Le, P. T. M., Shintani, S. A., Takadama, H., Ito, M., Kakutani, T., Kitagaki, H., et al. (2021). Bioactivation treatment with mixed acid and heat on titanium implants fabricated by selective laser melting enhances preosteoblast cell differentiation. *Nanomaterials* 11 (4), 987. doi:10.3390/nano11040987

Lin, K., Xia, L., Li, H., Jiang, X., Pan, H., Xu, Y., et al. (2013). Enhanced osteoporotic bone regeneration by strontium-substituted calcium silicate bioactive ceramics. *Biomaterials* 34 (38), 10028–10042. doi:10.1016/j.biomaterials.2013.09.056

Montagna, G., Cristofaro, F., Fassina, L., Bruni, G., Cucca, L., Kochen, A., et al. (2020). An *in vivo* comparison study between strontium nanoparticles and rhBMP2. *Front. Bioeng. Biotechnol.* 8, 499. doi:10.3389/fbioe.2020.00499

Naseri, R., Yaghini, J., and Feizi, A. (2020). Levels of smoking and dental implants failure: A systematic review and meta-analysis. *J. Clin. Periodontol.* 47 (4), 518–528. doi:10.1111/jcpe.13257

Okuzu, Y., Fujibayashi, S., Yamaguchi, S., Masamoto, K., Otsuki, B., Goto, K., et al. (2021). *In vitro* study of antibacterial and osteogenic activity of titanium metal releasing strontium and silver ions. *J. Biomater. Appl.* 35 (6), 670–680. doi:10.1177/0885328220959584

Park, Y. S., Lee, J. Y., Suh, J. S., Jin, Y. M., Yu, Y., Kim, H. Y., et al. (2014). Selective osteogenesis by a synthetic mineral inducing peptide for the treatment of osteoporosis. *Biomaterials* 35 (37), 9747–9754. doi:10.1016/j.biomaterials.2014.08.007

Peng, S., Zhou, G., Luk, K. D., Cheung, K. M., Li, Z., Lam, W. M., et al. (2009). Strontium promotes osteogenic differentiation of mesenchymal stem cells through the Ras/MAPK signaling pathway. *Cell Physiol. Biochem.* 23 (1-3), 165–174. doi:10.1159/000204105

Russow, G., Jahn, D., Appelt, J., Märdian, S., Tsitsilonis, S., and Keller, J. (2018). Anabolic therapies in osteoporosis and bone regeneration. *Ijms* 20 (1), 83. doi:10.3390/ijms20010083

Salou, L., Hoornaert, A., Louarn, G., and Layrolle, P. (2015). Enhanced osseointegration of titanium implants with nanostructured surfaces: An experimental study in rabbits. *Acta Biomater.* 11, 494–502. doi:10.1016/j.actbio.2014.10.017

Schmidt, R., Gebert, A., Schumacher, M., Hoffmann, V., Voss, A., Pilz, S., et al. (2020). Electrodeposition of Sr-substituted hydroxyapatite on low modulus beta-type Ti-45Nb and effect on *in vitro* Sr release and cell response. *Mater. Sci. Eng. C* 108, 110425. doi:10.1016/j.msec.2019.110425

Shu, T., Zhang, Y., Sun, G., Pan, Y., He, G., Cheng, Y., et al. (2020). Enhanced osseointegration by the hierarchical micro-nano topography on selective laser melting Ti-6Al-4V dental implants. *Front. Bioeng. Biotechnol.* 8, 621601. doi:10.3389/fbioe.2020.621601

Spriano, S., Yamaguchi, S., Baino, F., and Ferraris, S. (2018). A critical review of multifunctional titanium surfaces: New frontiers for improving osseointegration and host response, avoiding bacteria contamination. *Acta Biomater.* 79, 1–22. doi:10.1016/j.actbio.2018.08.013

Sun, Y., Li, Y., Zhang, Y., Wang, T., Lin, K., and Liu, J. (2021). A polydopamine-assisted strontium-substituted apatite coating for titanium promotes osteogenesis and angiogenesis via FAK/MAPK and PI3K/AKT signaling pathways. *Mater. Sci. Eng. C* 131, 112482. doi:10.1016/j.msec.2021.112482

Takahashi, T., Watanabe, T., Nakada, H., Tanimoto, Y., Kimoto, S., Mijares, D. Q., et al. (2016). Effect of a dietary supplement on peri-implant bone strength in a rat model of osteoporosis. *J. Prosthodont. Res.* 60 (2), 131–137. doi:10.1016/j.jpor.2015.12.006

Tao, Z. S., Lv, Y. X., Cui, W., Huang, Z. L., Tu, K. K., Zhou, Q., et al. (2016). Effect of teriparatide on repair of femoral metaphyseal defect in ovariectomized rats. *Z Gerontol. Geriat* 49 (5), 423–428. doi:10.1007/s00391-015-0949-1

Tao, Z. S., Zhou, W. S., Tu, K. K., Huang, Z. L., Zhou, Q., Sun, T., et al. (2015). Effect exerted by Teriparatide upon Repair Function of β-tricalcium phosphate to ovariectomised rat's femoral metaphysis defect caused by osteoporosis. *Injury* 46 (11), 2134–2141. doi:10.1016/j.injury.2015.07.042

Wan, H. Y., Shin, R. L. Y., Chen, J. C. H., Assunção, M., Wang, D., Nilsson, S. K., et al. (2022). Dextran sulfate-amplified extracellular matrix deposition promotes osteogenic differentiation of mesenchymal stem cells. *Acta Biomater.* 140, 163–177. doi:10.1016/j.actbio.2021.11.049

Wang, A., Yuan, W., Song, Y., Zang, Y., and Yu, Y. (2022). Osseointegration effect of micro-nano implants loaded with kaempferol in osteoporotic rats. *Front. Bioeng. Biotechnol.* 10, 842014. doi:10.3389/fbioe.2022.842014

Wang, H., Liu, J., Wang, C., Shen, S. G., Wang, X., and Lin, K. (2021a). The synergistic effect of 3D-printed microscale roughness surface and nanoscale feature on enhancing osteogenic differentiation and rapid osseointegration. *J. Mater. Sci. Technol.* 63 (04), 18–26. doi:10.1016/j.jmst.2019.12.030

Wang, H., Xu, Q., Hu, H., Shi, C., Lin, Z., Jiang, H., et al. (2020). The fabrication and function of strontium-modified hierarchical micro/nano titanium implant. *Ijn* Vol. 15, 8983–8998. doi:10.2147/IJN.S268657

Wang, H., Zhang, X., Wang, H., Zhang, J., Li, J., Ruan, C., et al. (2018). Enhancing the osteogenic differentiation and rapid osseointegration of 3D printed Ti6Al4V implants via nano-topographic modification. *J. Biomed. Nanotechnol.* 14 (4), 707–715. doi:10.1166/jbn.2018.2551

Wang, M., Li, H., Yang, Y., Yuan, K., Zhou, F., Liu, H., et al. (2021b). A 3D-bioprinted scaffold with doxycycline-controlled BMP2-expressing cells for inducing bone regeneration and inhibiting bacterial infection. *Bioact. Mater.* 6 (5), 1318–1329. doi:10.1016/j.bioactmat.2020.10.022

Wang, X., Li, Z., Wang, Z., Liu, H., Cui, Y., Liu, Y., et al. (2021c). Incorporation of bone morphogenetic protein-2 and osteoprotegerin in 3D-printed Ti6Al4V scaffolds enhances osseointegration under osteoporotic conditions. *Front. Bioeng. Biotechnol.* 9, 754205. doi:10.3389/fbioe.2021.754205

Wang, X., Ning, B., and Pei, X. (2021d). Tantalum and its derivatives in orthopedic and dental implants: Osteogenesis and antibacterial properties. *Colloids Surfaces B Biointerfaces* 208, 112055. doi:10.1016/j.colsurfb.2021.112055

Wei, H., Cui, J., Lin, K., Xie, J., and Wang, X. (2022). Recent advances in smart stimuli-responsive biomaterials for bone therapeutics and regeneration. *Bone Res.* 10 (1), 17. doi:10.1038/s41413-021-00180-y

Wilson, C. J., Clegg, R. E., Leavesley, D. I., and Pearcy, M. J. (2005). Mediation of biomaterial-cell interactions by adsorbed proteins: A review. *Tissue Eng.* 11 (1-2), 1–18. doi:10.1089/ten.2005.11.1

Xing, H., Li, R., Wei, Y., Ying, B., Li, D., and Qin, Y. (2020). Improved osteogenesis of selective-laser-melted titanium alloy by coating strontium-doped phosphate with high-efficiency air-plasma treatment. *Front. Bioeng. Biotechnol.* 8, 367. doi:10.3389/fbioe.2020.00367

Yu, X., Wang, X., Li, D., Sheng, R., Qian, Y., Zhu, R., et al. (2022). Mechanically reinforced injectable bioactive nanocomposite hydrogels for *in-situ* bone regeneration. *Chem. Eng. J.* 433, 132799. doi:10.1016/j.cej.2021.132799

Zhang, C., Zhang, T., Geng, T., Wang, X., Lin, K., and Wang, P. (2021a). Dental implants loaded with bioactive agents promote osseointegration in osteoporosis: A review. *Front. Bioeng. Biotechnol.* 9, 591796. doi:10.3389/fbioe.2021.591796

Zhang, J., Liu, J., Wang, C., Chen, F., Wang, X., and Lin, K. (2020). A comparative study of the osteogenic performance between the hierarchical micro/submicro-textured 3D-printed Ti6Al4V surface and the SLA surface. *Bioact. Mater.* 5 (1), 9–16. doi:10.1016/j.bioactmat.2019.12.008

Zhang, J., Zhao, S., Zhu, Y., Huang, Y., Zhu, M., Tao, C., et al. (2014). Three-dimensional printing of strontium-containing mesoporous bioactive glass scaffolds for bone regeneration. *Acta Biomater.* 10 (5), 2269–2281. doi:10.1016/j.actbio.2014.01.001

Zhang, W., Cao, H., Zhang, X., Li, G., Chang, Q., Zhao, J., et al. (2016). A strontium-incorporated nanoporous titanium implant surface for rapid osseointegration. *Nanoscale* 8 (9), 5291–5301. doi:10.1039/c5nr08580b

Zhang, X., Cui, J., Cheng, L., and Lin, K. (2021b). Enhancement of osteoporotic bone regeneration by strontium-substituted 45S5 bioglass via time-dependent modulation of autophagy and the Akt/mTOR signaling pathway. *J. Mat. Chem. B* 9 (16), 3489–3501. doi:10.1039/d0tb02991b

Zhang, X., Li, H., Lin, C., Ning, C., and Lin, K. (2018). Synergetic topography and chemistry cues guiding osteogenic differentiation in bone marrow stromal cells through ERK1/2 and p38 MAPK signaling pathway. *Biomater. Sci.* 6 (2), 418–430. doi:10.1039/c7bm01044c

Zhao, Q., Yi, L., Jiang, L., Ma, Y., Lin, H., and Dong, J. (2019). Surface functionalization of titanium with zinc/strontium-doped titanium dioxide microporous coating via microarc oxidation. *Nanomedicine Nanotechnol. Biol. Med.* 16, 149–161. doi:10.1016/j.nano.2018.12.006

frontiers | Frontiers in Bioengineering and Biotechnology

TYPE Review
PUBLISHED 16 September 2022
DOI 10.3389/fbioe.2022.1022368

OPEN ACCESS

EDITED BY
Qian Feng,
Chongqing University, China

REVIEWED BY
Xiaojun Zhou,
Donghua University, China
Feng Chen,
Tongji University, China

*CORRESPONDENCE
Changyong Yuan,
yuanchangyong1983@foxmail.com
Kaili Lin,
linkaili@sjtu.edu.cn

†These authors have contributed equally to this work

SPECIALTY SECTION
This article was submitted to Biomaterials, a section of the journal Frontiers in Bioengineering and Biotechnology

RECEIVED 18 August 2022
ACCEPTED 01 September 2022
PUBLISHED 16 September 2022

CITATION
Zhuang Y, Jiang S, Yuan C and Lin K (2022), The potential therapeutic role of extracellular vesicles in osteoarthritis. *Front. Bioeng. Biotechnol.* 10:1022368. doi: 10.3389/fbioe.2022.1022368

The potential therapeutic role of extracellular vesicles in osteoarthritis

Yu Zhuang[1,2,3†], Shengjie Jiang[1,2,3†], Changyong Yuan[4,5,6*] and Kaili Lin[1,2,3*]

[1]Department of Oral and Cranio-Maxillofacial Surgery, Shanghai Ninth People's Hospital, Shanghai Jiao Tong University School of Medicine, Shanghai, China, [2]College of Stomatology, Shanghai Jiao Tong University, Shanghai, China, [3]National Center for Stomatology, National Clinical Research Center for Oral Diseases, Shanghai Key Laboratory of Stomatology, Research Unit of Oral and Maxillofacial Regenerative Medicine, Chinese Academy of Medical Sciences, Shanghai, China, [4]School of Stomatology, Xuzhou Medical University, Shanghai, China, [5]Department of Dental Implant, The Affiliated Stomatological Hospital of Xuzhou Medical University, Shanghai, China, [6]Shanghai Key Laboratory of Stomatology, Department of Oral and Cranio-Maxillofacial Surgery, Shanghai Ninth People's Hospital, Shanghai Research Institute of Stomatology, Shanghai Jiao Tong University School of Medicine, Shanghai, China

Osteoarthritis (OA) is a worldwide and disabling disease, which cause severe pain and heavy socioeconomic burden. However, pharmacologic or surgical therapies cannot mitigate OA progression. Mesenchymal stem cells (MSCs) therapy has emerged as potential approach for OA treatment, while the immunogenicity and ethical audit of cell therapy are unavoidable. Compared with stem cell strategy, EVs induce less immunological rejection, and they are more stable for storage and *in vivo* application. MSC-EVs-based therapy possesses great potential in regulating inflammation and promoting cartilage matrix reconstruction in OA treatment. To enhance the therapeutic effect, delivery efficiency, tissue specificity and safety, EVs can be engineered via different modification strategies. Here, the application of MSC-EVs in OA treatment and the potential underlying mechanism were summarized. Moreover, EV modification strategies including indirect MSC modification and direct EV modification were reviewed.

KEYWORDS

extracellular vesicles, osteoarthritis, mesenchymal stem cells, therapeutic treatment, EV engineering

Introduction

Osteoarthritis (OA) is a worldwide and disabling disease, which cause severe pain and heavy socioeconomic burden (Glyn-Jones et al., 2015). The pathogenic risk factors for OA include trauma, aging, obesity, inheritance, etc. (Cisternas et al., 2016). OA is characterized as synovitis, degrading cartilage, damaged menisci and ligaments, and pathologically formed osteophytes (Loeser et al., 2012). Aging-related cell senescence, metabolic disorder and aberrant mechanical load can lead to senescence-associated secretory phenotype (SASP) release and local inflammation, which in turn aggravate cell senescence and cartilage matrix degradation (Glyn-Jones et al., 2015; Appleton, 2018;

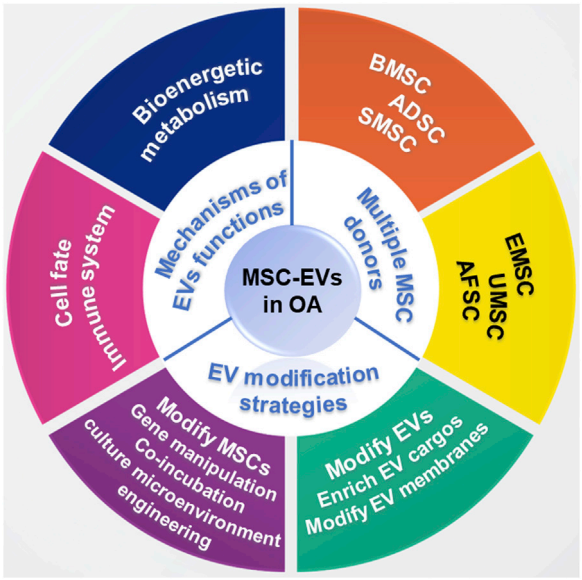

FIGURE 1
Schematic illustration for the application of MSC-EVs in OA treatment.

Boulestreau et al., 2021). Existing therapies for OA are symptomatic strategies like nonsteroidal anti-inflammatory drugs (NSAIDs), and surgical strategies like joint replacement (Tao et al., 2017). However, pharmacologic or surgical therapies cannot mitigate OA progression, or enhance damaged cartilage reconstruction. Recently, mesenchymal stem cells (MSCs) therapy has emerged as potential approach for OA treatment, while the immunogenicity and ethical audit of cell therapy are unavoidable (Zhuang et al., 2022). Effective strategies for inflammation regulation and cartilage regeneration are urgently required.

Extracellular vesicles (EVs), serving as cell-cell communication media, play a vital role in regulating tissue homeostasis and biological process. EVs derived from MSCs (MSCs-EVs) inherit the valuable characteristics of donor MSCs (Liu A. et al., 2021; Liu L. et al., 2021; Zhang X. et al., 2022). Compared with stem cell strategy, EVs induce less immunological rejection, and they are more stable for storage and *in vivo* application (Brennan et al., 2020). Multiple components (including miRNAs, lipids, proteins) make EVs potential candidates in promoting tissue regeneration and modulating immunity (Yu et al., 2022). MSCs-EVs have been reported to improve chondrocyte phenotype, attenuate cartilage degradation *in vitro* and ameliorate OA progression *in vivo* (Zhang S. et al., 2016; Tofiño-Vian et al., 2018; Woo et al., 2020). To enhance the therapeutic effect, delivery efficiency, tissue specificity and safety, EVs can be engineered via different modification strategies.

EV-based therapy possesses great potential in regulating inflammation and promoting cartilage matrix reconstruction in OA treatment. In this review, we summarize the application of MSC-EVs in OA treatment and the potential underlying mechanism. Moreover, EV modification strategies including indirect MSC modification and direct EV modification were also reviewed (Figure 1).

The application of extracellular vesicles in osteoarthritis treatment

There have been more and more studies indicating that MSC-EVs are potential in controlling inflammation, inhibiting cartilage matrix degradation, and promoting cartilage repair for OA treatment. The applications of EVs derived from different MSCs in OA treatment and the potential underlying mechanisms are summarized here.

The therapeutic role of different MSC-derived extracellular vesicles

The cargos of EVs may vary depending on their donor cells and consist of multiple bioactive molecules including proteins, lipids, and miRNAs, thus leading to specific characteristics of different MSC-EVs (Mianehsaz et al., 2019). MSCs therapy has been proved to attenuate inflammation, prevent cartilage matrix degradation, and ameliorate pain in clinical trials (Toh et al., 2017; Song et al., 2020). The mechanism underlying the MSCs therapeutic effect might be secretion of bioactive molecules (Eleuteri and Fierabracci, 2019), additionally, application of EVs secreted from MSCs possess inherent advantages compared to direct MSC therapy (lower immunogenicity, tumorigenicity, etc.) (Ankrum et al., 2014; Fichtel et al., 2022). Thus, EVs therapy has gained more and more attention in disease treatment and tissue reconstruction. EVs derived from different MSCs source for OA treatment have been summarized here (Table 1).

EVs derived from bone marrow mesenchymal stem cells (BMSC-EVs) has been widely applied for OA treatment. BMSC-EVs can play a role in promoting the proliferation and matrix components secretion of chondrocytes, and improve the framework of subchondral bone. He et al. (2020) treated OA rats with BMSC-EVs, and the results indicated that BMSC-EVs improved chondrocyte phenotype and alleviated pain *via* ameliorating function of dorsal root ganglion (DRG). Moreover, BMSC-EVs were reported to regulate inflammation through restraining NF-κB pathway (Li et al., 2020), controlling inflammation related factor Autotaxin-YAP (Wang Y. et al., 2021), modulating macrophagocyte polarization (Zhang et al., 2020), and prevent chondrocyte apoptosis (Chen et al., 2020; Wang X. et al., 2021; Jin et al., 2021).

TABLE 1 The therapeutic role of different MSC-EVs in OA treatment.

MSC source	Cargo	Model	Delivery strategies	Therapeutic effect	References
BMSCs	miR-92a-3p	Collagenase induced mice OA model	Local intra-articular injection	Promoting cartilage development and maintaining homeostasis via miR-92a-3p/ pathway	Mao et al. (2018)
	miR-320c	Chondrocytes isolated from OA articular cartilage samples	Co-culture	Enhancing cartilage extracellular matrix deposition (upregulate SOX9 and downregulate MMP13)	Sun et al. (2019)
	—	Collagenase induced mice OA model	Local intra-articular injection	Inhibiting inflammation, inducing expression of matrix formation-related genes and preventing OA progression	Cosenza et al. (2017)
	lncRNA MEG-3	Anterior cruciate ligament (ACL) transection and medial meniscectomy (MM) induced rat OA model	Local intra-articular injection	Reducing the senescence and apoptosis of chondrocytes	Jin et al. (2021)
	lncRNA LYRM4	IL-1β induced inflammatory chondrocyte	Co-culture	Reversing the carbolic changes of chondrocytes induced by IL-1β via lncRNA LYRM4-AS1/ GRPR/miR-6515–5p pathway	Wang et al. (2021a)
	miR-136–5p	Post-traumatic mice OA model	Local intra-articular injection	Promoting collagen II, aggrecan, and SOX9 expression of chondrocytes via miR-136–5p/ELF3, and inhibiting post-traumatic OA progression	Chen et al. (2020)
	—	Anterior cruciate ligament (ACL) transection induced rat OA model	Local intra-articular injection	Alleviating OA via promoting M2 polarization of synovial macrophages	Zhang et al. (2020)
	lncRNA NEAT1	Destabilization of the medial meniscus (DMM) induced mice OA model	Local intra-articular injection	Activating the proliferation and autophagy of chondrocytes via lncRNA NEAT1/miR-122–5p/ Sesn2/Nrf2 pathway	Zhang and Jin, (2022)
ADSCs	—	IL-1β induced inflammatory chondrocyte	Co-culture	Inhibiting inflammation and protecting chondrocytes via upregulating annexin A1 and downregulating NF-κB	Tofiño-Vian et al. (2018)
	miR-199a, 125b, 221, 92a)	Destabilisation of the medial meniscus (DMM) induced mice OA model	Local intra-articular injection	Enhancing cartilage matrix deposition and protecting cartilage from degradation	Woo et al. (2020)
	—	IL-1β induced inflammatory chondrocyte	Co-culture	Attenuating inflammatory micro-environment via inhibiting NF-κB pathway	Cavallo et al. (2021)
EMSCs	—	MIA injection induced rat TMJ-OA	Local intra-articular injection	Activating cartilage repair and restoring matrix via activating adenosine receptor, and phosphorylation of AKT, ERK and AMPK	Zhang et al. (2019)
UMSCs	miR-100–5p	Chondrocytes isolated from OA articular cartilage samples	Co-culture	Inhibiting ROS production and cell apoptosis through miR-100–5p/NOX4	Li et al. (2021d)
	miR-122–5p, 148a-3p, 486–5p, let-7a-5p, 100–5p	Anterior cruciate ligament (ACL) transection induced rat OA model	Local intra-articular injection	Enhancing M2 polarization through PI3K/AKT pathway, and alleviating OA progression	Li et al. (2022)
	miR-1208	Destabilisation of the medial meniscus (DMM) induced mice OA model	Local intra-articular injection	Reducing osteophyte production, and chondrocyte apoptosis via miR-1208/ METTL3 induced m6A level decrease of NLRP3 mRNA	Zhou et al. (2022)
AFSCs	TGF-β	Monoiodoacetate-induced rat OA model	Local intra-articular injection	Modulating macrophage polarization and preventing cartilage damage	Zavatti et al. (2020)
SMSCs	miR-129–5p	IL-1β induced inflammatory chondrocyte	Co-culture	Suppressing IL-1β-mediated OA via miR-129–5p/HMGB1 pathway	Qiu et al. (2021)
	miR-26a-5p	IL-1β induced inflammatory chondrocyte	Co-culture	Inhibiting apoptosis and inflammation of chondrocytes	Lu et al. (2021)

It has been reported that adipose mesenchymal stem cells (ADSCs) also showed potential in protecting cartilage (ter Huurne et al., 2012; Baharlou et al., 2017), and ADSC-EVs could play a role in regulating inflammation. (Mortati et al. (2020) utilized ADSC-EVs for OA treatment, and the results indicated that ADSC-EVs effectively promoted M2 polarization, inhibited inflammation and promoted cartilage matrix deposition. Apart from chondrocytes, ADSC-EVs could target

synovial cells, modulating the synthetase, catabolic enzymes and inflammatory cytokines secretion of synovial cells, and positively improve the biological performance of EVs secreted by endogenous synovial cells and chondrocytes (Cavallo et al., 2021). Promoting autophagy of chondrocyte *via* mTOR pathway could also be one of the mechanisms under the therapeutic effect of ADSC-EVs in preventing OA process (Wu et al., 2019).

Human perinatal stem cells, with outstanding self-renewal capacity, are widely applied in OA treatment (Matas et al., 2019). More and more studies indicated that EVs derived from perinatal stem cells, maintaining the excellent traits of donor cells, are ideal alternatives to MSCs in cartilage repair (Tang et al., 2021; Zhang Q. et al., 2022; Zhang S. et al., 2022; Li et al., 2022; Zhou et al., 2022). EVs derived from embryonic MSCs (EMSCs) were proved to inhibit inflammation, reconstruct cartilage matrix, and alleviate pain in OA model (Zhang S. et al., 2016; Zhang et al., 2019). Umbilical cord MSCs (UMSCs) also secreted EVs that were capable to control inflammation *via* promoting M2 polarization and inhibiting m6A of NLRP3 in macrophages, and enhance cartilage repair (Park et al., 2017; Li X. et al., 2021; Zhang Q. et al., 2022; Li et al., 2022; Zhou et al., 2022). It has been reported that EVs derived from amniotic MSCs (AMSCs) (Silini et al., 2017; Ragni et al., 2021) and amniotic fluid stem cells (AFSCs) (Maraldi et al., 2013; Zavatti et al., 2020) are also potential in inflammation modulation and OA treatment.

In addition, synovial mesenchymal stem cells (SMSCs) showed stronger potential in chondrocyte differentiation. EVs derived from SMSCs showed great potential in immunomodulation and cartilage repair, and were applied in OA treatment (Zhu et al., 2017; Lu et al., 2021; Qiu et al., 2021).

The potential mechanism under the therapeutic effect of MSC-derived extracellular vesicles

MSCEVs can effectively promote the synthesis of cartilage extracellular matrix (ECM) (Yeo et al., 2013). The mechanisms under the therapeutic effect of MSC-EVs attract much attention. Multiple MSCs can serve as donor cell source for EV production, and there are masses of various cargos in MSC-EVs, like nucleus acids and proteins. Considering that EVs derived from different MSCs possess similar therapeutic effect, MSC-EVs may share evolutionary conserved key bioactive molecules in their biological activity (Yeo et al., 2013; Toh et al., 2017). Proteins in MSC-EVs contain some housekeeping enzymes that play a role in reconstructing cartilage homeostasis *via* modulating cell fate of chondrocyte, remodeling bioenergetic metabolism, regulating immune system and promoting cartilage matrix synthesis (Lai et al., 2015).

Modulating cell fate of chondrocyte

In OA cartilage micro-environment, oxidative stress, ROS production and inflammatory factors boost intensively, which usually lead to cell apoptosis, cell death and cell dysfunction (Haslauer et al., 2013; Heard et al., 2015; Toh et al., 2016). There have been studies reporting that MSC-EVs could promote cell proliferation *via* activating the phosphorylation of ERK1/2 and AKT, the factors tightly connected with cell survival. In the repair process of damaged sites, excessive ATP can lead to cell death of neighbouring healthy cells. The ATP is metabolized *via* hydrolysis into AMP (Toh et al., 2017). CD73, the hallmark of EVs, serve as catalyst to activate the hydrolysis of AMP into adenosine, the activator of survival related enzymes (Colgan et al., 2006; Jacobson and Gao, 2006; Toh et al., 2017). The ability of MSC-EVs in converting ATP into pro-survival kinases make them potential in promoting cell proliferation for cartilage repair. Additionally, MSC-EVs are capable to inhibit apoptosis *via* mTOR pathway (Li X. et al., 2021; Jin et al., 2021; Lu et al., 2021; Zhou et al., 2022), and promote autophagy (Zhang and Jin, 2022) to improve cell performance of chondrocytes.

Remodeling bioenergetic metabolism

Mitochondria, the ATP production organelle, plays a key role in cartilage bioenergy homeostasis. Chondrocytes in OA are reported to suffer mitochondrial dysfunction and reduced electron transport chain (ETC) proteins activity. The inhibited ETC activity and ATP production in chondrocytes lead to abnormal bioenergetics, which then induce increased cell apoptosis, more ROS production, enhanced catabolism and inhibited anabolism of cartilage matrix (Vaamonde-García et al., 2012; Lee et al., 2020). MSC-EVs are enriched in enzymes to promote ATP production for decreased ATP generation compensation in defective chondrocytes, which make them potential in reconstructing bioenergetic homeostasis and repair capability of chondrocytes in OA (Pashoutan Sarvar et al., 2016; Toh et al., 2017).

Regulating immune system

Immune system is activated rapidly following tissue repair happening, which exerts vital influence on tissue reconstruction. Immune cell like macrophage, neutrophil and synovium cell release amount of pro-inflammation factors (IL-1β, IL-6, IL-8, MMPs, etc.), which then induce the cartilage matrix destruction and OA progression (Haslauer et al., 2013; Heard et al., 2015; Mianehsaz et al., 2019). Moreover, the modulation of macrophage M1-M2 polarization plays a role in maintaining inflammation balance during tissue repair process (Ding et al., 2016; Utomo et al., 2016). There have been many studies indicated that immunomodulation factors in MSC-EVs can synergistically reduce IL-1β, IL-6, TNF-α expression, promote M2 polarization, and enhance IL-10, TGF-β1 secretion, to construct a positive immuno-microenvironment for cartilage repair.

TABLE 2 Modification strategies for EV engineering.

Modification methods		Approaches	Results	References
Indirect MSC modification strategies	Manipulating gene transfection	Virus transfection	Overexpressing miR-140–5p, and alleviating OA progress through downregulating VEGFA	Liu et al. (2022)
		Plasmid transfection	Upregulating circRNA_0001236, and inhibiting cartilage degradation via miR-3677–3p/Sox9	Mao et al. (2021)
		Plasmid transfection	Overexpressing lncRNA H19, and promoting chondrogenesis through miR-29b-3p/FOXO3	Yan et al. (2021)
	Co-incubating donor cells with bioactive molecules	Co-incubation with curcumin	Reducing the oxidative stress and protecting chondrocytes	Xu et al. (2022)
		Co-incubation with TGF-β1	Enhancing the M2 polarization via miR-135b/MAPK6 axis	Wang and Xu, (2021)
		Co-incubation with IL-1β	Inhibiting inflammation of OA	Kim et al. (2021)
		Co-incubation with LPS	Inhibiting cartilage matrix degradation	Duan et al. (2021)
	Engineering cell culture micro-environment	3D culture	Promoting chondrogenesis	Yan and Wu, (2020)
		Dynamic mechanical stimulation	Inhibiting inflammation via NF-κB signal pathway	Liao et al. (2021)
		Hypoxia micro-environment culture	Enhancing cartilage repair	Rong et al. (2021)
Direct EV modification strategies	Enriching EV cargos	Direct mixture method	Loading COS into EVs, and promoting anabolic related genes expression of chondrocytes	Li et al. (2021a)
		Electroporation	Loading KGN into EVs, and improving cartilage repair	Xu et al. (2021)
	Modifying EV membrane	E7 peptide modifying EV surface	Targeting synovial fluid-derived MSCs	Xu et al. (2021)
		Fusing CAP with EV surface protein	Improving the chondrocyte target ability	Liang et al. (2020)
		Modifying EVs with PPD	Regulating EV surface charge potential, and promoting EV penetration into cartilage matrix	Feng et al. (2021)

Promoting cartilage matrix synthesis

ECM is the important component of cartilage structure and gradually destroyed during OA progression. The inflammatory pathological micro-environment tends to induce cartilage matrix degradation, and cartilage structure loss (Haslauer et al., 2013; Heard et al., 2015). Activating reparative responses and anabolic related gene expression of chondrocytes is important in promoting cartilage matrix re-deposition (Mizuta et al., 2004). MSC-EVs are proved to promote cartilage matrix deposition *via* upregulating SOX9, aggrecan, col2 expression and inhibit matrix degradation through downregulating MMP13, MMP3, ADAMTS-5 expression (Cosenza et al., 2017; Sun et al., 2019; Zhang et al., 2019; Chen et al., 2020; Woo et al., 2020; Wang X. et al., 2021).

The application of engineered extracellular vesicles in osteoarthritis treatment

MSC-EVs exert positive influence on immunomodulation, cell fate regulation, bioenergy homeostasis remodeling, and matrix synthesis modulation, which make MSC-EVs considered to be potential candidates for OA treatment. To further improve cargo delivery, cell specification and fusion efficiency, multiple strategies can be utilized to modify EVs, including direct (modify cargo and membrane of EVs) and indirect (modify MSCs) methods (Table 2).

Modifying MSCs for EVs engineering

EVs tend to inherit characteristics of their donor cells, and donor MSCs can be modified to obtain correspondingly customized miRNA enriched EVs (Kosaka et al., 2010; Ni et al., 2020). The advantage of indirect MSC modification lies in that the stimulation factors on MSCs are in control and can be quantified.

Manipulating gene transfection

Gene transfection manipulation, mainly *via* viral vectors, can not only improve EV yields, but also enhance functional cargos like miRNA, circRNA and LncRNA in engineered EVs for OA treatment Kosaka et al. (Kosaka et al., 2010) found that upregulating the expression of neutral sphingomyelinase 2

(nSMase2) in donor cells promoted the secretion of miRNAs, which are transferable and functional to target cells.

The functions of miRNAs are important in the biological performance of EVs in recipient cells. Through Microarray analysis and literature review, key miRNAs can be found out. Virus infection can effectively manipulate target gene expression of donor cells and cargos of EVS. It has been reported that upregulating expression of miR-26a–5p (Jin et al., 2020), miR-126–3p (Zhou et al., 2021), miR-155–5p (Wang Z. et al., 2021), miR-140–5p (Liu et al., 2022) in MSCs and EVs can effectively inhibit inflammation, matrix degradation, cell apoptosis and improve matrix secretion of chondrocytes. The miRNAs can bind to target mRNAs, induce mRNA degradation, and impact downstream signal pathways (Zhuang et al., 2022). Apart from miRNAs, circRNAs and lncRNAs are also potential in regulating cell behavior. CircRNAs like circRNA_0001236 (Mao et al., 2021), circHIPK3 (Li et al., 2021b) and lncRNAs like lncRNA H19 (Yan et al., 2021; Yang et al., 2021) can interact with target miRNAs, regulate downstream genes, inhibit catabolism and attenuate anabolism of chondrocytes. Thus, overexpression of functional circRNAs and lncRNAs in EVs can also be potential candidates for better OA therapeutic strategy.

Co-incubating donor cells with bioactive molecules

Bioactive molecules can be loaded into EVs *via* co-incubation with donor cells. The characteristic of donor cells obtained following compound co-incubation can be transmitted to EVs. Co-incubated with anti-inflammatory factors like curcumin (Li et al., 2021c; Xu et al., 2022), TGF-β1 (Wang and Xu, 2021) endows EVs with ideal capacity to modulate macrophage polarization, reduce oxidative stress and promote chondrocyte anabolism. Interestingly, IL-1β (Colombini et al., 2021; Kim et al., 2021) and LPS (Duan et al., 2021) preconditioned donor cell derived EVs are proved to inhibit inflammation, improve chondrocyte performance and ameliorate OA progression. The reason accounting for this lies in that MSCs treated with low concentration of LPS or IL-1β response adaptively, which is beneficial for immunomodulation.

Engineering cell culture microenvironment

MSCculture microenvironment changes can exert influence on the biological effect of EVs. Compared to 2D culture, 3D culture can enhance the yield and functions of EVs (Rocha et al., 2019). Yan et al. (Yan and Wu, 2020) constructed a hollow-fiber bioreactor to build a 3D culture microenvironment for cartilage restoration, and the results indicated that EVs isolated from 3D culture cells showed greater potential in promoting TGF-β1 expression and Smad2/3 pathway. Moreover, dynamic mechanical stimulation is also proved to be able to modulate cell proliferation and differentiation, and improve EV production and functions (Li et al., 2011; Guo et al., 2021). (Liao et al. (2021) utilized ultrasound to load BMSCs with mechanical stimulus, and found that the obtained EVs could inhibit inflammation *via* NF-κB pathway, and enhance cartilage matrix deposition (Figure 2). Apart from 3D culture and mechanical stimulation, hypoxia microenvironment regulates MSC performance *via* HIF-1α (Malladi et al., 2007). EVs derived from hypoxia pre-treatment MSCs were proved to promote repair capability of chondrocytes through miR-216a-5p/JAK2/STAT3 pathway (Rong et al., 2021).

Modifying EVs directly for EVs engineering

Indirect methods pre-synthesize components to enrich EV cargos *via* donor cell modification. Direct engineering strategies, including enriching EV cargos and modifying EV membranes, can endow EVs with specific and controllable functions.

Enriching EVs cargos

Multiple strategies can be utilized to transfer cargos into EVs, including direct co-incubation, physical and chemical methods. Hydrophobic molecules can pass across EV phospholipid membrane, which makes them suitable for the direct mixture method (Fuhrmann et al., 2015). Li et al. (2021) co-incubated EVs with chitosan oligosaccharides (COS) for 1 h at 37°C to make COS go into EVs and construct COS-EVs. The result indicated that compared to EVs, COS-EVs exhibited better ability in promoting anabolic related genes expression of chondrocytes. Strategies like electroporation (Kooijmans et al., 2013; Pomatto et al., 2018), sonication (Lamichhane et al., 2016), saponin permeabilization (Pomatto et al., 2019), freeze-thawing (Luan et al., 2017), and $CaCl_2$ mediated method (Zhang D. et al., 2016) can be utilized to directly load EVs with bioactive molecules. To enhance drug encapsulation rate, Xu et al. (Xu et al. (2021) encapsulated kartogenin (KGN) into EVs *via* electroporation, and the encapsulation rate was advanced to 40% compared to 8% of direct co-incubation. The enhanced KGN delivery efficiency could promote cartilage repair.

Modifying EVs membrane

To further improve the target and drug delivery efficiency of EVs, EVs membrane can be modified. Xu et al. (Xu et al. (2021) modified EV surface with E7 peptide *via* plasmids transfection of donor cells to target synovial fluid-derived MSCs for enhanced OA treatment. Through plasmids transfection, liang et al. (Liang et al., 2020) fused chondrocyte-affinity peptide (CAP) with EV surface protein, and improved the chondrocyte target ability of CAP-EVs. Apart from protein fusion, regulating EV surface charge potential can promote EV penetration since the block influence of negative cartilage matrix. Feng et al. (2021) utilized

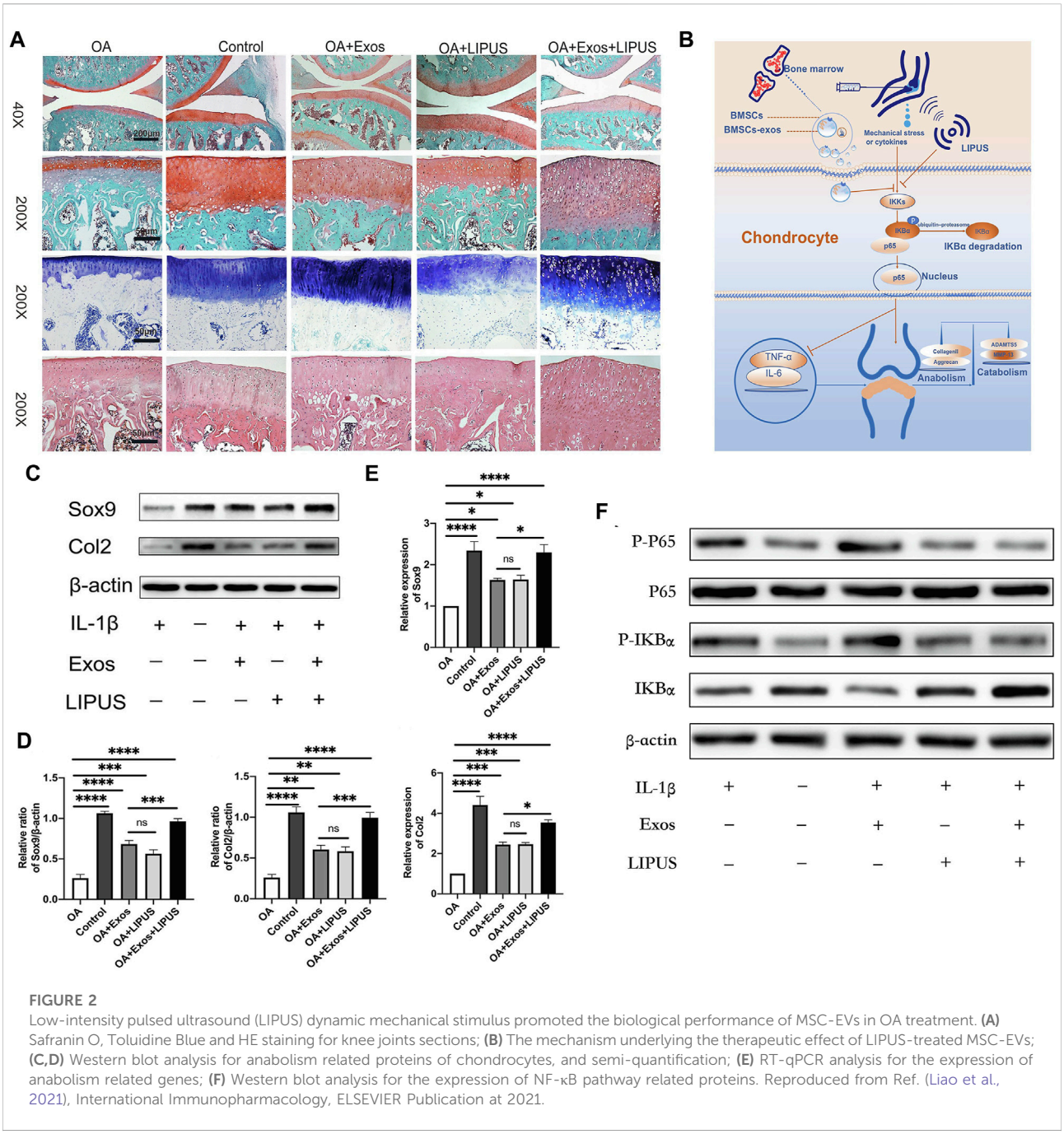

FIGURE 2
Low-intensity pulsed ultrasound (LIPUS) dynamic mechanical stimulus promoted the biological performance of MSC-EVs in OA treatment. **(A)** Safranin O, Toluidine Blue and HE staining for knee joints sections; **(B)** The mechanism underlying the therapeutic effect of LIPUS-treated MSC-EVs; **(C,D)** Western blot analysis for anabolism related proteins of chondrocytes, and semi-quantification; **(E)** RT-qPCR analysis for the expression of anabolism related genes; **(F)** Western blot analysis for the expression of NF-κB pathway related proteins. Reproduced from Ref. (Liao et al., 2021), International Immunopharmacology, ELSEVIER Publication at 2021.

ε-polylysine-polyethylene-distearyl phosphatidylethanolamine (PPD) modifying EVs to construct positively charged MSC-EVs for better cartilage matrix penetration. Wei et al. (Wei et al.) endowed EVs with amphiphilic positive potential through surface modification of cationic 1,2-dioleoyl-3-trimethylammonium propane (DOTAP), and the results showed that DOTAP modified EVs could promote the penetration of EVs into cartilage matrix, extend EV retention and attenuate OA destruction.

Conclusion and further perspectives

EVs derived from different MSCs, loaded with abundant cargos including miRNAs, lipids, and proteins, show great potential in OA treatment. The mechanisms underlying the MSC-EVs therapeutic effects lie in that MSC-EVs can play roles in modulating cell fate of chondrocyte, remodeling bioenergetic metabolism, regulating immune system and promoting cartilage matrix synthesis. To further enhance

target and delivery efficiency of EVs, gene transfection manipulation, co-incubation and cell culture microenvironment engineering can be utilized to modify donor cells, and EV cargo enrichment and EV membrane modification can be applied to directly modify EVs.Wei Y et al., 2021.

Although the wide application of MSC-EVs, in OA treatment, there are still challenges requiring further explorations.

1) Current studies mostly concentrate on the phenotype of chondrocytes following EV treatment, but the molecular mechanisms underlying the phenomenon are still unclear. For precise medical treatment, the discovery of specific target is crucial. Understanding the molecular mechanism in OA development and treatment can provide a new approach for treatment and facilitate precise intervention for patients.
2) Apart from the therapeutic effect of MSC-EVs, EVs also play a role in the pathological process of OA development. Studying the pathogenic effect of EVs can help better understand the molecular mechanism of OA progress, and facilitate the exploration of new therapeutic strategies. Moreover, EVs can serve as biomarkers for early OA diagnosis, and more specific and effective EVs as biomarkers are required to be found.
3) The MSC-EVs treatment can attenuate OA progression, but the effect of MSC-EVs on reversing chondrocyte function is short of demonstration. Whether applying EVs in early or late period of OA can reverse OA pathological changes, but not only mitigate OA progression, which needs more explorations.
4) The kinetics and bio-distribution of EVs, and dosage of EVs used in *vivo* experiments and further in clinical trials is still unclear, which needs more researches to clarify.
5) The MSC therapy has undergone clinical trial period, and can be applied in clinic, but the safety of MSC-EVs for clinical application requires more studies to verify.
6) Indirect EV engineering strategies are costly, time-consuming and hard to manipulate; utilizing new gene-editing technologies, like CRISPR-Cas9 can make the gene manipulation more efficient and accurate. Direct EV modification might exert negative influence on morphology and size of engineered EVs, and efficient and scatheless EV engineering strategies are required.

Author contributions

YZ and SJ have written the manuscript text. CY and KL have conceived the concept of this review.

Funding

This work was funded by the National Natural Science Foundation of China (82072396, 81871490), Program of Shanghai Academic/Technology Research Leader (19XD1434500), Science and Technology Commission of Shanghai Municipality (21490711700), Double Hundred Plan (20191819), Interdisciplinary Program of Shanghai Jiao Tong University (YG2021ZD12), and CAMS Innovation Fund for Medical Sciences (CIFMS) (2019-I2M-5-037).

Conflict of interest

The authors declare that the research was conducted in the absence of any commercial or financial relationships that could be construed as a potential conflict of interest.

Publisher's note

References

Ankrum, J. A., Ong, J. F., and Karp, J. M. (2014). Mesenchymal stem cells: Immune evasive, not immune privileged. *Nat. Biotechnol.* 32 (3), 252–260. doi:10.1038/nbt.2816

Appleton, C. T. (2018). Osteoarthritis year in review 2017: Biology. *Osteoarthr. Cartil.* 26 (3), 296–303. doi:10.1016/j.joca.2017.10.008

Baharlou, R., Ahmadi-Vasmehjani, A., Faraji, F., Atashzar, M. R., Khoubyari, M., Ahi, S., and Saiedeh, E. (2017). Human adipose tissue-derived mesenchymal stem cells in rheumatoid arthritis: Regulatory effects on peripheral blood mononuclear cells activation. *Int. Immunopharmacol.* 47, 59–69. doi:10.1016/j.intimp.2017.03.016

Boulestreau, J., Maumus, M., Jorgensen, C., and Noël, D. (2021). Extracellular vesicles from mesenchymal stromal cells: Therapeutic perspectives for targeting senescence in osteoarthritis. *Adv. Drug Deliv. Rev.* 175, 113836. doi:10.1016/j.addr.2021.113836

Brennan, M. Á., Layrolle, P., and Mooney, D. J. (2020). Biomaterials functionalized with MSC secreted extracellular vesicles and soluble factors for tissue regeneration. *Adv. Funct. Mat.* 30 (37), 1909125. doi:10.1002/adfm.201909125

Cavallo, C., Merli, G., Borzì, R. M., Zini, N., D'Adamo, S., and Guescini, M., (2021). Small Extracellular Vesicles from adipose derived stromal cells significantly attenuate *in vitro* the NF-κB dependent inflammatory/catabolic environment of osteoarthritis. *Sci. Rep.* 11 (1), 1053. doi:10.1038/s41598-020-80032-7

Chen, X., Shi, Y., Xue, P., Ma, X., Li, J., and Zhang, J. (2020). Mesenchymal stem cell-derived exosomal microRNA-136-5p inhibits chondrocyte degeneration in traumatic osteoarthritis by targeting ELF3. *Arthritis Res. Ther.* 22 (1), 256. doi:10.1186/s13075-020-02325-6

Cisternas, M. G., Murphy, L., Sacks, J. J., Solomon, D. H., Pasta, D. J., and Helmick, C. G. (2016). Alternative methods for defining osteoarthritis and the

impact on estimating prevalence in a US population-based survey. *Arthritis Care & Res.* 68 (5), 574–580. doi:10.1002/acr.22721

Colgan, S. P., Eltzschig, H. K., Eckle, T., and Thompson, L. F. (2006). Physiological roles for ecto-5'-nucleotidase (CD73). *Purinergic Signal.* 2 (2), 351–360. doi:10.1007/s11302-005-5302-5

Colombini, A., Ragni, E., Mortati, L., Libonati, F., Perucca Orfei, C., and Viganò, M., (2021). Adipose-derived mesenchymal stromal cells treated with interleukin 1 beta produced chondro-protective vesicles able to fast penetrate in cartilage. *Cells* 10 (5), 1180. doi:10.3390/cells10051180

Cosenza, S., Ruiz, M., Toupet, K., Jorgensen, C., and Noël, D. (2017). Mesenchymal stem cells derived exosomes and microparticles protect cartilage and bone from degradation in osteoarthritis. *Sci. Rep.* 7 (1), 16214. doi:10.1038/s41598-017-15376-8

Ding, J., Chen, B., Lv, T., Liu, X., Fu, X., Wang, Q., and Ran, X. (2016). Bone marrow mesenchymal stem cell-based engineered cartilage ameliorates polyglycolic acid/polylactic acid scaffold-induced inflammation through M2 polarization of macrophages in a pig model. *Stem Cells Transl. Med.* 5 (8), 1079–1089. doi:10.5966/sctm.2015-0263

Duan, A., Shen, K., Li, B., Li, C., Zhou, H., Kong, R., Wei, L., and Feng, L. (2021). Extracellular vesicles derived from LPS-preconditioned human synovial mesenchymal stem cells inhibit extracellular matrix degradation and prevent osteoarthritis of the knee in a mouse model. *Stem Cell. Res. Ther.* 12 (1), 427. doi:10.1186/s13287-021-02507-2

Eleuteri, S., and Fierabracci, A. (2019). Insights into the secretome of mesenchymal stem cells and its potential applications. *Int. J. Mol. Sci.* 20 (18), 4597. doi:10.3390/ijms20184597

Feng, K., Xie, X., Yuan, J., Gong, L., Zhu, Z., Zhang, J., and Yang, W. (2021). Reversing the surface charge of MSC-derived small extracellular vesicles by εPL-PEG-DSPE for enhanced osteoarthritis treatment. *J. Extracell. Vesicles* 10 (13), e12160. doi:10.1002/jev2.12160

Fichtel, P., von Bonin, M., Kuhnert, R., Möbus, K., Bornhäuser, M., and Wobus, M. (2022). Mesenchymal stromal cell-derived extracellular vesicles modulate hematopoietic stem and progenitor cell viability and the expression of cell cycle regulators in an age-dependent manner. *Front. Bioeng. Biotechnol.* 10, 892661. doi:10.3389/fbioe.2022.892661

Fuhrmann, G., Serio, A., Mazo, M., Nair, R., and Stevens, M. M. (2015). Active loading into extracellular vesicles significantly improves the cellular uptake and photodynamic effect of porphyrins. *J. Control. Release* 205, 35–44. doi:10.1016/j.jconrel.2014.11.029

Glyn-Jones, S., Palmer, A. J. R., Agricola, R., Price, A. J., Vincent, T. L., and Weinans, H., (2015). Osteoarthritis. *Lancet* 386 (9991), 376–387. doi:10.1016/S0140-6736(14)60802-3

Guo, S., Debbi, L., Zohar, B., Samuel, R., Arzi, R. S., Fried, A. I., Tahel, C., and Dudi, S. (2021). Stimulating extracellular vesicles production from engineered tissues by mechanical forces. *Nano Lett.* 21 (6), 2497–2504. doi:10.1021/acs.nanolett.0c04834

Haslauer, C. M., Elsaid, K. A., Fleming, B. C., Proffen, B. L., Johnson, V. M., and Murray, M. M. (2013). Loss of extracellular matrix from articular cartilage is mediated by the synovium and ligament after anterior cruciate ligament injury. *Osteoarthr. Cartil.* 21 (12), 1950–1957. doi:10.1016/j.joca.2013.09.003

He, L., He, T., Xing, J., Zhou, Q., Fan, L., Liu, C., and Rong, L. (2020). Bone marrow mesenchymal stem cell-derived exosomes protect cartilage damage and relieve knee osteoarthritis pain in a rat model of osteoarthritis. *Stem Cell. Res. Ther.* 11 (1), 276. doi:10.1186/s13287-020-01781-w

Heard, B. J., Barton, K. I., Chung, M., Achari, Y., Shrive, N. G., and Frank, C. B., (2015). Single intra-articular dexamethasone injection immediately post-surgery in a rabbit model mitigates early inflammatory responses and post-traumatic osteoarthritis-like alterations. *J. Orthop. Res.* 33 (12), 1826–1834. doi:10.1002/jor.22972

Jacobson, K. A., and Gao, Z.-G. (2006). Adenosine receptors as therapeutic targets. *Nat. Rev. Drug Discov.* 5 (3), 247–264. doi:10.1038/nrd1983

Jin, Y., Xu, M., Zhu, H., Dong, C., Ji, J., Liu, Y., Aidong, D., and Zhifeng, G. (2021). Therapeutic effects of bone marrow mesenchymal stem cells-derived exosomes on osteoarthritis. *J. Cell. Mol. Med.* 25 (19), 9281–9294. doi:10.1111/jcmm.16860

Jin, Z., Ren, J., and Qi, S. (2020). Human bone mesenchymal stem cells-derived exosomes overexpressing microRNA-26a-5p alleviate osteoarthritis via down-regulation of PTGS2. *Int. Immunopharmacol.* 78, 105946. doi:10.1016/j.intimp.2019.105946

Kim, M., Shin, D. I., Choi, B. H., and Min, B.-H. (2021). Exosomes from IL-1β-primed mesenchymal stem cells inhibited IL-1β- and TNF-α-mediated inflammatory responses in osteoarthritic SW982 cells. *Tissue Eng. Regen. Med.* 18 (4), 525–536. doi:10.1007/s13770-020-00324-x

Kooijmans, S. A. A., Stremersch, S., Braeckmans, K., de Smedt, S. C., Hendrix, A., and Wood, M. J. A., (2013). Electroporation-induced siRNA precipitation obscures the efficiency of siRNA loading into extracellular vesicles. *J. Control. Release* 172 (1), 229–238. doi:10.1016/j.jconrel.2013.08.014

Kosaka, N., Iguchi, H., Yoshioka, Y., Takeshita, F., Matsuki, Y., and Ochiya, T. (2010). Secretory mechanisms and intercellular transfer of microRNAs in living cells. *J. Biol. Chem.* 285 (23), 17442–17452. doi:10.1074/jbc.M110.107821

Lai, R. C., Yeo, R. W. Y., and Lim, S. K. (2015). Mesenchymal stem cell exosomes. *Seminars Cell. & Dev. Biol.* 40, 82–88. doi:10.1016/j.semcdb.2015.03.001

Lamichhane, T. N., Jeyaram, A., Patel, D. B., Parajuli, B., Livingston, N. K., Arumugasaamy, N., et al. (2016). Oncogene knockdown via active loading of small RNAs into extracellular vesicles by sonication. *Cell. Mol. Bioeng.* 9 (3), 315–324. doi:10.1007/s12195-016-0457-4

Lee, Y.-H., Park, H.-K., Auh, Q.-S., Nah, H., Lee, J. S., Moon, H.-J., In San, K., and Il Keun, K. (2020). Emerging potential of exosomes in regenerative medicine for temporomandibular joint osteoarthritis. *Int. J. Mol. Sci.* 21 (4), 1541. doi:10.3390/ijms21041541

Li, D., Zhou, J., Chowdhury, F., Cheng, J., Wang, N., and Wang, F. (2011). Role of mechanical factors in fate decisions of stem cells. *Regen. Med.* 6 (2), 229–240. doi:10.2217/rme.11.2

Li, K., Yan, G., Huang, H., Zheng, M., Ma, K., and Cui, X., (2022). Anti-inflammatory and immunomodulatory effects of the extracellular vesicles derived from human umbilical cord mesenchymal stem cells on osteoarthritis via M2 macrophages. *J. Nanobiotechnology* 20 (1), 38. doi:10.1186/s12951-021-01236-1

Li, S., Liu, J., Liu, S., Jiao, W., and Wang, X. (2021a). Chitosan oligosaccharides packaged into rat adipose mesenchymal stem cells-derived extracellular vesicles facilitating cartilage injury repair and alleviating osteoarthritis. *J. Nanobiotechnology* 19 (1), 343. doi:10.1186/s12951-021-01086-x

Li, S., Liu, J., Liu, S., Jiao, W., and Wang, X. (2021b). Mesenchymal stem cell-derived extracellular vesicles prevent the development of osteoarthritis via the circHIPK3/miR-124-3p/MYH9 axis. *J. Nanobiotechnology* 19 (1), 194. doi:10.1186/s12951-021-00940-2

Li, S., Stöckl, S., Lukas, C., Götz, J., Herrmann, M., Federlin, M., and Susanne, G. (2020). hBMSC-derived extracellular vesicles attenuate IL-1β-induced catabolic effects on OA-chondrocytes by regulating pro-inflammatory signaling pathways. *Front. Bioeng. Biotechnol.* 8, 603598. doi:10.3389/fbioe.2020.603598

Li, S., Stöckl, S., Lukas, C., Herrmann, M., Brochhausen, C., König, M. A., and Susanne, G. (2021c). Curcumin-primed human BMSC-derived extracellular vesicles reverse IL-1β-induced catabolic responses of OA chondrocytes by upregulating miR-126-3p. *Stem Cell. Res. Ther.* 12 (1), 252. doi:10.1186/s13287-021-02317-6

Li, X., Wang, Y., Cai, Z., Zhou, Q., Li, L., and Fu, P. (2021d). Exosomes from human umbilical cord mesenchymal stem cells inhibit ROS production and cell apoptosis in human articular chondrocytes via the miR-100-5p/NOX4 axis. *Cell. Biol. Int.* 45 (10), 2096–2106. doi:10.1002/cbin.11657

Liang, Y., Xu, X., Li, X., Xiong, J., Li, B., and Duan, L., (2020). Chondrocyte-targeted MicroRNA delivery by engineered exosomes toward a cell-free osteoarthritis therapy. *ACS Appl. Mat. Interfaces* 12 (33), 36938–36947. doi:10.1021/acsami.0c10458

Liao, Q., Li, B. J., Li, Y., Xiao, Y., Zeng, H., Liu, J. M., and Liu, G. (2021). Low-intensity pulsed ultrasound promotes osteoarthritic cartilage regeneration by BMSC-derived exosomes via modulating the NF-κB signaling pathway. *Int. Immunopharmacol.* 97, 107824. doi:10.1016/j.intimp.2021.107824

Liu, A., Lin, D., Zhao, H., Chen, L., Cai, B., and Lin, K., (2021a). Optimized BMSC-derived osteoinductive exosomes immobilized in hierarchical scaffold via lyophilization for bone repair through Bmpr2/Acvr2b competitive receptor-activated Smad pathway. *Biomaterials* 272, 120718. doi:10.1016/j.biomaterials.2021.120718

Liu, L., Yu, F., Li, L., Zhou, L., Zhou, T., Xu, Y., and Xia, L. (2021b). Bone marrow stromal cells stimulated by strontium-substituted calcium silicate ceramics: Release of exosomal miR-146a regulates osteogenesis and angiogenesis. *Acta Biomater.* 119, 444–457. doi:10.1016/j.actbio.2020.10.038

Liu, Y., Zeng, Y., Si, H.-B., Tang, L., Xie, H.-Q., and Shen, B. (2022). Exosomes derived from human urine–derived stem cells overexpressing miR-140-5p alleviate knee osteoarthritis through downregulation of VEGFA in a rat model. *Am. J. Sports Med.* 50 (4), 1088–1105. doi:10.1177/03635465221073991

Loeser, R. F., Goldring, S. R., Scanzello, C. R., and Goldring, M. B. (2012). Osteoarthritis: A disease of the joint as an organ. *Arthritis & Rheumatism* 64 (6), 1697–1707. doi:10.1002/art.34453

Lu, L., Wang, J., Fan, A., Wang, P., Chen, R., Lu, L., and Yin, F. (2021). Synovial mesenchymal stem cell-derived extracellular vesicles containing microRN555A-

26a-5p ameliorate cartilage damage of osteoarthritis. *J. Gene Med.* 23 (11), e3379. doi:10.1002/jgm.3379

Luan, X., Sansanaphongpricha, K., Myers, I., Chen, H., Yuan, H., and Sun, D. (2017). Engineering exosomes as refined biological nanoplatforms for drug delivery. *Acta Pharmacol. Sin.* 38 (6), 754–763. doi:10.1038/aps.2017.12

Malladi, P., Xu, Y., Chiou, M., Giaccia, A. J., and Longaker, M. T. (2007). Hypoxia inducible factor-1α deficiency affects chondrogenesis of adipose-derived adult stromal cells. *Tissue Eng.* 13 (6), 1159–1171. doi:10.1089/ten.2006.0265

Mao, G., Xu, Y., Long, D., Sun, H., Li, H., and Xin, R., (2021). Exosome-transported circRNA_0001236 enhances chondrogenesis and suppress cartilage degradation via the miR-3677-3p/Sox9 axis. *Stem Cell. Res. Ther.* 12 (1), 389. doi:10.1186/s13287-021-02431-5

Mao, G., Zhang, Z., Hu, S., Zhang, Z., Chang, Z., and Huang, Z., (2018). Exosomes derived from miR-92a-3p-overexpressing human mesenchymal stem cells enhance chondrogenesis and suppress cartilage degradation via targeting WNT5A. *Stem Cell. Res. Ther.* 9 (1), 247. doi:10.1186/s13287-018-1004-0

Maraldi, T., Riccio, M., Pisciotta, A., Zavatti, M., Carnevale, G., Beretti, F., and Nakamura, E. (2013). Human amniotic fluid-derived and dental pulp-derived stem cells seeded into collagen scaffold repair critical-size bone defects promoting vascularization. *Stem Cell. Res. Ther.* 4 (3), 53. doi:10.1186/scrt203

Matas, J., Orrego, M., Amenabar, D., Infante, C., Tapia-Limonchi, R., and Cadiz, M. I., (2019). Umbilical cord-derived mesenchymal stromal cells (MSCs) for knee osteoarthritis: Repeated MSC dosing is superior to a single MSC dose and to hyaluronic acid in a controlled randomized phase I/II trial. *Stem Cells Transl. Med.* 8 (3), 215–224. doi:10.1002/sctm.18-0053

Mianehsaz, E., Mirzaei, H. R., Mahjoubin-Tehran, M., Rezaee, A., Sahebnasagh, R., Pourhanifeh, M. H., and Nakamura, E. (2019). Mesenchymal stem cell-derived exosomes: A new therapeutic approach to osteoarthritis? *Stem Cell. Res. Ther.* 10 (1), 340. doi:10.1186/s13287-019-1445-0

Mizuta, H., Kudo, S., Nakamura, E., Otsuka, Y., Takagi, K., and Hiraki, Y. (2004). Active proliferation of mesenchymal cells prior to the chondrogenic repair response in rabbit full-thickness defects of articular cartilage. *Osteoarthr. Cartil.* 12 (7), 586–596. doi:10.1016/j.joca.2004.04.008

Mortati, L., de Girolamo, L., Perucca Orfei, C., Viganò, M., Brayda-Bruno, M., Ragni, E., and Alessandra, C. (2020). *In vitro* study of extracellular vesicles migration in cartilage-derived osteoarthritis samples using real-time quantitative multimodal nonlinear optics imaging. *Pharmaceutics* 12 (8), 734. doi:10.3390/pharmaceutics12080734

Ni, Z., Zhou, S., Li, S., Kuang, L., Chen, H., Luo, X., et al. (2020). Exosomes: Roles and therapeutic potential in osteoarthritis. *Bone Res.* 8 (1), 25. doi:10.1038/s41413-020-0100-9

Park, Y.-B., Ha, C.-W., Lee, C.-H., Yoon, Y. C., and Park, Y.-G. (2017). Cartilage regeneration in osteoarthritic patients by a composite of allogeneic umbilical cord blood-derived mesenchymal stem cells and hyaluronate hydrogel: Results from a clinical trial for safety and proof-of-concept with 7 Years of extended follow-up. *Stem Cells Transl. Med.* 6 (2), 613–621. doi:10.5966/sctm.2016-0157

Pashoutan Sarvar, D., Shamsasenjan, K., and Akbarzadehlaleh, P. (2016). Mesenchymal stem cell-derived exosomes: New opportunity in cell-free therapy. *Adv. Pharm. Bull.* 6 (3), 293–299. doi:10.15171/apb.2016.041

Pomatto, M. A. C., Bussolati, B., D'Antico, S., Ghiotto, S., Tetta, C., and Brizzi, M. F., (2019). Improved loading of plasma-derived extracellular vesicles to encapsulate antitumor miRNAs. *Mol. Ther. - Methods & Clin. Dev.* 13, 133–144. doi:10.1016/j.omtm.2019.01.001

Pomatto, M. A. C., Gai, C., Deregibus, M. C., Tetta, C., and Camussi, G. (2018). Noncoding RNAs carried by extracellular vesicles in endocrine diseases. *Int. J. Endocrinol.* 2018, 1–18. doi:10.1155/2018/4302096

Qiu, M., Liu, D., and Fu, Q. (2021). MiR-129-5p shuttled by human synovial mesenchymal stem cell-derived exosomes relieves IL-1β induced osteoarthritis via targeting HMGB1. *Life Sci.* 269, 118987. doi:10.1016/j.lfs.2020.118987

Ragni, E., Papait, A., Perucca Orfei, C., Silini, A. R., Colombini, A., Viganò, M., et al. (2021). Amniotic membrane-mesenchymal stromal cells secreted factors and extracellular vesicle-miRNAs: Anti-inflammatory and regenerative features for musculoskeletal tissues. *Stem Cells Transl. Med.* 10 (7), 1044–1062. doi:10.1002/sctm.20-0390

Rocha, S., Carvalho, J., Oliveira, P., Voglstaetter, M., Schvartz, D., Thomsen, A. R., et al. (2019). 3D cellular architecture affects MicroRNA and protein cargo of extracellular vesicles. *Adv. Sci. (Weinh).* 6 (4), 1800948. doi:10.1002/advs.201800948

Rong, Y., Zhang, J., Jiang, D., Ji, C., liu, W., and Wang, J., (2021). Hypoxic pretreatment of small extracellular vesicles mediates cartilage repair in osteoarthritis by delivering miR-216a-5p. *Acta Biomater.* 122, 325–342. doi:10.1016/j.actbio.2020.12.034

Silini, A. R., Magatti, M., Cargnoni, A., and Parolini, O. (2017). Is immune modulation the mechanism underlying the beneficial effects of amniotic cells and their derivatives in regenerative medicine? *Cell. Transpl.* 26 (4), 531–539. doi:10.3727/096368916X693699

Song, Y., Zhang, J., Xu, H., Lin, Z., Chang, H., Liu, W., and Kong, L. (2020). Mesenchymal stem cells in knee osteoarthritis treatment: A systematic review and meta-analysis. *J. Orthop. Transl.* 24, 121–130. doi:10.1016/j.jot.2020.03.015

Sun, H., Hu, S., Zhang, Z., Lun, J., Liao, W., and Zhang, Z. (2019). Expression of exosomal microRNAs during chondrogenic differentiation of human bone mesenchymal stem cells. *J. Cell. Biochem.* 120 (1), 171–181. doi:10.1002/jcb.27289

Tang, S., Chen, P., Zhang, H., Weng, H., Fang, Z., and Chen, C., (2021). Comparison of curative effect of human umbilical cord-derived mesenchymal stem cells and their small extracellular vesicles in treating osteoarthritis. *Int. J. Nanomedicine* 16, 8185–8202. doi:10.2147/ijn.S336062

Tao, S.-C., Yuan, T., Zhang, Y.-L., Yin, W.-J., Guo, S.-C., and Zhang, C.-Q. (2017). Exosomes derived from miR-140-5p-overexpressing human synovial mesenchymal stem cells enhance cartilage tissue regeneration and prevent osteoarthritis of the knee in a rat model. *Theranostics* 7 (1), 180–195. doi:10.7150/thno.17133

ter Huurne, M., Schelbergen, R., Blattes, R., Blom, A., de Munter, W., and Grevers, L. C., (2012). Antiinflammatory and chondroprotective effects of intraarticular injection of adipose-derived stem cells in experimental osteoarthritis. *Arthritis & Rheumatism* 64 (11), 3604–3613. doi:10.1002/art.34626

Tofiño-Vian, M., Guillén, M. I., Pérez del Caz, M. D., Silvestre, A., and Alcaraz, M. J. (2018). Microvesicles from human adipose tissue-derived mesenchymal stem cells as a new protective strategy in osteoarthritic chondrocytes. *Cell. Physiol. biochem.* 47 (1), 11–25. doi:10.1159/000489739

Toh, W. S., Brittberg, M., Farr, J., Foldager, C. B., Gomoll, A. H., Hui, J. H. P., and Kim, H. K. (2016). Cellular senescence in aging and osteoarthritis. *Acta Orthop.* 87 (sup363), 6–14. doi:10.1080/17453674.2016.1235087

Toh, W. S., Lai, R. C., Hui, J. H. P., and Lim, S. K. (2017). MSC exosome as a cell-free MSC therapy for cartilage regeneration: Implications for osteoarthritis treatment. *Seminars Cell. & Dev. Biol.* 67, 56–64. doi:10.1016/j.semcdb.2016.11.008

Utomo, L., van Osch, G. J. V. M., Bayon, Y., Verhaar, J. A. N., and Bastiaansen-Jenniskens, Y. M. (2016). Guiding synovial inflammation by macrophage phenotype modulation: An *in vitro* study towards a therapy for osteoarthritis. *Osteoarthr. Cartil.* 24 (9), 1629–1638. doi:10.1016/j.joca.2016.04.013

Vaamonde-García, C., Riveiro-Naveira, R. R., Valcárcel-Ares, M. N., Hermida-Carballo, L., Blanco, F. J., and López-Armada, M. J. (2012). Mitochondrial dysfunction increases inflammatory responsiveness to cytokines in normal human chondrocytes. *Arthritis & Rheumatism* 64 (9), 2927–2936. doi:10.1002/art.34508

Wang, R., and Xu, B. (2021). TGF-β1-modified MSC-derived exosomal miR-135b attenuates cartilage injury via promoting M2 synovial macrophage polarization by targeting MAPK6. *Cell. Tissue Res.* 384 (1), 113–127. doi:10.1007/s00441-020-03319-1

Wang, X., Li, Z., Cui, Y., Cui, X., Chen, C., and Wang, Z. (2021a). Exosomes isolated from bone marrow mesenchymal stem cells exert a protective effect on osteoarthritis via lncRNA LYRM4-AS1-GRPR-miR-6515-5p. *Front. Cell. Dev. Biol.* 9, 644380. doi:10.3389/fcell.2021.644380

Wang, Y., Zhao, M., Li, W., Yang, Y., Zhang, Z., Ma, R., et al. (2021b). BMSC-derived small extracellular vesicles induce cartilage reconstruction of temporomandibular joint osteoarthritis via autotaxin–YAP signaling Axis. *Front. Cell. Dev. Biol.* 9, 656153. doi:10.3389/fcell.2021.656153

Wang, Z., Yan, K., Ge, G., Zhang, D., Bai, J., Guo, X., and Kim, H. K. (2021c). Exosomes derived from miR-155-5p–overexpressing synovial mesenchymal stem cells prevent osteoarthritis via enhancing proliferation and migration, attenuating apoptosis, and modulating extracellular matrix secretion in chondrocytes. *Cell. Biol. Toxicol.* 37 (1), 85–96. doi:10.1007/s10565-020-09559-9

Wei, Y., Yan, L., Luo, L., Gui, T., Jang, B., Amirshaghaghi, A., and Kim, H. K. (2021). Phospholipase A2 inhibitor–loaded micellar nanoparticles attenuate inflammation and mitigate osteoarthritis progression. *Sci. Adv.* 7 (15), eabe6374. doi:10.1126/sciadv.abe6374

Woo, C. H., Kim, H. K., Jung, G. Y., Jung, Y. J., Lee, K. S., Yun, Y. E., and Li, T. (2020). Small extracellular vesicles from human adipose-derived stem cells attenuate cartilage degeneration. *J. Extracell. Vesicles* 9 (1), 1735249. doi:10.1080/20013078.2020.1735249

Wu, J., Kuang, L., Chen, C., Yang, J., Zeng, W.-N., Li, T., and Liu, Y. (2019). miR-100-5p-abundant exosomes derived from infrapatellar fat pad MSCs protect articular cartilage and ameliorate gait abnormalities via inhibition of mTOR in osteoarthritis. *Biomaterials* 206, 87–100. doi:10.1016/j.biomaterials.2019.03.022

Xu, C., Zhai, Z., Ying, H., Lu, L., Zhang, J., and Zeng, Y. (2022). Curcumin primed ADMSCs derived small extracellular vesicle exert enhanced protective effects on

osteoarthritis by inhibiting oxidative stress and chondrocyte apoptosis. *J. Nanobiotechnology* 20 (1), 123. doi:10.1186/s12951-022-01339-3

Xu, X., Liang, Y., Li, X., Ouyang, K., Wang, M., and Cao, T., (2021). Exosome-mediated delivery of kartogenin for chondrogenesis of synovial fluid-derived mesenchymal stem cells and cartilage regeneration. *Biomaterials* 269, 120539. doi:10.1016/j.biomaterials.2020.120539

Yan, L., Liu, G., and Wu, X. (2021). The umbilical cord mesenchymal stem cell-derived exosomal lncRNA H19 improves osteochondral activity through miR-29b-3p/FoxO3 axis. *Clin. Transl. Med.* 11 (1), e255. doi:10.1002/ctm2.255

Yan, L., and Wu, X. (2020). Exosomes produced from 3D cultures of umbilical cord mesenchymal stem cells in a hollow-fiber bioreactor show improved osteochondral regeneration activity. *Cell. Biol. Toxicol.* 36 (2), 165–178. doi:10.1007/s10565-019-09504-5

Yang, Q., Yao, Y., Zhao, D., Zou, H., Lai, C., Xiang, G., and Huang, X. (2021). LncRNA H19 secreted by umbilical cord blood mesenchymal stem cells through microRNA-29a-3p/FOS axis for central sensitization of pain in advanced osteoarthritis. *Am. J. Transl. Res.* 13 (3), 1245–1256.

Yeo, R. W. Y., Lai, R. C., Zhang, B., Tan, S. S., Yin, Y., Teh, B. J., and Sai Kiang, L. (2013). Mesenchymal stem cell: An efficient mass producer of exosomes for drug delivery. *Adv. Drug Deliv. Rev.* 65 (3), 336–341. doi:10.1016/j.addr.2012.07.001

Yu, W.-W., Wan, Q.-Q., Wei, Y., Li, Y.-T., Li, Q.-H., and Ye, T., (2022). Engineered extracellular vesicles: Regulating the crosstalk between the skeleton and immune system. *Eng. Regen.* 3 (3), 270–282. doi:10.1016/j.engreg.2022.06.004

Zavatti, M., Beretti, F., Casciaro, F., Bertucci, E., and Maraldi, T. (2020). Comparison of the therapeutic effect of amniotic fluid stem cells and their exosomes on monoiodoacetate-induced animal model of osteoarthritis. *BioFactors* 46 (1), 106–117. doi:10.1002/biof.1576

Zhang, D., Lee, H., Zhu, Z., Minhas, J. K., and Jin, Y. (2016a). Enrichment of selective miRNAs in exosomes and delivery of exosomal miRNAs *in vitro* and *in vivo*. *Am. J. Physiology-Lung Cell. Mol. Physiology* 312 (1), L110–L121. doi:10.1152/ajplung.00423.2016

Zhang, J., Rong, Y., Luo, C., and Cui, W. (2020). Bone marrow mesenchymal stem cell-derived exosomes prevent osteoarthritis by regulating synovial macrophage polarization. *Aging* 12 (24), 25138–25152. doi:10.18632/aging.104110

Zhang, Q., Cao, L., Zou, S., Feng, Y., Miao, X., Huang, L., and Yongping, W. (2022a). Human umbilical cord mesenchymal stem cell-derived extracellular vesicles carrying MicroRNA-181c-5p promote BMP2-induced repair of cartilage injury through inhibition of SMAD7 expression. *Stem Cells Int.* 2022, 1–14. doi:10.1155/2022/1157498

Zhang, S., Chu, W. C., Lai, R. C., Lim, S. K., Hui, J. H. P., and Toh, W. S. (2016b). Exosomes derived from human embryonic mesenchymal stem cells promote osteochondral regeneration. *Osteoarthr. Cartil.* 24 (12), 2135–2140. doi:10.1016/j.joca.2016.06.022

Zhang, S., and Jin, Z. (2022). Bone mesenchymal stem cell-derived extracellular vesicles containing long noncoding RNA NEAT1 relieve osteoarthritis. *Oxidative Med. Cell. Longev.* 2022, 1–21. doi:10.1155/2022/5517648

Zhang, S., Li, J., Li, C., Xie, X., He, J., Ling, F., and Zhilin, L. (2022b). CD73-Positive small extracellular vesicles derived from umbilical cord mesenchymal stem cells promote the proliferation and migration of pediatric urethral smooth muscle cells through adenosine pathway. *Front. Bioeng. Biotechnol.* 10, 895998. doi:10.3389/fbioe.2022.895998

Zhang, S., Teo, K. Y. W., Chuah, S. J., Lai, R. C., Lim, S. K., and Toh, W. S. (2019). MSC exosomes alleviate temporomandibular joint osteoarthritis by attenuating inflammation and restoring matrix homeostasis. *Biomaterials* 200, 35–47. doi:10.1016/j.biomaterials.2019.02.006

Zhang, X., Lu, Y., Wu, S., Zhang, S., Li, S., and Tan, J. (2022c). An overview of current research on mesenchymal stem cell-derived extracellular vesicles: A bibliometric analysis from 2009 to 2021. *Front. Bioeng. Biotechnol.* 10, 910812. doi:10.3389/fbioe.2022.910812

Zhou, H., Shen, X., Yan, C., Xiong, W., Ma, Z., and Tan, Z., (2022). Extracellular vesicles derived from human umbilical cord mesenchymal stem cells alleviate osteoarthritis of the knee in mice model by interacting with METTL3 to reduce m6A of NLRP3 in macrophage. *Stem Cell. Res. Ther.* 13 (1), 322. doi:10.1186/s13287-022-03005-9

Zhou, Y., Ming, J., Li, Y., Li, B., Deng, M., and Ma, Y., (2021). Exosomes derived from miR-126-3p-overexpressing synovial fibroblasts suppress chondrocyte inflammation and cartilage degradation in a rat model of osteoarthritis. *Cell. Death Discov.* 7 (1), 37. doi:10.1038/s41420-021-00418-y

Zhu, Y., Wang, Y., Zhao, B., Niu, X., Hu, B., and Li, Q., (2017). Comparison of exosomes secreted by induced pluripotent stem cell-derived mesenchymal stem cells and synovial membrane-derived mesenchymal stem cells for the treatment of osteoarthritis. *Stem Cell. Res. Ther.* 8 (1), 64. doi:10.1186/s13287-017-0510-9

Zhuang, Y., Cheng, M., Li, M., Cui, J., Huang, J., Zhang, C., and Yu, H. (2022). Small extracellular vesicles derived from hypoxic mesenchymal stem cells promote vascularized bone regeneration through the miR-210-3p/EFNA3/PI3K pathway. *Acta Biomater.* 150, 413–426. doi:10.1016/j.actbio.2022.07.015

frontiers | Frontiers in Bioengineering and Biotechnology

TYPE Original Research
PUBLISHED 16 September 2022
DOI 10.3389/fbioe.2022.1007535

OPEN ACCESS

EDITED BY
Qian Feng,
Chongqing University, China

REVIEWED BY
Long Bai,
East China University of Science and Technology, China
Yifan Wang,
Huazhong University of Science and Technology, China

*CORRESPONDENCE
Lei Chen,
chenlei689595@wmu.edu.cn
Jiang Chang,
jchang@mail.sic.ac.cn

†These authors have contributed equally to this work and share the first authorship

SPECIALTY SECTION
This article was submitted to Biomaterials, a section of the journal Frontiers in Bioengineering and Biotechnology

RECEIVED 30 July 2022
ACCEPTED 31 August 2022
PUBLISHED 16 September 2022

CITATION
Pan H, Deng L, Huang L, Zhang Q, Yu J, Huang Y, Chen L and Chang J (2022), 3D-printed $Sr_2ZnSi_2O_7$ scaffold facilitates vascularized bone regeneration through macrophage immunomodulation. *Front. Bioeng. Biotechnol.* 10:1007535. doi: 10.3389/fbioe.2022.1007535

3D-printed $Sr_2ZnSi_2O_7$ scaffold facilitates vascularized bone regeneration through macrophage immunomodulation

Hao Pan[1,2†], Li Deng[3†], Lingwei Huang[3,4], Qi Zhang[1,2], Jing Yu[3], Yueyue Huang[5], Lei Chen[1,2,5*] and Jiang Chang[1,3,4*]

[1]Joint Centre of Translational Medicine, the First Affiliated Hospital of Wenzhou Medical University, Wenzhou, Zhejiang, China, [2]Department of Orthopaedics, The First Affiliated Hospital of Wenzhou Medical University, Wenzhou, Zhejiang, China, [3]Wenzhou Institute, University of CAS, Wenzhou, Zhejiang, China, [4]Oujiang Laboratory, Wenzhou, Zhejiang, China, [5]Key Laboratory of Intelligent Treatment and Life Support for Critical Diseases of Zhejiang Province, Wenzhou, Zhejiang, China

Biomaterial-based bone grafts are emerged as an effective strategy for the treatment of large bone defects, especially for the scaffolds with enhanced osteogenic and angiogenic bioactivities. However, most studies focused on the direct interactions between scaffolds and bone-related cells such as osteoblasts and endothelial cells, and ignored the effects of material-triggered immunomodulation and the subsequent immune-regulated bone regeneration process. In this study, we developed a silicate bioceramic ($Sr_2ZnSi_2O_7$, SZS) scaffold with well-defined pore structures using a three-dimensional (3D) printing technique. The prepared scaffolds were biodegradable, and the released bioactive ions were beneficial for immunomodulation, which stimulated macrophages to release more pro-healing cytokines and less pro-inflammatory cytokines. The obtained scaffold/macrophage conditioned medium further promoted the proliferation and osteogenic differentiation of a murine preosteoblast cell line (MC3T3-E1), as well as the angiogenic activity of human umbilical vein endothelial cells (HUVECs). Moreover, the *in vivo* experiments of critical-sized calvarial defects in rats revealed that the 3D printed SZS scaffolds could facilitate more vascularized bone regeneration than the 3D printed β-tricalcium phosphate (β-TCP, a typical clinically used bioceramic) scaffolds, suggesting that the 3D-printed SZS scaffolds hold the potential as implantable biomaterials with favorable osteoimmunomodulation for bone repair.

KEYWORDS

3D printing, immunomodulation, osteogenesis, angiogenesis, bone defect

1 Introduction

Large bone defect is a common but serious medical problem in clinical practice, which is mostly caused by trauma, infection, or tumor resection and can't be self-healed when the lesion exceeds the "critical size" (Roddy et al., 2018; Sparks et al., 2020). Bone grafts are usually needed for the reconstruction of large bone defects, serving as an osteoconductive scaffold for new bone formation. The currently available bone grafts mainly include biological products (autologous or allogeneic implants), and synthetic biomaterials (Yang et al., 2018; Wei et al., 2022). Although both autologous and allogeneic bone grafts have been implemented clinically for many years and proved as effective strategies for bone restoration, their major disadvantages are still unsolved. For example, autologous bone grafting needs additional surgical intervention and is subject to the limited bone supply, while allogeneic bone grafting has the risk of immunological rejection and disease propagation (Zhao et al., 2021). Therefore, it is imperative to develop suitable artificial bone scaffolds for the repair of large bone defects.

An ideal bone scaffold requires many properties, among which the bioactivity of osteogenesis and angiogenesis are two of the principal elements (Yang et al., 2021b). Various methods have been developed to promote the osteogenic and angiogenic ability of the scaffold simultaneously (Shi et al., 2015; Feng et al., 2017; Kuttappan et al., 2018; Yang et al., 2019). Among these methods, modifying scaffolds with growth factors is the most direct way. For example, Yasuhiko Tabata *et al.* developed a fibrous scaffold loaded with both bone morphogenetic protein 2 (BMP-2, an osteogenic growth factor) and vascular endothelial growth factor (VEGF, an angiogenic growth factor) for the critical-sized calvarial defect in rats (Kuttappan et al., 2018). The results showed that the co-delivery of BMP-2 and VEGF by the scaffolds significantly stimulated the vascularized bone regeneration in the defect area. However, the drawbacks of high cost, instability and short life hinder the translational application of growth factors. Another commonly used strategy for enhancing osteogenesis and angiogenesis is based on material-mediated immune regulation. In general, bone reconstruction is a result of the interplay between the skeletal and immune systems, and the implanted scaffold-triggered inflammation has been recognized as the first stage of bone regeneration, which markedly affects the following bone healing and remodeling process (Chen et al., 2016). It has been widely proved that a beneficial immune microenvironment for osteogenesis and angiogenesis could be modulated by tailoring the composition or structure of a scaffold (Yang et al., 2019; Negrescu and Cimpean, 2021). For example, in our previous study, we proved that the decoration of micro/nano hierarchical structures on a hydroxyapatite (HA) ceramic could promote the polarization of macrophages from phenotype M1 towards M2, showing benefits for the pro-healing immune environment, which further increased the expressions of osteogenic genes in human bone marrow stromal cells (hBMSCs) and angiogenic genes in human umbilical vein endothelial cells (HUVECs) (Yang et al., 2019).

Apart from the structure of the implanted scaffolds, the component of the material is also a key factor in the regulation of the immune microenvironment. Scaffolds containing trace elements such as silicon (Si), zinc (Zn), and strontium (Sr) and has shown great potential in manipulating the immune microenvironment by affecting multiple immune cells including macrophages and Treg cells (Liu et al., 2018; Bai et al., 2021; Zhang et al., 2021; Zhong et al., 2022). In our previous study, a bioactive ceramic ($Sr_2ZnSi_2O_7$, SZS) containing Si, Zn, and Sr was synthesized and plasma-sprayed on a titanium alloy implant, which significantly inhibited the release of pro-inflammatory cytokines, showing a beneficial osteoimmunomodulation due to sustaining released of silicate ions (SiO_3^{2-}), zinc ions (Zn^{2+}) and strontium ions (Sr^{2+}) (Chen et al., 2014). However, it is unknown if the ions-regulated immune microenvironment is also beneficial for angiogenesis. Also, titanium alloy is non-biodegradable, which may require surgical removal due to possible complications such as infection and exposure. In contrast, a degradable SZS scaffold itself might be more suitable for bone regeneration. Therefore, in this study, we prepared SZS scaffolds by three-dimensional (3D) printing and investigated their effects on the immune microenvironment, as well as the following osteogenic and angiogenic potential both *in vitro* and *in vivo*. It is expected that the proposed SZS scaffolds could enhance osteogenesis and angiogenesis for bone tissue regeneration via immunomodulation.

2 Materials and methods

2.1 Preparation of SZS powders and scaffolds

SZS powders were compounded in a sol-gel method (Zhang et al., 2012). Briefly, nitric acid (HNO_3, Aladdin Reagent Co., Ltd, Shanghai, China) was added to 400 ml distilled water to adjust pH to 2 followed by adding 0.4 mol TEOS and stirring for 1.5 h. Then, strontium nitrate ($Sr(NO_3)_2$, Aladdin Reagent Co., Ltd, Shanghai, China) and zinc nitrate hexahydrate ($Zn(NO_3)_2{\cdot}6H_2O$, Aladdin Reagent Co., Ltd, Shanghai, China) were added to the tetraethyl orthosilicate (TEOS, Aladdin Reagent Co., Ltd, Shanghai, China) solution in a molar Sr: Zn: Si ratio of 2:1: 2 and stirred for 5 h. Sequentially, the mixture was put at 60°C for 24 h until gel formation, and the formed gel was stabilized at 60°C for another 1~2 h, which was followed by drying the gel at 120°C, as well as milling and filtering to acquire particles less than 200-mesh. Finally, the obtained particles were sintered in a high temperature furnace (KSL-1700X-A4, HF-kejing Co., Ltd, Anhui,

TABLE 1 Primers for gene expression analysis.

Gene	Forward primer	Reverse primer
IL-1β	AATGCCACCTTTTGACAGTGATG	TGATGTGCTGCTGCGAGATT
TNF-α	TAGCCCACGTCGTAGCAAAC	GCAGCCTTGTCCCTTGAAGA
iNOS	ACCCCTTGTGCTGTTCTCAG	GGGATTCTGGAACATTCTGTGC
IL-1α	GTCGGGAGGAGACGACTCTAA	GTTTCTGGCAACTCCTTCAGC
TGF-1β	TGATACGCCTGAGTGGCTGTCT	CACAAGAGCAGTGAGCGCTGAA
IL-1rα	AGAGCCCCTTATAGTCACGAA	TACACCCTGCAAAAGTTGTTCC
ARG	AACCTTGGCTTGCTTCGGAACTC	GTTCTGTCTGCTTTGCTGTGATGC
CD206	ATCCACGAGCAAATGTACCTCA	TAGCCAGTTCAGATACCGGAA
RUNX-2	GACTGTGGTTACCGTCATGGC	ACTTGGTTTTTCATAACAGCGGA
COL-1	TTCTCCTGGCAAAGACGGAC	CTCAAGGTCACGGTCACGAA
OCN	GAACAGACAAGTCCCACACAGC	TCAGCAGAGTGAGCAGAAAGAT
BMP-2	TCACTTATAGCCGCATTATCTTCTTC	TTGGTTTATCCATGAGGCTAACTG
bFGF	CAATTCCCATGTGCTGTGAC	ACCTTGACCTCTCAGCCTCA
VEGF	TATGCGGATCAAACCTCACCA	CACAGGGATTTTTCTTGTCTTGCT
FGF-2	AAAAGGCAAGATGCAGGAGA	TTTTGCAGCCTTACCCAATC
HIF-1α	ATCCATGTGACCATGAGGAAAT	CTCGGCTAGTTAGGGTACACTT
eNOS	GATGTTACCATGGCAACCAAC	GAAAATGTCTTCGTGGTAGCG

China) at 1,200°C for 3 h at a heating rate of 2°C/min and ground for further use.

For scaffolds, the printing paste was first prepared by mixing SZS powders (2 g) with sodium alginate (Alg, 0.01 g), and Pluronic®F-127 (F-127,2 ml, 20 wt%). Then, the 3D printer (BioMaker, SunP Biotech, Beijing, China) was applied to prepare porous SZS scaffolds with a 45°-crossed lay-down pattern at a printing speed of 4.4 mm/s. As a control, β-tricalcium phosphate (β-TCP) scaffolds were also 3D printed similarly. The obtained 3D printed ceramic embryos were further sintered at 1,200–1,400°C for SZS, and 1,100°C for β-TCP.

2.2 Characterization of the 3D printed scaffolds

The component of the SZS scaffolds was characterized using an X-ray diffractometer (XRD, Bruker, Germany) with 40 kV and 40 mA. The structure and surface morphology of the scaffolds were examined with a scanning electron microscope (SEM, SU8010, HITACHI, Japan). To study the release of SiO_3^{2-}, Zn^{2+} and Sr^{2+} ions from SZS scaffolds, SZS scaffolds were placed in a 48-well plate with 1 ml/well deionized water for 2 days, and the extracts were collected and filtered using Millipore filters with pore size of 0.22 μm before quantifying the concentration of these ions by an inductively coupled plasma-mass spectrometry (ICP-MS, Agilent7850, Singapore). The mechanical properties of the scaffolds were evaluated with a universal testing machine (Instron 5,944, America). The porosity (P) of the scaffolds was measured using a drainage method (Yang et al., 2017). Briefly, the weight of the scaffolds was measured in dried (M1), water-filled (M2) and water-immersion (M3) conditions, respectively. The porosity (P) of the scaffolds was calculated by the following formula.

$$P = \frac{M2 - M1}{M2 - M3} \times 100\% \quad (1)$$

For the degradation test, scaffolds were immersed into Tris-HCl buffer solution in a ratio of 50 ml/g at 37°C for 1, 3, and 7 days. Then, the scaffolds were weighed after drying at 120°C for 12 h. The degradation rate was calculated as the percentage of weight loss of scaffolds during the immersion.

2.3 Cell experiment

2.3.1 Inflammatory reaction of the scaffolds

For the cytotoxicity assay, RAW264.7 macrophages were seeded on the scaffolds in a 48-well plate at a density of 1×10^4 cells/well and cultured for 1 day. For, imflammatory reaction assay, RAW264.7 macrophages were seeded on scaffolds in a 6-well plate with a density of 2×10^5 cells/well and cultured for 2 days. Then, the total RNA was extracted using an RNA kit (YISHEN, China), and transferred into cDNA using a reverse transcription kit (YISHEN, China). Gene expression of inflammation factors including interleukin-1α (IL-1α),interleukin-1β (IL-1β), inducible nitric oxide synthase (iNOS), tumor necrosis factor-α (TNF-α), transforming growth factor-1β (TGF-1β), interleukin-1 receptor antagonist (IL-1rα), cluster of differentiation 206

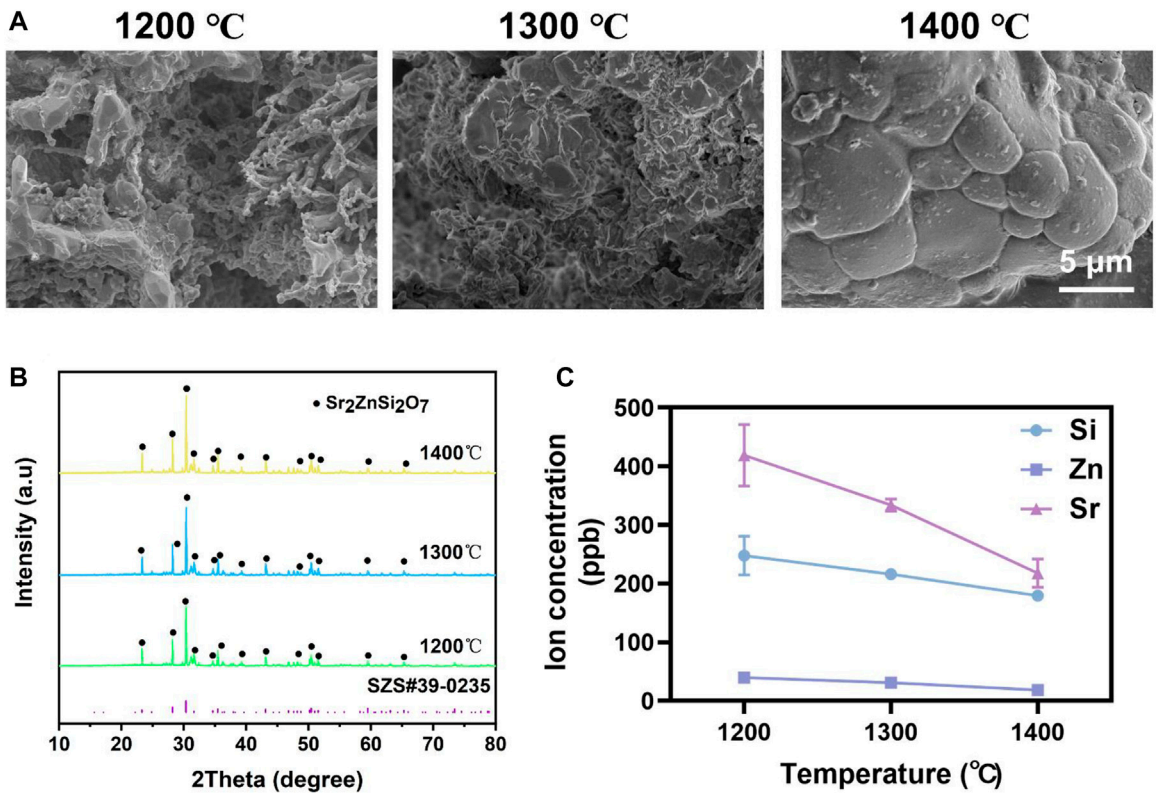

FIGURE 1
Characterization of SZS scaffolds sintered at 1,200°C, 1,300°C, and 1,400°C, respectively. **(A)** SEM characterization of the surface morphology. **(B)** XRD analysis of the crystalline. **(C)** Ions release profile of SiO_3^{2-}, Zn^{2+} or Sr^{2+}. (n = 3).

(CD206), arginine (ARG) was evaluated using a real-time polymerase chain reaction (RT-PCR) combined with SYBR Green PCR Master Mix (YISHEN, China). The gene expression was normalized to GADPH. The primer sequences are shown in Table 1.

2.3.2 Effect of conditional medium on MC3T3-E1 cells

To prepare scaffold/macrophage conditional media, the supernatant from the cell experiment of 2.3.1 was collected and mixed with Dulbecco's modified eagle medium (DMEM) at a ratio of 1:1. The following cell experiments were implemented under the stimulation of conditional media. For the cell proliferation study, MC3T3-E1 cells were seeded in a 96-well plate with a density of 1,000 cells/well, and cultured in humidified 5% CO_2 at 37°C for 12 h. Then, the culture medium was replaced by the conditional medium, and the cells were cultured for 1, 3 and 5 days, during which the culture medium was exchanged every other day. Cell proliferation was evaluated by the cell counting kit-8 (CCK-8, YESEN, China) assay using a microplate reader (EPOCH2NS, BioTek instruments, America) at a wavelength of 450 nm. For the alkaline phosphatase (ALP) and alizarin red staining (ARS) experiments, cells were cultured with the conditional medium for 7 days and stained by kits purchased from Solarbio (Beijing, China). For the gene expression study, MC3T3-E1 cells were seeded in a 6-well plate with a density of 1×10^5 cells/well and cultured in the conditional medium for 7 days. Then, the osteogenic genes of osteocalcin (OCN), type I collagen (COL-1), runt-related transcription factor 2 (RUNX-2) and BMP-2 were evaluated following the same procedure above.

2.3.3 Effect of conditional medium on HUVECs

The cell proliferation study of HUVECs under the conditional medium was assessed using a CCK-8 assay kit with an initial cell density of 1,000 cells/well in 96-well plates on day 1, 3 and 5. For the cell migration study, HUVECs were seeded in a 6-well plate with a density of 4×10^5 cells/well and cultured for 12 h. Then, scratches were made with a pipette tip followed by phosphate buffered solution (PBS) washing twice. After microscopy, the conditional medium was added and cultured for another 24 h. The cells were imaged again after fixation with 4% paraformaldehyde and staining with methylrosanilnium chloride solution. The acquired images were processed using ImageJ software, where the original width (A_0) and final width (A_1) of the scratches were measured. The immigration rate (A) was calculated by the following formula.

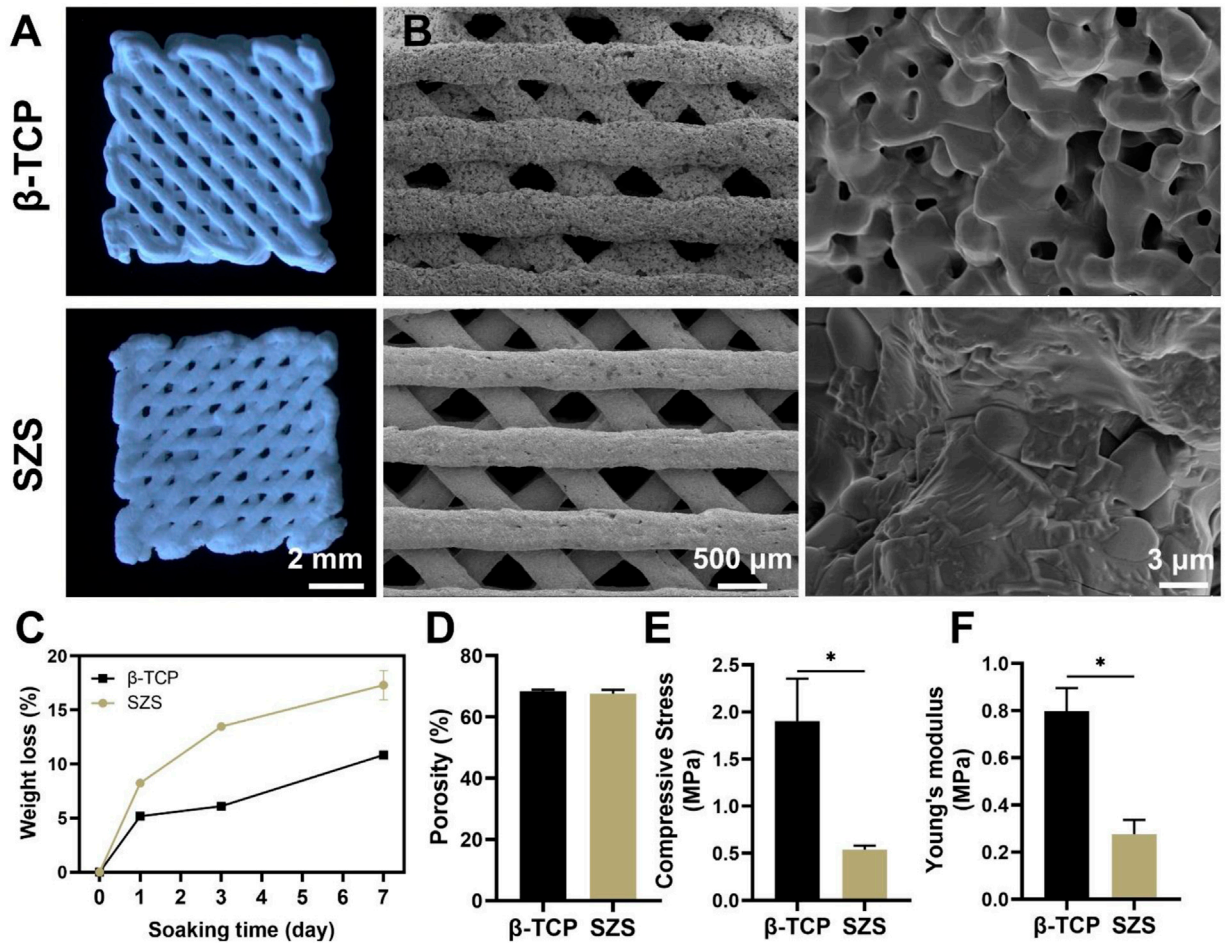

FIGURE 2
Characterization of 3D printed SZS and β-TCP scaffolds. **(A)** Optimal images. **(B)** SEM characterization of the macroporous structure and surface morphology. **(C)** *In vitro* degradation assay. (n = 3). **(D)** Porosity of scaffolds. (n = 4). **(E)** Compressive stress and **(F)** Young's modulus of scaffolds. (n = 3). *p < 0.05 and **p < 0.01.

$$A = \frac{A0 - A1}{A0} \times 100\% \quad (2)$$

The *in vitro* tube formation experiment was conducted by seeding HUVECs (4×10^4 cells/well) on matrigel (ABW®Matrigengel, China) in a 48-well plate and incubating with the conditional medium for 4 h. Microscopy images were taken using optical microscope (ckx53, Olympus, China) and analyzed with the ImageJ software (National Institutes of Health, United States). In addition, the gene expression experiments of HUVECs were performed similarly to the above studies, and the angiogenic genes of vascular endothelial growth factor (VEGF), fibroblast growth fator 2 (FGF-2), basic fibroblast growth factor (bFGF), hypoxia inducible factor 1α (HIF-1α) and bmpendothelial nitric oxide synthase (eNOS) were evaluated.

2.4 Animal experiment

2.4.1 Animal model and grouping

Sprague-Dawley mature male rats (8-week-old) were purchased from the Zhejiang Provincial Laboratory Animal Center, and the experiment was approved by the Animal Research and Ethics Committee of Wenzhou Institute of University of Chinese Academy of Sciences. A rat critical-sized cranial bone defect model was established according to a previous study (Yang et al., 2021c). Briefly, rats were anesthetized by intraperitoneal injection of pentobarbital. Then, full-thickness bone defects (5 mm) were created on both sides of the calvarium by a trephine drill. After implanting the 3D printed porous SZS (experimental group) or β-TCP (control group) scaffolds (with a diameter of 5 mm and a height of 1 mm) into the defects, the skin wound was sutured.

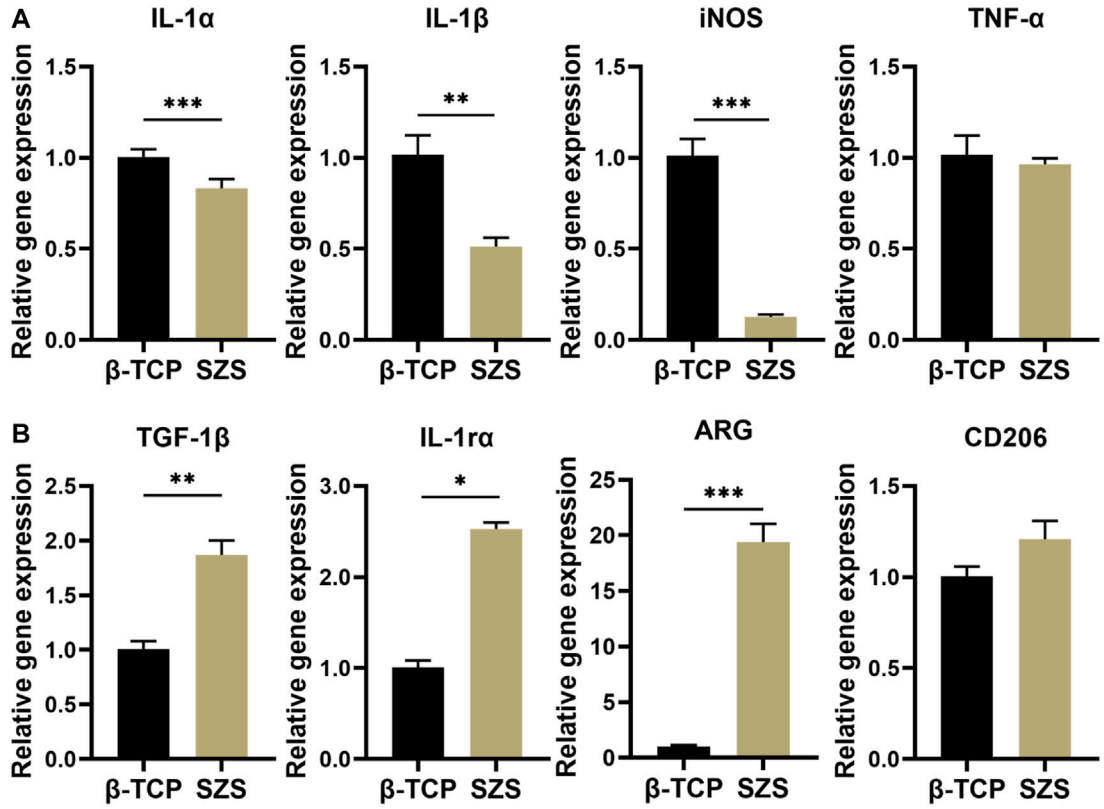

FIGURE 3
Gene expression of **(A)** inflammatory factors (IL-1α, IL-1β, iNOS, and TNF-α) (n = 4) and **(B)** pro-healing factors (TGF-1β, IL-1rα, ARG, and CD 206) in RAW264.7 macrophages after the treatment of different 3D printed scaffolds. (n = 4). *p < 0.05; **p < 0.01; ***p < 0.001.

2.4.2 Evaluation of bone regeneration

After an 8-weeks recovery, the rats were sacrificed and their skulls were collected for fixation with 4% paraformaldehyde and micro-computed tomography (micro-CT) scanning (Skyscan1176, Bruker, Germany). Bone mineral density and bone microstructure were quantified using the manufacturer's analysis software (CTAn, Bruker, Germany). Then, the samples were decalcified with ethylenediamine tetraacetic acid (EDTA), dehydrated with gradient alcohol, embedded in paraffin, and sectioned into slices with a thickness of 4 μm. Histological analysis was performed following hematoxylin-eosin (H&E) staining and Masson's trichrome staining, as well as immunohistochemistry staining of platelet endothelial cell adhesion molecule-1 (PECAM-1, CD31) and osteocalcin (OCN).

2.5 Statistical analysis

A one-way analysis of variance (ANOVA) was used to compare the difference between groups (≥3), and a Student's t-test was used to analyze data between the two groups using GraphPad software. All the data were presented as mean ± SEM, and the significance level for tests was $p < 0.05$.

3 Results

3.1 Comparison of the SZS scaffolds sintered at different temperatures

The effect of sintered temperature on SZS scaffolds was firstly investigated. As shown in Figure 1A, the density of the ceramic increased gradually with the elevated sintered temperature from 1,200°C to 1,400°C. Although the XRD patterns demonstrated that the SZS phase (JCPDS card: no. 39–0,235) contributed to the main component of the scaffolds in all groups without apparent differences (Figure 1B), the concentration of the released ions (SiO_3^{2-}, Zn^{2+} or Sr^{2+}) from the scaffolds was negatively correlated to sintering temperature (Figure 1C). In consideration of the possible cytotoxicity of excess ion release, SZS scaffolds sintered at 1,400°C were chosen for further studies.

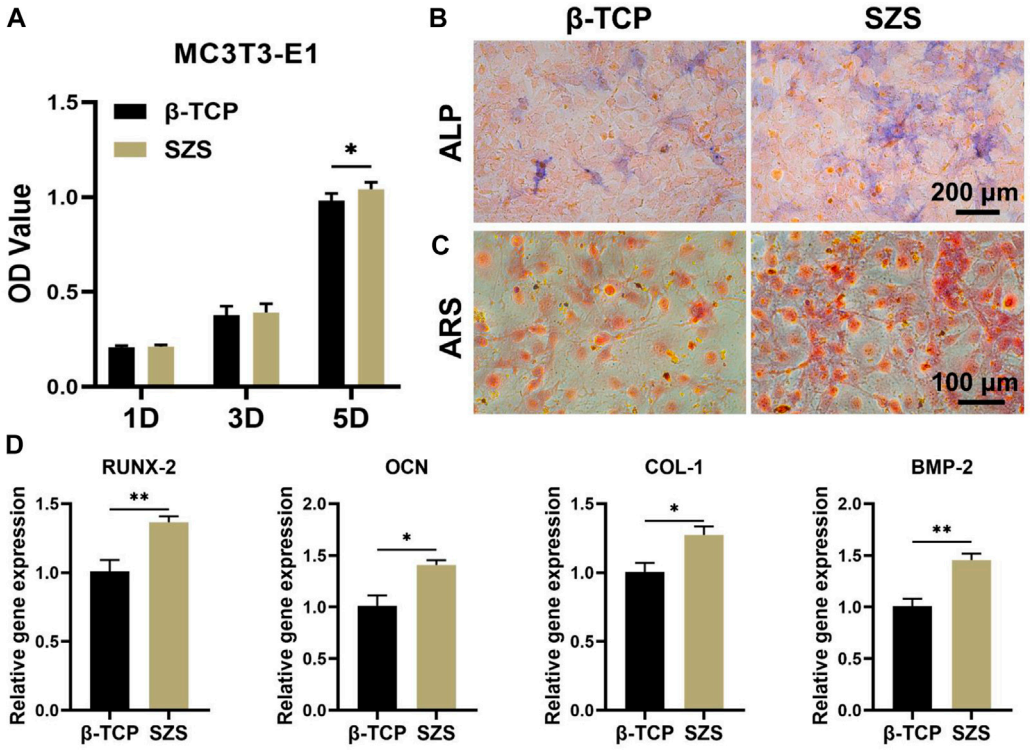

FIGURE 4
Effect of macrophage/scaffold conditional medium on MC3T3-E1 cells. **(A)** Cell proliferation on day 1, 3, and 5. (n = 6). **(B)** Representative images of ALP staining after 7 days' culture. Blue color represents ALP. **(C)** Representative images of Alizarin red s (ARS) staining after 7 days' culture. Orange-red color represents calcium nodules. **(D)** The osteogenic genes (RUNX-2, OCN, COL-1, and BMP-2) expression in cells by q-PCR assessment after 7 days' culture. (n = 4). *p < 0.05; **p < 0.01.

3.2 Characterization of the 3D printed porous SZS scaffolds

3D printed porous scaffolds of SZS and β-TCP with the uniform 45° interlaced architectures were shown by the optical images (Figure 2A). SEM images (Figure 2B) revealed that the pore size in both the scaffolds was about 450 μm. The porosities of the SZS and β-TCP scaffolds were 67.6 and 68.46%, respectively (Figure 2D). There are no significant differences in the macro pore structures between SZS and β-TCP scaffolds, indicating the excellent controllability of 3D printing technique. Furthermore, the mechanical properties of the scaffolds were evaluated, and the 3D printed β-TCP scaffolds showed higher compressive stress and Young's modulus than the 3D printed SZS scaffolds (Figures 2E,F). Correspondingly, the *in vitro* degradation rate of SZS scaffolds was also faster than β-TCP scaffolds (Figure 2C), which reached 17.41% after 7 days.

3.3 Immunomodulation behavior of the 3D printed porous SZS scaffolds

The cytotoxicity of scaffolds on RAW264.7 macrophages was first evaluated and the result was shown in Supplementary Figure S1. Both β-TCP and SZS scaffolds were non-toxic and SZS scaffolds could even promote the cell viability of macrophages. The mRNA expressions of inflammatory factors secreted from RAW264.7 macrophages in presence of the scaffolds were investigated and the results are shown in Figure 3. Downregulation of Pro-inflammatory factors such as IL-α, IL-1β and iNOS were exhibited in SZS group as compared to β-TCP group (Figure 3A). Also, significant upregulation of pro-healing factors after the treatment of SZS scaffolds was exhibited compared with β-TCP scaffolds, especially for factors of TGF-1β, IL-1rα, ARG (Figure 3B). All these results indicated that 3D printed SZS scaffolds had a beneficial pro-healing immune regulation ability.

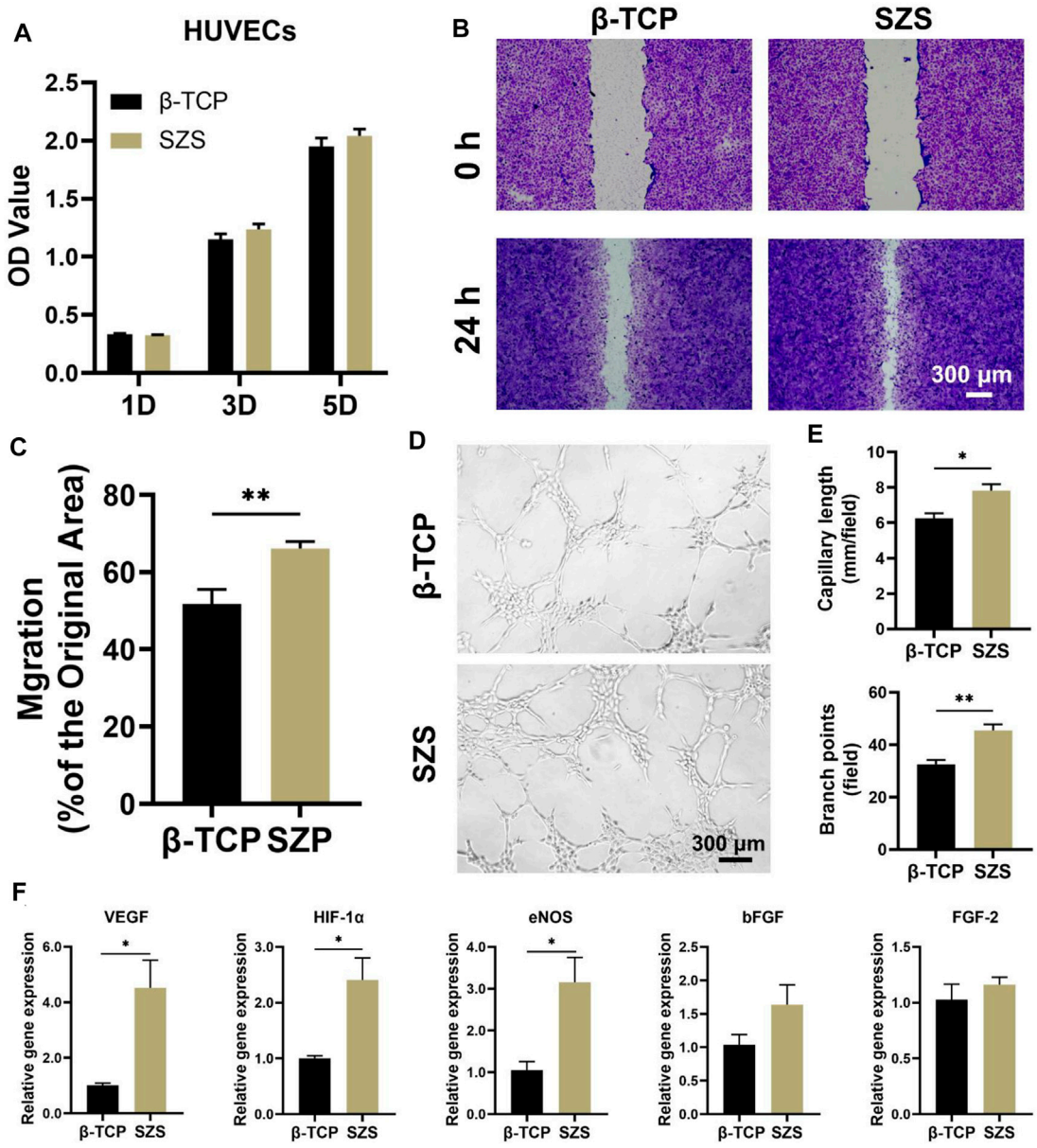

FIGURE 5
Effect of macrophage/scaffold conditional medium on HUVECs. **(A)** Cell proliferation on day 1, 3, and 5. (n = 6). **(B)** Representative images of cell migration after 1 day's culture. **(C)** Quantitative analysis of cell migration rate. (n = 8 for β-TCP; n = 9 for SZS). **(D)** Representative images and **(E)** quantitative analysis of the *in vitro* tube formation. (n = 4). **(F)** The angiogenic genes (VEGF, HIF-1α, eNOS, bFGF and FGF-2) expression in cells by q-PCR assessment after 3 days's culture. (n = 4). *p < 0.05; **p < 0.01.

3.4 Promotion of *in vitro* osteogenesis by the macrophage/scaffold conditional medium

To further evaluate the osteoimmunomodulation ability of the scaffolds, the macrophage/scaffold conditional medium was prepared. The cell proliferation results showed that more MC3T3-E1 cells proliferated after the culture with SZS mediated conditional medium as compared to β-TCP group, especially on day 5 since a significant difference was shown between SZS and β-TCP group (Figure 4A). Also, the ALP and alizarin red staining of cells treated with different conditional media for 7 days were conducted, which displayed that higher expression of ALP and more calcium nodules appeared in group SZS as compared to group β-TCP (Figures 4B,C). Moreover, the osteogenic gene expression of MC3T3-E1cells cultured with

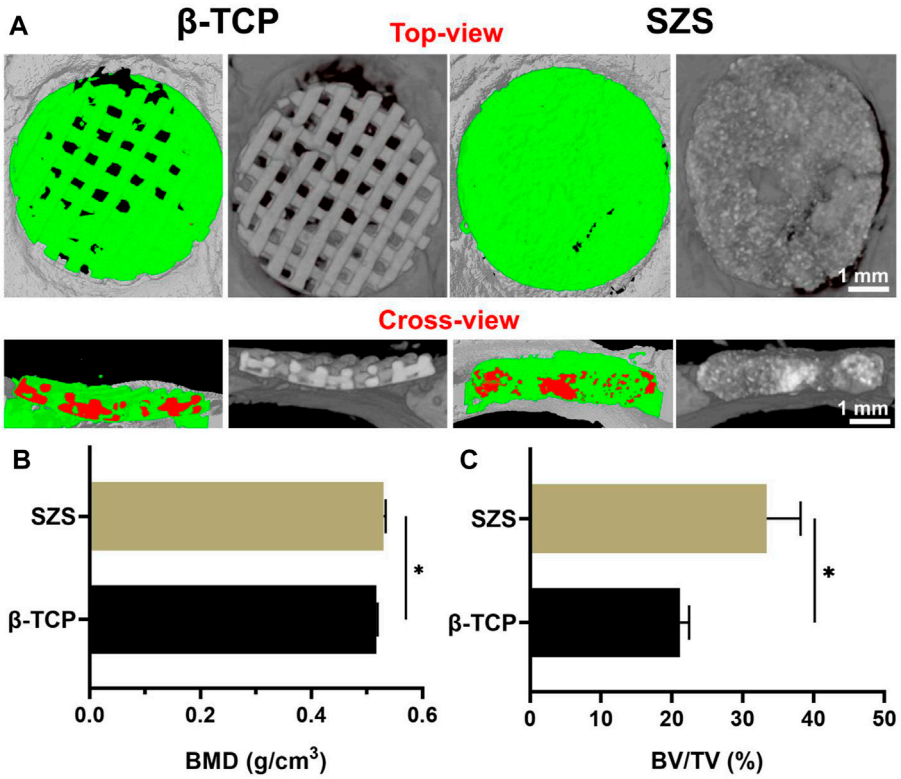

FIGURE 6
Micro-CT analysis of new bone formation in defect areas after implantation of 3D printed SZS and β-TCP scaffolds for 2 months **(A)** Typical 3D reconstruction of micro-CT images from the top view and cross-view. Green color shows newly formed bone, and red color represents materials. Quantitative analysis of **(B)** bone mineral density (BMD) (n = 4) and **(C)** bone volume/total volume (BV/TV) from micro-CT data. (n = 4). *p < 0.05.

different conditional media for 7 days was estimated by the q-PCR method. As shown in Figure 4D, significantly higher expressions of COL-1, BMP-2, OCN, and RUNX-2 were observed in the SZS group than that in the β-TCP group. All these outcomes implied that SZS scaffolds had better osteoimmunomodulation activity than β-TCP scaffolds.

3.5 Promotion of *in vitro* angiogenesis by the macrophage/scaffold conditional medium

Apart from the osteoimmunomodulation performance of the scaffolds, the immune-regulated angiogenic performance was also explored in our study. The effect of conditional medium on HUVECs was investigated including cell proliferation, migration, and differentiation. The cell proliferation study showed that a slight proliferative promotion of HUVECs was observed in the SZS group as compared to the β-TCP group without significant differences (Figure 5A). However, the cell migration rate in the SZS group was significantly higher than that in the SZS group (Figures 5B,C). More interestingly, the *in vitro* tube formation assay exhibited that the SZS group promoted more tubes formation in Matrigel after culture for 4 h as compared to the β-TCP group (Figure 5D). The corresponding quantitative analysis showed that the number of branch points and the capillary length in the SZS group was about 1.4 and 1.2 folds of that in group β-TCP, respectively (Figure 5E). Finally, significantly higher expression of angiogenic genes including VEGF, HIF-1α and eNOS in HUVECs were observed in the SZS group as compared to the β-TCP group (Figure 5F). The outcomes indicated that SZS scaffolds had a better immune regulation effect on the pro-angiogenesis of HUVECs than β-TCP scaffolds.

3.6 *In vivo* vascularized bone regeneration by the scaffolds in critical-sized calvarial defects

To further evaluated the *in vivo* bone regeneration ability of the 3D printed scaffolds, a typical rat calvarial defect model in rats was built and filled with both 3D printed β-TCP and β-TCP

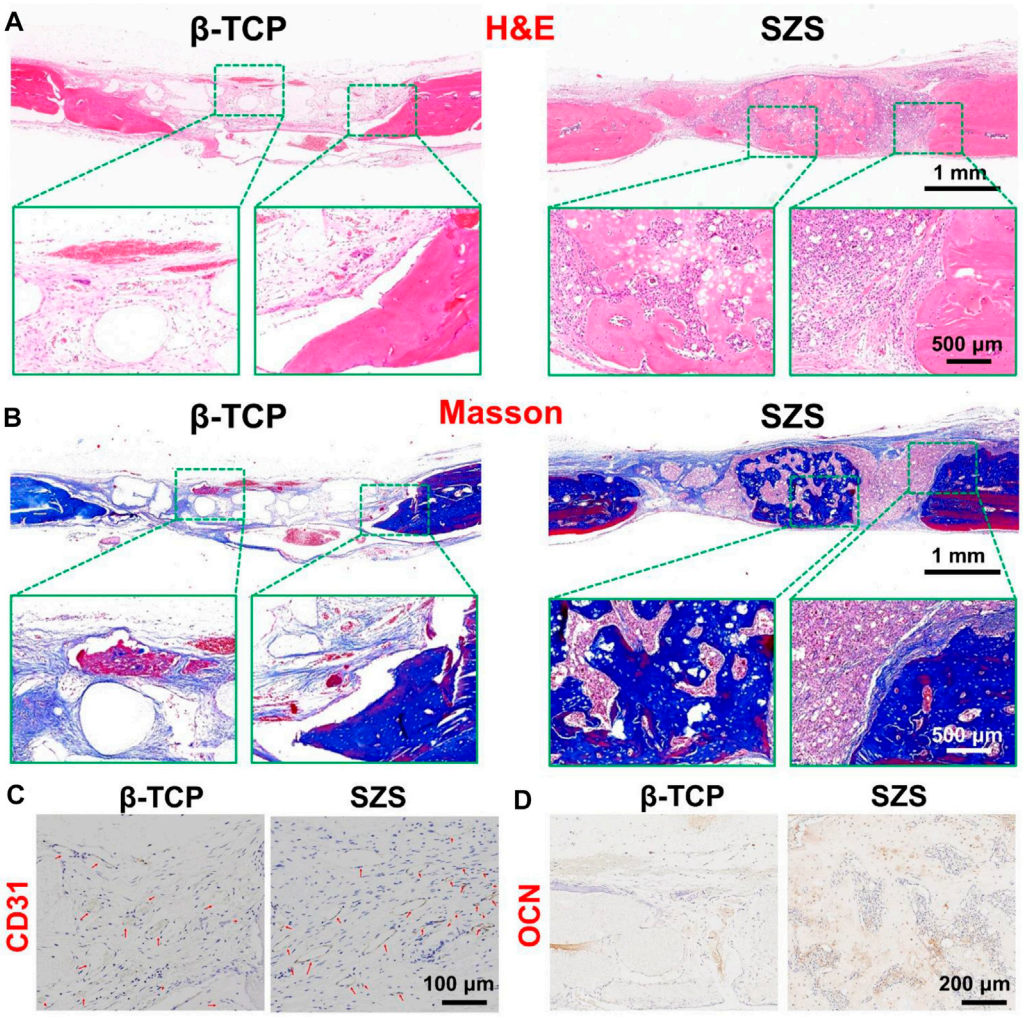

FIGURE 7
Representative H&E staining **(A)** and Masson's trichrome staining **(B)** of the craniums with cranial defects after implantation of 3D printed SZS and β-TCP scaffolds for 2 months. Representative immunohistochemistry staining images targeting angiogenic marker CD31 **(C)** and osteogenic marker OCN **(D)** in new-formed tissues.

scaffolds for 2 months, respectively. The 3D reconstructed micro-CT images revealed that more new bone tissues were deposited in the SZS scaffolds compared with the β-TCP scaffolds, which was confirmed by the quantitative analysis of bone mineral density (BMD) and bone volume fraction (BV/TV) (Figures 6A–C). It is worth mentioning that SZS scaffolds degraded much faster than β-TCP scaffolds as the porous structure was fragmentized in the SZS group, whereas it was maintained in the β-TCP group. The histological analysis of H&E staining and Masson's trichrome staining also showed consistent results where more newly formed tissues including collagen were found in defects treated with SZS scaffolds than those treated with β-TCP scaffolds (Figures 7A,B). Furthermore, the immunohistochemical staining of osteogenic biomarker OCN and angiogenic biomarker CD31 showed that SZS scaffolds had a better promotion of osteogenesis and angiogenesis in newly formed bone tissues (Figures 7C,D). All these results demonstrated that 3D printed SZS scaffolds had the bioactivity to promote vascularized bone regeneration.

4 Discussion

Scaffolds serve as a bridge guiding tissue regeneration in bone defects, which require essential mechanical properties and befitting porous structures. The technique of 3D printing emerged in the 1990s and has been proved as a critical fabrication method of bone scaffolds due to its flexibility in controlling the bulk geometry and internal structures, showing the ability in balancing mechanical properties and

porous structures (Zhen et al., 2021). Here, both SZS and β-TCP scaffolds with high porosity were fabricated by 3D printing, which was demonstrated beneficial for bone regeneration (Indranath et al., 2021). Therefore, 3D printed SZS porous scaffolds might be available for bone regeneration. Apart from the structure, the component of scaffolds also affect the outcomes of bone repair. Silicate biomaterials usually show better bioactivity for the deposition of bone-like apatite compared with phosphate biomaterials such as HA and β-TCP due to the exposed siloxane groups, and the commercial products of silicate bioglass (e.g., 45S5Bioglass® and BonAlive®) have been widely used in the field of bone regeneration for many years (Cannio et al., 2021). Recently, increasing evidences show that the released bioactive ions including SiO_3^{2-} ions and the corresponding metal ions (e.g., Ca^{2+}, Mg^{2+}, and Sr^{2+}) from the silicate biomaterials make the main contributions to biological activities such as osteogenesis and angiogenesis (Yang et al., 2021a; Dong et al., 2022; Fan et al., 2022). It is revealed that SiO_3^{2-} ions could stimulate osteogenesis through multiple signaling pathways including Wnt/β-catenin, Shh, MAPK/Erk, and antagonizing nuclear factor kappa-B (NF-κB) signaling pathways (Han et al., 2013; Shie and Ding, 2013; Guan et al., 2015; Mao et al., 2017). Also, SiO_3^{2-} ions could stimulate angiogenesis by upregulating the expression of pro-angiogenic factors such as VEGF, bFGF and HIF-1α (Li and Chang, 2013; Xu et al., 2021; Que et al., 2022). More interestingly, the combination of SiO_3^{2-} ions with other bioactive ions may result in a synergetic effect on both osteogenesis and angiogenesis (Mao et al., 2017; Xing et al., 2018).

However, most studies focused on the direct effects of silicate biomaterials on bone relative cells and ignored the relationship between the immune system and the skeleton system. As a matter of fact, immune cells first respond to the implanted biomaterials among all types of cells and play an indispensable role in the following tissue healing process by collaboration with other cells. Taking the most common studied immune cells such as macrophages as an example, they are aggregated onto the surface of the materials when scaffolds are implanted, stimulated by the local microenvironment, and then release specific chemokines or cytokines to affect the behaviors of other cells such as osteoblasts and endothelial cells involved in bone regeneration (Chen et al., 2016). Our study proved that 3D printed SZS scaffolds could significantly increase the anti-inflammatory cytokines such as TGF-1β but decrease the pro-inflammatory cytokines such as IL-1α secreted from macrophages, showing a simulation of a pro-healing immune microenvironment. The following studies using the conditioned medium to culture MC3T3-E1 cells and HUVECs confirmed the beneficial immunomodulation effects on osteogenesis and angiogenesis with the treatment of 3D printed SZS scaffolds as compared to β-TCP scaffolds. The mechanism might be ascribed to the sustained release of the bioactive ions (SiO_3^{2-}, Zn^{2+} and Sr^{2+}) from SZS as either SiO_3^{2-}, Zn^{2+} or Sr^{2+} exhibits a regulatory effect on immune cells depending on the concentrations (Chen et al., 2014; Zhong et al., 2022). Since the ions released in our study were in the active concentration range, their combination may result in higher efficiency in stimulating the pro-healing immune microenvironment for bone regeneration, which was also proved by the *in vivo* study as more new vascularized bone formed in 3D printed SZS scaffolds as compared to β-TCP scaffold. Our study demonstrated that 3D printed bioceramic scaffolds containing suitable nutrient elements could regulate the inflammatory response of macrophages and further prompt osteogenesis and angiogenesis. However, the disadvantages of SZS scaffolds are also apparent such as the relatively low compressive mechanical strength and fast degradation rate, which should be seriously considered in future applications.

5 Conclusion

In summary, porous SZS scaffolds were successfully fabricated using the 3D printing technique. The obtained SZS scaffolds could regulate the inflammatory response of macrophages and create a beneficial immune microenvironment for bone regeneration. Thus, the osteogenic activity of MC3T3-E1 cells and the angiogenic activity of HUVECs could be enhanced by the scaffold/macrophage conditioned medium. In addition, the *in vivo* study of skull defect model in rats demonstrated the excellent vascularized bone reconstruction performance of 3D printed SZS scaffolds. Our results suggested that 3D printed porous SZS scaffolds have the potential for repairing large bone defects.

Data availability statement

The original contributions presented in the study are included in the article/Supplementary Material, further inquiries can be directed to the corresponding authors.

Ethics statement

The animal study was approved by the ethics Committee of Wenzhou Research Institute in the University of Chinese Academy of Sciences.

Author contributions

HP and LD performed the main experiments and analyzed the data, LH wrote the manuscript, QZ and YH performed the animal experiment, JY prepared ceramic powders, LC and JC formulated the hypothesis, designed the research and revised the manuscript.

Funding

This work was supported by National Natural Science Foundation of China (31900945, 81873949), Zhejiang

Traditional Chinese Medicine Scientific Research Fund Project (2022ZB342), Zhejiang Province Medical and Health Science and Technology Project (2022512117), Major Science and Technology Project of Wenzhou Science and Technology Bureau (2018ZY002), the seed grants from the Wenzhou Institute, University of Chinese Academy of Sciences (WIUCASQD2020013, WIUCASQD2021030), and the founding from First Affiliated Hospital of Wenzhou Medical University.

Conflict of interest

The authors declare that the research was conducted in the absence of any commercial or financial relationships that could be construed as a potential conflict of interest.

Publisher's note

Supplementary material

The Supplementary Material for this article can be found online at: https://www.frontiersin.org/articles/10.3389/fbioe.2022.1007535/full#supplementary-material

References

Bai, X., Liu, W., Xu, L., Ye, Q., Zhou, H., Berg, C., et al. (2021). Sequential macrophage transition facilitates endogenous bone regeneration induced by Zn-doped porous microcrystalline bioactive glass. *J. Mat. Chem. B* 9 (12), 2885–2898. doi:10.1039/d0tb02884c

Cannio, M., Bellucci, D., Roether, J. A., Boccaccini, D. N., and Cannillo, V. (2021). Bioactive glass applications: A literature review of human clinical trials. *Materials* 14 (18), 5440. doi:10.3390/ma14185440

Chen, Z. T., Klein, T., Murray, R. Z., Crawford, R., Chang, J., Wu, C. T., et al. (2016). Osteoimmunomodulation for the development of advanced bone biomaterials. *Mater. Today* 19 (6), 304–321. doi:10.1016/j.mattod.2015.11.004

Chen, Z., Yi, D., Zheng, X., Chang, J., Wu, C., and Xiao, Y. (2014). Nutrient element-based bioceramic coatings on titanium alloy stimulating osteogenesis by inducing beneficial osteoimmmunomodulation. *J. Mat. Chem. B* 2 (36), 6030–6043. doi:10.1039/c4tb00837e

Dong, C., Yang, C., Younis, M. R., Zhang, J., He, G., Qiu, X., et al. (2022). Bioactive NIR-II light-responsive shape memory composite based on cuprorivaite nanosheets for endometrial regeneration. *Adv. Sci. (Weinh).* 9, e2102220. doi:10.1002/advs.202102220

Fan, C., Xu, Q., Hao, R., Wang, C., Que, Y., Chen, Y., et al. (2022). Multi-functional wound dressings based on silicate bioactive materials. *Biomaterials* 287, 121652. doi:10.1016/j.biomaterials.2022.121652

Feng, C., Zhang, W., Deng, C., Li, G., Chang, J., Zhang, Z., et al. (2017). 3D printing of Lotus root-like biomimetic materials for cell delivery and tissue regeneration. *Adv. Sci. (Weinh).* 4 (12), 1700401. doi:10.1002/advs.201700401

Guan, J., Zhang, J., Guo, S., Zhu, H., Zhu, Z., Li, H., et al. (2015). Human urine-derived stem cells can be induced into osteogenic lineage by silicate bioceramics via activation of the Wnt/β-catenin signaling pathway. *Biomaterials* 55, 1–11. doi:10.1016/j.biomaterials.2015.03.029

Han, P., Wu, C., and Xiao, Y. (2013). The effect of silicate ions on proliferation, osteogenic differentiation and cell signalling pathways (WNT and SHH) of bone marrow stromal cells. *Biomater. Sci.* 1 (4), 379–392. doi:10.1039/c2bm00108j

Indranath, M., Susmita, B., William, S. D., Nairanjana, D., Chrissy, E., Jim, H., et al. (2021). 3D Printing in alloy design to improve biocompatibility in metallic implants. *Mater. Today* 45, 20–34. doi:10.1016/j.mattod.2020.11.021

Kuttappan, S., Mathew, D., Jo, J-I., Tanaka, R., Menon, D., Ishimoto, T., et al. (2018). Dual release of growth factor from nanocomposite fibrous scaffold promotes vascularisation and bone regeneration in rat critical sized calvarial defect. *Acta Biomater.* 78, 36–47. doi:10.1016/j.actbio.2018.07.050

Li, H., and Chang, J. (2013). Stimulation of proangiogenesis by calcium silicate bioactive ceramic. *Acta Biomater.* 9 (2), 5379–5389. doi:10.1016/j.actbio.2012.10.019

Liu, W., Li, J., Cheng, M., Wang, Q., Yeung, K. W., Chu, P. K., et al. (2018). Zinc-modified sulfonated polyetheretherketone surface with immunomodulatory function for guiding cell fate and bone regeneration. *Adv. Sci. (Weinh).* 5 (10), 1800749. doi:10.1002/advs.201800749

Mao, L., Xia, L., Chang, J., Liu, J., Jiang, L., Wu, C., et al. (2017). The synergistic effects of Sr and Si bioactive ions on osteogenesis, osteoclastogenesis and angiogenesis for osteoporotic bone regeneration. *Acta Biomater.* 61, 217–232. doi:10.1016/j.actbio.2017.08.015

Negrescu, A-M., and Cimpean, A. (2021). The state of the art and prospects for osteoimmunomodulatory biomaterials. *Materials* 14 (6), 1357. doi:10.3390/ma14061357

Que, Y., Zhang, Z., Zhang, Y., Li, X., Chen, L., Chen, P., et al. (2022). Silicate ions as soluble form of bioactive ceramics alleviate aortic aneurysm and dissection. *Bioact. Mater.* 07, 005. doi:10.1016/j.bioactmat.2022.07.005

Roddy, E., Debaun, M. R., Daoud-Gray, A., Yang, Y. P., and Gardner, M. J. (2018). Treatment of critical-sized bone defects: Clinical and tissue engineering perspectives. *Eur. J. Orthop. Surg. Traumatol.* 28 (3), 351–362. doi:10.1007/s00590-017-2063-0

Shi, M., Zhou, Y., Shao, J., Chen, Z., Song, B., Chang, J., et al. (2015). Stimulation of osteogenesis and angiogenesis of hBMSCs by delivering Si ions and functional drug from mesoporous silica nanospheres. *Acta Biomater.* 21, 178–189. doi:10.1016/j.actbio.2015.04.019

Shie, M-Y., and Ding, S-J. (2013). Integrin binding and MAPK signal pathways in primary cell responses to surface chemistry of calcium silicate cements. *Biomaterials* 34 (28), 6589–6606. doi:10.1016/j.biomaterials.2013.05.075

Sparks, D. S., Saifzadeh, S., Savi, F. M., Dlaska, C. E., Berner, A., Henkel, J., et al. (2020). A preclinical large-animal model for the assessment of critical-size load-bearing bone defect reconstruction. *Nat. Protoc.* 15 (3), 877–924. doi:10.1038/s41596-019-0271-2

Wei, H., Cui, J., Lin, K., Xie, J., and Wang, X. (2022). Recent advances in smart stimuli-responsive biomaterials for bone therapeutics and regeneration. *Bone Res.* 10 (1), 17–19. doi:10.1038/s41413-021-00180-y

Xing, M., Wang, X., Wang, E., Gao, L., and Chang, J. (2018). Bone tissue engineering strategy based on the synergistic effects of silicon and strontium ions. *Acta Biomater.* 72, 381–395. doi:10.1016/j.actbio.2018.03.051

Xu, Q., Jiang, F., Guo, G., Wang, E., Younis, M. R., Zhang, Z., et al. (2021). Targeted hot ion therapy of infected wound by glycol chitosan and polydopamine grafted Cu-SiO2 nanoparticles. *Nano Today* 41, 101330. doi:10.1016/j.nantod.2021.101330

Yang, C., Gao, X., Younis, M. R., Blum, N. T., Lei, S., Zhang, D., et al. (2021a). Non-invasive monitoring of *in vivo* bone regeneration based on alkaline phosphatase-responsive scaffolds. *Chem. Eng. J.* 408, 127959. doi:10.1016/j.cej.2020.127959

Yang, C., Huan, Z., Wang, X., Wu, C., and Chang, J. (2018). 3D printed Fe scaffolds with HA nanocoating for bone regeneration. *ACS Biomater. Sci. Eng.* 4 (2), 608–616. doi:10.1021/acsbiomaterials.7b00885

Yang, C., Ma, H., Wang, Z., Younis, M. R., Liu, C., Wu, C., et al. (2021b). 3D printed wesselsite nanosheets functionalized scaffold facilitates NIR-II

photothermal therapy and vascularized bone regeneration. *Adv. Sci. (Weinh).* 8, 2100894. doi:10.1002/advs.202100894

Yang, C., Wang, X. Y., Ma, B., Zhu, H. B., Huan, Z. G., Ma, N., et al. (2017). 3D-printed bioactive Ca3SiO5 bone cement scaffolds with nano surface structure for bone regeneration. *ACS Appl. Mat. Interfaces* 9 (7), 5757–5767. doi:10.1021/acsami.6b14297

Yang, C., Zhao, C., Wang, X., Shi, M., Zhu, Y., Jing, L., et al. (2019). Stimulation of osteogenesis and angiogenesis by micro/nano hierarchical hydroxyapatite via macrophage immunomodulation. *Nanoscale* 11 (38), 17699–17708. doi:10.1039/c9nr05730g

Yang, C., Zheng, Z., Younis, M. R., Dong, C., Chen, Y., Lei, S., et al. (2021c). 3D printed enzyme-functionalized scaffold facilitates diabetic bone regeneration. *Adv. Funct. Mat.* 31 (20), 2106571. doi:10.1002/adfm.202106571

Zhang, B., Su, Y., Zhou, J., Zheng, Y., and Zhu, D. (2021). Toward a better regeneration through implant-mediated immunomodulation: Harnessing the immune responses. *Adv. Sci.* 8 (16), 2100446. doi:10.1002/advs.202100446

Zhang, M. L., Lin, K. L., and Chang, J. (2012). Preparation and characterization of Sr-hardystonite (Sr2ZnSi2O7) for bone repair applications. *Mater. Sci. Eng. C* 32 (2), 184–188. doi:10.1016/j.msec.2011.10.017

Zhao, D., Zhu, T., Li, J., Cui, L., Zhang, Z., Zhuang, X., et al. (2021). Poly (lactic-co-glycolic acid)-based composite bone-substitute materials. *Bioact. Mater.* 6 (2), 346–360. doi:10.1016/j.bioactmat.2020.08.016

Zhen, W., Yichuan, W., Jiaqi, Y., Keshi, Z., Feng, L., Lei, X., et al. (2021). Pharmaceutical electrospinning and 3D printing scaffold design for bone regeneration. *Adv. Drug Deliv. Rev.* 174, 504–534. doi:10.1016/j.addr.2021.05.007

Zhong, Z., Wu, X., Wang, Y., Li, M., Li, Y., Liu, X., et al. (2022). Zn/Sr dual ions-collagen co-assembly hydroxyapatite enhances bone regeneration through procedural osteo-immunomodulation and osteogenesis. *Bioact. Mater.* 10, 195–206. doi:10.1016/j.bioactmat.2021.09.013

frontiers | Frontiers in Bioengineering and Biotechnology

TYPE Original Research
PUBLISHED 02 November 2022
DOI 10.3389/fbioe.2022.1046476

OPEN ACCESS

EDITED BY
Qian Feng,
Chongqing University, China

REVIEWED BY
Uriel Zapata,
EAFIT University, Colombia
Antonio López-Valverde,
University of Salamanca, Spain

*CORRESPONDENCE
Yi Zhang,
zhangyi0205@csu.edu.cn
Min Wang,
minwang@csu.edu.cn

†These authors have contributed equally to this work and share first authorship

SPECIALTY SECTION
This article was submitted to Biomaterials, a section of the journal Frontiers in Bioengineering and Biotechnology

RECEIVED 16 September 2022
ACCEPTED 18 October 2022
PUBLISHED 02 November 2022

CITATION
Liu Q, Liang J, Liu Z, Guo H, Wang M and Zhang Y (2022), Global trends and current status of distraction osteogenesis: Bibliometric analysis of publications from 1980 to 2021. *Front. Bioeng. Biotechnol.* 10:1046476. doi: 10.3389/fbioe.2022.1046476

Global trends and current status of distraction osteogenesis: Bibliometric analysis of publications from 1980 to 2021

Qi Liu[1,2†], Jieyu Liang[1,2†], Ze Liu[1,2], Hongbin Guo[1,2], Min Wang[3*] and Yi Zhang[1,2*]

[1]Department of Orthopaedics, Xiangya Hospital, Central South University, Changsha, Hunan, China, [2]National Clinical Research Center for Geriatric Disorders, Xiangya Hospital, Central South University, Changsha, Hunan, China, [3]Department of Endocrinology, Xiangya Hospital, Central South University, Changsha, Hunan, China

Introduction: Distraction osteogenesis (DO) has become an important technology for the correction of various congenital and acquired skeletal ridge deformities. It is widely used in oral and maxillofacial surgery, orthopedics, and other disciplines. From 1980 to 2021, the cutting-edge research of DO has been continuously promoted, and the interaction between disciplines has also been deepening. However, the analysis on the global trend and status of DO is relatively rare. Therefore, the aim of our study was to summarize the global trends and current status of DO through bibliometrics.

Materials and methods: Web of Science (WOS) core collection database and Medline were used to search DO-related literatures published during 1980–2021. The collected data are imported into Microsoft Excel, Microsoft Word, VOSviewer software for analysis and drawing figure/table.

Results: A total of 7,721 publications were included in this study. The United States is the main contributing country to DO (ranking first in terms of total publications, sum of times cited and H-index). Harvard University was the main contributing institution to DO. Journal of Craniofacial Surgery is the main contributing journal of DO related articles. Buchman, SR is the main contributing author to DO related articles. DO related publications can be summarized into 7 clusters: 1) "mechanism study", 2) "limb bone distraction study", 3) "alveolar bone distraction study", 4) "temporomandibular joint ankylosis study", 5) "maxillofacial surgery study", 6) "skull distraction study" and 7) "mandible distraction study". Mandible distraction study has been a hot topic in recent years. In addition, the "management", "osteogenesis" and "reconstruction" of DO have been the research hotspots from 1980 to 2021.

Conclusion: From 1980 to 2021, the total number of DO articles has increased rapidly and maintained a steady trend. The United States is the predominant country in the field. Surgery, dental, and oral surgery and orthopaedics are hot fields of DO research. The study of mandible distraction has been paid more and more attention and will become a hotspot in the future. Our study is beneficial for scientists to specify the research hotspot and development direction of DO.

KEYWORDS
distraction osteogenesis, bibliometrics, web of science, VOSviewer, visual analyses

1 Introduction

Distraction osteogenesis (DO) was first used by Codivilla (1905) to lengthen the femur axially (Codivilla, 2008). The principle of DO is that the regenerative signal system of the body is activated under the action of continuous, stable and slow pulling force, which stimulates the division and regeneration of tissue cells, and the bone tissue. The attached muscles, fascia, blood vessels, nerves, and skin will grow synchronously. In the 1950s, Professor Ilizarov, a physician of the former Soviet Union, used DO to correct long bone defects and deformities of limbs, and developed the technology into mature (Liu et al., 2022). In 1992, McCarthy et al. (1992a) first used DO technique to correct hemifacial micrognathia and Nagers' syndrome. Since then, DO technique has been widely used to correct various congenital and acquired maxillofacial deformities.

From 1980 to 2021, more and more publications have reported the clinical application of DO in orthopaedics, oral and maxillofacial surgery and neurosurgery around the world (Sandhaus and Johnson, 2021; Shevtsov and Leonchuk, 2021; Kosyk et al., 2022). However, the bibliometric analysis on the global trend and status of DO is relatively rare. Bibliometrics is a cross-discipline that uses mathematical and statistical methods to quantitatively analyze knowledge carriers, which can effectively avoid the subjectivity and arbitrariness of literature analysis and improve the formality and credibility of the results (Mayr and Scharnhorst, 2015). Through the systematic arrangement and reflection of literature, it is helpful for scholars to find a research breakthrough, and guide the future research direction. Therefore, the purpose of this study is to analyze the DO-related publications from 1980 to 2021 by bibliometrics, and to study the country, institutions, journal and authors in the field of DO. The results of our study may be helpful to facilitate the communication and cooperation among researchers, and then grasp the research trends in this field.

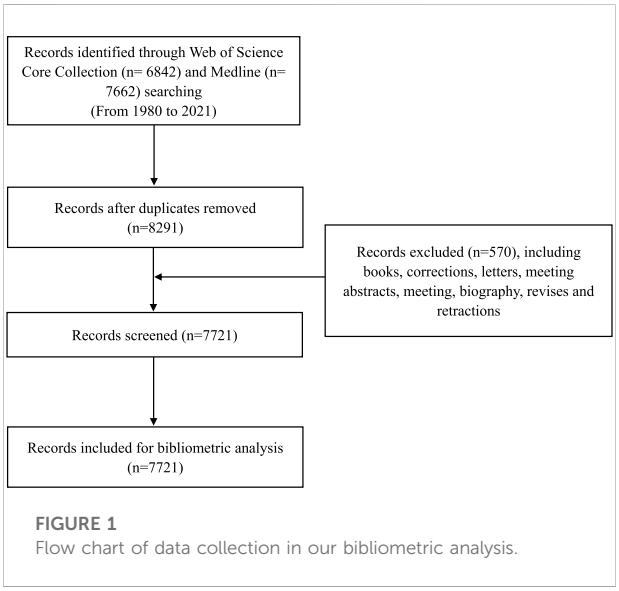

FIGURE 1
Flow chart of data collection in our bibliometric analysis.

2 Materials and methods

2.1 Data sources

All publications were sourced from Web of Science (WOS) Core Collection database (SCI-Expanded, SSCI, A&HCI, CPCI-S, CPCI-SSH, ESCI, CCR-Expanded, and IC) and Medline (Figure 1).

2.2 Search strategy

All publications were searched in WOS on October 2022. The search terms were TS = ("distraction osteogenesis" OR "bone lengthening") and document types: (Article OR Review). We selected publications with publication dates ranging from 1 January 1980 to 31 December 2021.

2.3 Data collection

The full records (including title, publication year, author nationalities, institutions of authors, funding sources, journals of publications, abstracts, keywords, total number of publications, sum times of cited, average citations per item, and H-index) were extracted from the retrieved literature by two independent authors (QL and YZ). The disagreements were resolved by discussions to prevent potential bias. The obtained publication information was exported in TXT format, and then imported into Microsoft Excel 2019 and VOSviewer (v.1.6.18) for analysis.

2.4 Bibliometric analysis

Microsoft Excel 2019 was used to analyze literature data and draw graphs. Bibliometric indicators, including total publications, sum of times cited, average citations per item, H-index and self-citation times, were included in this study. Total publications are widely used to measure the contribution to a field. Sum of times cited and average citations per item reflects the level of attention (Taubes, 1993). The H-index reflects the number and quality of an author's publications, which means that a scholar has published H papers, each of which has been

cited at least H times by other publications (Roldan-Valadez et al., 2019; Lu et al., 2022). In addition, it can now also define the publication quality of a country/region, institution or journal (Noruzi et al., 2022).

VOSviewer is one of the much scientific knowledge graph software, which can demonstrate the influence, cooperation and evolution of research field through bibliographic coupling analysis, co-authorship analysis, co-citation analysis and co-occurrence analysis. Bibliographic coupling analysis is a way of showing similar relationships between items by the number of references co-cited by items. Co-authorship analysis is a way to assess the intensity of collaboration between items by counting the number of co-authored publications. Co-citation analysis is a way of presenting the relevance of items based on how many times an item is cited together. Co-occurrence network visualization is created by analyzing the number of publications in which keywords appear together in the title or abstract. The aim is to identify hot research directions and topics that are essential to tracking scientific developments (Wang et al., 2019). In some way, the total link strength (TLS) can measure the degree of influence, collaboration of the items as a bibliometric index. In network visualization, the circle and label form items. The larger the circle, the more the number of publications. The thickness of line represents the correlation strength, and the circle color represents different cluster.

3 Results and discussion

3.1 Trend analysis of distraction osteogenesis-related publications

Our study identified 7721 DO-related publications, including article 6685) and review (1036), published between 1980 and 2021. The annual publications related to DO have maintained a steady trend after rapid growth. During 1980 to 2021, the number of annual publications on DO increased fifteenfold, from 22 in 1980 to 350 in 2021 (Figure 2A). It showed a steady upward trend from 1980 to 2012, and the publication volume tended to be stable from 2013 to 2021. A total of 99 countries participated in the DO study, and Figure 2B shows the top 20 countries. Among them, The United States ranks first in total publications (2010, 30%), followed by China (722, 11%), Japan (550, 8%), Germany (433, 7%), and Italy (354, 5%). In addition, among the top 5 countries, the United States and China showed an upward trend year by year, while the number of publications issued in other countries did not increase significantly (Figure 2C).

As shown in this study, from 1980 to 2021, the number of DO-related publications peaked in 2012 and then leveled off. We can predict that there will be more than 250 DO-related publications per year in the next few years. In addition, DO-related publications in the United States and China will continue to increase. From the fan chart, we can see that DO related researchers come from all over the world, especially in the United States, China, and Japan.

3.2 Quality analysis of distraction osteogenesis-related publications

3.2.1 Country

Figure 3A shows the quality measurement indicators (including sum times for cited, the average times of citations per item, H-index and self-citation times) of the top 10 DO-related publications. Among the top 10 countries in the total number of publications, the United States ranked first, has higher sum times of cited (64436) and H-index (105) than the other 9 countries. Although China ranked second in total publications, it ranked 9th in the average times of citations per item (15.87), slightly ahead of Turkey (13.42). Other developed countries, including Italy (40.23), England (32.88), Canada (30.57), Germany (27.16), Japan (21.87), France (17.09), and South Korea (16.25), despite the small total publications, the average times of citations per item is relatively high, of which Italy ranks first in the world. The above studies suggested that the quality of publications in the United States is comparatively high, while those in China are relatively low. The reason for the situation maybe that China's past scientific evaluation system paid more attention to the quantity rather than the quality of publications.

3.2.2 Institution

From 1980 to 2021, about 5742 institutions around the world have studied DO. Figure 3B shows the top 10 global main contributing institutions. Among the 10 institutions, there are 5 in the United States (Harvard University, University of California, New York University, University of Michigan, University of Pennsylvania), 2 in France (Udice French Research Universities, Assistance Publique Hopitaux Paris), 1 in China (Shanghai Jiaotong University), 1 in Egypt (Egyptian Knowledge Bank) and 1 in England (University of London), respectively. Harvard University ranks No. 1 in the total publication of DO research, which has published 138 papers. The University of California ranked second (131 publications), followed by Egyptian Knowledge Bank (102 publications), New York University (102 publications), and Udice French Research Universities (102 publications). The above data show that Harvard University is the most contributing institution in the world.

3.2.3 Author

The top 10 main contributing authors to the analysis of the quality of the author's publication are shown in Figure 3C. Among these authors, seven are from the United States

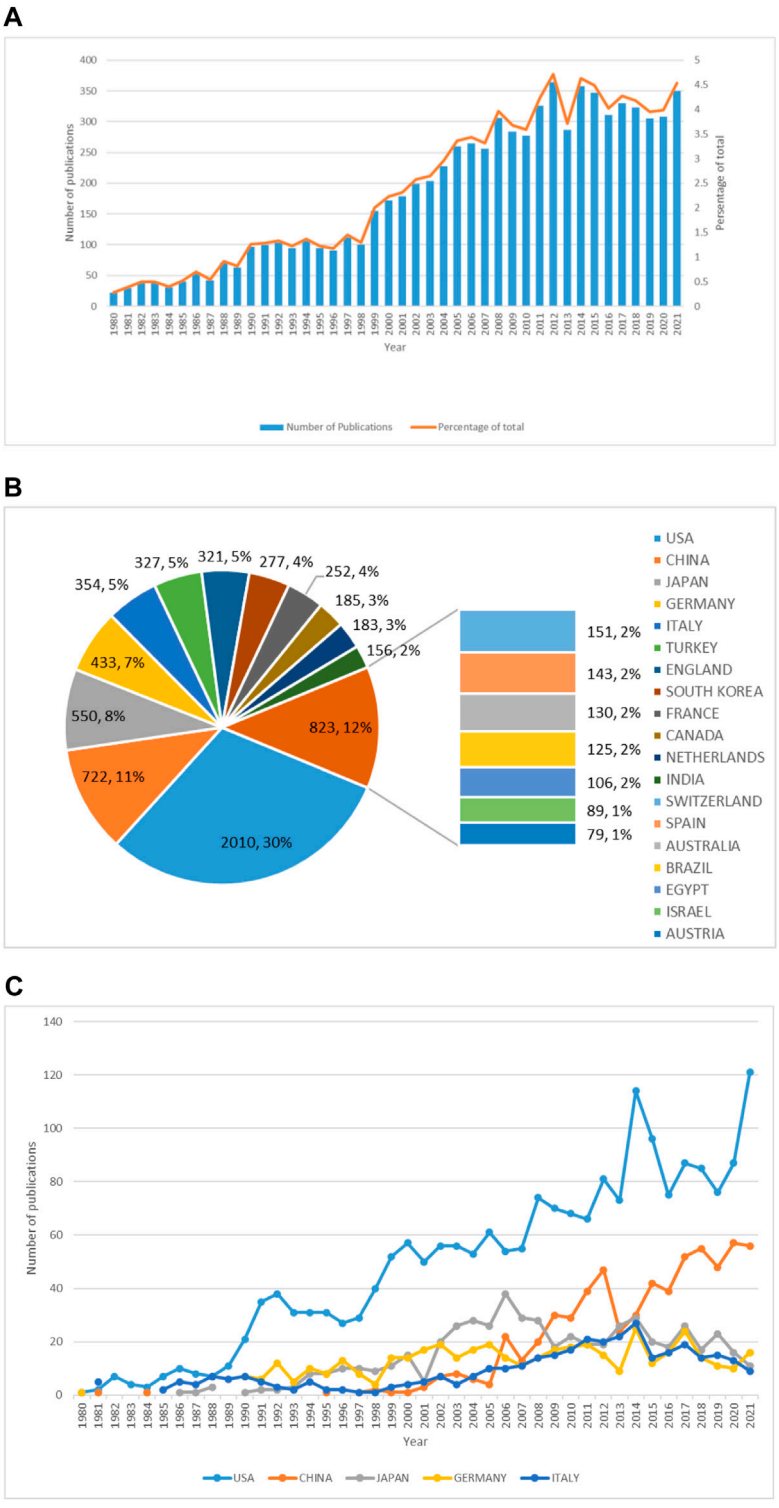

FIGURE 2
Global trends of publications on distraction osteogenesis (DO) in the last 42 years. **(A)** Annual DO-related publications worldwide. **(B)** The total number and percentage of DO-related publications from the top twenty countries. **(C)** DO-related publications of the top five countries over time.

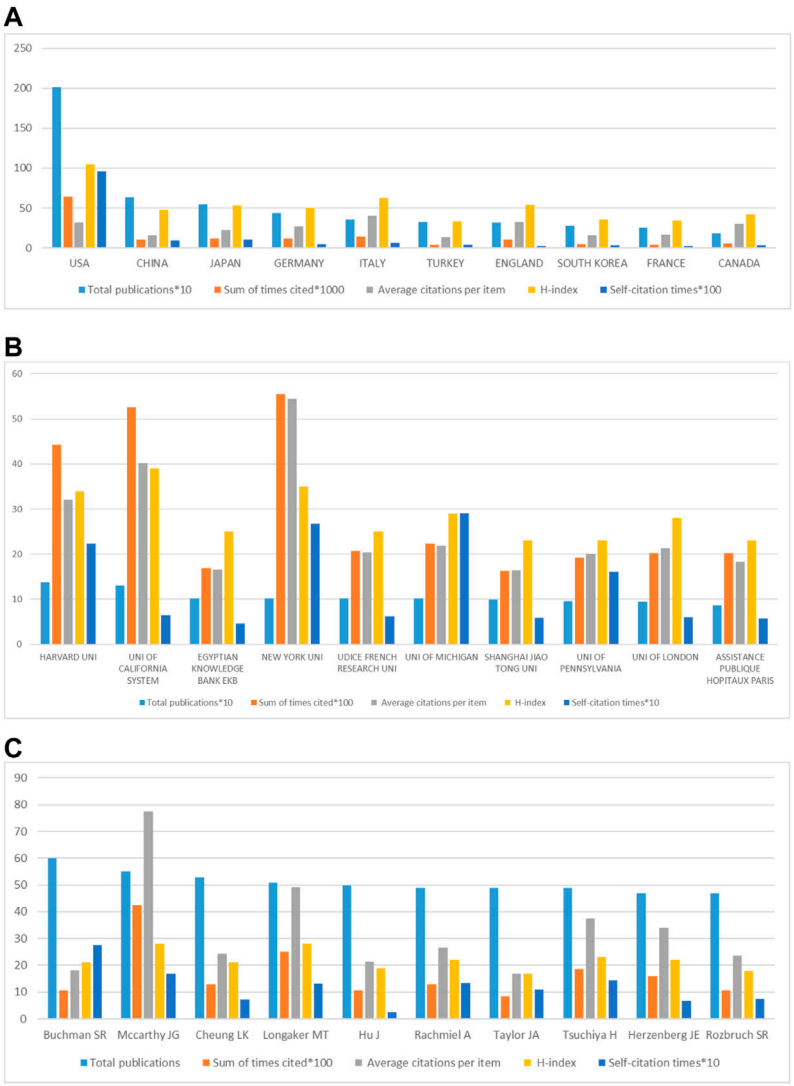

FIGURE 3
Quality analysis of global publications in DO in the last 42 years. **(A)** Total publications, sum of times cited, average citations per item, H-index and self-citation times of the top ten countries by contributions. **(B)** Total publications, sum of times cited, average citations per item, H-index and self-citation times of the top ten institutions by contributions. **(C)** Total publications, sum of times cited, average citations per item, H-index and self-citation times of the top ten authors by contributions.

(Buchman SR, Mccarthy JG, Longaker MT, Rachmiel A, Taylor JA, Herzenberg JE, and Rozbruch SR), two from China (Cheung LK and Hu J), one from Japan (Tsuchiya H). In addition, two from the University of Michigan (Buchman SR, Rachmiel A), one from the Children's Hospital of Philadelphia (Taylor JA), Mccarthy JG from New York University, Cheung LK from the University of Hong Kong, Longaker MT from Stanford University, Hu J from Sichuan University, Tsuchiya, H from Kanazawa University, Herzenberg JE from Sinai Hospital of Baltimore, Rozbruch SR from Cornell University. The biggest contributing authors is Buchman SR, which has published 60 papers with 1081 citations, with average citations per item of 18.02 and a H-index of 21. Mccarthy JG (55 articles, 4256 citations, average citations of 18.02, H-Index 28), which ranks second in the total number of publications, ranks first in the number of citations, and his H-index ranks first with Longaker MT. The above data show that Buchman SR is the author of DO-related publications with the greatest contribution. Interestingly, most of the authors with high contributions come from countries and institutions with high contributions, which shows that top research platforms can enable authors to create more contributions.

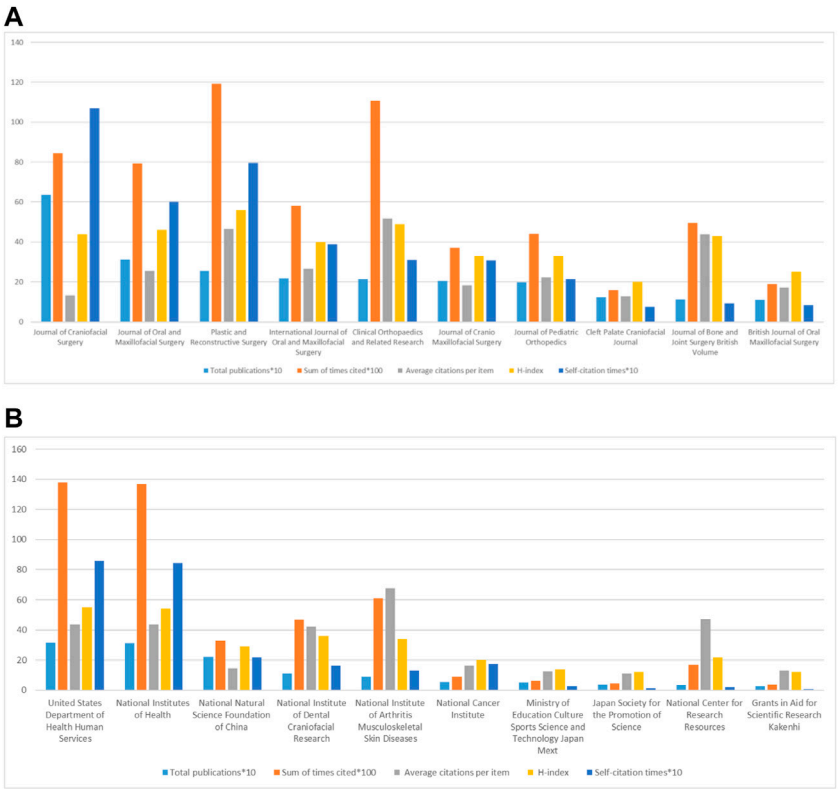

FIGURE 4
Analysis of highly contributing journals and funding agencies in DO in the last 42 years. **(A)** Total publications, sum of times cited, average citations per item, H-index and self-citation times of the top ten journals. **(B)** Total publications, sum of times cited, average citations per item, H-index and self-citation times of the top ten funding agencies.

3.2.4 Journal

Figure 4A shows the top 10 journals that have published the most DO-related publications. Journal of Craniofacial Surgery (IF = 1.172, 2022) is the largest number of DO-related publications (635 publications), followed by Journal of Oral and Maxillofacial Surgery (IF = 2.136, 2022) with 311 publications, Plastic and Reconstructive Surgery (IF = 5.169, 2022) with 256 publications, International Journal of Oral and Maxillofacial Surgery (IF = 2.986, 2022) with 219 publications, Clinical Orthopaedics and Related Research (IF = 4.755, 2022) with 214 publications.

Among the top 10 journals, Journal of Craniofacial Surgery rank first, which is the journal with the largest contribution to DO-related publications. In addition, Plastic and Reconstructive Surgery ranked third, ranking first in the sum of citations and H-index. The higher average citations per item indicate that a higher level of attention for its publication (Garcia et al., 2021). However, journals' excessive self-citation can artificially affect journal metrics (Sanfilippo et al., 2021). We found that Journal of Craniofacial Surgery had a relatively high self-citation rate (12.6%), while the remaining nine journals were all below 10%. The above shows that Plastic and Reconstructive Surgery and Clinical Orthopaedics and Related Research are journals with high publication quality.

3.2.5 Funding agency

Figure 4B presents the top 10 funding organizations of the largest of DO-related publications. The top funding agency in the number of publications is the United States Department of Health and Human Services (HHS, United States), followed by the National Institutes of Health (NIH, United States), the National Natural Science Foundation of China (NSFC, China), which indicates that these institutions made a significant contribution to DO-related publications. The higher average citations per item funding agencies are National Institute of Arthritis Musculoskeletal Skin Diseases (NIAMS, United States), National Center for Research Resources and the United States Department of Health and Human Services (HHS, United States), which indicates that the publications funded by these funding agencies are of high quality.

TABLE 1 Top ten most cited publications in DO in the world.

Title	Authors	Journal	Year	Type	IF	Times cited
Lengthening the human mandible by gradual distraction	McCarthy JG et al	Plastic and reconstructive surgery	1992	Article	5.169	1566
The tension-stress effect on the genesis and growth of tissues: Part II. The influence of the rate and frequency of distraction	Ilizarov GA	Clinical orthopaedics and related research	1989	Article	4.755	1411
Chitosan: A versatile biopolymer for orthopaedic tissue-engineering	Di Martino A et al	Biomaterials	2005	Review	2.69	1255
Bone regeneration: current concepts and future directions	Dimitriou, R et al	BMC medicine	2011	Review	11.15	1032
Problems, obstacles, and complications of limb lengthening by the Ilizarov technique	Paley D	Clinical orthopaedics and related research	1990	Article	4.755	1024
Optimizing esthetics for implant restorations in the anterior maxilla: Anatomic and surgical considerations	Buser D et al	International journal of oral and maxillofacial implants	2004	Article	2.912	706
Fracture healing under healthy and inflammatory conditions	Claes L et al	Nature reviews rheumatology	2012	Review	32.286	660
Which hard tissue augmentation techniques are the most successful in furnishing bony support for implant placement?	Aghaloo T et al	International journal of oral and maxillofacial implants	2007	Review	2.912	620
Mechanobiology of skeletal regeneration	Carter DR et al	Clinical orthopaedics and related research	1998	Article	4.755	526
Clinical application of the tension-stress effect for limb lengthening	Ilizarov GA	Clinical orthopaedics and related research	1990	Article	4.755	520

3.3 Analysis of highly cited distraction osteogenesis-related publications

Table 1 indicates the top 10 most cited DO-related publications with citations ranging from 520 to 1566. McCarthy et al. (1992b), Buser et al. (2004), Aghaloo and Moy (2007) wrote the first, sixth, eighth most cited publications, respectively. They all made a comprehensive summary and analysis of the anatomy, treatment plan and matters needing attention of DO operation of oral and maxillofacial bone. Ilizarov (1989a) and Ilizarov (1990), Paley (1990) wrote the second and 10th, fifth most cited publications, respectively. They detailed the best strategy and complications of DO operation of limb bone. Di Martino et al. (2005), Dimitriou et al. (2011), Claes et al. (2012), Carter et al. (1998) wrote the third, fourth, seventh, and ninth most cited publications, respectively. They summarized and studied the therapeutic strategies, influencing factors and mechanobiology mechanisms of promoting bone regeneration in the process of DO.

3.4 Analysis of distraction osteogenesis-related research areas

DO-related publications are divided into 118 different research fields on WOS. We analyzed the top 10 research areas of DO-related publications. Figure 5 shows the corresponding number of DO-related publications in all research areas, among which surgery area receiving the most attention (6659, 86.245%), followed by orthopaedics area (6504,84.238%), anatomy morphology area (3472,44.968%), dentistry oral surgery medicine area (3464,44.865%), pediatrics area (3183,41.225%), physiology area (2862,37.068%), radiology nuclear medicine medical imaging area (2045,26.486%), rehabilitation area (1026,13.288%), pathology area (996,12.9%), and research experimental medicine area (995,12.887%).

Surgery, dentistry oral surgery medicine, orthopaedics and radiology nuclear medicine medical imaging have been widely and deeply studied for their attention to the influencing factors, surgical methods, diagnosis and treatment of DO. Meanwhile, anatomy morphology had also been intensively investigated within the development of surgery. In the field of pediatrics, the emphasis was placed on DO bone reconstruction surgery for the treatment of skeletal dysplasia in children. DO can correct skeletal deformities such as limb and head deformities in children, so as to promote the recovery of skeletal function and morphology in patients. Vogt et al. (2011) studied the use of DO technique to correct forearm deformities caused by multiple chondroectogenesis in children. With the progress of research experimental medicine, more and more studies have applied animal experiments or clinical trials to the pathology and physiology of DO. In addition, researchers combine physiology, pathology, and experimental medical research to explore the biological mechanism of DO. For example, Hamushan et al. (2021) demonstrated that high purity magnesium needles can promote bone growth by mechanical test, radiology and histological analysis of rat

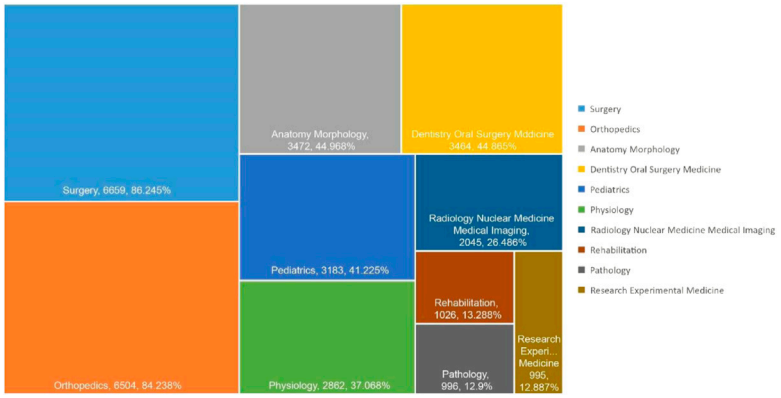

FIGURE 5
Research area analysis of global publications in DO in the last 42 years.

femur, which may be related to the regulation of Ptch protein activating Hedgehog pathway instead of Wnt signal transduction. Meanwhile, some studies have also shown that the growth hormone can promote callus regeneration in patients with X-linked hypophosphatemic rickets during DO (Canete et al., 2014). In the field of rehabilitation, it mainly focuses on the role of physical therapy (such as low-intensity pulse ultrasound, exercise therapy) in promoting callus growth and limb function recovery in the process of DO. El-Mowafi and Mohsen (2005) found that low-intensity pulsed ultrasound stimulation was effective in promoting tibia maturation and shortening bone formation time.

3.5 Bibliographic coupling analysis

3.5.1 Country

Figure 6A presents the relevance of 54 identified countries (the minimum number of documents of a country more than 5). The top five countries with TLS are as follows: the United States (TLS = 1142009), China (TLS = 461186), Japan (TLS = 405909), Germany (TLS = 309495) and Turkey (TLS = 276394). Therefore, according to bibliographic coupling analysis, the United States is the leading country in DO around the world.

3.5.2 Institution

Figure 6B shows the relevance of 399 identified institutions (the minimum number of documents of an institution is more than 5). The top five institutions with TLS are New York University (TLS = 103555), Harvard University (TLS = 99245), University of Michigan (TLS = 96046), University of Hong Kong (TLS = 85036) and McGill University of Canada (TLS = 84412). Therefore, through the above analysis, New York University is the leading institution of DO in the world.

3.5.3 Journal

Figure 6C shows the relevance of 141 identified journals (the minimum number of documents of a journal is more than 5). The top five journals with TLS are as follows: Journal of Craniofacial Surgery (TLS = 406287), Journal of Oral And Maxillofacial Surgery (TLS = 268937), Plastic and Reconstructive Surgery (TLS = 231890), International Journal of Oral and Maxillofacial Surgery (TLS = 209614) and Journal of Cranio-Maxillofacial Surgery (TLS = 157150). Therefore, according to bibliographic coupling analysis, Journal of Craniofacial Surgery is the leading global journal in DO.

3.6 Co-authorship analysis

3.6.1 Country

Figure 7A presents the relevance of 53 identified countries (the minimum number of documents of a country is more than 5) in TLS. The top five countries with TLS are the United States (TLS = 399), the England (TLS = 163), Germany (TLS = 148), and Italy (TLS = 125), the Switzerland (TLS = 115). Therefore, according to the co-authorship analysis, American authors are more cooperative than their authors in other countries.

3.6.2 Institution

Figure 7B shows the relevance of 371 identified institutions (the minimum number of documents of an institution is more than 5) in TLS. The top five institutions with TLS are Harvard University (TLS = 68), University of Bologna (TLS = 55), University of Michigan (TLS = 51), Boston Children's Hospital (TLS = 50), Shanghai Jiaotong University (TLS = 48). Therefore, according to the co-authorship analysis, Harvard University is more cooperative than other universities.

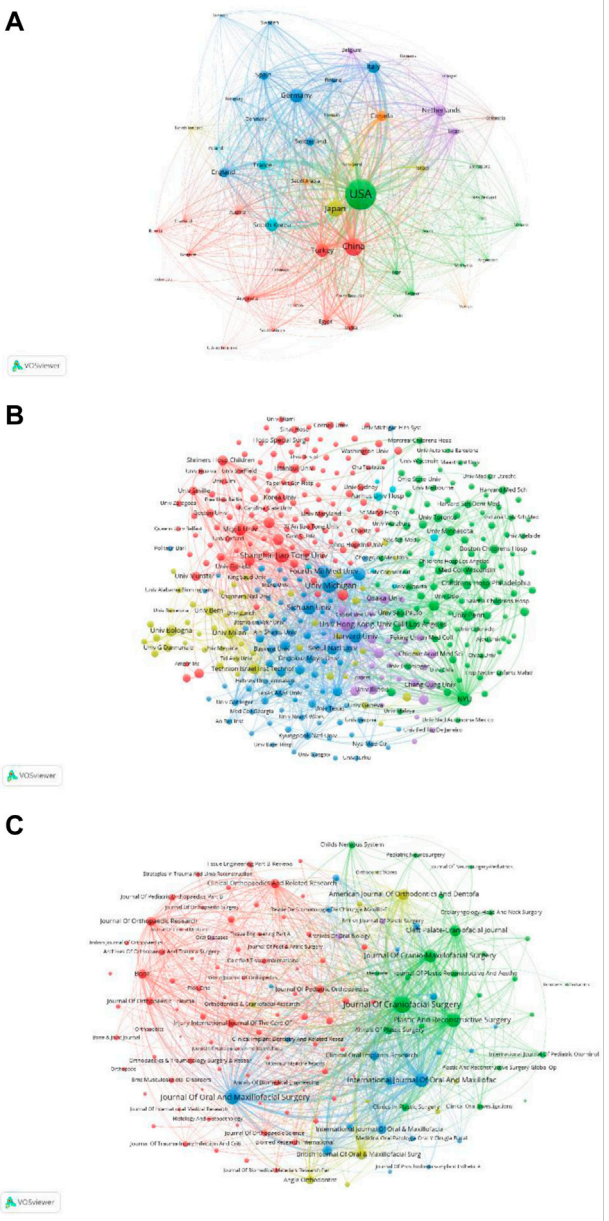

FIGURE 6
Bibliographic coupling analysis of global publications in DO in the last 42 years. **(A)** Network visualization of the 54 identified countries in DO. **(B)** Network visualization of the 399 identified institutions in DO. **(C)** Network visualization of the 141 identified journals in DO. In the visualized network, items are represented by circles. The larger the circle, the more the number of publications; the thickness of line represents the correlation strength; and the circle color represents different cluster.

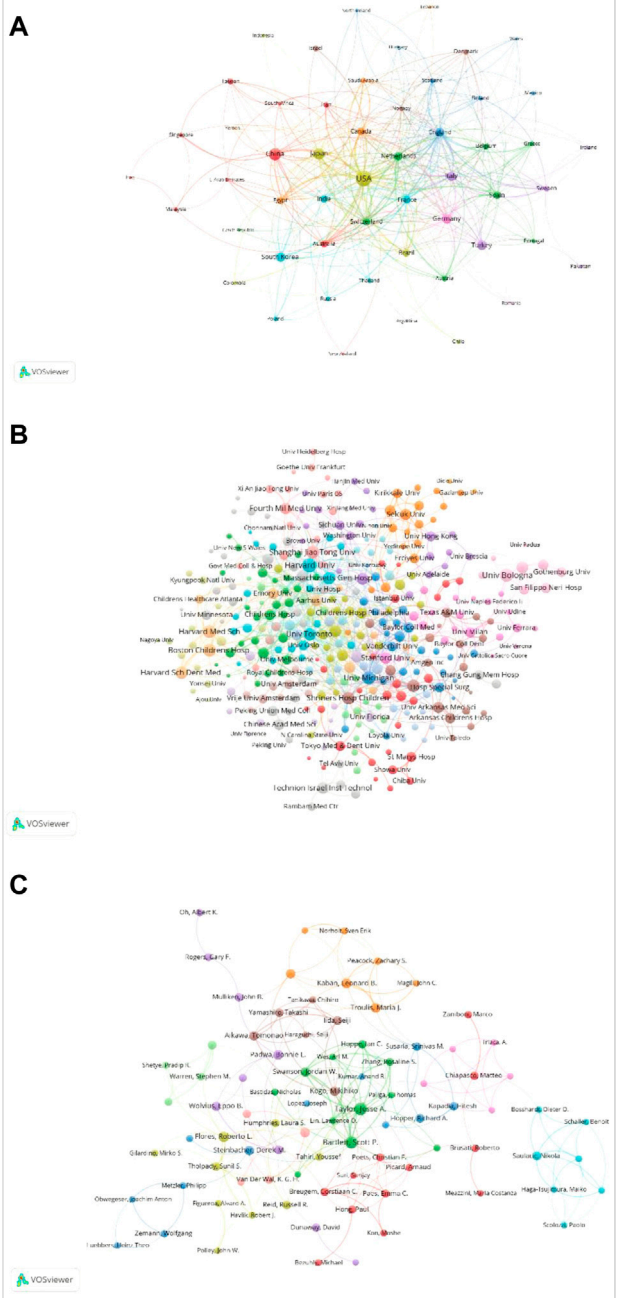

FIGURE 7
Co-authorship analysis of global publications in DO in the last 42 years. **(A)** Network visualization of the 53 identified countries in DO. **(B)** Network visualization of the 371 identified institutions in DO. **(C)** Network visualization of the 86 identified authors in DO.

3.6.3 Author

Figure 7C shows the relevance of 86 identified author (the minimum number of documents of an author is more than 5) in TLS. The top five authors are as follows: Bartlett, Scott P. (TLS = 92), Taylor, Jesse A. (TLS = 88), Swanson, Jordan W. (TLS = 53), Hoppe, Ian C. (TLS = 41), and Zhang, Rosaline S. (TLS = 39). Therefore, according to the co-authorship analysis, Bartlett, Scott P. is the most cooperative author.

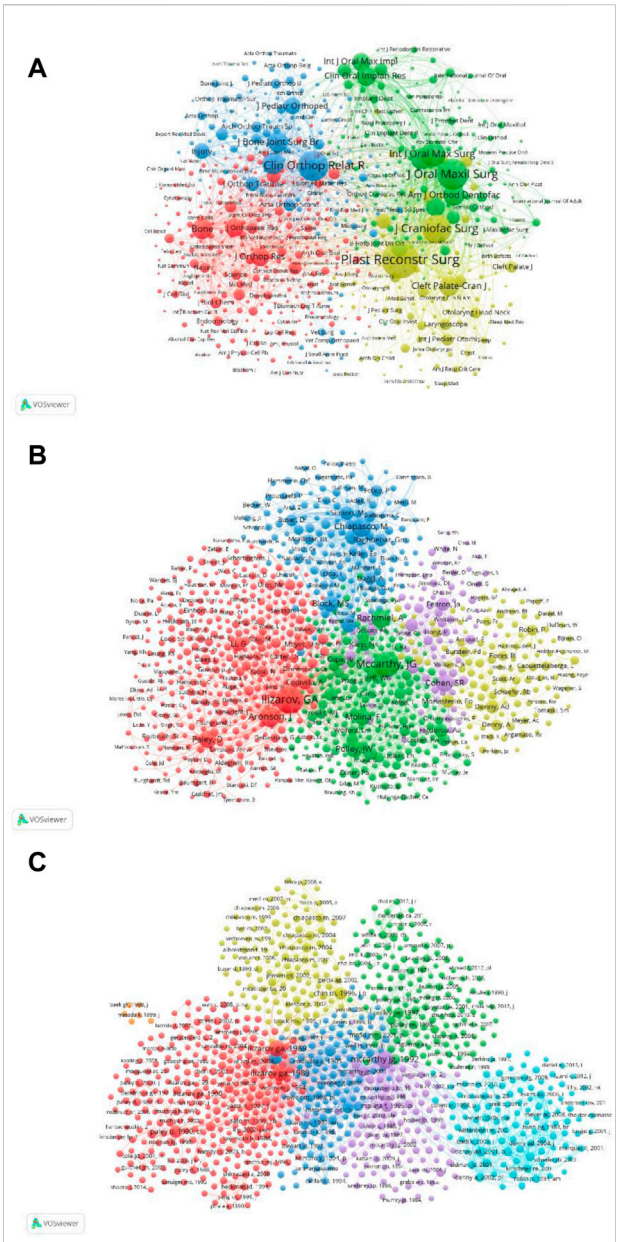

FIGURE 8
Co-citation analysis of global publications in DO in the last 42 years. **(A)** Network visualization of the 712 identified journals in DO. **(B)** Network visualization of the 1257 identified authors in DO. **(C)** Network visualization of the 906 identified references in DO.

3.7 Co-citation analysis

3.7.1 Journal

Figure 8A shows the relevance between the TLS of 712 identified journals (the minimum number of citations of a journal is more than 20). The top five journals with TLS are as follows: Plast Reconstr Surg (TLS = 427555), J Oral Maxil Surg (TLS = 355213), J Craniofac Surg (TLS = 273571), Clin Orthop Relat R (TLS = 269309) and Int J Oral Max Surg (TLS = 201085). Therefore, according to the co-citation analysis, Plast Reconstr Surg is the influential journal of DO in the world.

3.7.2 Authors

Figure 8B reveals the relevance between the TLS of the 1257 identified authors (the minimum number of references to a publication is more than 20). The top five publications with TLS are Ilizarov GA (TLS = 42691), Mccarthy JG (TLS = 34527), Aronson J (TLS = 18810), Chiapasco M (TLS = 17265), and Rachmiel A (TLS = 15678). Therefore, according to the co-citation analysis, Ilizarov GA are the most influential authors of DO in the world.

3.7.3 References

Figure 8C reveals the relevance between the TLS of the 906 identified publications (the minimum number of references a publication is more than 20). The top five publications with TLS are as follows: McCarthy et al. (1992b) (TLS = 11983), Ilizarov (1989b), Ilizarov (1989c) (TLS = 9124 and 8692), Molina and Ortiz Monasterio (1995) (TLS = 3959) and Chin and Toth (1996) (TLS = 3875). Therefore, according to the co-citation analysis, The paper by McCarthy et al. (1992b) is the most influential publications of DO in the world.

3.8 Co-occurrence analysis

As shown in Figure 9A, 1,000 identified keywords (the minimum number of occurrences of a keyword in titles and abstracts is more than 10) are divided into 7 clusters: “mechanism study”, “limb bone distraction study”, “alveolar bone distraction study”, “temporomandibular joint ankylosis study”, “maxillofacial surgery study”, “skull distraction study” and “mandible distraction study”. The top 10 keywords in DO are “distraction osteogenesis”, “management”, “osteogenesis”, “reconstruction”, “growth”, “children”, “complications”, “bone”, “mandibular distraction osteogenesis,” and “expression”. These results can provide new insights into the hot research directions and topics of DO, which indicates that further attention should be paid to these promising areas in the future.

The overlay visualization can give items different colors depending on the average time of keyword appearance. The bluer the color, the earlier the keyword appears, the more yellow the color, the later the keyword appears (Figure 9B). By comparing Figure 9A with Figure 9B, we can find that the cluster 7 region is more yellow in Figure 9B, which means that the keywords related to mandibular distraction appeared later. Therefore, “mandible distraction study” is a hot topic of

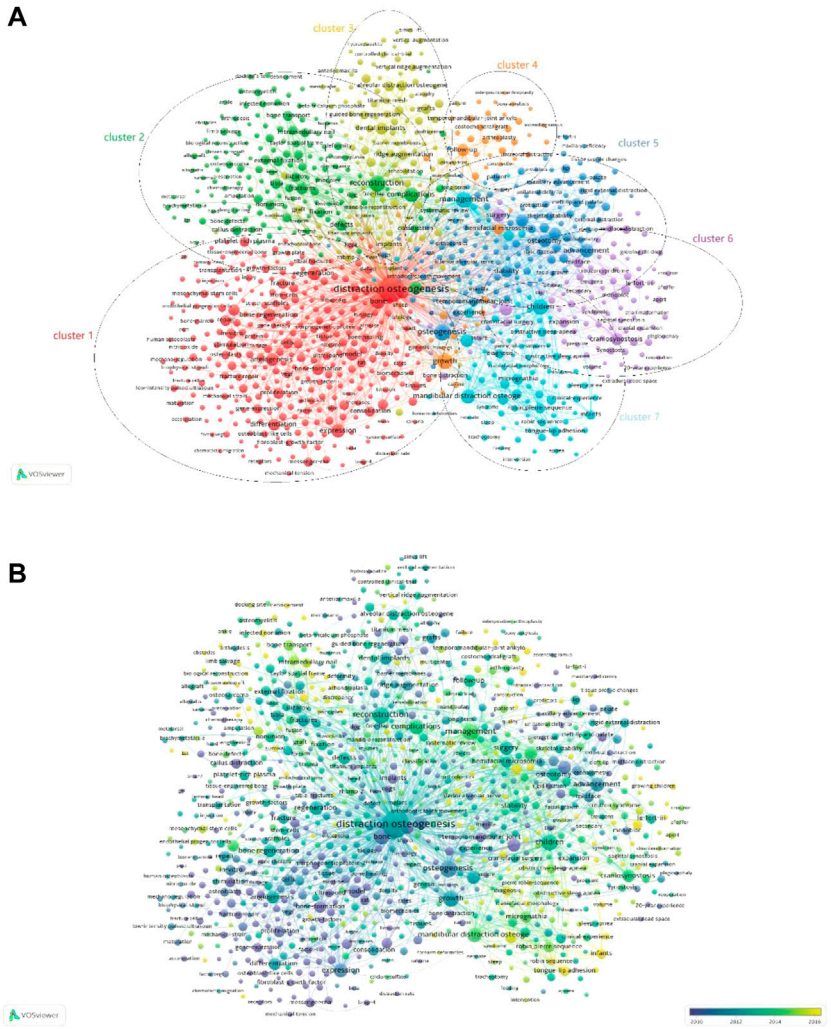

FIGURE 9
Co-occurrence analysis of global publications in DO in the last 42 years. **(A)** Network visualization of 1000 identified keywords in DO. All the keywords are divided into 7 clusters: 1) "mechanism study", 2) "limb bone distraction study", 3) "alveolar bone distraction study", 4) "temporomandibular joint ankylosis study", 5) "maxillofacial surgery study", 6) "skull distraction study" and 7) "mandible distraction study". **(B)** Overlay visualization of the identified 662 keywords in DO based on the average time they appeared in the publications. The blue keyword appeared earlier, while the yellow keyword appeared later.

DO-related research in recent years and may become the focus of future research. While before 2012, most studies focus on "mechanism study."

4 Strengths and limitations

Our study employs bibliometric research methods to provide a comprehensive and objective picture of global trends and the current state of DO-related publications from 1980 to 2021. However, the study also has some limitations. First, the study measures the quality of publications primarily by comparing the number of citations and the average times of citations for per item. However, highly cited publications do not equate to high scientific quality. The number of citations can be influenced by some factors, such as the hot issue of research topic, fame degree of researcher, or even over-cited artificially. Secondly, there are differences in publications from different databases, and we used only the WOS core collection database and Medline for literature data search, which may have an impact on the accuracy of the study results. Finally, the influence of publication time on the total number of citations was not considered. The fact that the most

recent high-quality articles are rarely cited may be overlooked. Therefore, it is also important to pay attention to the most recent publications.

5 Conclusion

Our study identifies DO-related publications from 1980 to 2021 and introduces their global trends and status. In the past 42 years, the number of total publications of DO research has maintained a steady trend after rapid growth. The United States ranks first in terms of total publications, sum of times cited, the H-Index and self-citation times. Harvard University, University of California and Egyptian Knowledge Bank are the top 3 contributing institutions to DO. Journal of Craniofacial Surgery, Journal of Oral and Maxillofacial Surgery and Plastic and Reconstructive Surgery are the top 3 contributing journals to DO. Buchman SR, Mccarthy JG and Cheung LK are the top 3 contributing authors to DO. Surgery, orthopaedics and anatomy morphology are the top 3 fields of DO research. In addition, the DO research on the mandible will become the focus of scholars in the future.

Data availability statement

The original contributions presented in the study are included in the article/supplementary material, further inquiries can be directed to the corresponding authors.

Author contributions

YZ decided and conceptualized this article, and revised the draft. QL and YZ wrote the manuscript. JL, ZL collected and analyzed the data. HG prepared the figures and tables. YZ and MW was the guarantor of the overall content. All authors approved the final version of the manuscript and agreed to be accountable for all specs of the work.

Funding

This study was supported by National Natural Science Foundation of China (82102581, 82270930), National Postdoctoral Science Foundation of China (2021M693562), Provincial Natural Science Foundation of Hunan (2019JJ40517, 2022JJ40843), Provincial Outstanding Postdoctoral Innovative Talents Program of Hunan (2021RC2020), Young Investigator Grant of Xiangya Hospital, Central South University (2020Q14), FuQing Postdoc Program of Xiangya Hospital, Central South University (176) and Fund of Reform and Practice of Ideological and Political in Xiangya Hospital, Central South University (36, 40).

Conflict of interest

The authors declare that the research was conducted in the absence of any commercial or financial relationships that could be construed as a potential conflict of interest.

Publisher's note

All claims expressed in this article are solely those of the authors and do not necessarily represent those of their affiliated organizations, or those of the publisher, the editors and the reviewers. Any product that may be evaluated in this article, or claim that may be made by its manufacturer, is not guaranteed or endorsed by the publisher.

References

Aghaloo, T. L., and Moy, P. K. (2007). Which hard tissue augmentation techniques are the most successful in furnishing bony support for implant placement? *Int. J. Oral Maxillofac. Implants* 22, 49–70.

Buser, D., Martin, W., and Belser, U. C. (2004). Optimizing esthetics for implant restorations in the anterior maxilla: Anatomic and surgical considerations. *Int. J. Oral Maxillofac. Implants* 19, 43–61.

Canete, R., Caballero-Villarraso, J., Aguilar-Quintero, M., and Vazquez-Rueda, F. (2014). Beneficial effects of growth hormone therapy for ossification defects after bone distraction in X linked hypophosphataemic rickets. *Case Rep. Child. Meml. Hosp. Chic.* 2014, bcr2013203069. doi:10.1136/bcr-2013-203069

Carter, D. R., Beaupre, G. S., Giori, N. J., and Helms, J. A. (1998). Mechanobiology of skeletal regeneration. *Clin. Orthop. Relat. Res.* 335, S41–S55.

Chin, M., and Toth, B. A. (1996). Distraction osteogenesis in maxillofacial surgery using internal devices: Review of five cases. *J. Oral Maxillofac. Surg.* 54, 45–53. doi:10.1016/s0278-2391(96)90303-1

Claes, L., Recknagel, S., and Ignatius, A. (2012). Fracture healing under healthy and inflammatory conditions. *Nat. Rev. Rheumatol.* 8, 133–143. doi:10.1038/nrrheum.2012.1

Codivilla, A. (2008). The Classic: On the means of lengthening, in the lower limbs, the muscles and tissues which are shortened through deformity, 1905). *Clin. Orthop. Relat. Res.* 466, 2903–2909. doi:10.1007/s11999-008-0518-7

Di Martino, A., Sittinger, M., and Risbud, M. V. (2005). Chitosan: A versatile biopolymer for orthopaedic tissue-engineering. *Biomaterials* 26, 5983–5990. doi:10.1016/j.biomaterials.2005.03.016

Dimitriou, R., Jones, E., McGonagle, D., and Giannoudis, P. V. (2011). Bone regeneration: Current concepts and future directions. *BMC Med.* 9, 66. doi:10.1186/1741-7015-9-66

El-Mowafi, H., and Mohsen, M. (2005). The effect of low-intensity pulsed ultrasound on callus maturation in tibial distraction osteogenesis. *Int. Orthop.* 29, 121–124. doi:10.1007/s00264-004-0625-3

Garcia, J. B. S., de Moraes É, B., and Neto, J. O. B. (2021). A bibliometric analysis of published literature in Postoperative Pain in Elderly patients in low- and Middle-Income countries. *J. Clin. Med.* 10, 2334. doi:10.3390/jcm10112334

Hamushan, M., Cai, W., Zhang, Y., Ren, Z., Du, J., Zhang, S., et al. (2021). High-purity magnesium pin enhances bone consolidation in distraction osteogenesis via regulating Ptch protein activating Hedgehog-alternative Wnt signaling. *Bioact. Mater.* 6, 1563–1574. doi:10.1016/j.bioactmat.2020.11.008

Ilizarov, G. A. (1990). Clinical-application of the tension-stress effect for limb lengthening. *Clin. Orthop. Relat. Res.* 250, 8–26. doi:10.1097/00003086-199001000-00003

Ilizarov, G. A. (1989). The tension-stress effect on the genesis and growth of tissues. *Clin. Orthop. Relat. Res.* 239, 263–285. doi:10.1097/00003086-198902000-00029

Ilizarov, G. A. (1989). The tension-stress effect on the Genesis and growth of tissues: Part II. The influence of the rate and frequency of distraction. *Clin. Orthop. Relat. Res.* 239, 263–285. doi:10.1097/00003086-198902000-00029

Ilizarov, G. A. (1989). The tension-stress effect on the Genesis and growth of tissues. Part I. The influence of stability of fixation and soft-tissue preservation. *Clin. Orthop. Relat. Res.* 238, 249–281. doi:10.1097/00003086-198901000-00038

Kosyk, M. S., Carlson, A. R., Zapatero, Z. D., Kalmar, C. L., Cielo, C. M., Lioy, J., et al. (2022). Mandibular distraction osteogenesis for Tongue-based Airway Obstruction without micrognathia. *Ann. Plast. Surg.* 88, 54–58. doi:10.1097/sap.0000000000002891

Liu, Q., Liu, Z., Guo, H., Liang, J., and Zhang, Y. (2022). The progress in quantitative evaluation of callus during distraction osteogenesis. *BMC Musculoskelet. Disord.* 23, 490. doi:10.1186/s12891-022-05458-8

Lu, Y., Zhang, X., Wu, S., Zhang, S., and Tan, J. (2022). A bibliometric analysis of global research on vitamin D and reproductive health between 2012 and 2021: Learning from the past, planning for the future. *Front. Nutr.* 9, 973332. doi:10.3389/fnut.2022.973332

Mayr, P., and Scharnhorst, A. (2015). Combining bibliometrics and information retrieval: Preface. *Scientometrics* 102, 2191–2192. doi:10.1007/s11192-015-1529-2

McCarthy, J. G., Schreiber, J., Karp, N., Thorne, C. H., and Grayson, B. H. (1992). Lengthening the human mandible by gradual distraction. *Plastic Reconstr. Surg.* 89, 1–8. doi:10.1097/00006534-199289010-00001

Molina, F., and Ortiz Monasterio, F. (1995). Mandibular elongation and remodeling by distraction: A farewell to major osteotomies. *Plastic Reconstr. Surg.* 96, 825–840. doi:10.1097/00006534-199509001-00010

Noruzi, A., Gholampour, B., Gholampour, S., Jafari, S., Farshid, R., Stanek, A., et al. (2022). Current and future Perspectives on the COVID-19 Vaccine: A Scientometric review. *J. Clin. Med.* 11, 750. doi:10.3390/jcm11030750

Paley, D. (1990). Problems, Obstacles, and complications of limb lengthening by the Ilizarov technique. *Clin. Orthop. Relat. Res.* 250, 81–104. doi:10.1097/00003086-199001000-00011

Roldan-Valadez, E., Salazar-Ruiz, S. Y., Ibarra-Contreras, R., and Rios, C. (2019). Current concepts on bibliometrics: A brief review about impact factor, Eigenfactor score, CiteScore, SCImago journal rank, Source-Normalised impact per paper, H-index, and alternative metrics. *Ir. J. Med. Sci.* 188, 939–951. doi:10.1007/s11845-018-1936-5

Sandhaus, H., and Johnson, M. D. (2021). Distraction osteogenesis in craniosynostosis. *Curr. Opin. Otolaryngol. Head. Neck Surg.* 29, 304–313. doi:10.1097/moo.0000000000000724

Sanfilippo, F., Tigano, S., Morgana, A., Murabito, P., and Astuto, M. (2021). Self-citation policies and journal self-citation rate among Critical Care Medicine journals. *J. intensive care* 9, 15. doi:10.1186/s40560-021-00530-2

Shevtsov, V. I., and Leonchuk, S. S. (2021). Stimulation of distraction osteogenesis in limb lengthening: Our Concept. *Traumatology Orthop. Russ.* 27, 75–85. doi:10.21823/2311-2905-2021-27-1-75-85

Taubes, G. (1993). Measure for measure in science. *Science* 260, 884–886. doi:10.1126/science.8493516

Vogt, B., Tretow, H. L., Daniilidis, K., Wacker, S., Buller, T. C., Henrichs, M. P., et al. (2011). Reconstruction of forearm deformity by distraction osteogenesis in children with relative shortening of the ulna due to multiple cartilaginous exostosis. *J. Pediatr. Orthop.* 31, 393–401. doi:10.1097/BPO.0b013e31821a5e27

Wang, K., Xing, D., Dong, S., and Lin, J. (2019). The global state of research in nonsurgical treatment of knee osteoarthritis: A bibliometric and visualized study. *BMC Musculoskelet. Disord.* 20, 407. doi:10.1186/s12891-019-2804-9

Frontiers in
Bioengineering and Biotechnology

Accelerates the development of therapies, devices, and technologies to improve our lives

A multidisciplinary journal that accelerates the development of biological therapies, devices, processes and technologies to improve our lives by bridging the gap between discoveries and their application.

Discover the latest Research Topics

See more →

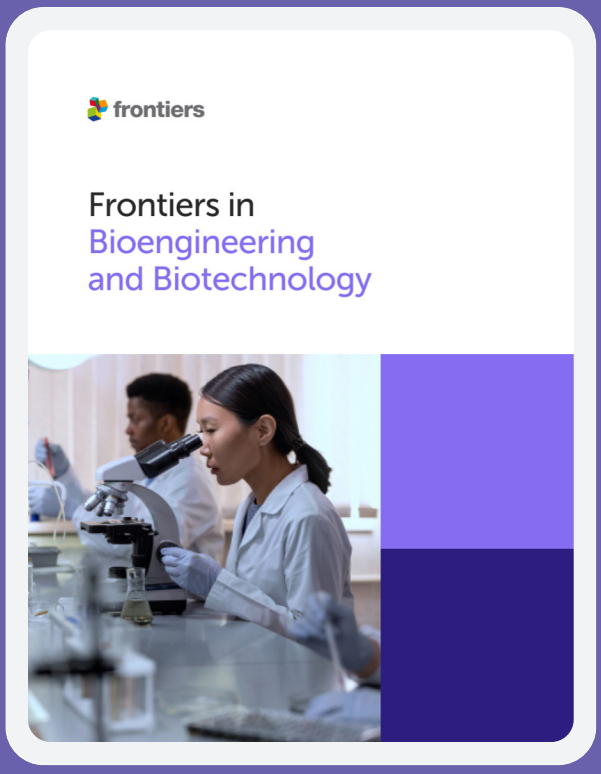

Frontiers

Avenue du Tribunal-Fédéral 34
1005 Lausanne, Switzerland
frontiersin.org

Contact us

+41 (0)21 510 17 00
frontiersin.org/about/contact